

UNCLASSIFIED

AD NUMBER

AD820957

LIMITATION CHANGES

TO:

Approved for public release; distribution is unlimited.

FROM:

Distribution authorized to U.S. Gov't. agencies and their contractors; Critical Technology; JUL 1967. Other requests shall be referred to Naval Air Systems Command, Department of the Navy, Washington, DC 20362. This document contains export-controlled technical data.

AUTHORITY

USNASC ltr, 15 Oct 1975

THIS PAGE IS UNCLASSIFIED

THIS REPORT HAS BEEN DELIMITED
AND CLEARED FOR PUBLIC RELEASE
UNDER E.O. DIRECTIVE 2850.20 AND
NO RESTRICTIONS ARE IMPOSED UPON
ITS USE AND DISCLOSURE.

DISTRIBUTION STATEMENT A

APPROVED FOR PUBLIC RELEASE;
DISTRIBUTION UNLIMITED.

AD820957

**DEVELOPMENT OF AN EJECTOR PUMP
ENGINE FUEL FEED SYSTEM**

**FINAL REPORT
(6 JUNE 1966 TO 6 JULY 1967)
JULY 1967**

**BY
H. F. WINCHESTER
R. H. VAN DYKE
C. J. MOINAT**

PREPARED UNDER CONTRACT NOW 66-0602-c

**FOR
NAVAL AIR SYSTEMS COMMAND
DEPARTMENT OF THE NAVY**

**BY
DOUGLAS AIRCRAFT COMPANY
AIRCRAFT DIVISION
3855 LAKEWOOD BLVD.
LONG BEACH 1, CALIFORNIA**

**THIS DOCUMENT IS SUBJECT TO
SPECIAL EXPORT CONTROLS AND EACH
TRANSMITTAL TO FOREIGN GOVERNMENTS
OR FOREIGN NATIONALS MAY BE MADE
ONLY WITH THE PRIOR APPROVAL OF
COMMANDER, NAVAL AIR SYSTEMS COMMAND**

ENCLOSURE 1 / 1

ERRATA
DEVELOPMENT OF AN EJECTOR PUMP
ENGINE FUEL FEED SYSTEM

FINAL REPORT
(6 JUNE 1966 TO 6 JULY 1967)
JULY 1967

BY
H. F. WINCHESTER
R. H. VAN DYKE
C. J. MOINAT

PREPARED UNDER CONTRACT NOW 66-0602-c
FOR
NAVAL AIR SYSTEMS COMMAND
DEPARTMENT OF THE NAVY

Page vii - List of Illustrations

1. Figure 90 - Correct text to read "Fluid Acceleration to Right"
Correct page number from "217" to "127"
2. Figure 91 - Correct page number from "217" to "127"

Page 9 - Paragraph 3.2 - Ejector Pump

3. Fourth sentence - Correct to read "This will provide a pump which will not continuously bleed a large volume of motive fuel when not in after-burner operation."

Page 10 - Figure 4 - Ejector Pump Engine Fuel Feed System

4. Top center of page - Correct the word "contrifugal" to "centrifugal"

Page 13 - Under Symbols

5. Correct the second "S" to "S'"

Page 15 - Under Symbols

6. Correct the fifth symbol from " δ " to " γ "

Pages 16 and 17

Correct the symbol " δ " to " γ " in the following places:

7. Equation (1)
8. Equation (2)
9. Equation (3)

Page 21

10. In the bottom paragraph - correct the symbol "s" to "S" in 4 places.

Page 24

11. In equation (7) correct " W_m " to " W_n "

Page 33

12. In the first equation correct " V_{sl} " to " V_{sL} "

Page 36

13. In the third ^{Paragraph}~~sentence~~ from bottom of the page - correct last sentence to read:

"It is probable that the entrainment process is most efficient when d_m nearly equals $d_{S'}$ or is near the S' downstream entrainment point."

Page 37 - Paragraph 4.2.4.1 - Ejector Inlet and Throat Entry Geometry

14. Fifth subparagraph - the first sentence should read:

"Tests were run which varied the nozzle exit to throat spacing, S, ... etc."

Page 37 - Paragraph 4.2.4.2 - Optimum Mixing Tube Length

15. First paragraph - first sentence should read:

"Where nozzle exit to throat spacing, S, ... etc."

Page 40

16. Tenth line from top of page - correct sentence "Figure 17 shows pictorially ... etc." to read "Figure 18 shows pictorially ... etc."

Page 43 - Paragraph 4.2.4.4 - Optimum Motive Nozzle Configuration

17. In the 12th line correct "car" to "care"

Page 45 - Paragraph 4.2.5 - Performance Results

18. In the ninth line from the bottom correct "ration" to ratio"

Page 50 - Paragraph 4.3.1 - The Annular Motive Flow

19. The third line should read: "Section 4.2.3.1 with the exception that d_n becomes the slot width c_n ."

Page 53

20. The second line from the bottom should read, "Thus, the second ph of entrainment and mixing takes place at a lower rate."

Page 55 - Paragraph 4.4 - Altitude and Temperature Effects on Ejector Performance

21. The third sentence should read: "The ejector used for these tests is shown in Figure 15, Configuration 3, except with a nozzle exit to throat spacing $S = 3-11/16$."
22. The second paragraph, first sentence should read: "Pressure altitude of both tanks was changed in accordance with a time schedule as shown in Figure 30."

Page 57

23. In the second paragraph, the second sentence should read: "On the JP-4 tests, when attempting to reduce the pressure on both tanks below that used for ... etc."

Page 61

24. The third equation should be numbered "(15)"
25. Correct the sixth equation to read:

$$(\bar{P}_i - \bar{P}_o)_1 / (\bar{P}_i - \bar{P}_o)_2$$

Page 65

26. The first equation should be corrected to read:

$$(\bar{P}_i - \bar{P}_d)_2 = (\bar{P}_d - \bar{P}_o)_1 - (\bar{P}_d - \bar{P}_o)_2 = \frac{(\bar{P}_d - \bar{P}_o)_1}{(1 + K_1)_2} \left[1 + K_1 - 2b_2 + (1 + K_{34})_2 b_2^2 \right]$$

Page 67

27. In the third paragraph, first line, correct "apparant" to "apparent"

Page 68

28. The bottom equation should read:

$$\frac{W_{n1}}{W_{n2}} = \frac{\phi_2}{1 + \phi_1}$$

Page 70

29. In the second line correct "ration" to "ratio"

30. Second equation should be corrected to read:

$$R_m = \sqrt{b} (1 + \phi) R_n$$

Page 74

31. The fourth line should read "As applied to two stage series ejectors, the main engine pump . . . etc"

Page 80

32. Tenth line from the bottom of page correct the word "stubstantiate" to "substantiate"

33. Third line from the bottom of page correct the word "parrallel" to "parallel"

Page 130

34. Second paragraph, last sentence should read "The test setup is shown schematically in Figure 93."

Page 133

35. In the third sentence correct "recivery" to "recovery"

36. In the third sentence correct "tha" to "the"

Page 135 - Paragraph 6.4 - Summary

37. In the first paragraph, second sentence, delete "a" at the end of the second line.

Page 146 - Paragraph 9.2 - Recommendations

38. In the last paragraph, third line, correct "coducted" to "conducted"

Last page (DD 1473)

39. Under Paragraph 5, Author, correct "R. H. Van Dyne" to "R. H. Van Dyke"

TABLE OF CONTENTS

Section	Page
I INTRODUCTION	1
II DESIGN REQUIREMENTS	3
III DESIGN APPROACH.	9
3.1 FUEL FEED SYSTEM.	9
3.2 EJECTOR PUMP.	9
3.3 FUEL TANK SUMP	9
3.4 FLUIDIC AMPLIFIER.	11
IV EJECTOR PUMP.	13
4.1 DESIGN OBJECTIVES.	13
4.2 THE SIMPLE EJECTOR	13
4.3 THE ANNULAR EJECTOR	50
4.4 ALTITUDE AND TEMPERATURE EFFECTS ON EJECTOR PERFORMANCE.	55
4.5 EJECTOR PUMP COMBINATIONS	59
4.6 LABORATORY TEST SETUP.	76
4.7 SUMMARY	76
V FUEL TANK SUMP	83
5.1 INTRODUCTION	83
5.2 DESIGN AND ANALYSIS	85
5.3 FUEL TANK SUMP TESTS	93
5.4 SUMMARY	128
VI FLUIDIC AMPLIFIER.	129
6.1 INTRODUCTION	129
6.2 DESIGN	129
6.3 TEST RESULTS.	130
6.4 SUMMARY	135
VII EVALUATION OF EXISTING ENGINE FUEL PUMPS	137
7.1 INTRODUCTION	137
7.2 J79 ENGINE	137
7.3 TF 30 ENGINE	139
7.4 SUMMARY	140
VIII QUANTITATIVE TRADEOFF ANALYSIS	143
IX CONCLUSIONS AND RECOMMENDATIONS.	145
9.1 CONCLUSIONS	145
9.2 RECOMMENDATIONS	146

TABLE OF CONTENTS (Continued)

Section	Page
X REFERENCES.....	147

LIST OF ILLUSTRATIONS

Figure		Page
1.	Fuel Flow Rates for Various Altitudes	3
2.	Fuel Line Pressure Loss	4
3.	Engine Fuel Flow Requirements	6
4.	Ejector Pump Engine Fuel Feed System.	10
5.	Simple Ejector Configuration	14
6.	Typical Ejector Performance.	18
7.	Ejector Pump Performance Curves.	19
8.	Nozzle Calibration	22
9.	Throat Entrance Loss.	23
10.	Combined Friction and Bend Loss Coefficient vs Reynolds Number for Smooth Pipe Flow	25
11.	Viscosity vs Temperature of Jet Fuels	27
12.	Total-Pressure-Loss Coefficient Factor K_4 for Straight- Wall Conical Diffusers	28
13.	Pictorial Presentation of the First Vortices Forming in the Contact Surface Between Two Fluids Flowing at Different Velocities	29
14.	Motive Nozzle Fluid Plume Model	30
15.	Throat Entry Configurations	38
16.	Pump Performance for Configurations 1, 2, & 3	39
17.	Nozzle and Mixing Tube Section of Ejector Pump Test Model	40
18.	Mixing Tube Configurations	41
19.	Mixing Tube Performance	42
20.	Motive Nozzle Configurations.	44
21.	Ejector Pump Test Configurations	46
22.	Ejector Performance	47
23.	Ejector Performance	48
24.	Ejector Performance	49
25.	Annular Nozzle Pump Configurations.	51
26.	Annular Ejector Performance of Configuration Number Four.	52
27.	Center Line Velocity ($V_s = 0$)	53
28.	Comparative Performance Annular Ejector with Blunt Nozzle Exit and with Sharp Nozzle Exit	54
29.	Climb Test Performance.	56
30.	Altitude Climb Schedule	57

LIST OF ILLUSTRATIONS (Continued)

Figure		Page
31.	Annular Ejector Altitude Performance	58
32.	Series Induced Flow Ejector	60
33.	Operating Curves for Series Induced Pump.	63
34.	Test Curves for Series Induced Pump	64
35.	Series - Parallel Staged Ejector.	72
36.	Series - Parallel Ejector Performance Sea Level Operation	73
37.	Dual Nozzle Simple Ejector Pump.	75
38.	Ejector Pump Test Setup.	77
39.	Ejector Pump Test Facility - General View	78
40.	Ejector Pump Test Facility - Motive Nozzle Supply Pumps . .	78
41.	Pump Section	79
42.	Ejector Nozzle and Mixing Inlet Area	79
43.	Tangential Velocity Required at Periphery to Develop Various Levels of Acceleration	86
44.	Skin Friction Drag Coefficient for a Smooth Flat Plate Parallel to Flow	87
45.	Dimensionless Moment Coefficient for Rotating Disk	89
46.	Total Drag Coefficient for a Cylinder	91
47.	Flexible Pickup	92
48.	Swirl Test System Schematic	93
49.	Swirl Test Setup	94
50.	Swirl Test Tank	94
51.	Variation in Pitot Reading with Angle of Incidence	96
52.	Swirl Velocity vs Distance from Center of Tank	97
53.	Comparison of Calculated Versus Observed Drag	98
54.	Drag Correction Factor	99
55.	Effect of Outlet Location on Velocity Head	100
56.	Velocity Head vs Time for Swirl Initiation	101
57.	Velocity Head vs Time for Frictional Slowdown.	102
58.	Velocity Head vs Time for Frictional Slowdown.	103
59.	Estimated Performance with Sustaining Flow During Slowdown	104
60.	Tank Sump System Schematic.	105

LIST OF ILLUSTRATIONS (Continued)

Figure		Page
61.	Sump Tank Setup	106
62.	View Looking Down into Sump Tank Showing Adjustable Baffles and Center Body	107
63.	Typical Velocity Head vs Distance from Center.	108
64.	Comparison of Velocity Head vs Sump Corner Radius.	109
65.	Schematic - Zero-G Flight Test of Swirl Tank.	111
66.	Flight Test System - Ground Checkout.	112
67.	End of Test Box with Control Switches.	112
68.	Inside View of Test Box	113
69.	Swirl Test Tank Mounted in Test Box	114
70.	Auxiliary Tank Mounted in Baggage Compartment	115
71.	Swirl Jet "On".	117
72.	Tank Pump Down.	117
73.	Sight Glass Cavitation.	118
74.	Pump Pressure Decay	118
75.	Pullout Prior to Weightlessness	119
76.	Initial Migration of Fluid.	119
77.	Continued Migration of Fluid	120
78.	Continued Migration of Fluid	120
79.	Fuel Pickup Unported.	121
80.	Air in Sight Glass	121
81.	Initial Zero Gravity	122
82.	Swirl Jet On	122
83.	Swirl Jet On	123
84.	Sight Glass Indicates Air.	123
85.	Cavitation of Pump.	124
86.	Pullout of Dive	125
87.	Bubble Forming at Top of Tank	125
88.	Bubble Migrates Down	126
89.	Coherent Vertical Bubble	126
90.	Fluid Acceleration the Right	217
91.	Fluid Acceleration to Left.	217
92.	Fluidic Amplifier.	129

LIST OF ILLUSTRATIONS (Continued)

Figure		Page
93.	Schematic of Test Setup for Fluidic Amplifier.	130
94.	Fluidic Amplifier Performance	131
95.	Fluidic Amplifier Performance	132
96.	Fluidic Amplifier Performance	133
97.	Fluidic Amplifier Performance	134
98.	Fluidic Amplifier Performance	134
99.	Fluidic Amplifier Performance	135
100.	J79 Main Engine Fuel Pump Flow at Sea Level	138
101.	J79 Afterburner Fuel Pump Performance.	139
102.	TF30 Main Engine Pump Performance - Sea Level	141
103.	TF-30 Afterburner Pump Performance	142

SECTION I

INTRODUCTION

The Naval Air Systems Command, Department of the Navy, has established a long range goal of providing aircraft fuel systems with as few moving parts as possible. As a result, a Research and Development contract NOW 66-0602-c was awarded to the Douglas Aircraft Company to develop and test an Ejector Pump Engine Fuel Feed System to supply fuel to the engine at a rate up to 70,000 pounds per hour, at altitudes up to 60,000 feet and under various gravity conditions as specified in the contract.

An ejector pump is a device by which a fluid stream may be pumped by the action of a high velocity jet of a second fluid stream. The pumping action is a result of a transfer of momentum from the jet fluid to the fluid being pumped. The use of ejector pumps in the past has been limited to transfer applications and relatively low flow rates and pressures. It is expected that the next application of ejector pumps will be to replace the aircraft booster pump in aircraft such as the F-4, A-5 or the F-111. Requirements may consist of large fuel flows, two stage fuel flow for main engine and afterburner operation or high fuel temperatures of approximately +200°F. Sufficient research has been done to design a system to satisfy these conditions.

Negative and zero gravity conditions require special methods for maintaining a continuous supply of fuel at the inlet to the fuel boost pump. This program has studied a means of introducing an artificial gravity force to maintain the fuel at the wall of the tank for pickup to supply the pump.

SECTION II

DESIGN REQUIREMENTS

The contract specifies that an ejector pump engine fuel feed system shall be developed for a single tank with dual engine feed provisions.

The system shall be capable of supplying fuel to both engines under the following conditions:

- Fuel flow rates as shown in Figure 1.

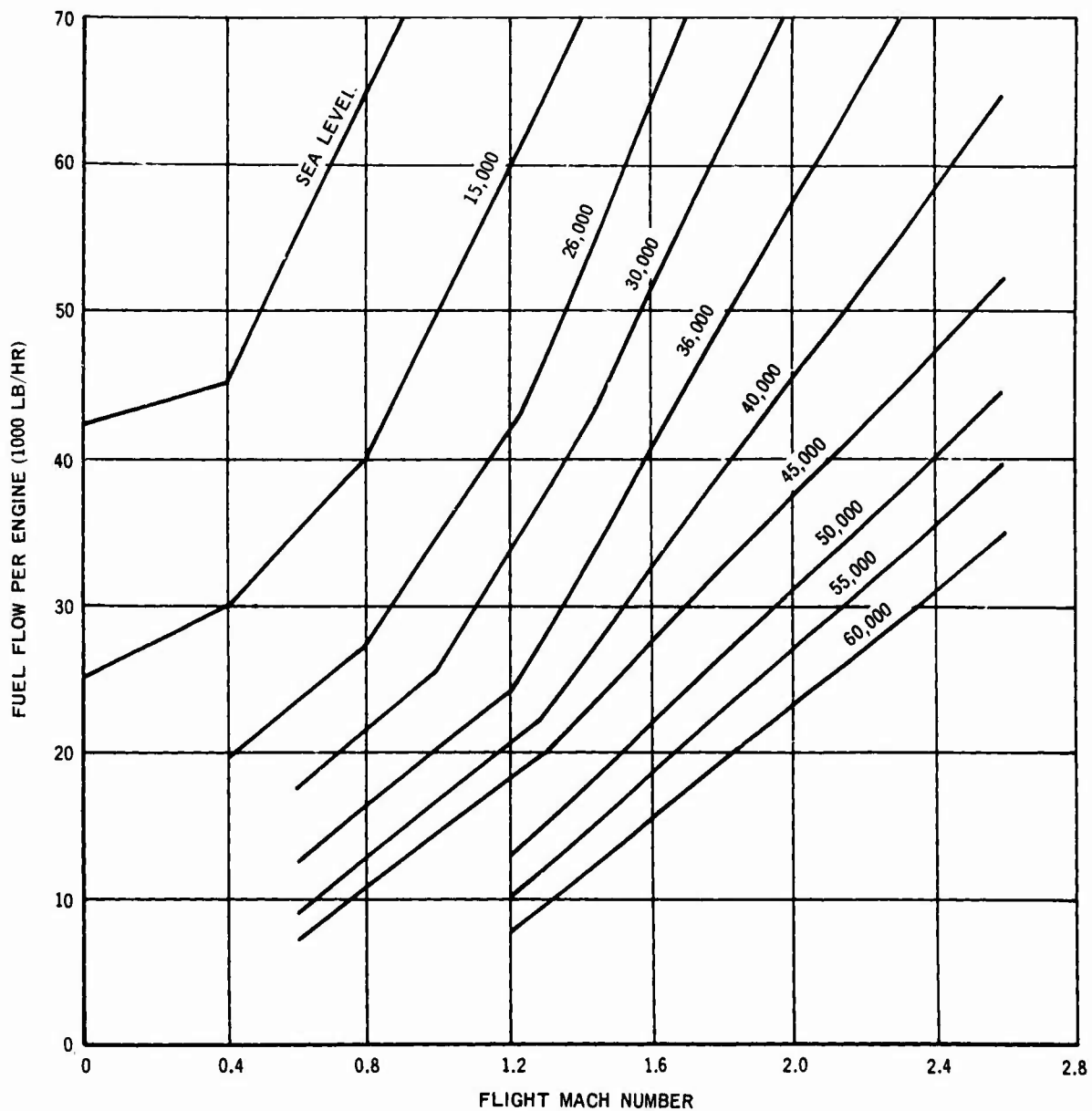


FIGURE 1. FUEL FLOW RATES FOR VARIOUS ALTITUDES

- Maximum allowable pressure drop through the fuel feed line as shown in Figure 2.

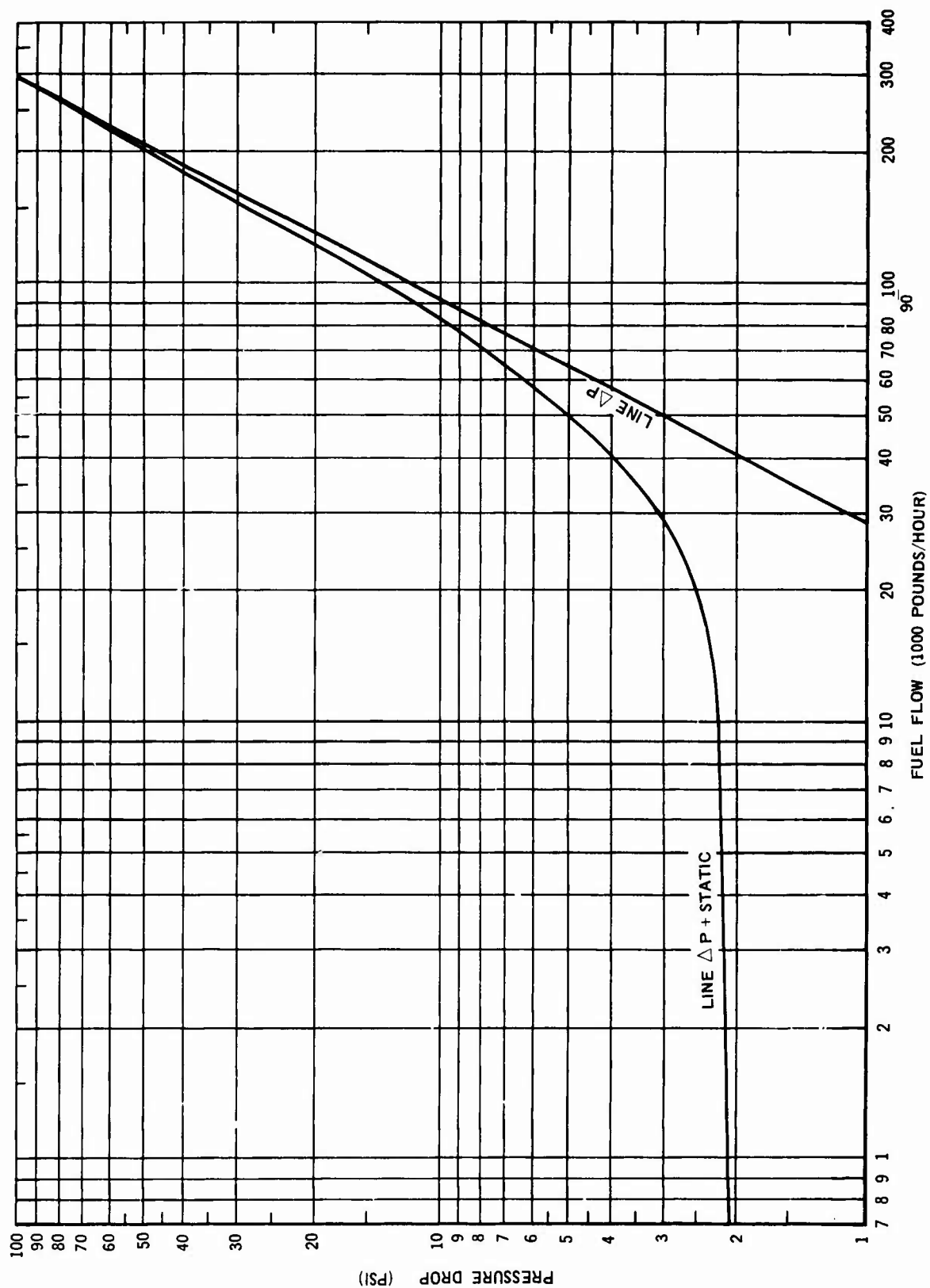


FIGURE 2. FUEL LINE PRESSURE LOSS

- Fuel temperatures from a maximum of +200°F down to -65°F, or to a temperature corresponding to a fuel viscosity of 12 centistokes.
- Fuel at the inlet of the engine driven pumps at pressures between 30 psi (relative to atmosphere) and 5 psi plus true vapor pressure of the fuel and vapor-liquid ratios of not more than 0.45.
- All normal flight attitudes.
- Altitudes from sea level to 60,000 feet.
- Flight operations under negative 1g for 60 seconds.
- Flight operations under zero g for 30 seconds.
- A horizontal loading during catapult of 7g's minimum to 8g's maximum. A horizontal loading during arrested landing of 4g's minimum to 5g's maximum.

The following ground rules were established at the beginning of the program with regard to fuel flow and fuel temperature:

- The fuel flow as shown in Figure 1 was made up of two components, main engine fuel flow and afterburner fuel flow. The proportional division is shown in Figure 3.
- A single ejector pump must provide two engine fuel flow for maximum main engine power, but need supply fuel flow for operating with only one engine afterburner.
- The fuel temperature in the tank will be a maximum of +135°F and heat inputs between the ejector pump and the engine inlet will raise the fuel temperature at the engine inlet to +200°F.
- In order to meet the requirements of MIL-F-17874 for a maximum evaporation of two percent of the fuel, the tank must be pressurized to maintain a minimum of 5 psia.

Based on the above requirements and assumptions, the pump performance as shown in Table I is required.

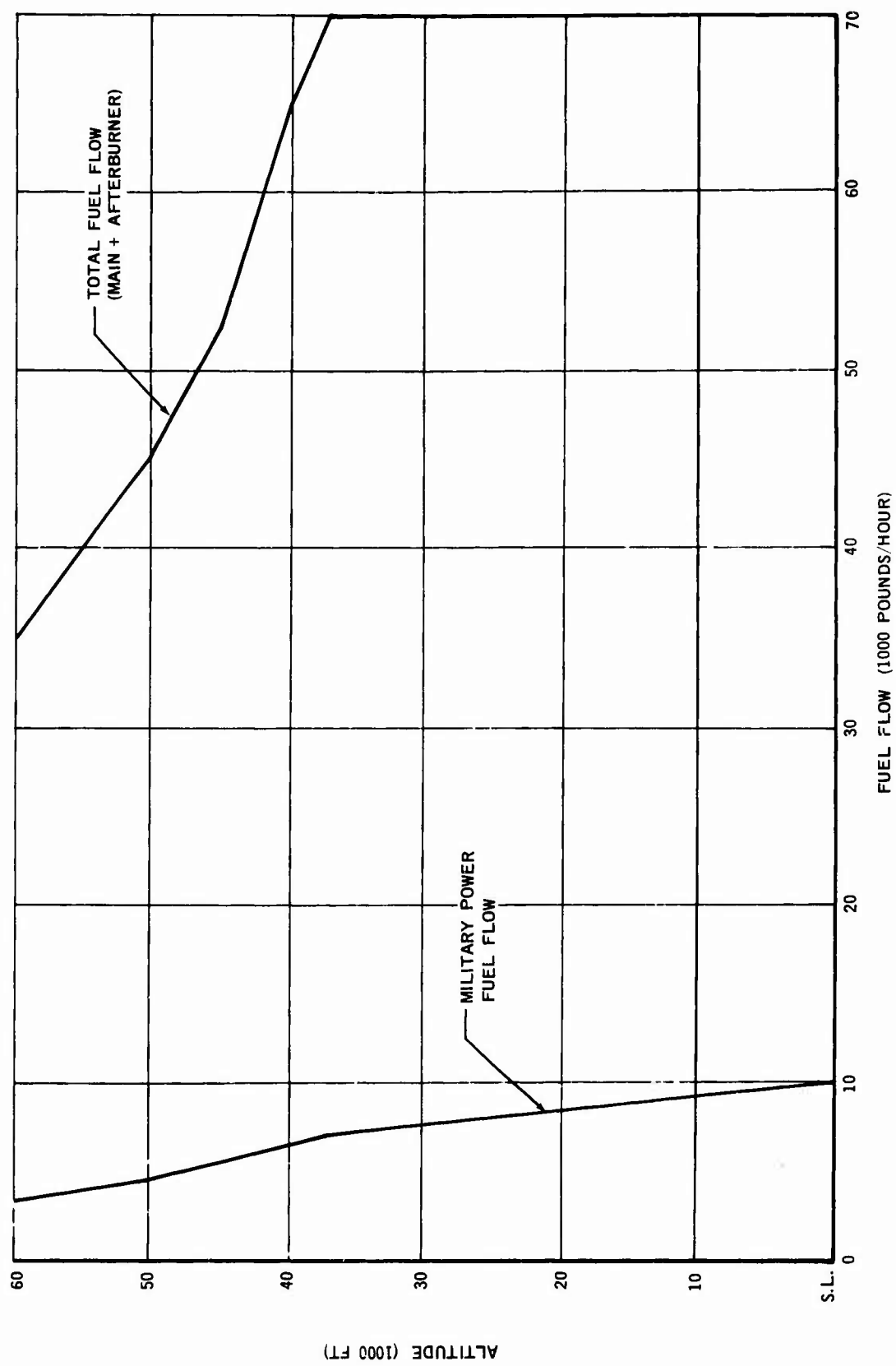


FIGURE 3. ENGINE FUEL FLOW REQUIREMENTS

TABLE I
EJECTOR PUMP DISCHARGE PRESSURE REQUIREMENTS (MINIMUM)

2 Engine Military Power	
Sea Level	- 21 psia (1 psig) @ 20,000 P. P. H.
37,000 feet	- 21 psia (13 psig) @ 14,000 P. P. H.
60,000 feet	- 21 psia (15 psig) @ 7,000 P. P. H.
Afterburner Power	
Sea Level	- 34 psia (14 psig) @ 70,000 P. P. H.
37,000 feet	- 34 psia (26 psig) @ 70,000 P. P. H.
60,000 feet	- 26 psia (20 psig) @ 35,000 P. P. H.

SECTION III

DESIGN APPROACH

3.1 FUEL FEED SYSTEM

To meet the design requirements, a system as shown in Figure 4, was designed and developed to make use of the following basic components:

- Two-stage ejector fuel pump where one stage operates for main engine operation and an additional stage is activated when the afterburner flow is required.
- A fluidic proportional amplifier which would sense ejector pump discharge pressure and divert sufficient motive fluid to reduce the ejector pump operating performance.
- A flexible fuel inlet which will stay at the bottom of the tank sump during normal flight and move upward to the top of the sump for negative g conditions.
- A swirl jet which will induce fluid rotation in the sump area of the main fuel tank and, by centrifugal force, keep fuel at the wall of the sump during zero g conditions.

3.2 EJECTOR PUMP

The ejector pump is powered by motive fuel which is bled from the discharge of the high pressure stage of the engine fuel pump. The primary stage nozzle will take fuel from the main engine fuel pump at all times. The secondary stage nozzle will take fuel from the afterburner fuel pump only when the afterburner system is actuated. This will provide a pump which will not continuously bleed a large volume of motive fuel when not in the afterburner. The primary stage delivers a sufficient amount of fuel, at the required pressure, to supply two engine flow requirements. See Section IV for analysis and development testing.

3.3 FUEL TANK SUMP

3.3.1 Flexible Pickup

The flexible pickup consists of a flexible hose mounted approximately mid-height in the sump so that the loose end can move up or down. On the end of the hose, there is a pickup which is heavy enough to keep the hose deflected down and shaped to allow the swirling fuel to produce a slight side force to keep the pickup against the tank wall. As the airplane enters a negative g condition, the weighted pickup will move to the top of the sump and continue to pick up the fuel. See Section V for details on design and testing of the flexible pickup.

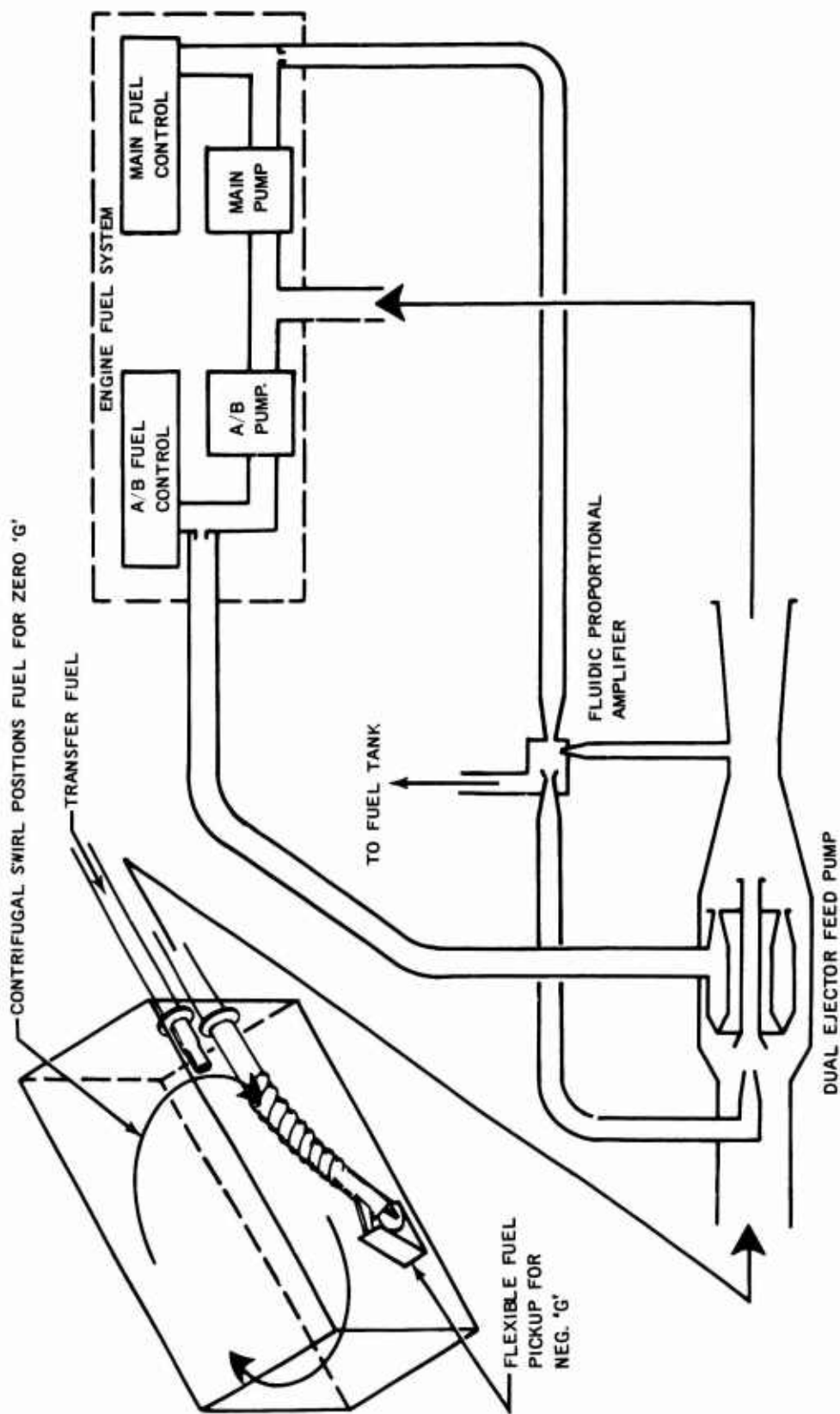


FIGURE 4. EJECTOR PUMP ENGINE FUEL FEED SYSTEM

3.3.2 Swirl Jet

For zero g flight condition the fuel could be located anywhere in the sump and may not be replaced from the main portion of the tank as fuel is removed for engine consumption. The design concept used was to purposely place the fuel at the tank wall where it could be picked up. This is done by introducing a jet of fuel along the wall of the sump and creating a fuel rotation which by centrifugal force keeps the fuel at the tank wall where the fuel pickup is located. The intertank transfer fuel could be supplied to the main tank in a manner to provide the fuel for the swirl jet. If under zero g conditions the intertank transfer stops, then there must be an additional means of providing a sustaining swirl jet. The sustaining jet need not be as large as the jet required to start the swirl. See Section V for details on swirl analysis and testing.

3.4 FLUIDIC AMPLIFIER

The fluidic proportional amplifier is a momentum exchange device located in the primary stage motive fluid line. The main flow enters the amplifier, exits through a nozzle, traverses a gap, and is caught by a receiver tube where the flow then continues on to the ejector pump. As the discharge pressure of the ejector pump increases, a control flow will be fed back to the amplifier. This control flow is introduced normal to the main flow. The higher the ejector pressure the more the flow in the amplifier is deflected, thus tending to reduce the flow available for the nozzle usage in the ejector pump. The flow which is diverted will be returned to the aircraft fuel tank. See Section VI for analysis and testing of the fluid amplifier.

SECTION IV

EJECTOR PUMP

4.1 DESIGN OBJECTIVES

The objectives of this investigation were; (a) to determine those parameters which best describe the operation of the ejector type pumps, (b) to examine and test various ejector configurations and their adaptation to fuel feed systems, and (c) to derive methods for rapid solution of ejector fuel feed system sizing problems.

4.2 THE SIMPLE EJECTOR

4.2.1 General Description

An ejector, also called jet pump, eductor, or injector, is a device which uses the energy of one fluid stream to pump or entrain another fluid stream. The two streams may be of the same type of fluid, as in the water-well jet pump, or different fluids as in steam ejectors used to pump air.

Ejectors are of interest in pump engineering primarily because of their mechanical simplicity. Having no moving parts other than the two fluid streams themselves, wear, vibration and other mechanisms of mechanical failure are reduced to a minimum. This enhancement of reliability has led to much interest in the use of ejectors for aircraft systems.

Figure 5 shows schematically the arrangement of the simple ejector. A nozzle directs the motive fluid stream into the area occupied by the pumped or secondary fluid. The secondary fluid is entrained within the region between the motive nozzle exit and the end of the mixing tube. The mixed fluids are then discharged, usually through a diffuser, into a receiver tank or feed line.

The following discussion will be limited to the case of pumping where both motive and secondary fluids have the same physical properties are the same temperature and are incompressible. The nomenclature used is as follows and is taken mainly from Reference 1, as are most of the equations used.

Symbols

A	cross sectional area - in. ²
d	diameter - inches
g	gravitational constant - 32.2 ft/sec ²
L	mixing tube length - inches
P	static pressure - Lb/in. ²
\bar{P}	total pressure - Lb/in. ²
S	nozzle to throat spacing - inches
S	length of high velocity core - inches
T	temperature

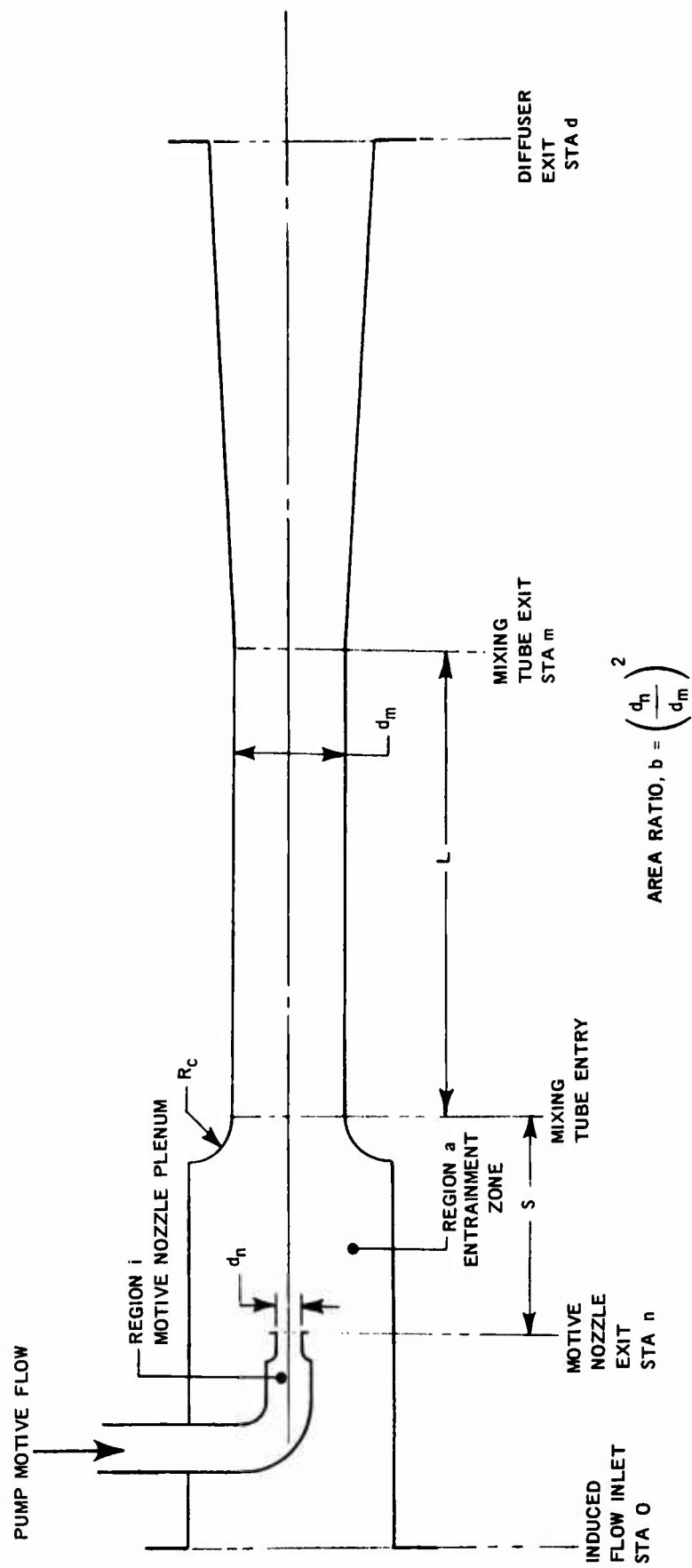


FIGURE 5. SIMPLE EJECTOR CONFIGURATION

Symbols (Continued)

V	velocity - Ft/sec
W	weight flow rate - Lb/hr
Y	cavitation function - Lb/in. ²
μ	fluid viscosity - Lb/ft-hr
δ	fluid density - Lb/ft ³

Subscripts

1	Stage 1
2	Stage 2
a	throat entry
d	discharge, diffuser exit
i	nozzle entry
L	limiting
m	throat section
mep	maximum efficiency point
n	nozzle or motive fluid
o	inlet entry, secondary fluid
s	secondary fluid

Dimensionless Ratios

b	nozzle to throat area ratio = $\frac{A_n}{A_m}$
f	friction factor = Kd/L
N	pressure ratio = $\frac{\bar{P}_d - \bar{P}_o}{\bar{P}_i - \bar{P}_d}$
R	Reynolds number = $\frac{Vd}{\mu}$
η	efficiency = ϕN
λ	velocity ratio = $\frac{V_s}{V_n}$
ϕ	flow ratio = $\frac{W_s}{W_n}$

Friction
Loss Coefficients

K_e	expansion loss
K_1	nozzle
K_2	throat - entry
K_3	mixing tube wall friction
K_4	diffuser
K_{34}	mixing tube - diffuser, $K_3 + K_4$

The motive nozzle pressure drop is

$$\bar{P}_i - \bar{P}_o = \frac{1.11 \times 10^{-5} W_n^2}{2g \delta A_n^2} (1 + K_1) \quad (1)$$

where

$$1.11 \times 10^{-5}$$

is a conversion factor permitting calculation using dimensional units as described in the nomenclature, $(144 \text{ in.}^2/\text{ft}^2 \div 3600^2 \text{ sec}^2/\text{hr}^2)$

The output pressure rise of the ejector is,

$$\bar{P}_d - \bar{P}_o = \frac{1.11 \times 10^{-5} W_n^2}{2g \delta A_n^2} \left[2b + \frac{2\phi^2 b^2}{1-b} - \frac{(1 + K_{34}) b^2 (1 + \phi)^2 - (1 + K_2) \frac{\phi^2 b^2}{(1-b)^2}}{(1-b)^2} \right] \quad (2)$$

The overall pressure drop, motive nozzle entry to ejector discharge is,

$$\bar{P}_i - \bar{P}_d = \frac{1.11 \times 10^{-5} W_n^2}{2g \delta A_n^2} \left[1 + K_1 - 2b - \frac{2\phi^2 b^2}{1-b} + \right. \\ \left. (1 + K_{34}) b^2 (1 + \phi)^2 + (1 + K_2) \frac{\phi^2 b^2}{(1-b)^2} \right] \quad (3)$$

Ejector efficiency is defined as the ratio of energy output to energy input

$$\eta = \frac{W_s}{W_n} \cdot \frac{\bar{P}_d - \bar{P}_o}{\bar{P}_i - \bar{P}_d} = \phi N \quad (4)$$

Figure 6 shows typical ejector pump-down curves for two different nozzle pressures. As the ejector discharge pressure is increased, as by closing a downstream throttling valve, the quantity of induced fluid pumped decreases. The pump-down curve for an ejector is similar to that of a centrifugal pump. Also shown in Figure 6 is the efficiency curve of the ejector. For a given ejector geometry there is a discrete operating point which gives best operating efficiency. This point is usually designated as the maximum efficiency point or mep.

In Figure 7, the pressure difference ratio versus flow ratio is plotted for ejectors with area ratios of 0.05, 0.10, 0.15, 0.20 and 0.30. The presentation of pressure difference ratio versus flow ratio has been used for some time as a method for estimation of ejector performance. The semi-logrithmic plot used in Figure 7 was selected to show more clearly the N versus ϕ relationships for small values of N . The dependency of ejector flow ratio on the pressure difference ratio can clearly be seen. For any given area ratio and nozzle pressure increasing pump, discharge pressure reduces flow ratio. Flow ratio is at a maximum where $P_d = 0$. Conversely, for each ejector size (area ratio) there is a maximum pressure difference ratio available which is indicated at the $\phi = 0 (W_s = 0)$ point. Throttling the flow beyond this point results in expelling motive fluid from the inlet port of the ejector. Ejectors with high area ratios have a greater potential discharge pressure than those with low area ratios. However, low area ratio ejectors have a greater flow ratio potential than high area ratio ejectors.

4.2.2 The Flow Losses in the Ejector

The prediction of the flow loss coefficients is of importance to the estimation of ejector performance. These losses are dependent upon the shape of the ejector passages, i.e., contour of motive nozzle inlet, contour of throat entry and discharge diffuser, length of mixing tube, and nozzle to throat spacing.

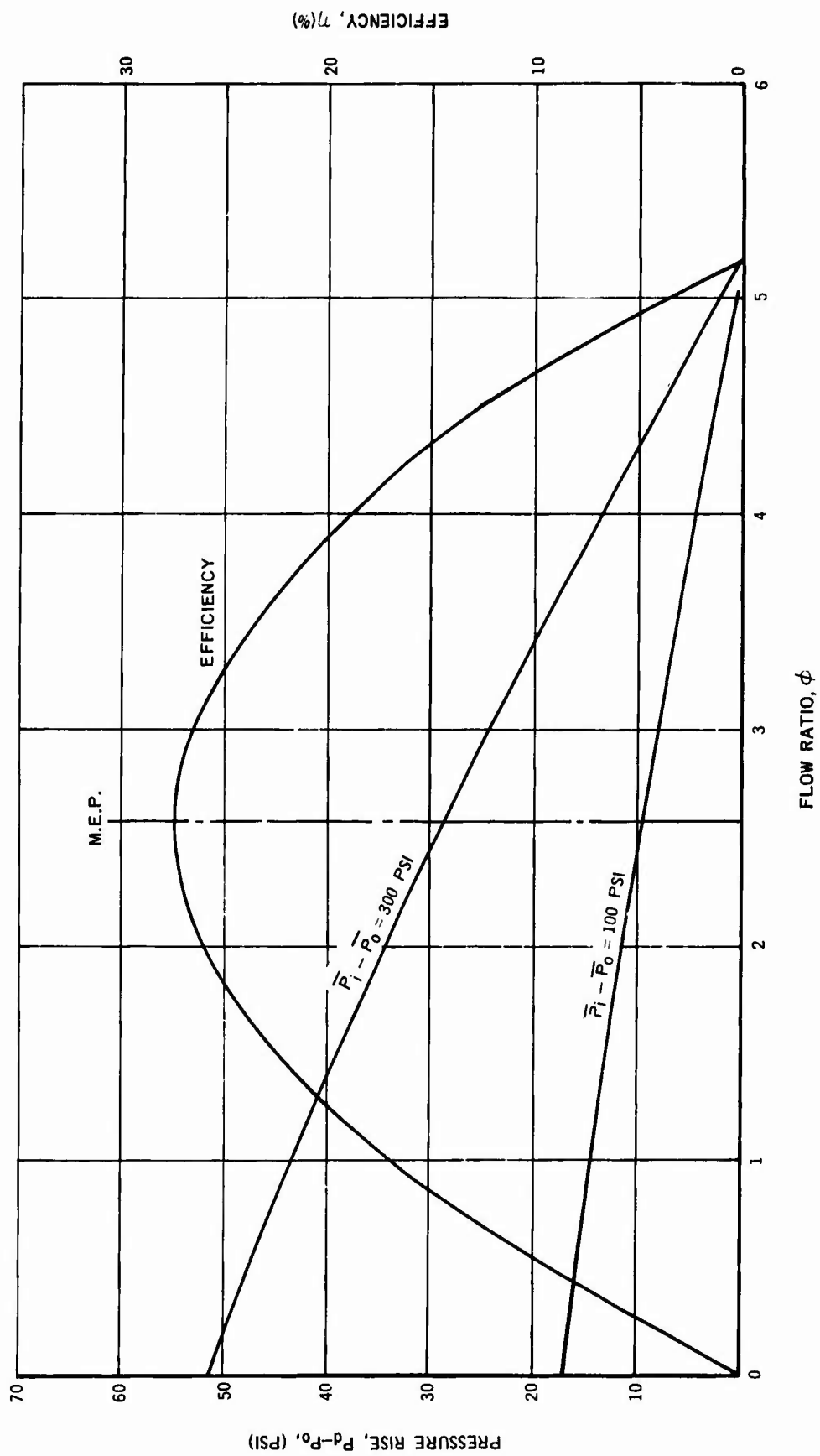
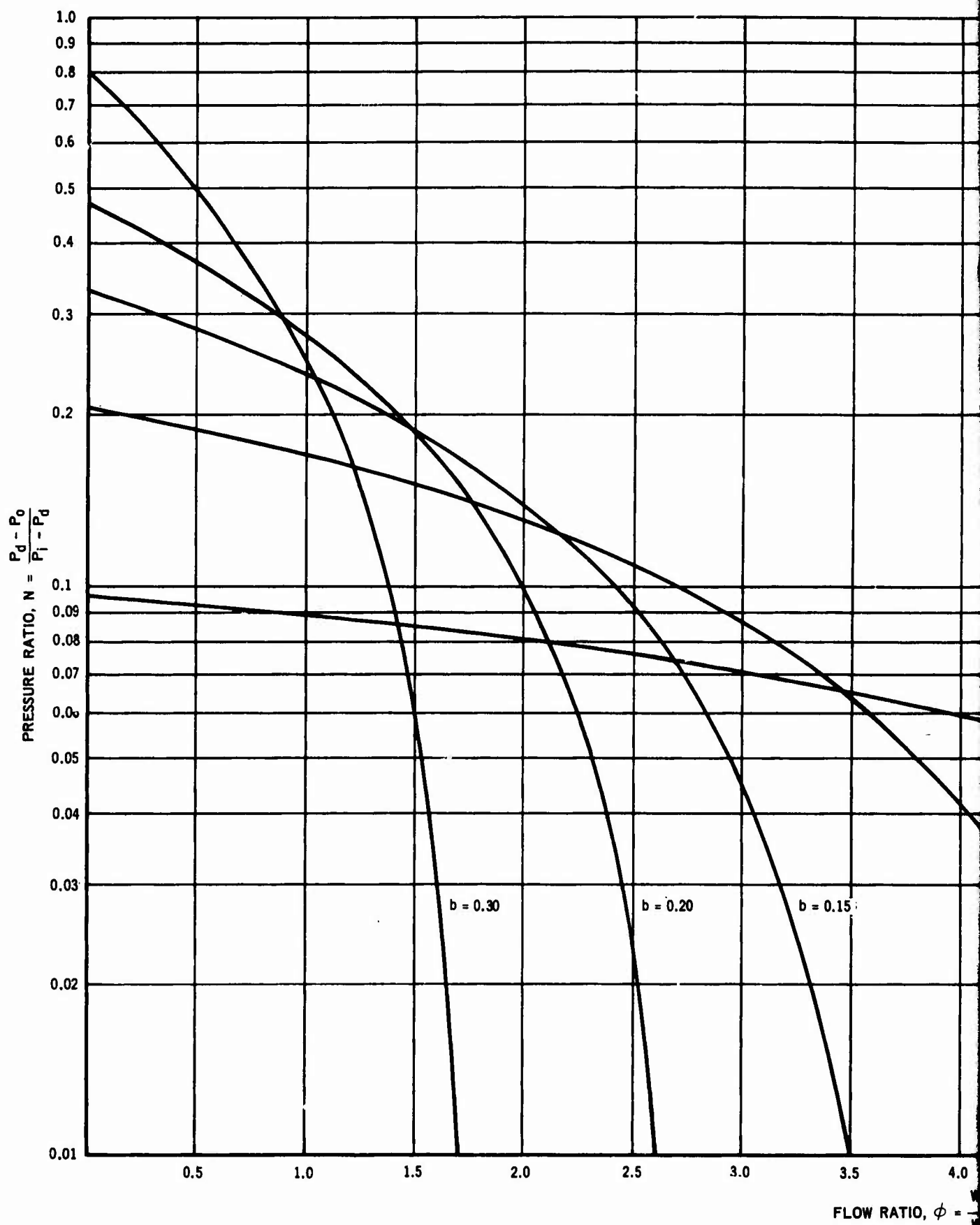
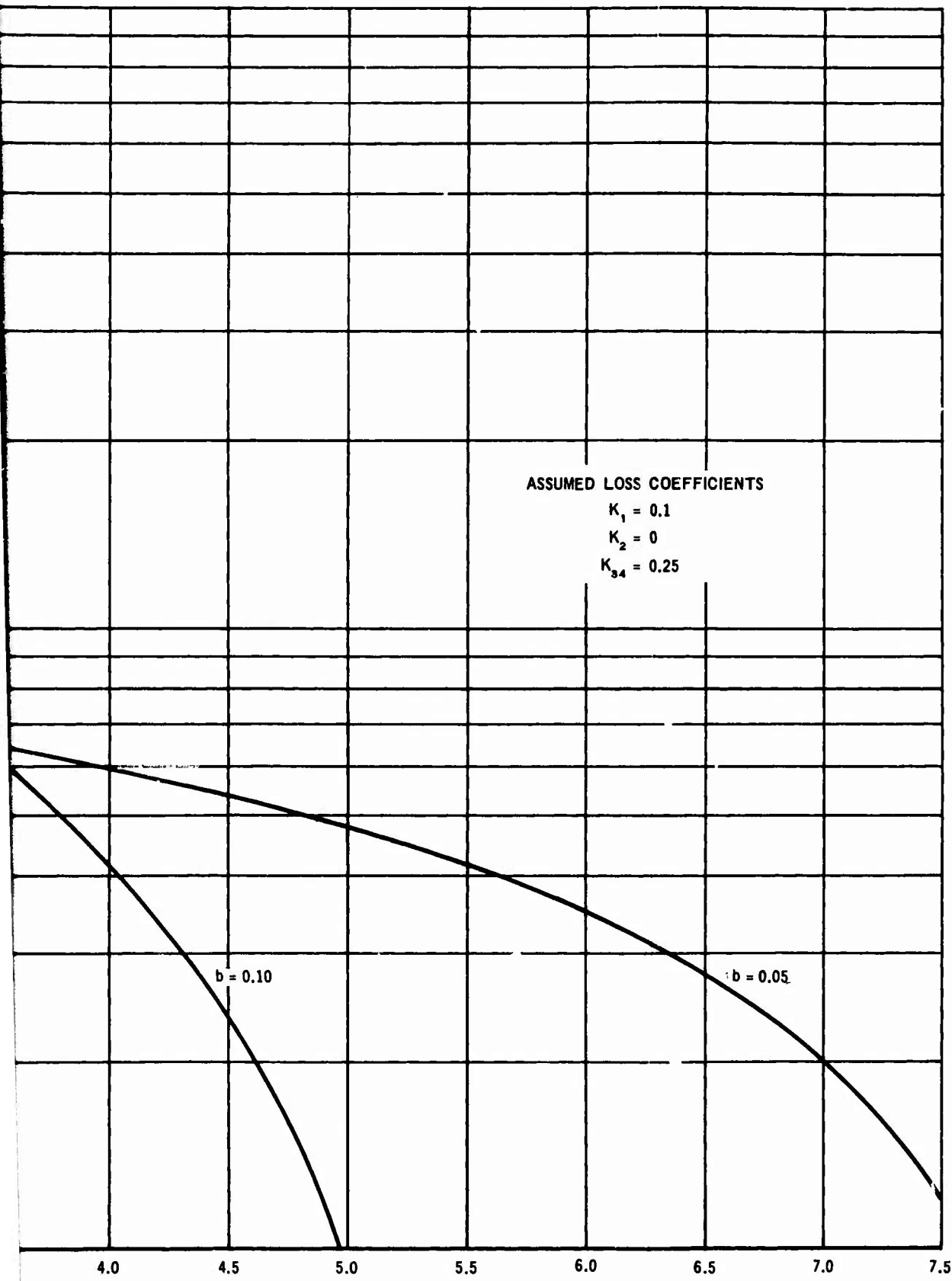


FIGURE 6. TYPICAL EJECTOR PERFORMANCE





RATIO, $\phi = \frac{W_s}{W_n}$

FIGURE 7. EJECTOR PUMP PERFORMANCE CURVES

2

4.2.2.1 The Motive Nozzle Loss Coefficient

K_1 , the motive nozzle loss coefficient can be derived by tests of the contemplated nozzle configuration or can be estimated by reference to literature. Cunningham (Reference 1) suggests a value of $K_1 = 0.10$ for Reynolds numbers of about 20,000 and greater. This value appears to be reasonable as compared with testing accomplished under this contract, although somewhat conservative at high Reynolds numbers (100,000 and above). Accurate determination of the loss coefficient can be obtained by testing the contemplated nozzle design, at various flow rates and nozzle pressures, and calculating the nozzle discharge coefficient. The loss coefficient can then be determined by the equation,

$$K_1 = \frac{1}{(\text{Discharge Coefficient})^2} - 1 \quad (5)$$

or the loss coefficient may be calculated directly by use of equation (1). The relationship of discharge coefficient, sometimes denoted as C_D , to K_1 is given here because it is sometimes of interest to compare C_D with values obtained from other literature sources.

Figure 8 shows the flow versus nozzle pressure drop for the initial test ejector nozzles used in this study. A comparison curve for an equivalent nozzle having a loss coefficient of $K_1 = 0$ is also shown with each nozzle test curve. The annular nozzle performance is comparable to that of a simple nozzle. More discussion of nozzle geometry and performance will be presented in the section on ejector geometry.

4.2.2.2 The Throat Entry Loss Coefficient

K_2 , the throat entry loss coefficient, is usually small, especially for the case where the motive nozzle exit is withdrawn some distance from the throat entry itself. The curves shown in Figure 9 give good values for entry loss, using radius type entries. Due to manufacturing complexity, it is probably more desirable to use a conical entry. Cunningham (Reference 1) recommends use of a 120° angle conical entry with slightly rounded throat entry. Hansen, (Reference 2) in his work, used 26-55 degree conical entries. Hansen achieved a very high ejector efficiency, 42 percent maximum, with an ejector having an area ratio of 0.295 using a 40° conical throat entry. Cunningham was never able to directly measure K_2 and therefore assumed that $K_2 = 0$, in his theoretical performance calculations.

It appears that for ejector configurations using a very small s spacing, in some cases $s = 0$, that throat entry configuration and external motive nozzle shape play an important role in ejector performance. Flugel (Reference 3) evaluated different throat entry shapes with small s spacing as did Keenan, Neumann, and Lustwerk (Reference 4). Both studies show the importance of throat shaping on ejector performance using small s spacing. Throat entry geometry will be discussed further in the section on cavitation characteristics of ejectors.

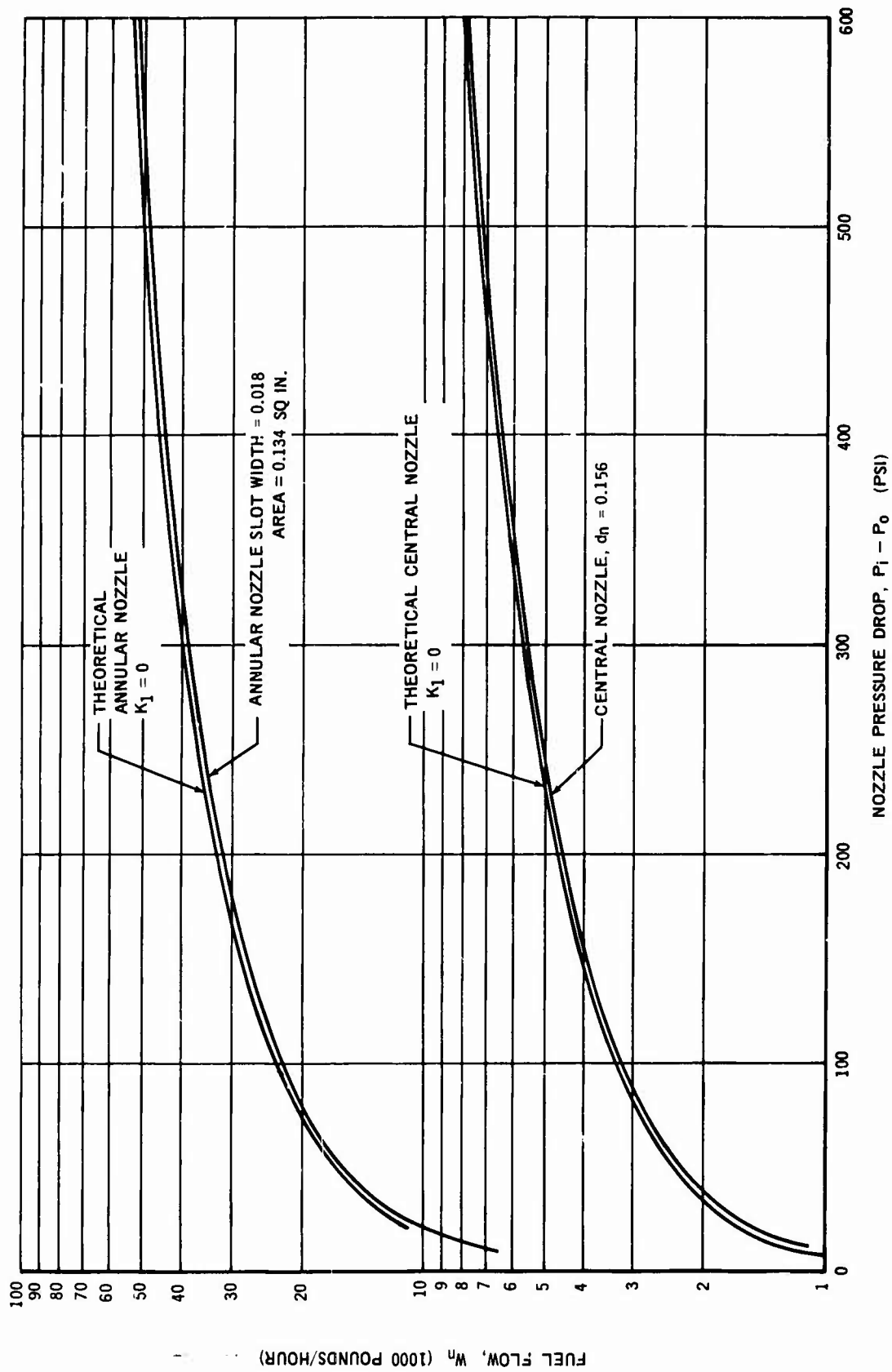


FIGURE 8. NOZZLE CALIBRATION

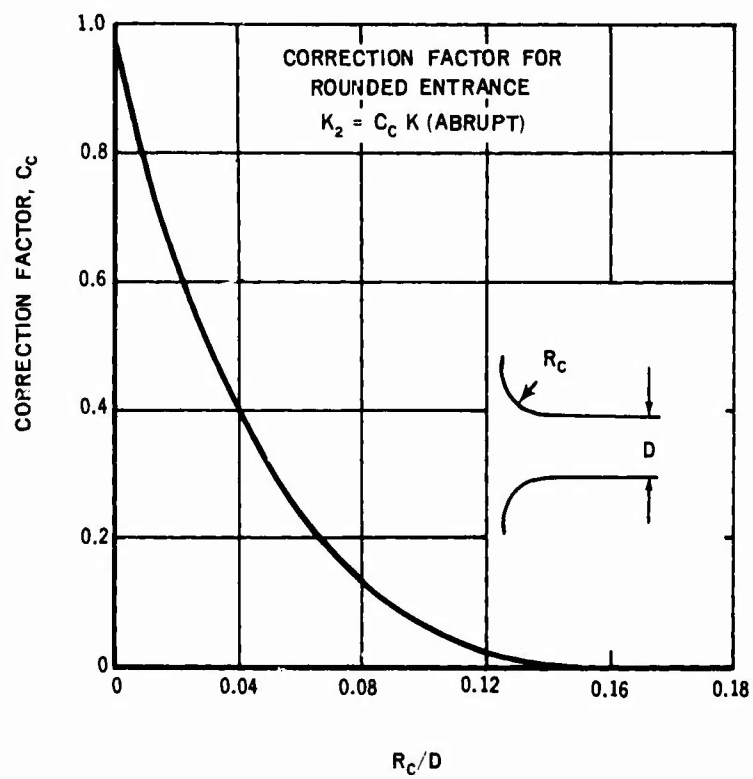
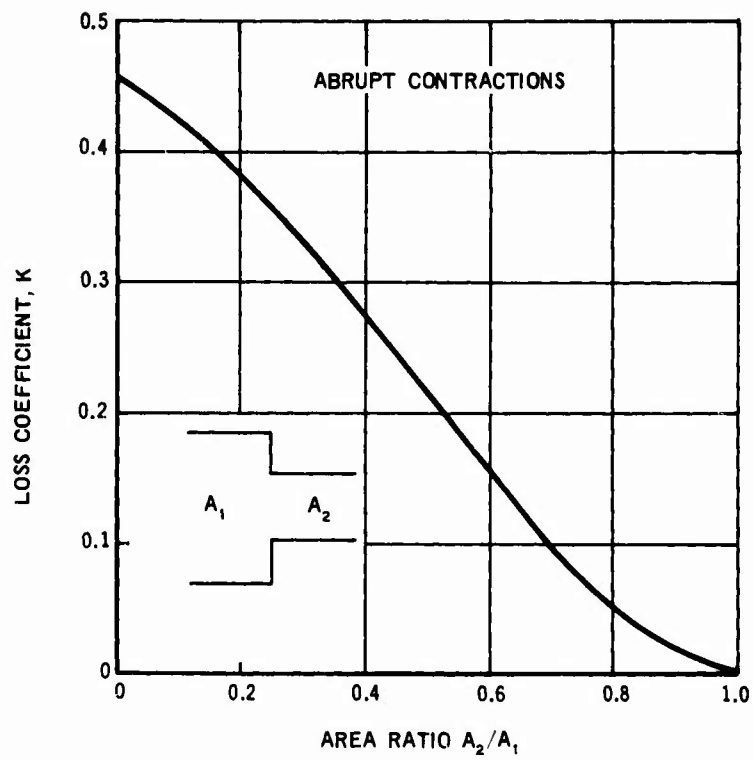


FIGURE 9. THROAT ENTRANCE LOSS

4.2.2.3 The Mixing Tube Loss Coefficient

K_3 , the mixing tube loss coefficient, can be estimated by the equation:

$$K_3 = f \frac{L}{d} \quad (6)$$

Where f is the friction factor, L is the constant section mixing tube length and d is the throat diameter. For convenience of the reader in determining K_3 ,

Figure 10 gives the relationship of friction factor and Reynolds number for flow in smooth tubing. Reynolds number may be calculated from.

$$R = \frac{48 (W_s + W_m)}{\pi d_m \mu} = \frac{48 W_n (1 + \phi)}{\pi d_m \mu} \quad (7)$$

A curve of viscosity versus temperature for JP-3, JP-4, and JP-5 fuels is presented in Figure 11.

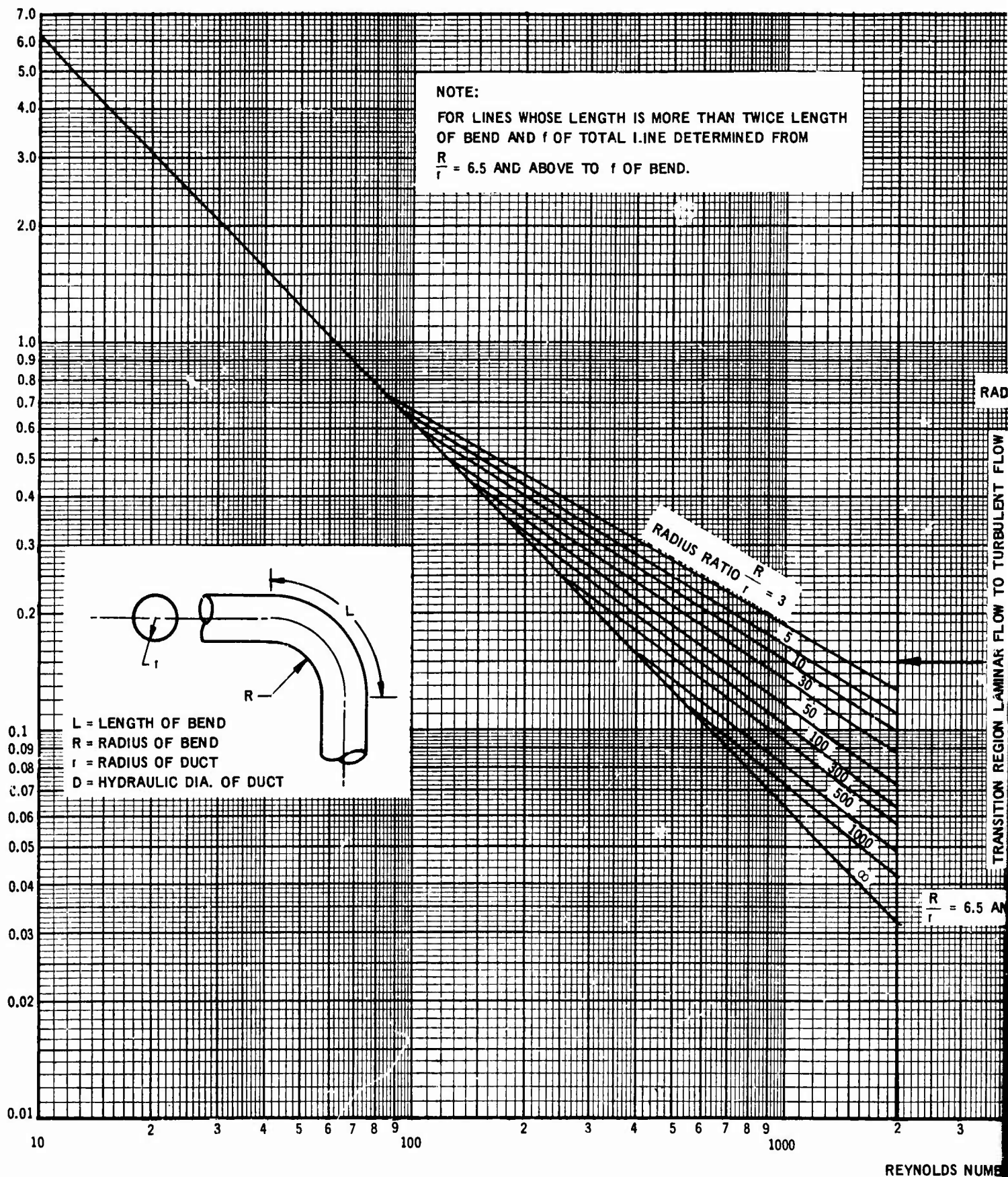
4.2.2.4 The Diffuser Loss Coefficient

K_4 , the diffuser loss coefficient may be determined from Figure 12 knowing the diffuser half angle and area ratio. From this figure note that diffuser loss is at a minimum for a diffuser cone half angle of 3° .

K_3 and K_4 are combined in equations (2) and (3). The resultant $K_{34} = K_3 + K_4$ represents the combined mixing tube and diffuser losses encountered in the ejector. Good design makes it imperative to reduce K_{34} as much as possible to obtain high ejector efficiency.

4.2.3 The Mechanism of Pumping

An interesting photograph is presented by Flugel (Reference 3) showing the mixing vortices forming in the contact surface between two fluids flowing at different velocities. For purposes of discussion this vortex formation is shown pictorially in Figure 13. The mechanism of pumping appears to depend on vortex formation and the pushing-action of the high velocity fluid on the low velocity or secondary fluid. The fact that turbulent vortex formation plays an important part in pumping as it occurs in the ejector is further substantiated by Cunningham who observed rapid degradation in ejector performance during tests at flow Reynolds numbers of 3,000 and lower. Remembering that such low Reynolds numbers represent flow in the laminar flow region where vortexing is nonexistent, seems to bear out the importance of flow turbulence in pumping. The results of other investigations, as summarized in Stepanoff's "Centrifugal and Axial Flow Pumps" (Reference 5), indicate that ejector pump efficiency increases almost tenfold from a Reynolds number of less than 1000 to a Reynolds number of 800,000 to 1,000,000.



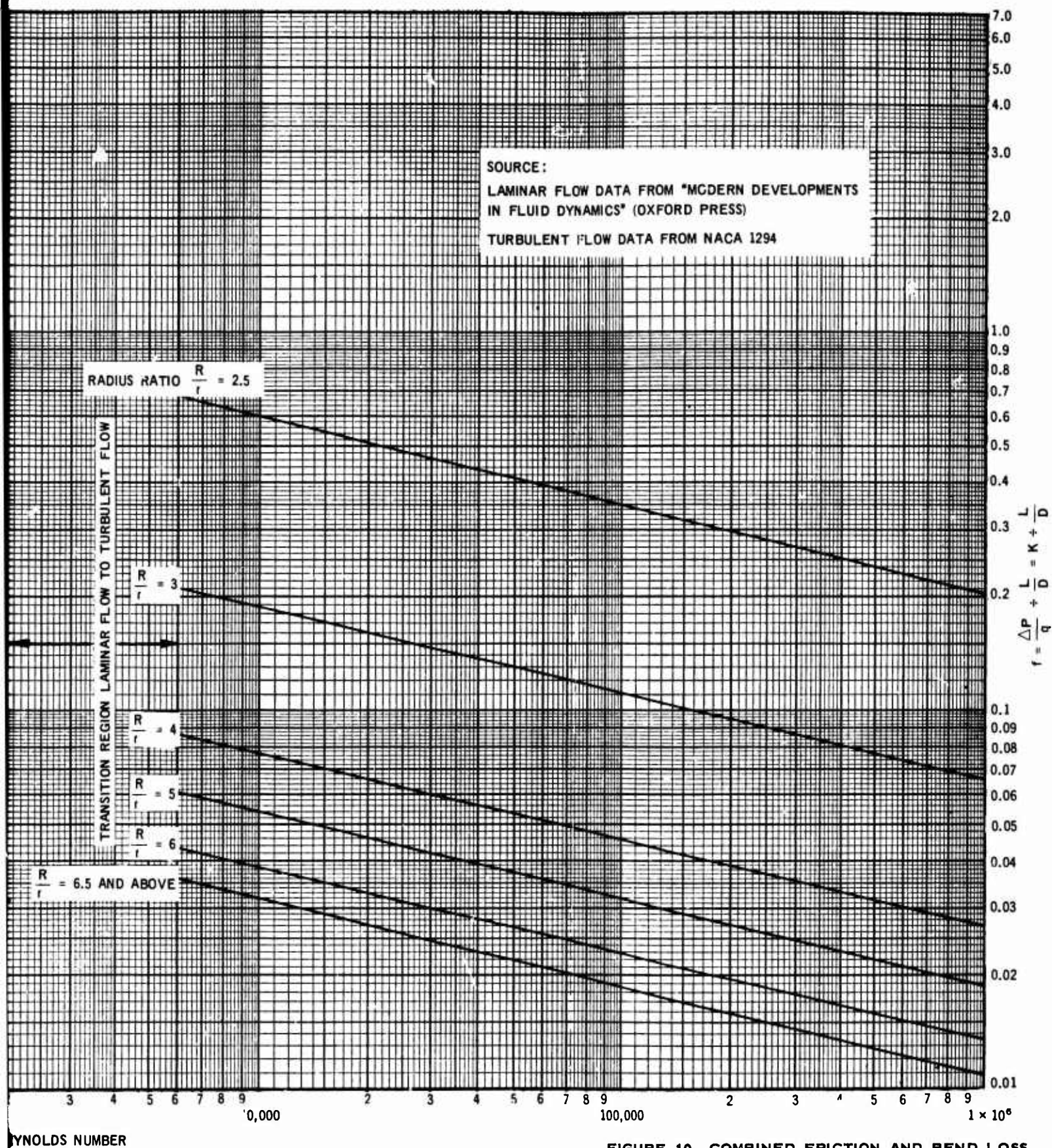


FIGURE 10. COMBINED FRICTION AND BEND LOSS
COEFFICIENT VS REYNOLDS NUMBER
FOR SMOOTH PIPE FLOW

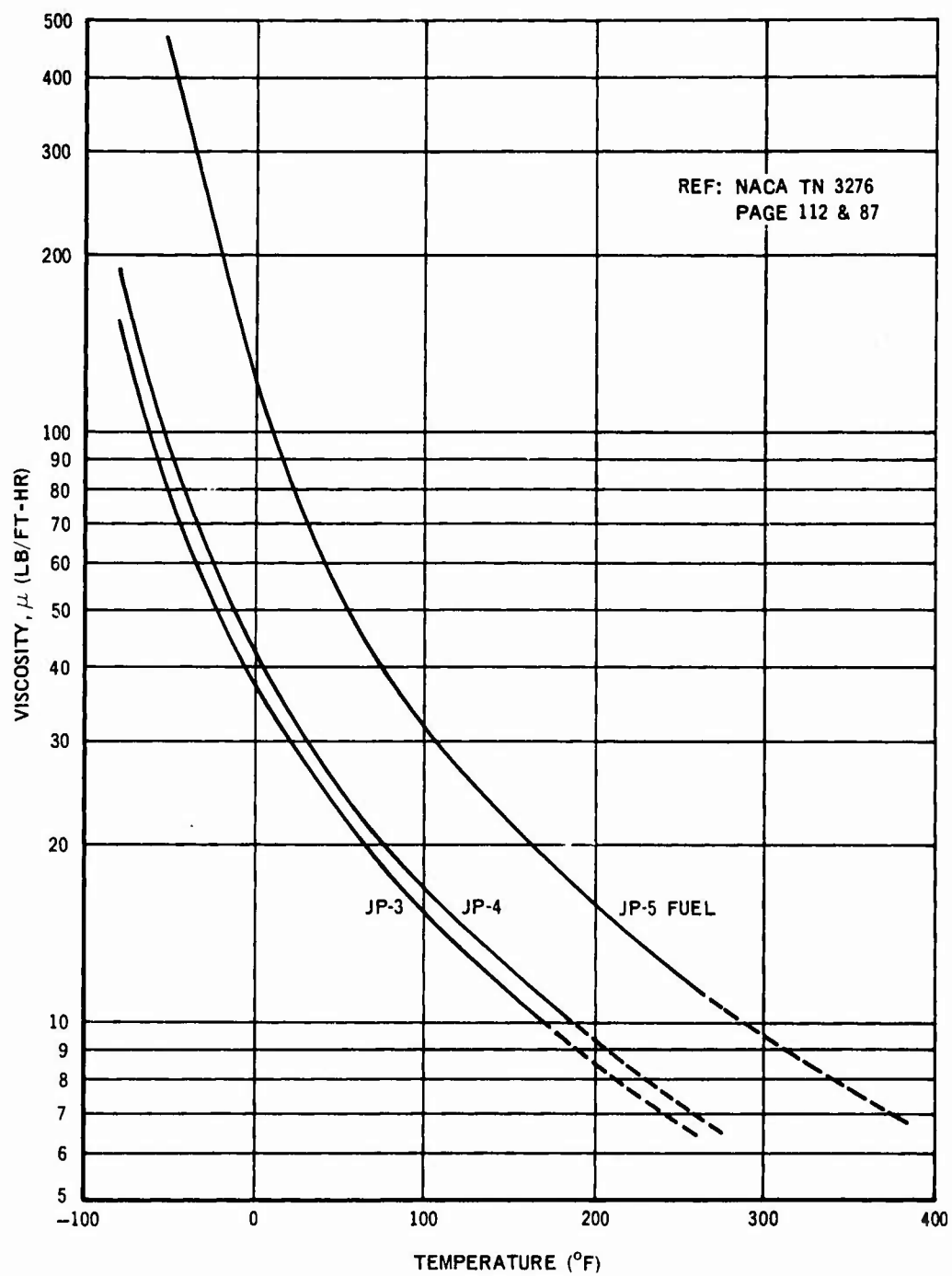


FIGURE 11. VISCOSITY VS TEMPERATURE OF JET FUELS

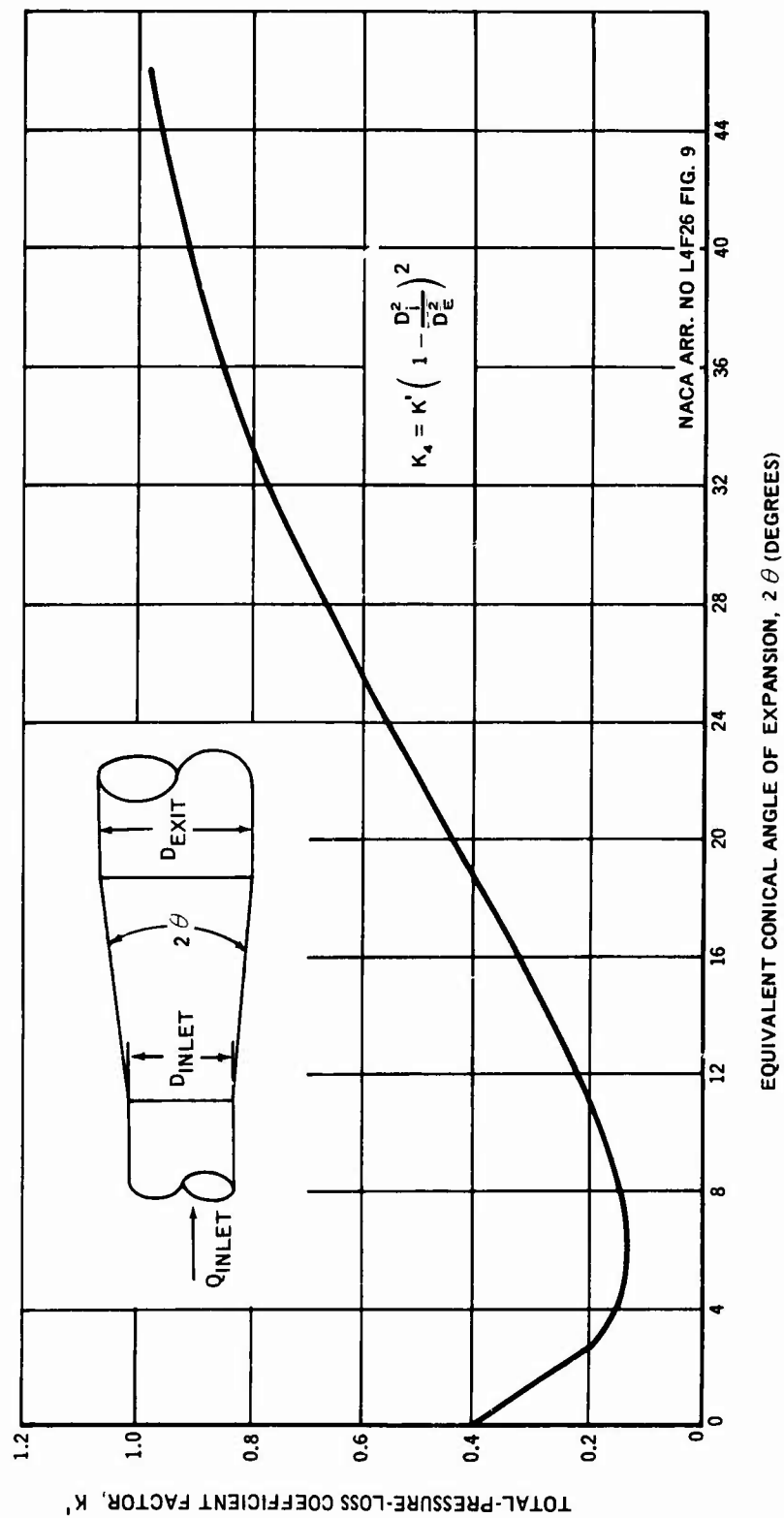


FIGURE 12. TOTAL-PRESSURE-LOSS COEFFICIENT FACTOR K_4 FOR STRAIGHT-WALL CONICAL DIFFUSERS

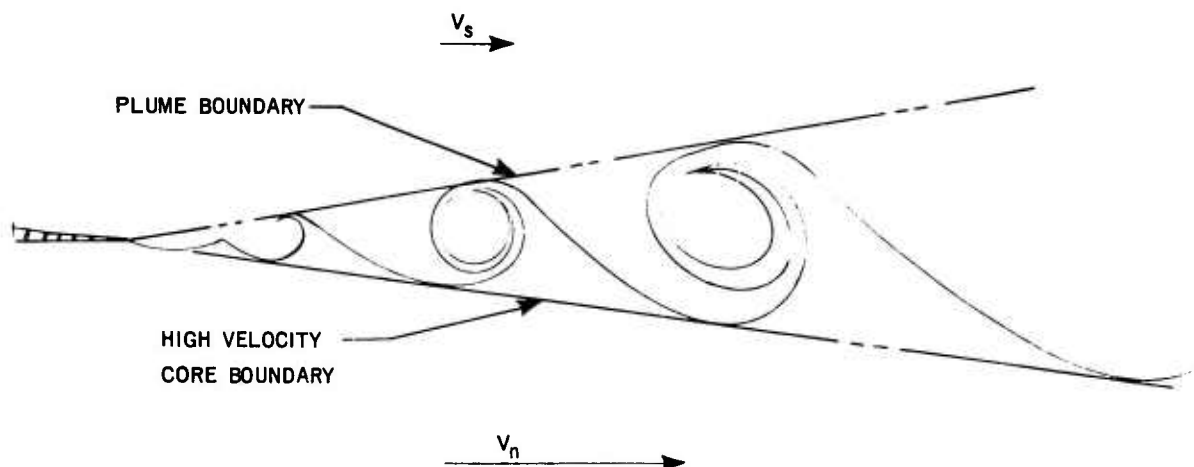


FIGURE 13. PICTORIAL PRESENTATION OF THE FIRST VORTICES FORMING IN THE CONTACT SURFACE BETWEEN TWO FLUIDS FLOWING AT DIFFERENT VELOCITIES

4.2.3.1 The Motive Fluid Jet Stream Model

For high pumping efficiency, it appears that the motive nozzle design pressure should be high enough to provide a velocity indicative of flow in the turbulent flow region. An approximate model of the motive nozzle flow and entrainment process can be established by reference to the work of Pabst, Corrsin, Ruden, and others as summarized in Reference 6. These studies established the velocity and temperature profiles in a round air jet emerging into still-air.

Figure 14 shows an approximate "plume" of a fluid jet as it emerges from the nozzle exit and as entrainment occurs at various stages downstream of the nozzle exit. The outer line, or virtual boundary, of the jet is defined as the point at which the velocity parallel to the axis is 10 percent of the velocity at the axis of the jet. Initially this boundary forms a cone with an included angle of approximately 90° . The entrainment process continues at a uniformly increasing rate to a point four to six nozzle diameters downstream of the nozzle exit. At this point the plume boundary expands, forming a cone with an included angle of approximately 180° and the velocity at the center axis of the jet begins to decrease below its initial value. Further entrainment takes place until the jet velocity at the center axis decays, presumably to a low laminar flow velocity. It appears that entrainment occurs in two definable stages. Initial entrainment is the interaction between motive fluid from the nozzle and the secondary fluid occupying an area extending from the nozzle exit to a region four to six nozzle diameters downstream of the nozzle exit. A second stage of entrainment occurs downstream of this point and involves the interaction, not only of the motive nozzle fluid and surrounding still-fluid, but also the secondary fluid entrained in initial entrainment region. It appears

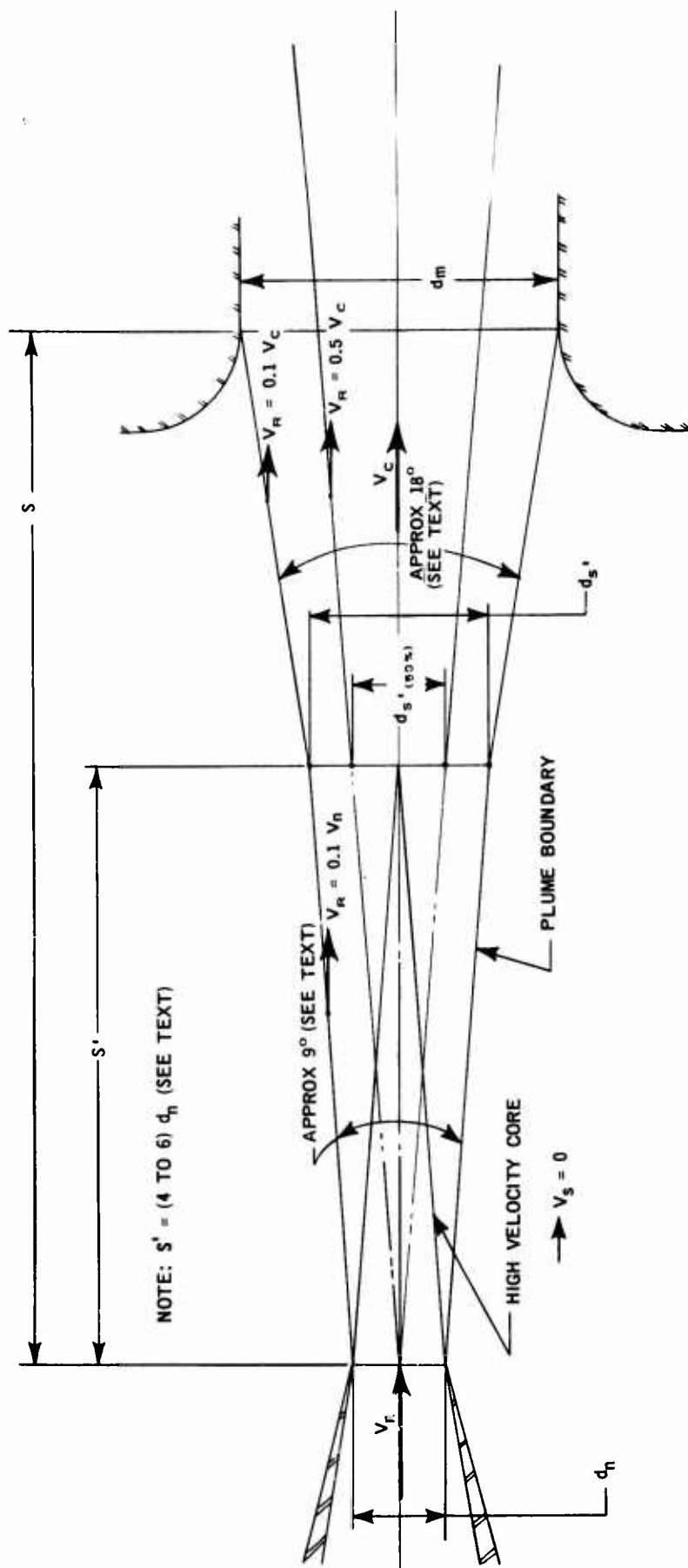


FIGURE 14. MOTIVE NOZZLE FLUID PLUME MODEL

that the additional interaction is the essential ingredient for the increased pluming effect beyond the four to six nozzle diameter downstream point in the flow.

The model presented is based upon motive nozzle flow which can be defined as nearly incompressible and turbulent (Reynolds numbers from approximately 10,000 to 1,000,000 for JP type fuels). The nozzle is convergent with a sharp-exit. The flow emerges into a region occupied by a nearly still-fluid with the same physical properties as the nozzle fluid.

4.2.3.2 Effect of Secondary Flow Approach Velocity

The motive nozzle plume model of Figure 14 is based upon an induced flow approach velocity of, theoretically, zero. As axial induced flow velocity is increased, the motive nozzle plume angle decreases. The entrainment process is the same as for the still-fluid model, at least in theory, except that for any given increment in time the process occurs over a longer axial distance, as secondary fluid approach velocity is increased. For the constant velocity cone of the motive nozzle flow, the still-air or $V_s = 0$ condition has been found to give a length of from 4 to $6d_n$. For $V_s > 0$, the constant velocity cone length becomes approximately $6d_n / 1 - \lambda$ (Reference 6),

where

$$\lambda = \frac{V_s}{V_n}$$

Nozzle bluntness appears to affect the length of the high velocity core. The core length, as observed from tests of various nozzle configurations, is discussed in section 4.2.4.4.

4.2.3.3 Cavitation and Its Effect on Induced Flow Approach Velocity

Cunningham (Reference 1) made a thorough study of the cavitation phenomenon as it occurs in the ejector. From tests and the use of the momentum exchange theory, he established a relationship for predicting the limiting flow ratio which an ejector of given area ratio can attain. Cavitation appears to depend upon the ejector geometry, the inlet or supply pressure to the ejector, the motive nozzle pressure, and an empirically determined Y function. The resultant equation for limiting flow is

$$\phi_L = \frac{1 - b}{b} \left(\frac{(1 + K_1) Y}{\bar{P}_i - \bar{P}_o} \right)^{1/2} \quad (8)$$

Viewed as an ejector performance phenomenon, an ejector operating at a fixed inlet pressure and motive nozzle pressure will respond to decreasing discharge pressure (such as opening a downstream throttling valve) by an increase in induced flow, to a point. Beyond this point the ejector fails to respond in the predicted manner. The induced flow fails to increase in response to a decrease in discharge pressure.

Cunningham observed cavitation in a special ejector made of plastic and instrumented with static pressure taps located at various distances down the mixing tube. During his tests, a discrete front or wall of cloudy fluid formed starting near the throat of the mixing tube. This visual observation was accompanied by a corresponding sudden increase in static pressure across this front. Increasing the nozzle pressure under these conditions caused the front to move progressively further downstream in the mixing tube. This cavitation phenomenon was accompanied by a high pitched whistling sound and the visual detection of large quantities of air bubbling out of solution.

The oil used in these tests was known to contain up to 15 percent by volume of dissolved air. Fuel can also contain relatively large amounts of air in solution.

The release of air dissolved in either fuel or oil is caused by a reduction in static pressure of the surrounding environment. The entrainment process is accompanied by a corresponding increase in induced fluid velocity. Where the motive nozzle is located close to the throat of the mixing tube, the secondary or induced fluid velocity may increase to a very high value because of the restricted opening available to flow proceeding to the throat of the mixing tube. Air dissolved in the liquid will come out of solution. The higher the induced liquid velocity, with a resulting decrease in static pressure, the more air will be evolved. Induced air and liquid are accelerated as the entrainment process proceeds into the mixing tube.

The sonic velocity of air is approximately 25 percent of that for fuel or oil. Since the air is carried along with the liquid at equal velocity, the assumption can be made that as induced flow velocity is increased, a point will be reached where a shock front caused by evolved air will develop.

For a perfect gas, the critical or sonic velocity can be defined as

$$V_c = \sqrt{kg R_c T_c}$$

where:

$$k = \text{ratio of specific heats } \frac{c_p}{c_v}$$

$$R_c = \text{gas constant}$$

$$T_c = \text{absolute temperature at the critical condition}$$

Cunningham defined the Y function as:

$$Y = \gamma \frac{V_{sL}^2}{2g} \text{ which is the dynamic pressure of the induced flow.}$$

$$V_{sL} \text{ for air} = V_{sl} \text{ for the liquid being induced.}$$

Since there is no physical reason for the liquid flow to be choked other than the presence of large quantities of air or fuel vapor,

$$Y = \frac{\gamma k g R_c T_c}{2g} = \frac{\gamma k R_c T_c}{2}$$

Since

$$\frac{P}{\gamma} = R_c T_c \text{ for a perfect gas}$$

$$Y = \frac{Pk R_c T_c}{2 R_c T_c} = \frac{k}{2} P$$

$k = 1.4$ approximately for air at room temperature.

$$Y = 0.7P$$

Assuming the fuel in the ejector inlet is flowing at low velocity, $\bar{P}_o \approx P_o$. As the velocity increases in the approach to the mixing tube, and assuming negligible throat entry loss, the limiting flow condition will be reached at

$$Y \approx 0.7 \bar{P}_o$$

From the results of many tests, Cunningham derived the empirical relationship

$$Y = 0.68 \bar{P}_o$$

which agrees closely with the assumed condition.

At altitude, or under conditions for extremely high nozzle velocities, pumping high temperature and/or high vapor pressure liquids, the above relationship appears to yield too optimistic an induced flow rate. Reference 7 refers to tests run on low-area ratio ejectors using nozzle pressures of up to 600 psig.

The fluid used was JP-4 at 110°F. In these tests the cavitation limit was reached at a lower induced flow than that indicated using equation (8) with $Y = 0.68 \bar{P}_o$. In this case the light-ends of JP-4 fuel boiling out of solution could cause the shock phenomenon of limiting flow. Assuming this to be so

$$Y = \frac{k}{2} \bar{P}_o \approx \frac{1.034}{2} P_o = 0.517 \bar{P}_o$$

The value for k was calculated using the relationships

$$k = C_p / C_v$$

$$C_v = C_p - \frac{R}{J}$$

where

$$J = 778 \text{ Ft Lb/Btu}$$

$$C_p = 0.493 \text{ for JP-4}$$

$$R = \frac{1545}{\text{molecular weight of JP-4}} = \frac{1545}{125} = 12.352$$

Although this determination of the Y function is rather crude, close agreement with the limiting flow achieved during the tests described in Reference 7 was found.

Assuming $K_2 = 0$, $\bar{P}_o = P_a + Y$. The static pressure in the area of the entrainment region should be maintained above a value

$$P_a \approx 0.5 \bar{P}_o$$

where the gaseous products of fuel are considered to exist due to high fuel vapor pressure, low inlet total pressure and high motive nozzle pressure.

For limiting flow conditions due to air entrainment when using low vapor pressure fuel (such as JP-5) the static pressure can be lower.

$$P_a \approx 0.3 \bar{P}_o$$

The limits of static pressure reduction impose definite limits on the induced flow approach velocity and thus on the throat entry geometry and nozzle-exit to throat-entry spacing, or S distance.

For the purpose of the following analysis, it is assumed that

$$S' = \text{the constant velocity cone length} = \frac{6 d_n}{1 - \lambda}$$

where

$$\lambda = \frac{V_s}{V_n}$$

For JP-4,

$$\frac{\gamma V_{sL}^2}{2g} = 0.5 \bar{P}_o$$

$$V_{sL}^2 = \frac{g \bar{P}_o}{\gamma}$$

From equation (1) and the relationship

$$V_n = \frac{W_n}{A_n \gamma}$$

$$V_n^2 = \frac{2 g (P_i - P_o)}{\gamma (1 + K_1)}$$

$$\frac{V_{sL}}{V_n} = \sqrt{\frac{g \bar{P}_o \gamma (1 + K_1)}{2g \gamma (\bar{P}_i - \bar{P}_o)}} = \sqrt{\frac{0.5 (1 + K_1) \bar{P}_o}{(\bar{P}_i - \bar{P}_o)}} \quad (9)$$

$$S' = \frac{6d_n}{1 - \sqrt{\frac{0.5 (1 + K_1) \bar{P}_o}{\bar{P}_i - \bar{P}_o}}} \quad (10)$$

It can be seen from this equation that as $\bar{P}_i - \bar{P}_o$ is increased, the plume model must approach the "still" secondary fluid ($V_s = 0$) model in order to prevent limiting flow cavitation.

Equation (9) can be used to determine the limiting value for V_s and thus define the minimum cross sectional area of the ejector inlet plenum.^s For most cases the inlet plenum cross sectional area should be larger than this minimum. Ideally, the plenum should be infinite in cross section with $V_s = 0$.

To eliminate gas evolution, all entrainment should occur before the induced flow enters the restrictive mixing tube throat.

Referring again to the still-fluid model of Figure 14, the entrainment zone boundary is approximately defined by the motive nozzle plume angles. By placing the mixing tube throat at the point where mixing tube diameter d_m equals the plume diameter, as shown in Figure 14, the condition for the

desired degree of entrainment will be fulfilled. For the condition where $V_s > 0$, distance S' in the plume model must be modified to accommodate this approach velocity. The relation previously cited should be used, namely

$$S' = \frac{6d_n}{1 - (V_s/V_n)} \quad (11)$$

If the plume diameter is measured at the point S' and compared to the nozzle diameter, it is found that

$$\frac{d_n}{d_{S'}} = 0.5143 \quad (12)$$

This value is a constant which can be used for any value of V_s/V_n . In other words the entrainment reaction always occupies the same cross sectional area at the point S' downstream of the nozzle. The numerical value of S' however, is dependent on V_s/V_n . (See Equation 11.)

It is interesting to note that

$$\left(\frac{d_n}{d_{S'}}\right)^2 = 0.264$$

From many literary sources comparing η_{mep} to area ratio, b , it has been established that ejectors with area ratios from 0.25 to 0.3 give the highest mep efficiencies. It is probable that the entrainment process is most efficient if d_m is located at or near the S' downstream entrainment point.

4.2.4 Ejector Geometry

From the previous discussion some conclusions as to proper ejector geometry can be reached, especially for the ejector used to pump high vapor pressure fuel under the adverse conditions of low inlet pressure to be encountered at high altitude.

4.2.4.1 Ejector Inlet and Throat Entry Geometry

Because of the cavitation problem, the secondary flow velocity in the approach to the entrainment region should be low. Theoretically the entrainment plenum should be infinite in cross-section and $V_s = 0$.

An approach to this hypothetical condition can be achieved by designing the plenum with as large a cross section as possible and allowing all entrainment to take place before the mixed flow reaches the mixing tube throat.

Since there is a rate associated with dissolved air coming out of solution and/or fuel vaporizing due to reduction of static pressure, the transition from the plenum to the mixing tube must be accomplished rapidly, such that the elapsed time is very short. Once the flow has entered the mixing tube the static pressure will gradually increase from the throat to the discharge port of the ejector, inhibiting further vapor evolution.

A number of throat inlet configurations were tested under this contract. Three of these configurations are shown in Figure 15. Corresponding performance curves for these three configurations are shown in Figure 16. Best pressure recovery was obtained with Configuration 1 and best flow ratio was obtained with Configuration 2.

It appears that a short, rounded entry would produce best results. The throat entry of Configuration 2 most nearly conforms to this configuration. Figure 16 shows that this throat entry permitted the best flow recovery. The optimum nozzle exit to throat spacing for Configuration 2 was approximately 3-11/16.

Tests were run which varied the nozzle to throat spacing, S , to confirm the assumption that optimum S is that length at which the entrainment plume diameter equals the throat diameter. At this point, best flow recovery is obtained. Configuration 1 appeared to provide best pressure recovery even though the nozzle plume extended into the mixing tube. As will be discussed later, it is likely that high pressure recovery was achieved because the mixing tube length more nearly approached optimum than with Configurations 2 and 3. Note that the 50% V_c cone for Configuration 1 impinges on the wall of the mixing tube very near the end of the tube or the beginning of the diffuser (Figure 15).

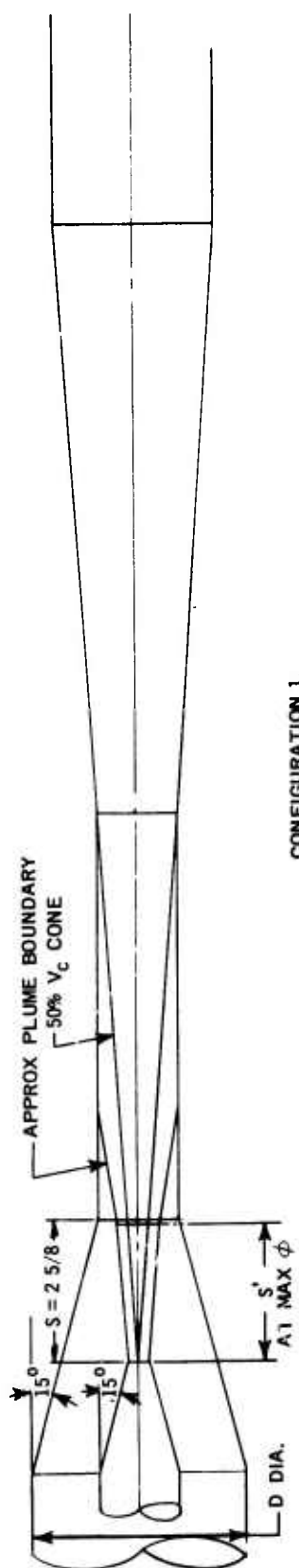
4.2.4.2 Optimum Mixing Tube Length

Where nozzle to throat spacing is that point at which the nozzle plume diameter equals the mixing tube diameter, once the flow has entered the mixing tube throat, no further entrainment is possible. Secondary fluid access to the mixing tube is blocked by the boundary of the entrainment reaction as it impinges on the throat wall. The mixing tube serves to stabilize the flow, by establishing an equilibrium axial velocity flow profile. For turbulent flow the equilibrium condition exists when the axial velocity near the wall is approximately 50 percent of the velocity at the tube center line. (Reference 8).

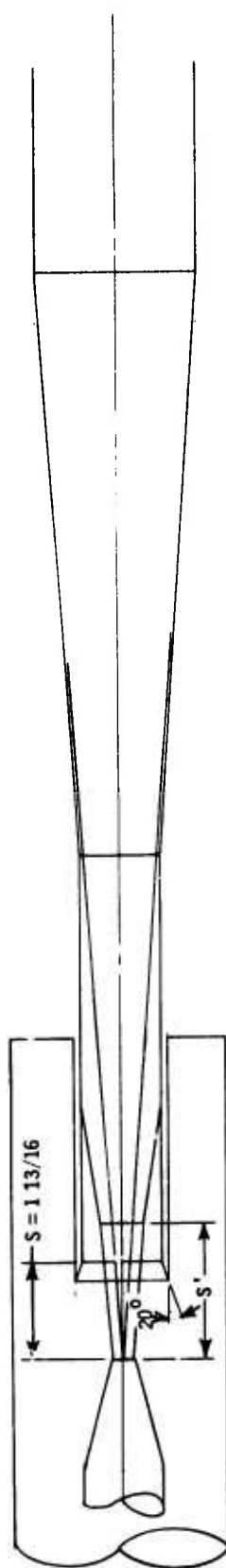
Again referring to the motive nozzle plume model of Figure 14, the 50 percent velocity cone, with its apex at the center of the motive nozzle exit, passes through the station S' downstream of the nozzle exit such that

$$d_{S' 50\%} = d_n \quad (13)$$

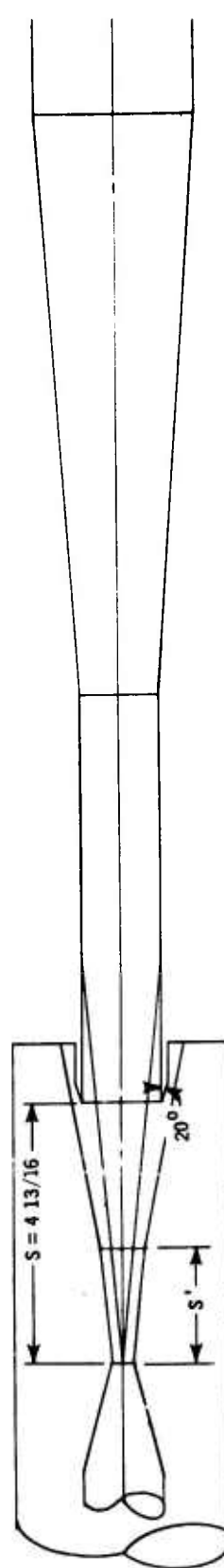
Extending this line to the mixing tube wall provides a downstream point where the velocity at the wall is 50 percent of the velocity at the center of the tube.



CONFIGURATION 1.



CONFIGURATION 2.



CONFIGURATION 3.

ALL CONFIGURATIONS - NOZZLE DIA, $d_n = 0.421$ THROAT DIA, $d_m = 1.500$ $b = 0.0785$
 MIXING TUBE LENGTH, $L = 7.5$ PLENUM DIA., $D = 4$ DIFFUSER CONE ANGLE 8°

FIGURE 15. THROAT ENTRY CONFIGURATIONS

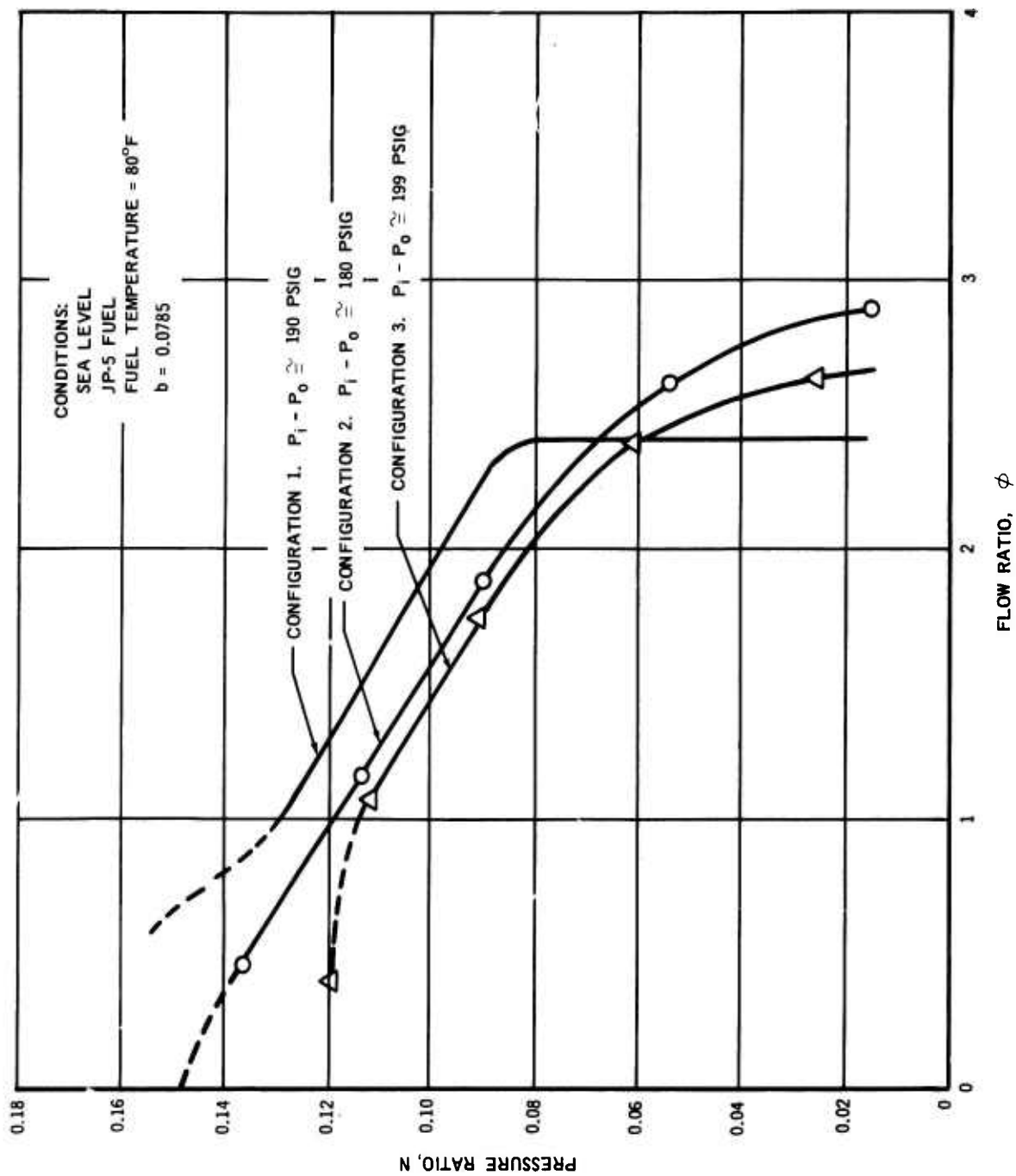


FIGURE 16. PUMP PERFORMANCE FOR CONFIGURATIONS 1, 2, & 3

At this point the flow should be stabilized sufficiently that the constant area mixing tube can be terminated.

One ejector configuration, tested under this contract, shows that the throat entry and a part of the mixing tube were made of acrylic (See Figure 17).

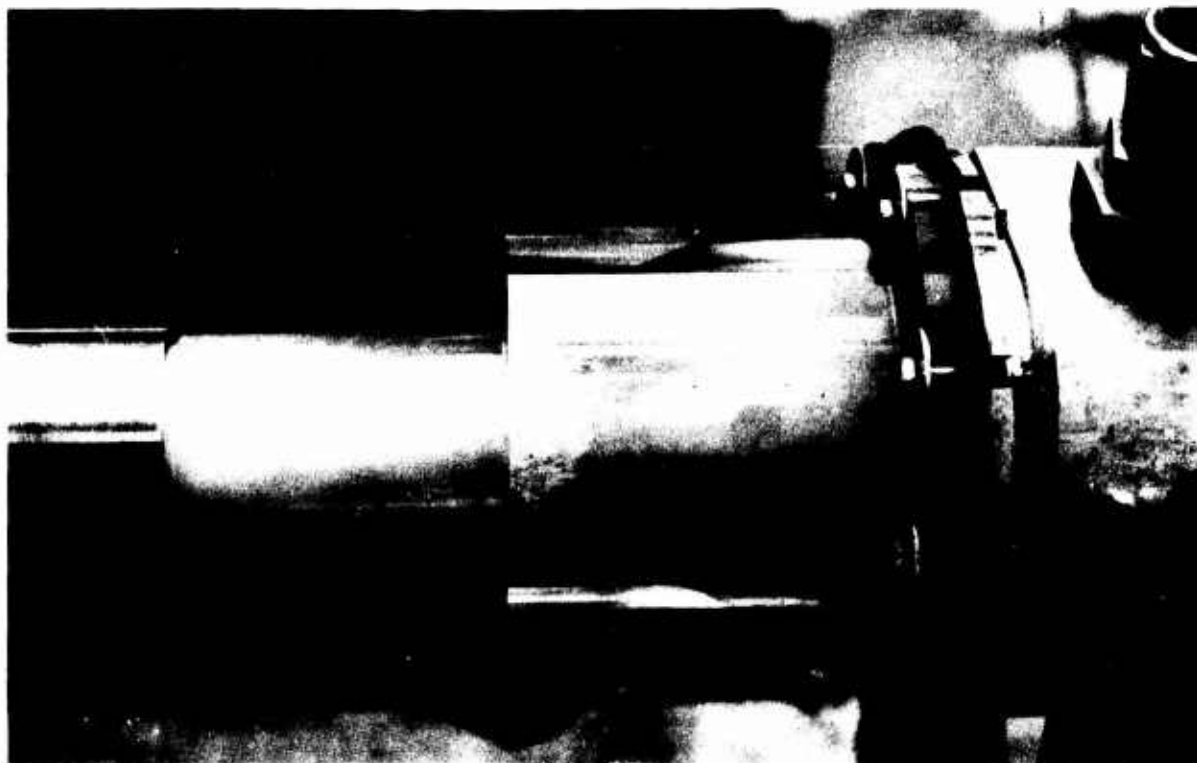


FIGURE 17. NOZZLE AND MIXING TUBE SECTION OF EJECTOR PUMP TEST MODEL

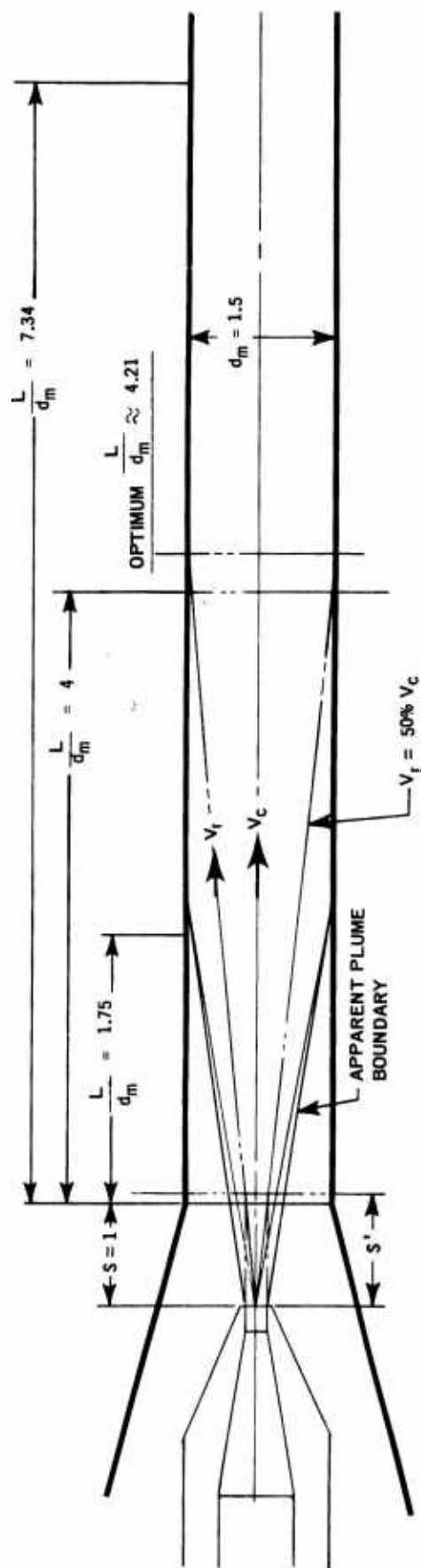
Visibility into the ejector permitted some estimations to be made concerning the nozzle plume and secondary flow aeration. From visual observation, the apparent plume half angle of the motive flow nozzle was determined to be approximately 9 to 10°. The downstream change of plume angle is extremely difficult to determine visually, due mainly to the flow turbulence at the entrainment boundary. Figure 17 shows picturally Configuration 1 of Figure 15. The motive nozzle used with this configuration was blunt at the exit station. Use of a blunt nozzle, instead of a sharp exit nozzle, apparently has the effect of shortening the S' initial entrainment distance. The velocity ratios experienced

ranged up to approximately $\frac{V_s}{V_n} = 0.19$. Assuming a S' shortening from

$S' = \frac{6d_n}{1 - (V_s/V_n)}$ to $S' = \frac{4d_n}{1 - (V_s/V_n)}$ the resultant apparent plume boundary half angle is 9°. The cone for the $V_r = 50\% V_c$ condition as shown in Figure 18

gives the optimum $\frac{L}{d_m} = 4.21$. Three pump-down runs were made with this

configuration, varying only the mixing tube length as shown on the drawing. Motive nozzle flow was held to 25.5 ± 0.5 gpm. The results of these runs are shown in the curves of Figure 19, pressure difference ratio versus $\frac{L}{d_m}$, at



$$s' = \frac{4dn}{V_s} \approx \frac{(4)(0.2188)}{1-0.19} \approx 1.08$$

$$\frac{V_s}{V_n} \approx 0.19$$

FIGURE 18. MIXING TUBE CONFIGURATIONS

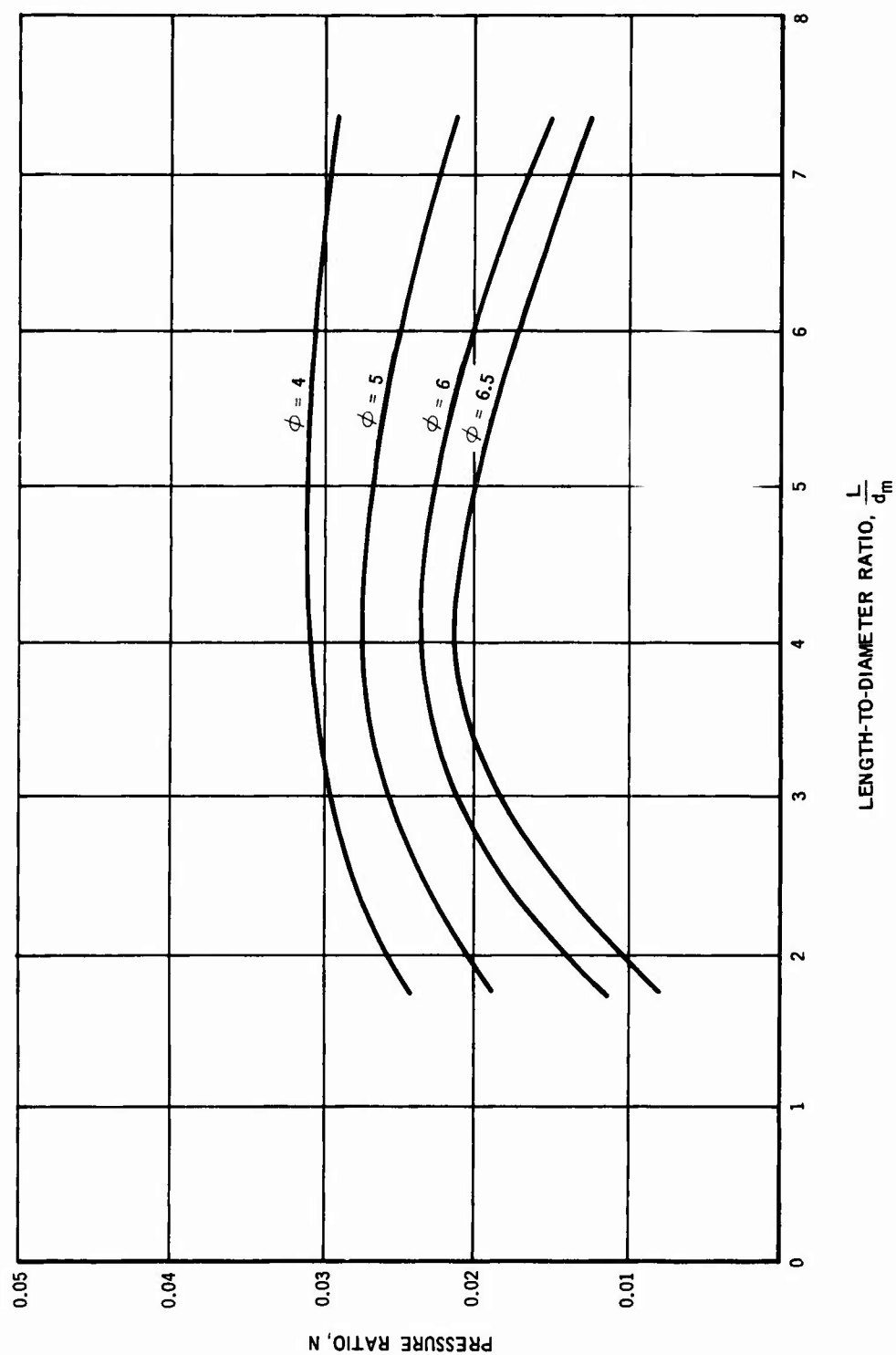


FIGURE 19. MIXING TUBE PERFORMANCE

various flow ratios. Depending on flow ratio, optimum $\frac{L}{d_m}$ occurs at values from 4 to 4.75. At the high flow ratio, $\phi = 6.5$, the peak occurs at $\frac{L}{d_m} \approx 4.2$.

These values appear to confirm the theoretical assumption for mixing tube length (at least for this configuration).

A mixing tube which is too short appears to more adversely affect ejector performance than a mixing tube which is too long. Underdeveloped flow probably expands abruptly within the diffuser rather than diffusing gradually. The resultant flow reversal in the diffuser creates a higher pressure loss than the added wall friction encountered in greater than optimum mixing tube length.

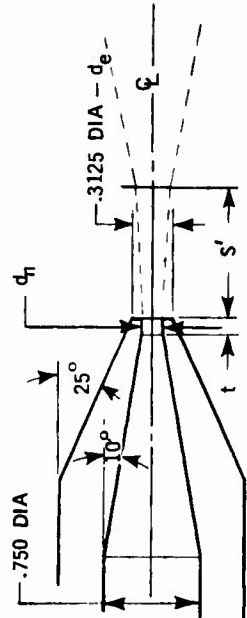
4.2.4.3 Optimum Diffuser Configuration

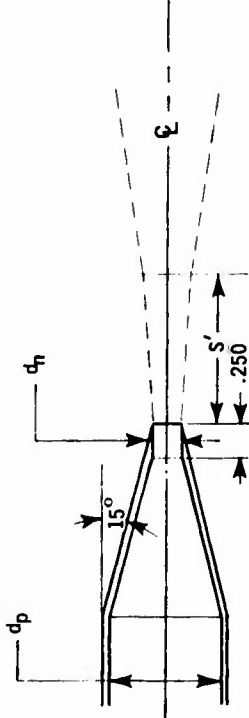
Since the flow entering the diffuser will be stabilized, the choice of diffuser angle is one based on minimum loss. As was noted in Section 4.2.2.4, a conical diffuser with a cone angle of 60° (30° half angle) gives minimum loss. This will result in a long diffuser which would be more difficult to adapt to some aircraft installations. Increasing the diffuser angle to a value equal to the $50\% V_c$ angle of the nozzle plume will probably still give satisfactory performance without flow reversal, i. e., abrupt expansion loss in the diffuser. For the test ejector shown in Figure 18, a diffuser cone angle of 120° would probably be satisfactory, although the diffuser actually used had a cone angle of 80° .

4.2.4.4 Optimum Motive Nozzle Configuration

Figure 20 shows some of the motive flow nozzles used during testing under this contract. Also included is the theoretical sharp nozzle on which the "still" induced flow plume model is based. For the $V_s = 0$ condition the external shape of the nozzle has no significant effect on \dot{S} . However, for $V_s > 0$, even though V_s may be small, the effect of external nozzle surface divergence angle and the bluntness of the nozzle exit will affect \dot{S} . For this case, the ideal nozzle configuration must have an external shape which prevents secondary flow separation at the nozzle exit and introduces this flow parallel to the motive flow. Ideally such a nozzle will have an infinitesimally thin wall at the exit. A nozzle configuration approaching the ideal nozzle would be difficult to fabricate and impractical for service because of susceptibility to handling damage. The nozzles of Configuration 2 required care in handling to avoid denting the sharp edge.

The nozzle discharge coefficients for the various nozzle configurations were calculated at the Reynolds number shown in the table accompanying Figure 20. The nozzle dimensions are given either in the figure or the accompanying table. No distinct trend toward optimum nozzle configuration is apparent. It appears that internal conical convergence angles of 20° and 30° (10° and 15° half angle) provide approximately equal performance. d_n/d_p ratios as low as 0.208 did not appear to adversely affect nozzle performance. Testing accomplished under this contract appears to substantiate the use of a nozzle loss

														CONFIGURATION NO. 1			
R_n	d_n	$d_n/.750$	t	C_D	d_e/d_h	$s' \approx$											
156,500	.156	.208	.125	.96	2	$\frac{4d_h}{1 - \frac{V_s}{V_n}}$											
192,500	.192	.256	.187	.95	1.63	$\frac{4d_h}{1 - \frac{V_s}{V_n}}$											
204,500	.219	.292	.240	.94	1.43	$\frac{4d_h}{1 - \frac{V_s}{V_n}}$											
R_n	d_n	d_n/d_p	t	C_D	d_e/d_h	$s' \approx$											
332,000	.219	.252	.250	.98	0	$\frac{4.5d_h}{1 - \frac{V_s}{V_n}}$											
338,000	.375	.232	.250	.94	0	$\frac{4.5d_h}{1 - \frac{V_s}{V_n}}$											
384,000	.421	.260	.250	.93	0	$\frac{4.5d_h}{1 - \frac{V_s}{V_n}}$											
							t	C_D	d_e/d_h	s'							
							0	1.0	0	$\frac{6d_h}{1 - \frac{V_s}{V_n}}$							

														CONFIGURATION NO. 2			
R_n	d_n	d_n/d_p	t	C_D	d_e/d_h	$s' \approx$											
332,000	.219	.252	.250	.98	0	$\frac{4.5d_h}{1 - \frac{V_s}{V_n}}$											
338,000	.375	.232	.250	.94	0	$\frac{4.5d_h}{1 - \frac{V_s}{V_n}}$											
384,000	.421	.260	.250	.93	0	$\frac{4.5d_h}{1 - \frac{V_s}{V_n}}$											
							t	C_D	d_e/d_h	s'							
							0	1.0	0	$\frac{6d_h}{1 - \frac{V_s}{V_n}}$							

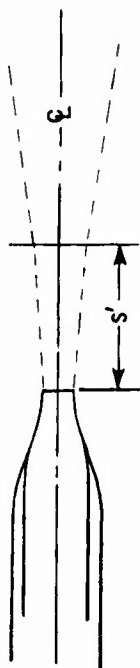
														"IDEAL" CONFIGURATION			
R_n	d_n	d_n/d_p	t	C_D	d_e/d_h	$s' \approx$											
332,000	.219	.252	.250	.98	0	$\frac{4.5d_h}{1 - \frac{V_s}{V_n}}$											
338,000	.375	.232	.250	.94	0	$\frac{4.5d_h}{1 - \frac{V_s}{V_n}}$											
384,000	.421	.260	.250	.93	0	$\frac{4.5d_h}{1 - \frac{V_s}{V_n}}$											
							t	C_D	d_e/d_h	s'							
							0	1.0	0	$\frac{6d_h}{1 - \frac{V_s}{V_n}}$							

FIGURE 20. MOTIVE NOZZLE CONFIGURATIONS

coefficient $K_1 \approx 0.1$ as advised by Cunningham (Reference 1) for high Reynolds number flow.

The nozzle external configuration may depend upon other ejector geometric considerations such as inlet plenum size and area ratio. From nozzle testing, it may be concluded that the combination of shallow diffusion angle (15° half angle) and sharp exit provide a larger \bar{S} high velocity core distance. None of the nozzles tested attained the $\bar{S} = 6d_n$ length assumed. Even in reference 6 there is a question as to the exactness of this value. It appears that for most practical nozzle designs $\bar{S} = 4d_n$ to $4.5d_n$ would yield satisfactory design

results for the $\frac{V_s}{V_n} \approx 0$ case.

4.2.5 Performance Results

Three different configurations of the simple ejectors tested are shown in Figure 21. Figures 22, 23 and 24 show the N versus ϕ performance curves obtained for these configurations. Two performance curves are shown for each configuration. The optimistic curve was derived by analysis using loss coefficients determined by methods described in Section 4.2.2. Test results are indicated by coded points and a faired curve. All tests were limited to maximum of 500 psi nozzle pressure as this was determined to be the operating range of main engine fuel pumps.

The deviation from analytical prediction is apparent. The ejector loss coefficient K_{34} , determined at various test data points, varied from a low of about 0.38 to a high of approximately 0.75. In determining K_{34} from tests, K_1 was calculated from the test data, K_2 was assumed to be zero and K_{34} was calculated using equation (2). Since K_2 may have a discrete value for the throat inlet used, the values of K_{34} may be somewhat pessimistic. However, from visual observation through the acrylic parts of the ejector during tests, it would appear that the high value of K_{34} was more a function of the aeration of the induced flow rather than a high throat entry loss. The effect of a shallow convergent cone angle throat entry permitted relatively large quantities of entrained air to come out of solution due to the high approach velocity of the induced flow. At high induced flow rates, the interior of the ejector throat and mixing tube were completely obscured by foamy fluid. Even with the ejector flow throttled to a low flow ration, aeration was visible.

Induced flow aeration was also a function of motive nozzle pressure. At 200 psi nozzle pressure, the throat entry and mixing tube were relatively clear (See Figure 17). Increasing the nozzle pressure produced increasing cloudiness in the throat entry section. At 500 psi nozzle pressure, this cloudiness was present almost to the $\phi = 0$ throttled condition. Multi-phase or aerated flow is known to substantially increase losses in piping systems. It would appear that this is the basic reason for deviation of the loss coefficient, K_{34} , from that assumed for all-liquid flow.

$d_m = 1.500$
 $S = 1.000$
 $L = 6.000$

DIFFUSER CONE ANGLE 8°
 EXIT DIA. 3.000

PUMP CONFIGURATION	d_n	b
1	0.156	0.0108
2	0.192	0.0163
3	0.219	0.0213

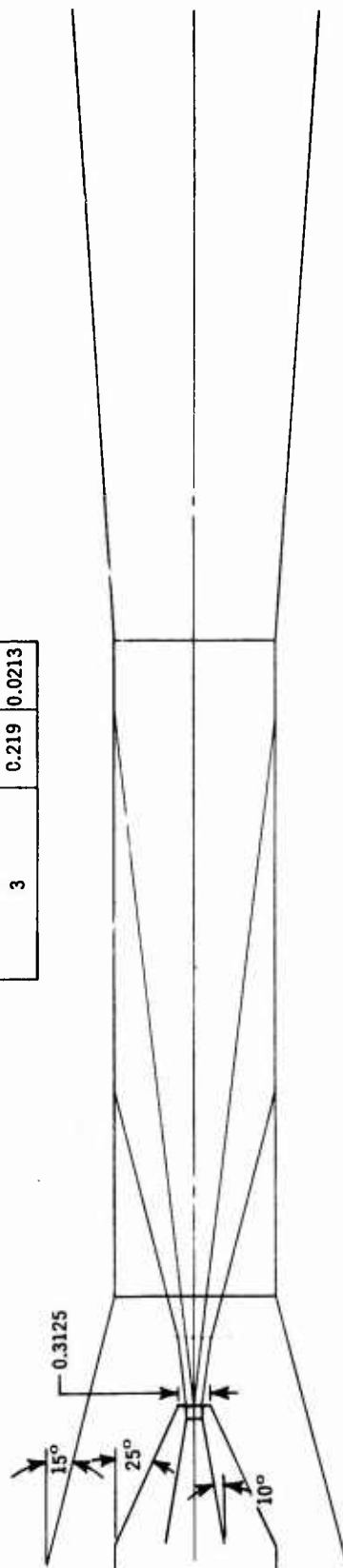


FIGURE 21. EJECTOR PUMP TEST CONFIGURATIONS

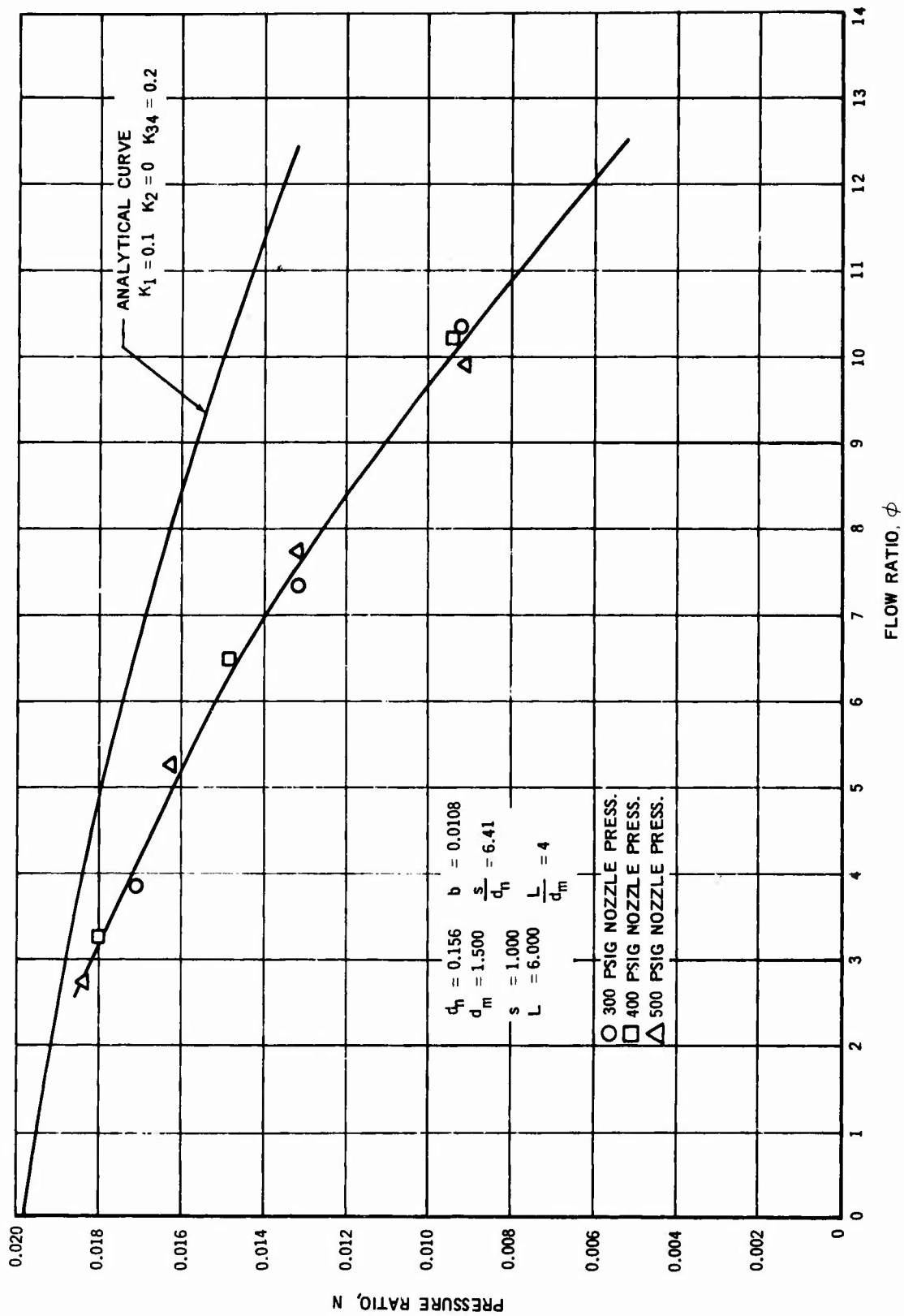


FIGURE 22. EJECTOR PERFORMANCE

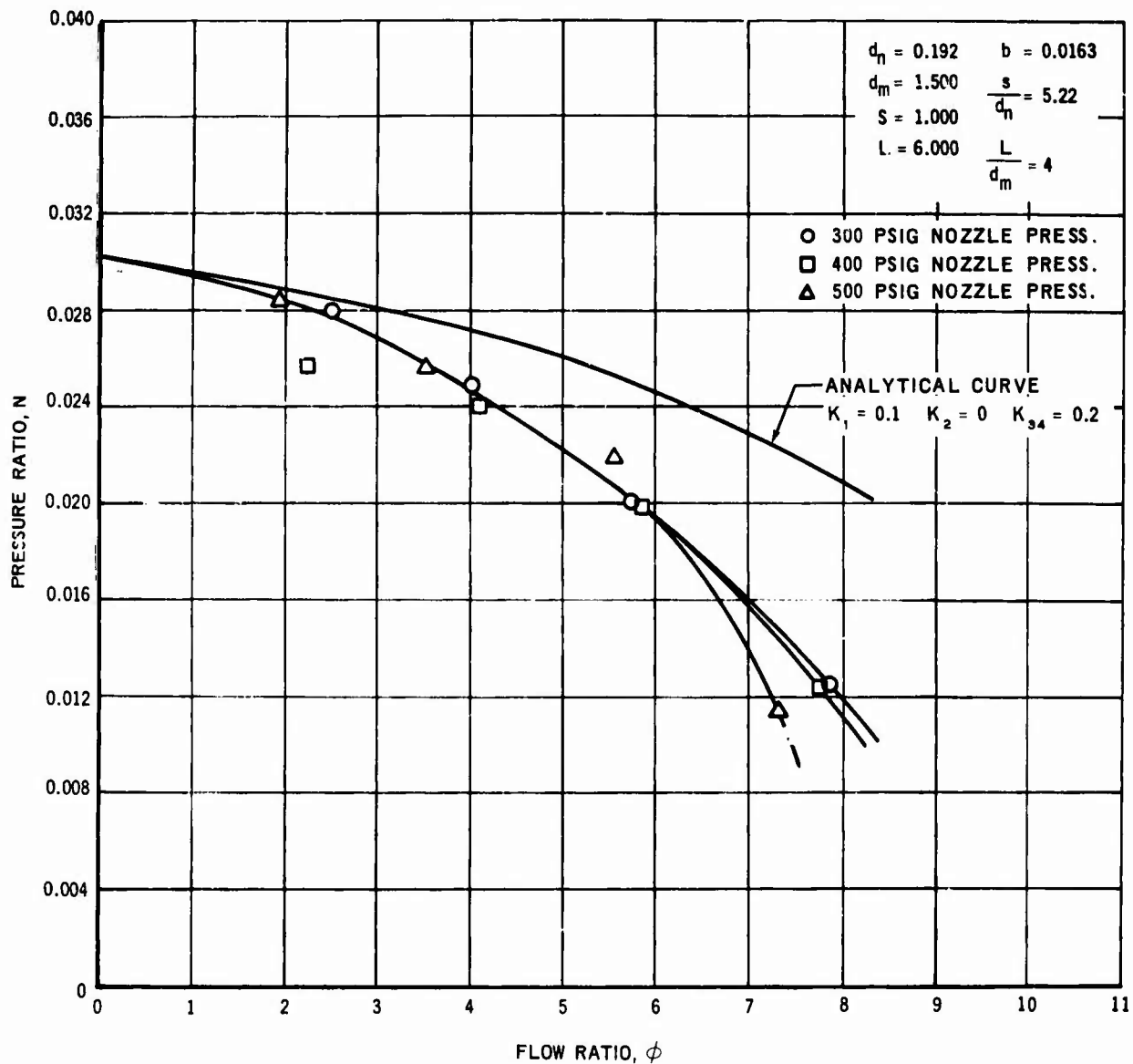


FIGURE 23. EJECTOR PERFORMANCE

The case of the $b = 0.0163$ ejector tested, Figure 23, is of particular interest here. The mixing tube length for this configuration was very near optimum. The loss coefficient (K_{34}) $\cong 0.38$ at low flow ratios and ≈ 0.7 at a flow ratio of 7.85 using 300 psig nozzle pressure. Extrapolating the test curve to $\phi = 0$ gives an N value equal to the analytical point using $K_{34} = 0.2$.

It would appear that high induced flow velocity initiates flow aeration, in this case, at a relatively low flow ratio. Flow aeration has a marked effect on ejector performance. This appears to substantiate the design need for a large inlet plenum and short throat entry. The plenum diameter to throat diameter

ratio for these ejectors was $\frac{d_o}{d_m} = 2.67$. This ratio appears to be inadequate even using a short throat entry. This ratio is discussed further in Section 4.5.1.

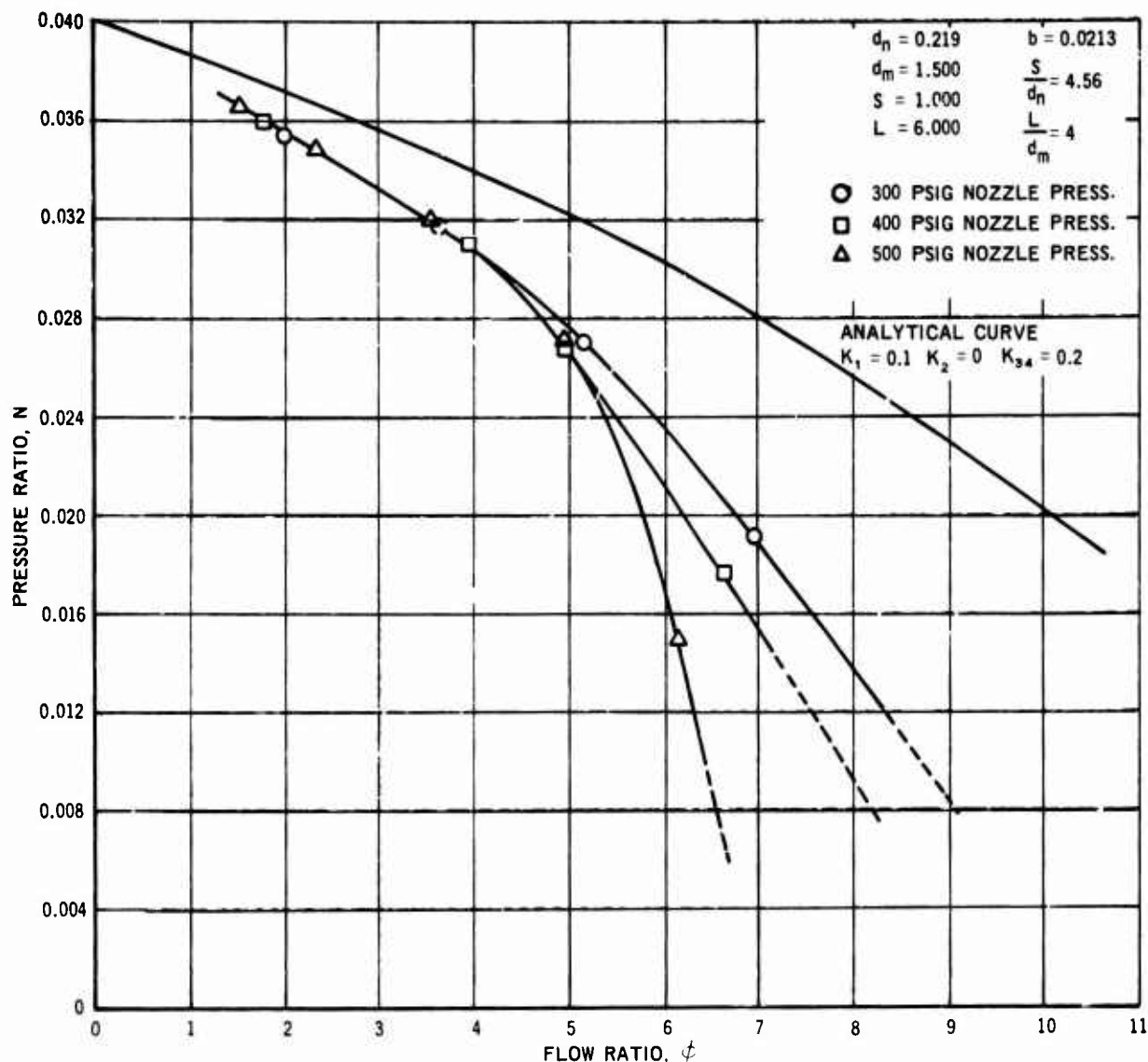


FIGURE 24. EJECTOR PERFORMANCE

For any given ejector geometry with a finite plenum diameter, the effect of throttling the ejector outflow is manifest in a change in motive nozzle plume angle. As induced flow is reduced, the nozzle plume angle tends to increase. This change is predicted by Equation (11). A reduction in V_s decreases the ratio V_s/V_n , which in turn, reduces \dot{S} . The entrainment reaction occurring at the \dot{S} station takes place closer to the nozzle exit. Since the reaction occupies the same area (as defined by Equation (12)) the effect is an increase in plume angle. An increase in motive nozzle pressure, thus increasing V_n while maintaining induced flow at a constant level, produces the same effect. Both of these characteristics were confirmed visually during the testing program. For an ejector required to operate at a number of flow points, as in an aircraft engine feed system, the above characteristics have an important bearing on ejector geometry. Where the plenum diameter is large with respect

to mixing tube diameter (V small) plume changes will be minimal. However, where the plenum diameter^s is small, plume changes will require a reduction in nozzle exit to throat spacing to permit efficient operation at low flow ratios. The effect of too large an S spacing at reduced flow ratios is a decrease in pressure recovery due to plume splatter, where a part of the plume misses the throat entry. Configuration 3 of Figure 15 shows this condition. The performance curve of Configuration 3 (Figure 16) substantiates this conclusion.

4.3 THE ANNULAR EJECTOR

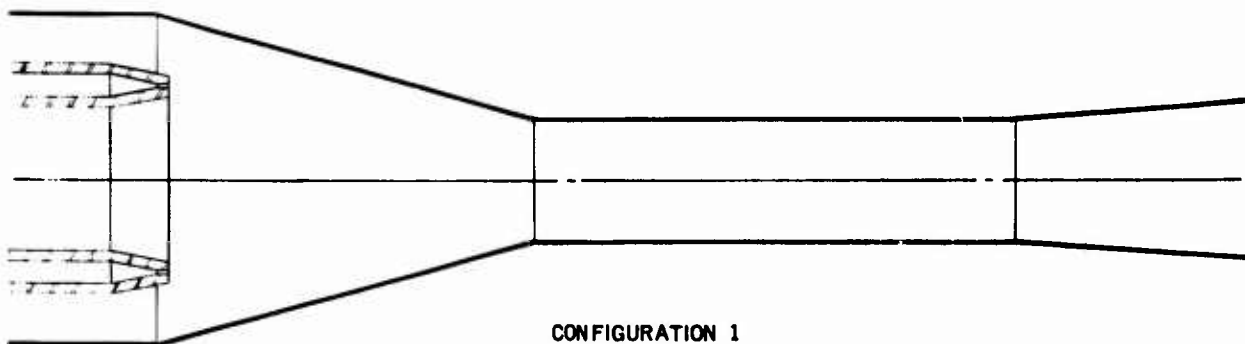
A definition of the term annular ejector is required before any discussion of this device is presented. For purposes of this report, an annular ejector is one using an annulus slot motive flow nozzle which discharges the motive fluid into either an annular throat or a circular throat. The motive nozzle slot may be located near the plenum wall or at some intermediate radial distance between the wall and the pumps axis of symmetry. Some of the possible arrangements are shown in Figure 25. Under this definition the annular ejector discharges the mixed fluids into a circular pipe.

All of the combinations shown in Figure 25 were tested. Of those shown, Configuration 4 gave best results. Most of the following discussion will be concerned with this configuration. Configuration 1 was very poor. The converging ramp entry to the throat appeared to hamper the entrainment process. Considerable turbulence was evidenced during operation of this configuration. Configuration 2 and a modification of this configuration using a centerbody (as shown in Configuration 4) gave some improvement. However, the presence of a wall in close proximity to the motive flow appeared to hamper entrainment even though the wall was parallel to the motive flow. The performance of Configuration 3 more nearly approached analytical prediction based on classical momentum relationships than did Configurations 1 and 2. The performance was poor due to the low area ratio. The addition of a centerbody, as shown in Configuration 4, raised the area ratio and improved the performance very much.

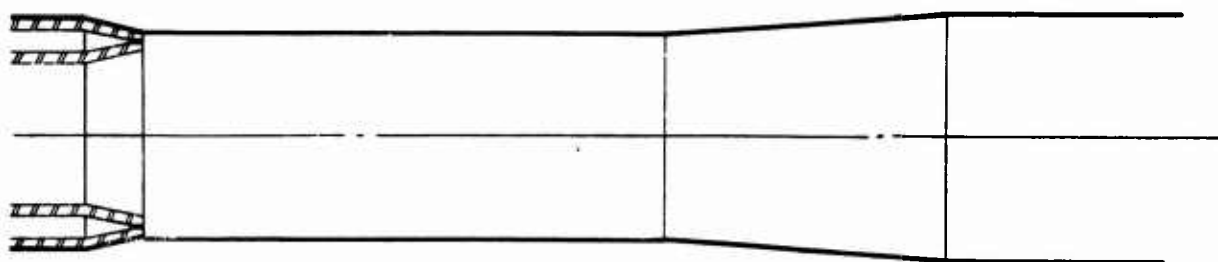
Figure 26 shows the performance of an annular ejector based on Configuration 4. A comparison curve of the anticipated performance for a simple ejector is also shown. The annular ejector curve indicates poorer performance. Further study and testing of this type of ejector is required to find a configuration which will provide performance which more nearly matches that of the analytical curve. One of the significant factors concerning these curves is the close parallel between them, which indicates that accurate estimation of the losses (K_1 , K_2 , and K_{34}) should enable the designer to predict annular ejector performance using the same basic equations (Equations (1) through (4)) as are used for simple ejectors.

4.3.1 The Annular Motive Flow Nozzle Plume Model

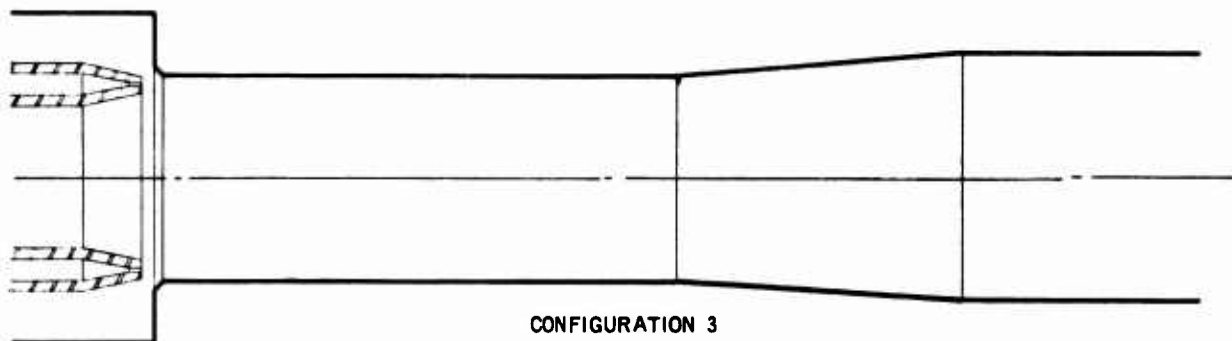
From the results of the tests described in Reference 9, the annular nozzle plume model is approximately the same as was presented for the round jet in Section 4.2.3.1 with the exception that the slot width d_n becomes c_n . S , the length of the high velocity core, was shown to be approximately $4.5 c_n$. This is dependent upon the relative bluntness of the nozzle. Thus, the geometry of



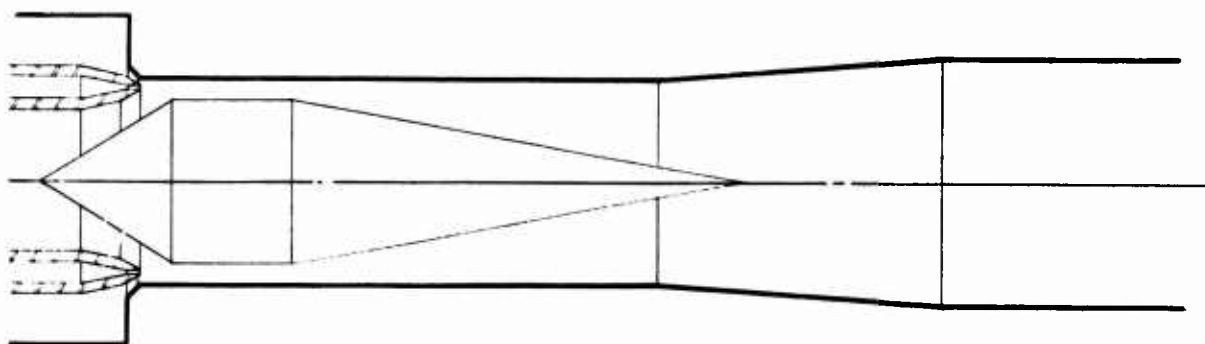
CONFIGURATION 1



CONFIGURATION 2



CONFIGURATION 3



CONFIGURATION 4

FIGURE 25. ANNULAR NOZZLE PUMP CONFIGURATIONS

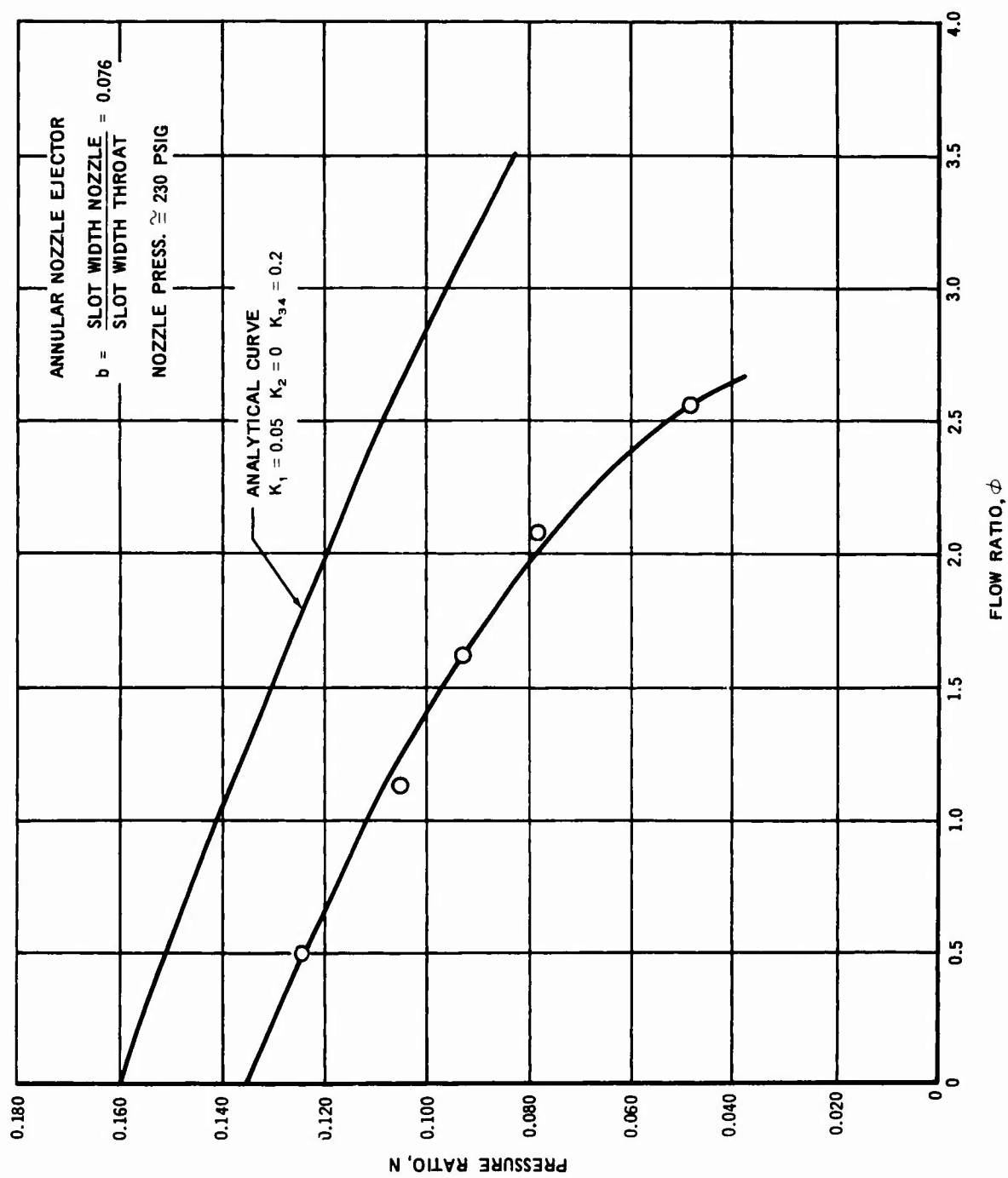


FIGURE 26. ANNULAR EJECTOR PERFORMANCE OF CONFIGURATION NUMBER FOUR

the annular ejector is governed by similar considerations discussed for the simple ejector, only based upon slot width considerations rather than nozzle diameter.

For the annular motive nozzle with a sharp exit $\frac{S}{c_n} \cong 4.5$ for $V_s = 0$. The above assumption is based upon information from Reference 9. Figure 27

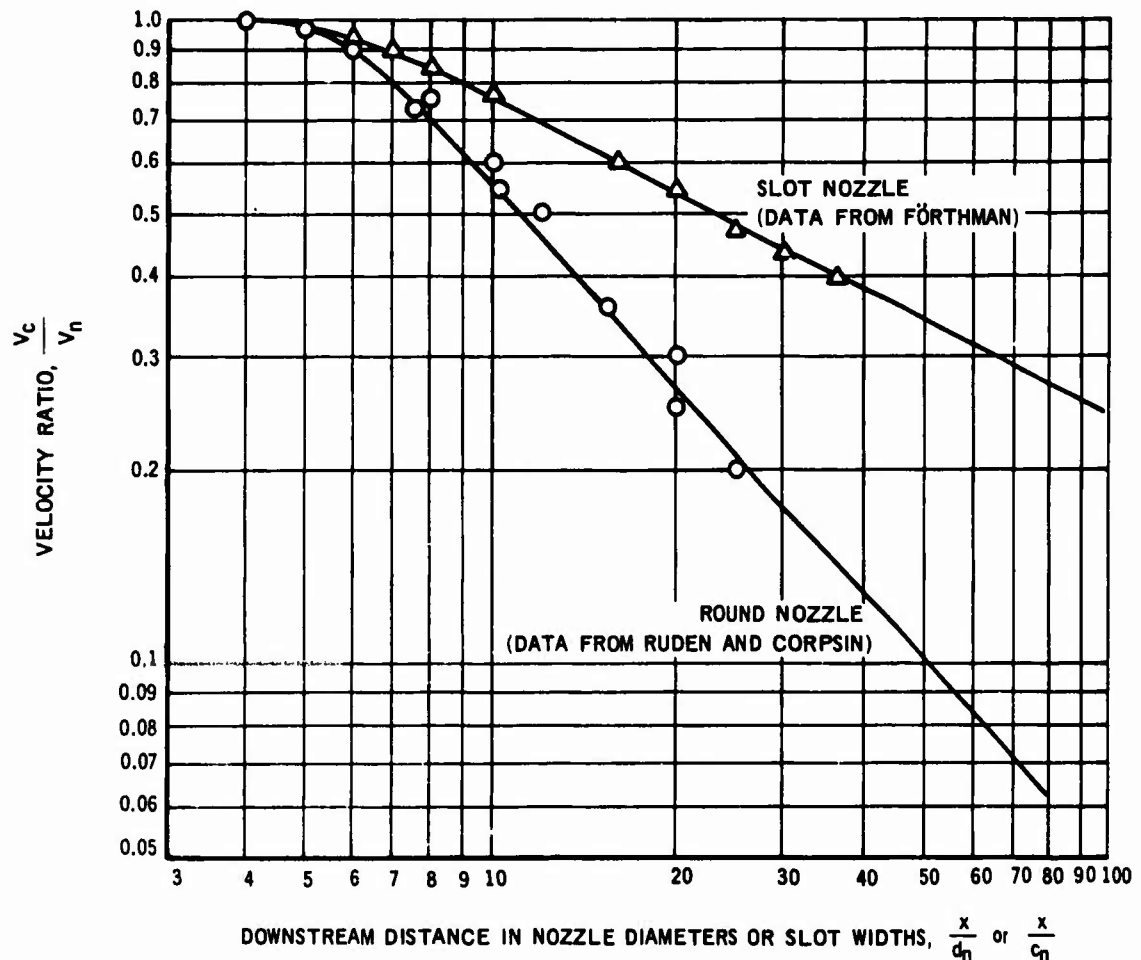


FIGURE 27. CENTER LINE VELOCITY ($V_s = 0$)

shows the centerline velocity decay for the annular and round jet, based upon the information obtained from the above reference for the slot nozzle, and Reference 6 for the round nozzle. From the figure it appears that the high velocity cone length is the same for both slot and round nozzles. The velocity decay rate is lower for the slot nozzle beyond the high velocity cone point. Thus, the second phase on entrainment and mixing takes place at a lower rate. This does not appear to affect the 50% V_c cone angle. Comparison between

the cone geometry for the round jet and the slot jet show negligible difference. It may be that nozzle exit to throat entry spacing, S , for annular ejectors with area ratios less than 0.265 needs to be slightly larger than for the equivalent simple ejector, in order to provide equivalent flow ratio. Further investigation is necessary to determine optimum ejector configuration and establish the criteria for optimization.

4.3.2 Annular Nozzle Performance

Only one basic annular nozzle was used in testing under this contract. The nozzle calibration curve has been previously presented in Figure 8. The nozzle discharge coefficient for this configuration was approximately 0.97, which is comparable to round nozzles tested under this contract. The original nozzle, shown in Configuration 3, Figure 25, was quite blunt at the exit station. The nozzle was later modified as shown in Configuration 4 Figure 25. Considerable improvement in ejector performance was attained by this change as shown in Figure 28. This improvement is attributed mainly to the increase in S length attained with the sharp exit configuration.

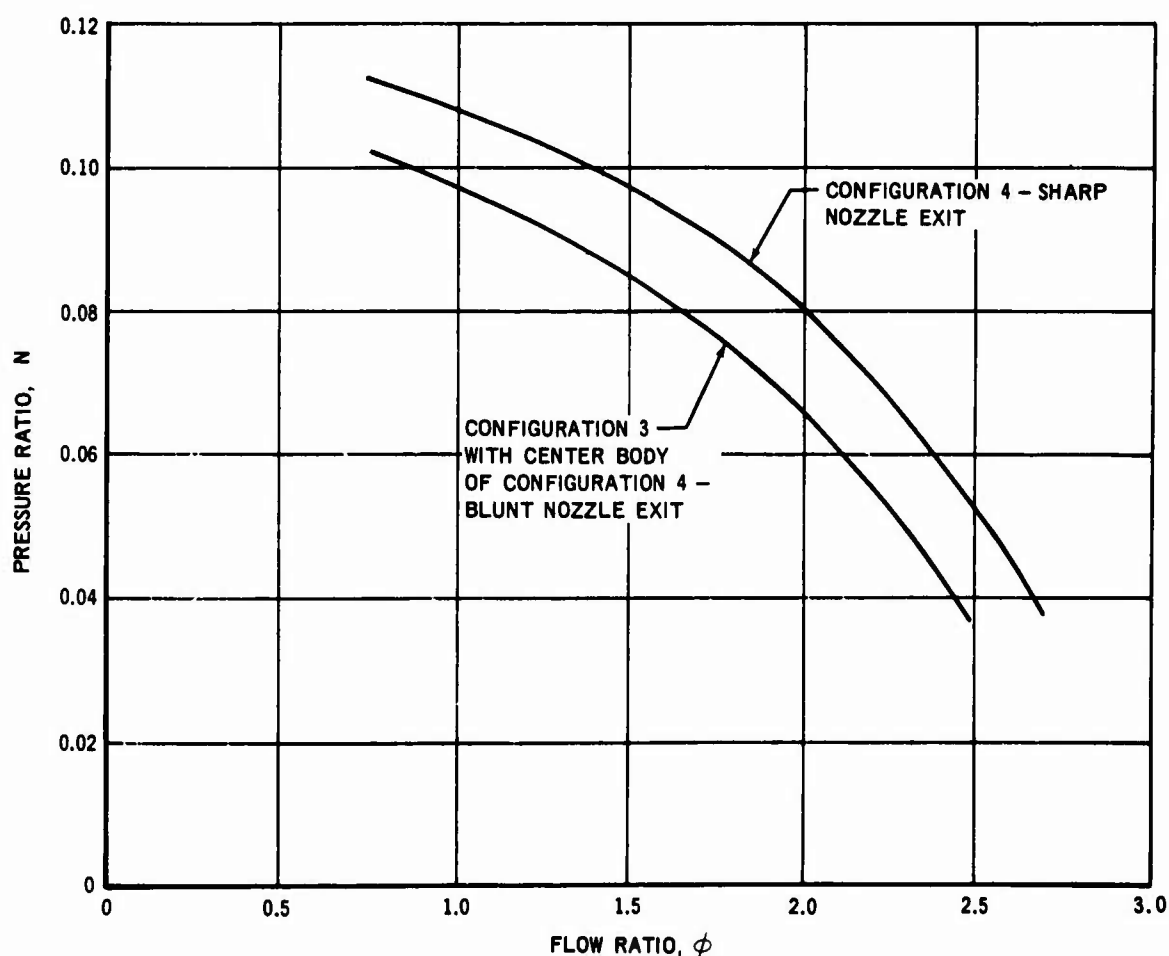


FIGURE 28. COMPARATIVE PERFORMANCE ANNULAR EJECTOR WITH BLUNT NOZZLE EXIT AND WITH SHARP NOZZLE EXIT

4.4 ALTITUDE AND TEMPERATURE EFFECTS ON EJECTOR PERFORMANCE

To determine the effects of altitude change on ejector performance, a series of simulated aircraft climbs were made. The results of these climb tests are shown in Figure 29. The ejector used for these tests is shown in Figure 15, Configuration 3, with a nozzle exit to throat spacing $S = 3\text{-}11/16$. The actual pump used is shown in Figure 37. The climb procedure was as follows. The ejector was operated at sea level and throttled to obtain maximum pressure at the maximum flow ratio point. Maintaining this condition the supply and receiver tank pressures were reduced to simulate a desired altitude.

Tank pressure altitude was changed in accordance with a time schedule as shown in Figure 30. The tank pressure variation was based on a typical high speed fighter which would climb from sea level to 60,000 feet in five minutes. The tank altitude pressure was corrected by adding 5 psi. The 5 psi was introduced as a requirement to prevent 135°F fuel boil-off in excess of 2 percent as specified in MIL-F-17874.

Three runs were made, using JP-5, at various temperatures as noted in Figure 29. T_o is the average ejector inlet fuel temperature and T_i the average motive nozzle fuel temperature for the run. One run was made, using JP-4, with an ejector inlet temperature of 130°F and motive nozzle temperature of 178°F average. Temperature variation for the runs was 10°F or less. An additional run, not shown on Figure 29, was made with JP-5 at 10°F. Flow ratios for this run corresponded closely with the -30°F JP-5 cold test shown in Figure 29.

Ejector pressure rise was set at sea level. The pressure at maximum flow ratio is shown in the following table with corresponding nozzle pressure.

Nozzle Pressure	Ejector Pressure Rise	Maximum Flow Ratio	Test.
$P_i - P_o$, psig	$P_d - P_o$, psi		
405	34	1.76	JP-5 ambient
380	26	1.97	JP-5 cold
405	32	1.71	JP-5 hot
400	37	1.58	JP-4 hot

A plot of equation (8) for limiting flow due to cavitation is shown in Figure 29, for $Y = 0.7 P_o$ and $Y = 0.5 P_o$. The value of K_1 used was 0.1. The cavitation predictions correspond well for $Y = 0.7 P_o$ and the JP-5 cold and ambient runs. For the hot JP-5 and JP-4 runs, the $Y = 0.5 P_o$ prediction

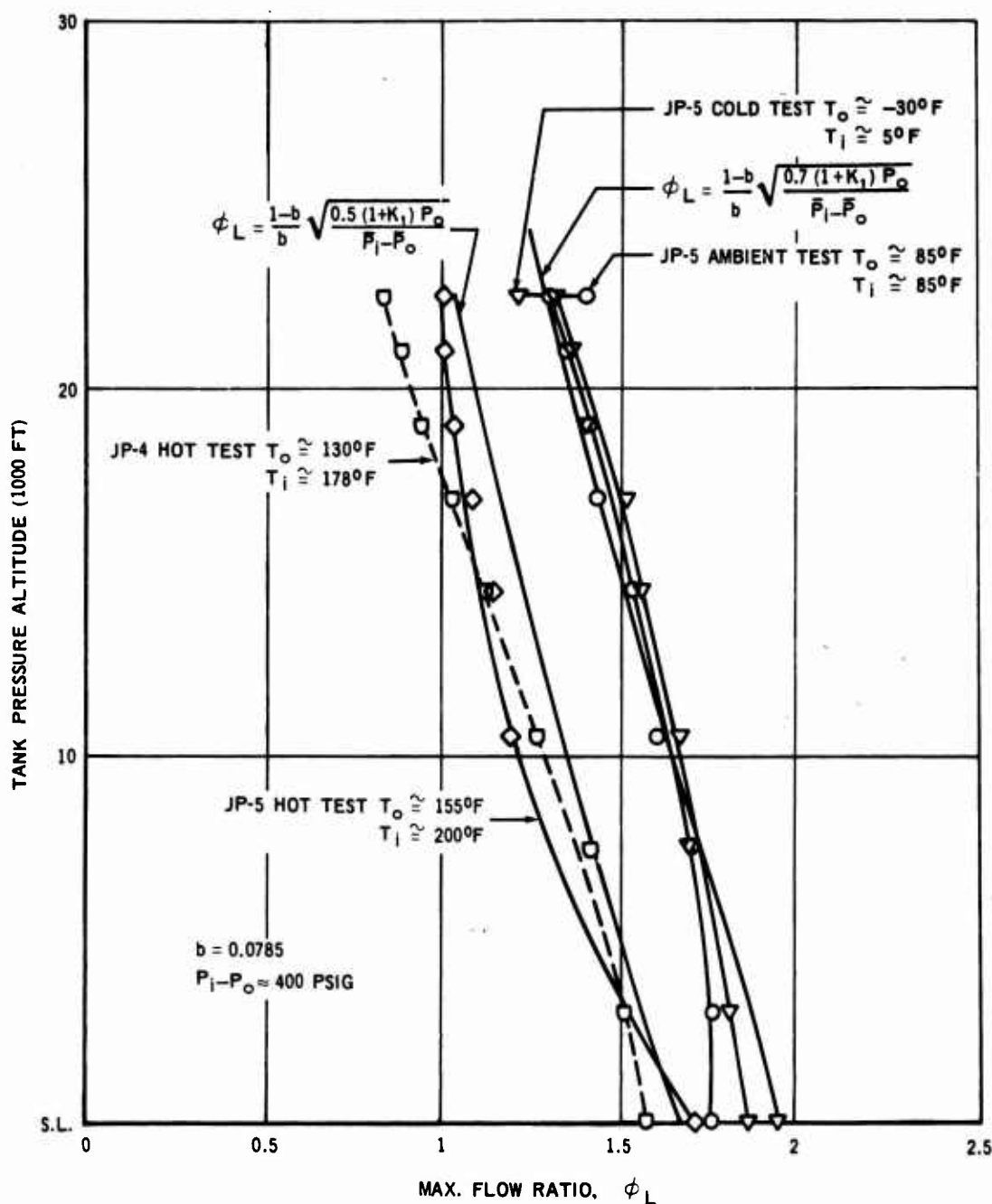


FIGURE 29. CLIMB TEST PERFORMANCE

is somewhat optimistic. Due to the climb rate, insufficient time for vapor boil-off in the tank may have provided a supersaturated fuel-vapor solution in the entrainment region of the ejector.

Visual observation of the ejector entrainment region, during these hot climb tests, indicated the presence of a large volume of vapor trapped in the area between the extended part of the mixing tube and the plenum (see Figure 15). From visual observation it appeared that the volume of vapor increased until some vapor was forced into the nozzle plume. The vapor was entrained in large quantities as altitude was increased. Vapor entrainment was unsteady creating an ejector discharge pressure surge. Ejector discharge pressure

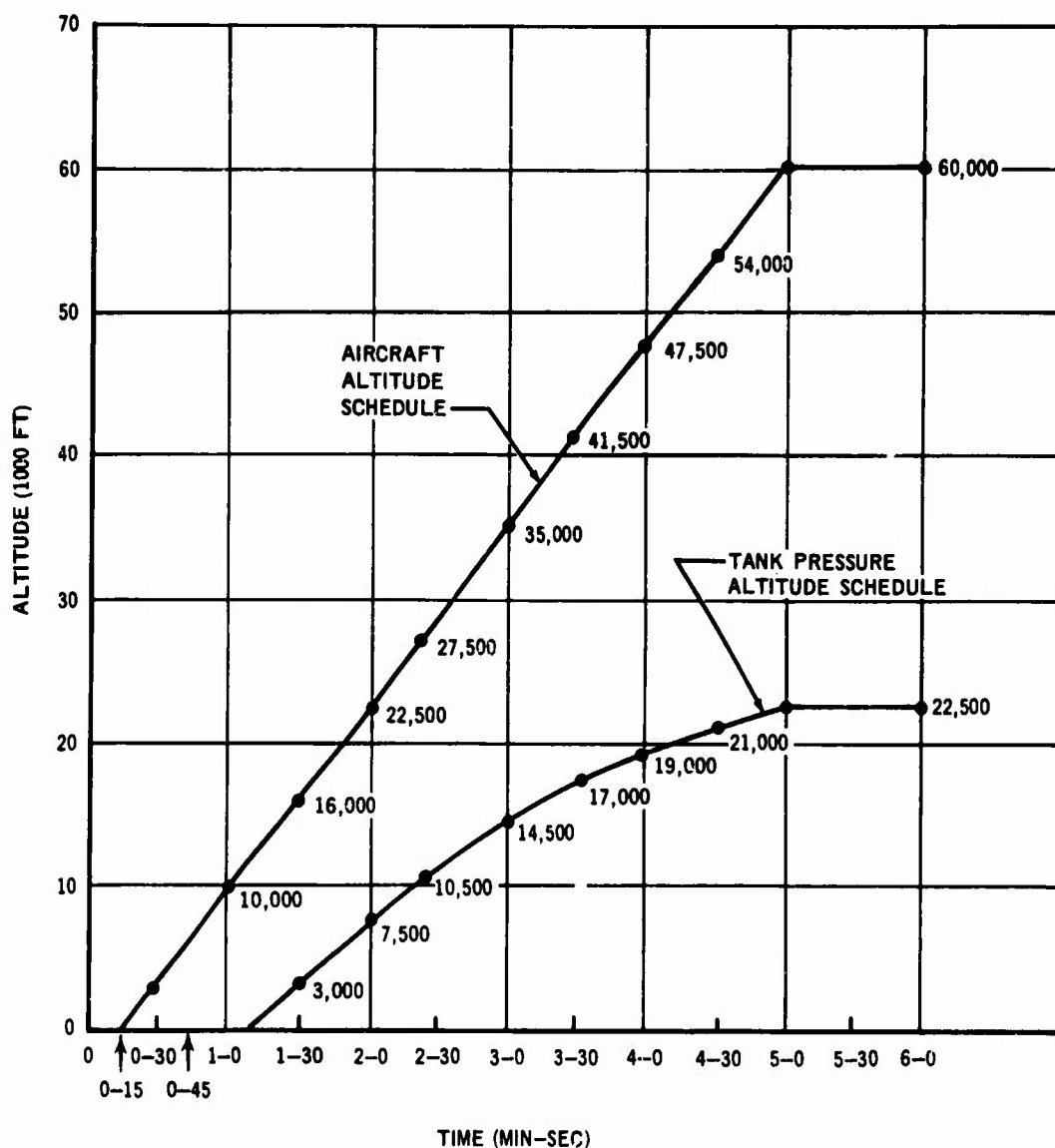


FIGURE 30. ALTITUDE CLIMB SCHEDULE

decreased from a reasonable value to zero and back again. The pressure cycling was fairly rapid, on the order of one cycle per every 2 to 3 seconds. This condition was probably the cause of the deterioration in performance below that anticipated. Vapor collection can be reduced by eliminating the trapping area.

The hot JP-4 and hot JP-5 acted very nearly the same during the climb test. This is attributed to the tank pressurization which prevented boiling. On the JP-4 tests, when attempting to reduce the tank pressure below that used for 60,000 feet plus 5 psi (6 psia), the fuel began to boil with a rapid degradation in performance.

An altitude test was performed using the annular ejector configuration as shown in Figure 25, configuration 4, except that nozzle to throat spacing, S , was approximately 0.6. This spacing appeared to be larger than optimum.

The results of the altitude test are shown in Figure 31. The test results conform closely to the predicted performance using equation (8) with $Y = 0.7 P_0$. No time schedule or tank pressurization was used for this altitude test. Nozzle flow was maintained at 85 gpm throughout the run. As maximum flow ratio decreased with altitude the ejector was throttled to obtain maximum discharge pressure at maximum flow ratio. The maximum pressures followed the normal pump-down curve as would be expected.

These tests appear to confirm Cunningham's (Reference 1) observations on the cavitation phenomenon. Cavitation can be predicted with reasonable accuracy by the use of equation (8) and the use of proper Y function values. The cavitation phenomenon has the same effect on annular ejector performance as on simple ejector performance.

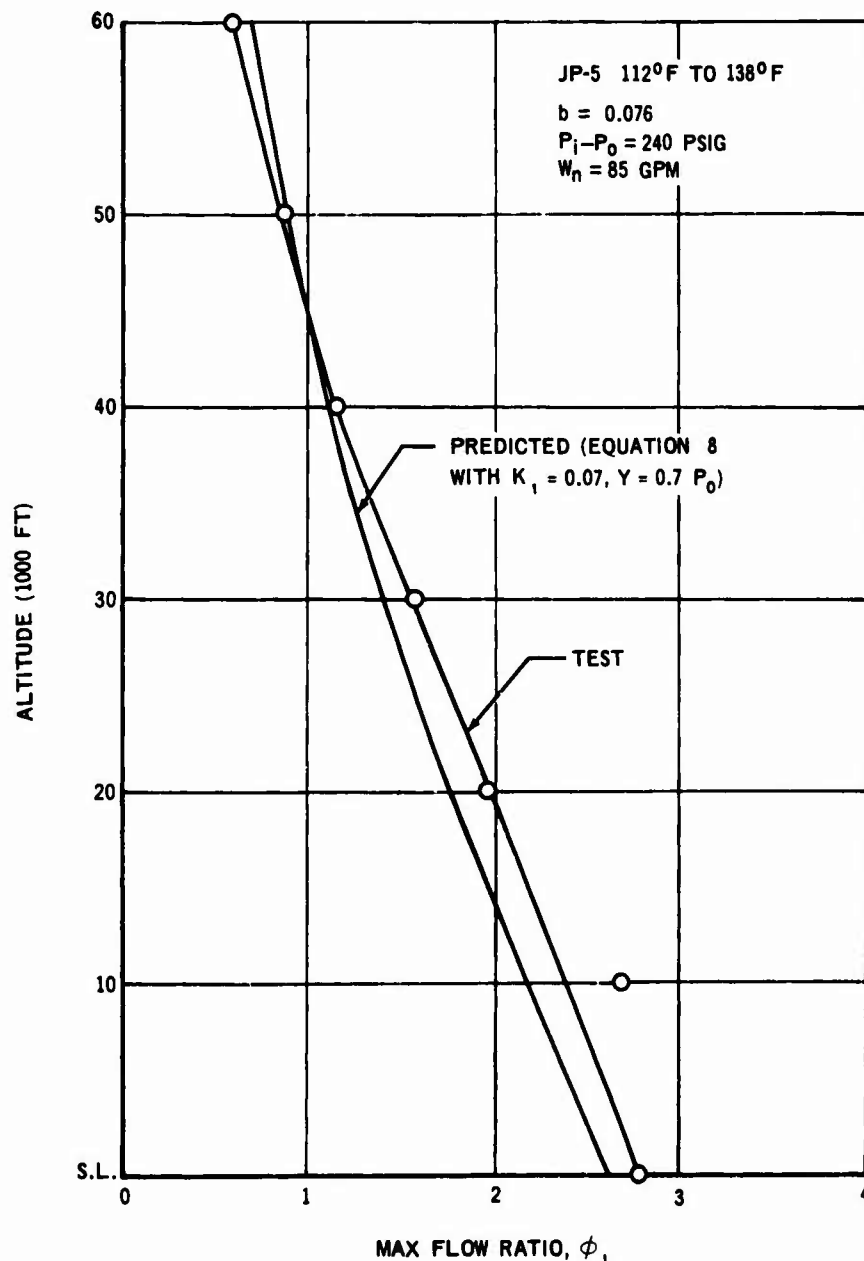


FIGURE 31. ANNULAR EJECTOR ALTITUDE PERFORMANCE

4.5 EJECTOR PUMP COMBINATIONS

There are innumerable combinations of ejectors which can be considered. Some of the combinations considered under this contract are described in the following discussion. All can be listed in the following categories:

- a. Series induced flow ejectors
- b. Series staged ejectors
- c. Series parallel staged ejectors
- d. Dual operation ejectors

4.5.1 Series Induced Flow Ejector

A series induced flow ejector is one using a single motive flow nozzle in which induced flow is entrained in steps. This type of ejector has two or more mixing sections. Such an ejector with two steps of entrainment is shown in Figure 32. Motive flow entrains fluid in the first stage. The mixed flow of the first stage is then used as motive flow for the second stage. Thus,

$$\phi_1 = \frac{W_{s1}}{W_n} \quad , \quad \phi_2 = \frac{W_{s2}}{W_n + W_{s1}}$$

The total induced flow $W_{st} = W_{s1} + W_{s2}$ and the total flow ratio

$$\phi_T = \frac{W_{s1} + W_{s2}}{W_n} = \phi_1 + \phi_2 (1 + \phi_1) \quad (14)$$

The equation for N can be modified to

$$N = \frac{\bar{P}_d - \bar{P}_o}{(\bar{P}_i - \bar{P}_o) - (\bar{P}_d - \bar{P}_o)}$$

$$N_1 = \frac{(\bar{P}_d - \bar{P}_o)_1}{(\bar{P}_i - \bar{P}_o) - (\bar{P}_d - \bar{P}_o)_1}$$

$$N_2 = \frac{(\bar{P}_d - \bar{P}_o)_2}{(\bar{P}_i - \bar{P}_o)_2 - (\bar{P}_d - \bar{P}_o)_2}$$

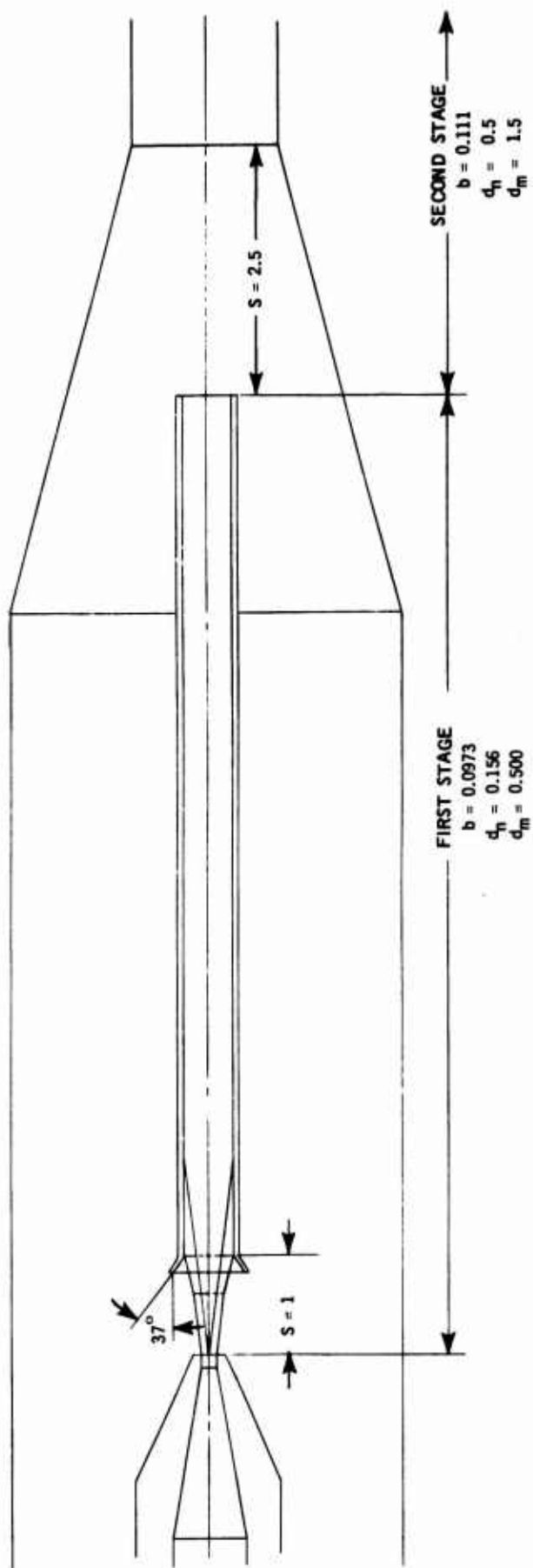


FIGURE 32. SERIES INDUCED FLOW EJECTOR

Since the discharge pressure of the first stage is essentially the motive nozzle pressure of the second stage

$$(\bar{P}_i - \bar{P}_o)_2 = (P_d - P_o)_1$$

The total pressure difference ratio for the pump combination is

$$N_T = \frac{(\bar{P}_d - \bar{P}_o)_2}{(\bar{P}_i - \bar{P}_o) - (\bar{P}_d - \bar{P}_o)_2}$$

by mathematical manipulation

$$N_T = \frac{N_1 N_2}{1 + N_1 + N_2}$$

In the above equations it has been assumed that the inlet pressure of both stages is approximately the same. Thus

$$\bar{P}_{o1} = \bar{P}_{o2}$$

Reference 10 presents a system which is similar to that being discussed here in which two separate ejectors are plumbed to provide a system comparable to that of Figure 32. The relationship of the first stage to the second stage as derived was determined by the ratio of the first stage motive nozzle diameter to the second stage nozzle diameter. The resultant equation is

$$\frac{d_{n1}}{d_{n2}} = \left(\frac{1}{1 + \phi_1} \right)^{1/2} \cdot \left(\frac{N_1}{1 + N_1} \right)^{1/4} \left[\frac{(1 + K_1)_1}{(1 + K_1)_2} \right]^{1/4} \quad (16)$$

The equation is derived from the motive nozzle pressure drop ratio (equation (1)) of the first stage to the second stage,

$$P_i - P_o)_1 (P_i - P_o)_2$$

Assuming the motive nozzle loss coefficients of both stages are the same

$$\frac{d_{n1}}{d_{n2}} = \left(\frac{1}{1 + \phi_1} \right)^{1/2} \left(\frac{N_1}{1 + N_1} \right)^{1/4} \quad (17)$$

For the case of Figure 32, $d_{n2} = d_{m1}$. Thus equation (17) becomes

$$\frac{d_{n1}}{d_{m1}} = \left(\frac{1}{1 + \phi_1} \right)^{1/2} \left(\frac{N_1}{1 + N_1} \right)^{1/4} = \sqrt{b_1}$$

In this specialized case $b_1 b_2 = b_T$ where

$$b_T = \left(\frac{d_{n1}}{d_{m2}} \right)^2$$

or the overall area ratio of the ejector combination. In accordance with Reference 10, the first stage will operate at one point which is the point of intersection of the N versus ϕ character-curve for the first stage and a plot of equation (17). Such a plot is shown in Figure 33 for the configuration of Figure 32. The intersection point gives $N_1 = 0.116$ and $\phi_1 = 2.32$. At this point $\phi_2 = 0$. Thus, the second stage will start to entrain fluid at the point where $\phi_1 = 2.32 = \phi_T$. Throttling the ejector to a flow ratio less than $\phi_1 = 2.32$ will result in recirculation of induced fluid between the second and first stages. The value of N_t at, say $\phi_1 = \phi_T = 1$ will be a function of the pressure balance between the feed line pressure drop and the pressure drop of the recirculation path; i. e., the fluid back flow from the second stage to the first stage.

Test results for the ejector configuration of Figure 32 as shown in Figure 34. During the tests, the ejector was throttled to the $\phi_2 = 0$ point by visually observing the flow through the acrylic parts of the pump. The point at which second stage induced flow stopped is noted in Figure 34. The flow ratio at that point was approximately 3.94. The two curves are for a motive nozzle pressure of 100 and 300 psig.

It is apparent that the $\phi_2 = 0$ does not match that anticipated by equation (17). $N_T = 0.0149$ for the 300 psig nozzle pressure curve at the $\phi_2 = 0$ point; at 100 psig nozzle pressure the corresponding $N_T = 0.0316$. Since the area ratio of the second stage is $b = 0.111$, at the $\phi_2 = 0$ point, $N_2 \cong 0.260$ ($K_1 = 0.1$, $K_{34} = 0.25$). From equation (15);

$$N_{1(300)} = \frac{(0.0149)(1.260)}{0.245} = 0.0765$$

$$N_{1(100)} = \frac{(0.0136)(1.260)}{0.246} = 0.0696$$

$$(\bar{P}_d - \bar{P}_o)_1 (300) = \frac{(0.0765)(300)}{1.0765} = 21.4 \text{ psi}$$

$$(\bar{P}_d - \bar{P}_o)_1 (100) = \frac{(0.0696)(100)}{1.0696} = 6.5 \text{ psi}$$

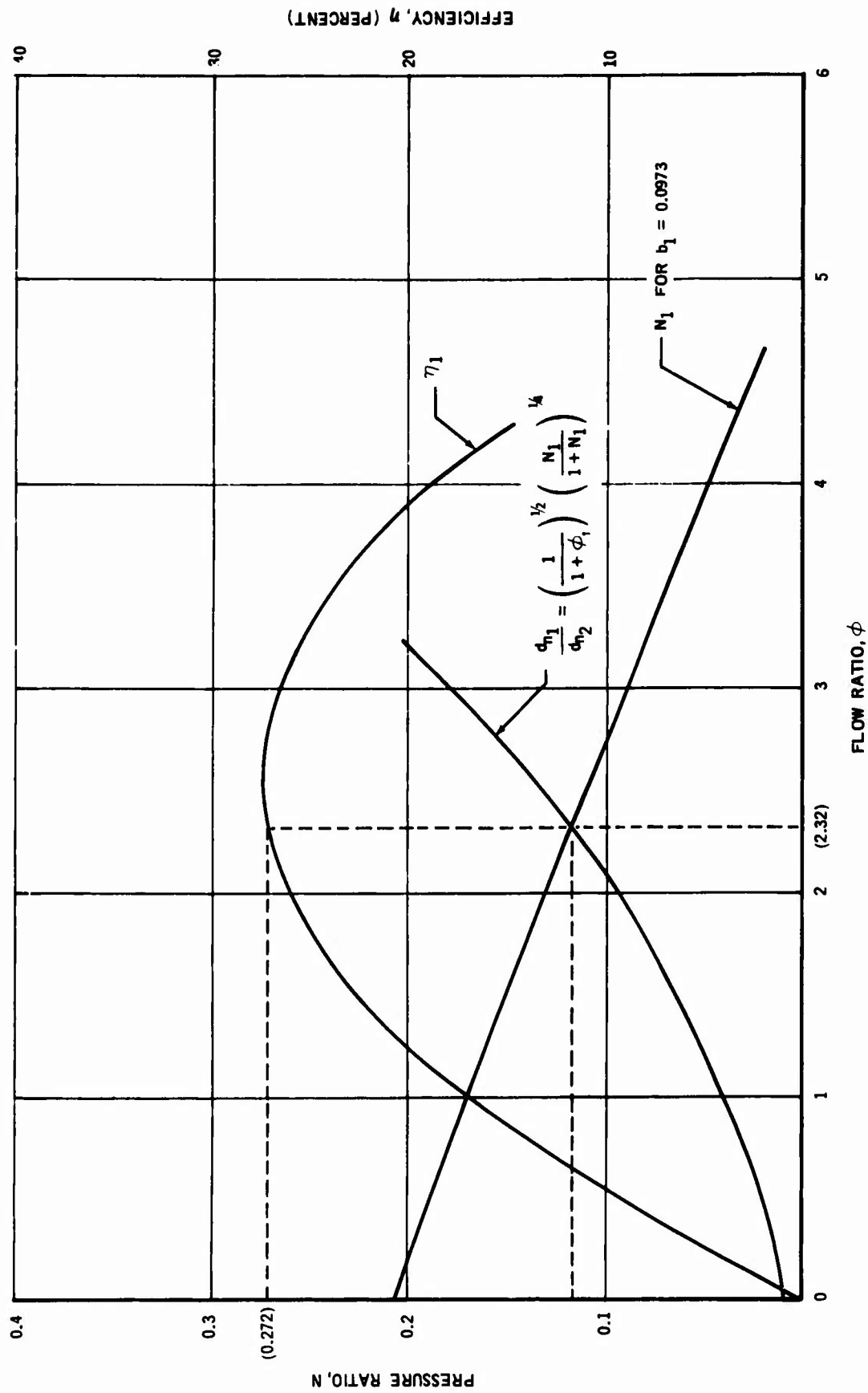


FIGURE 33. OPERATING CURVES FOR SERIES INDUCED PUMP

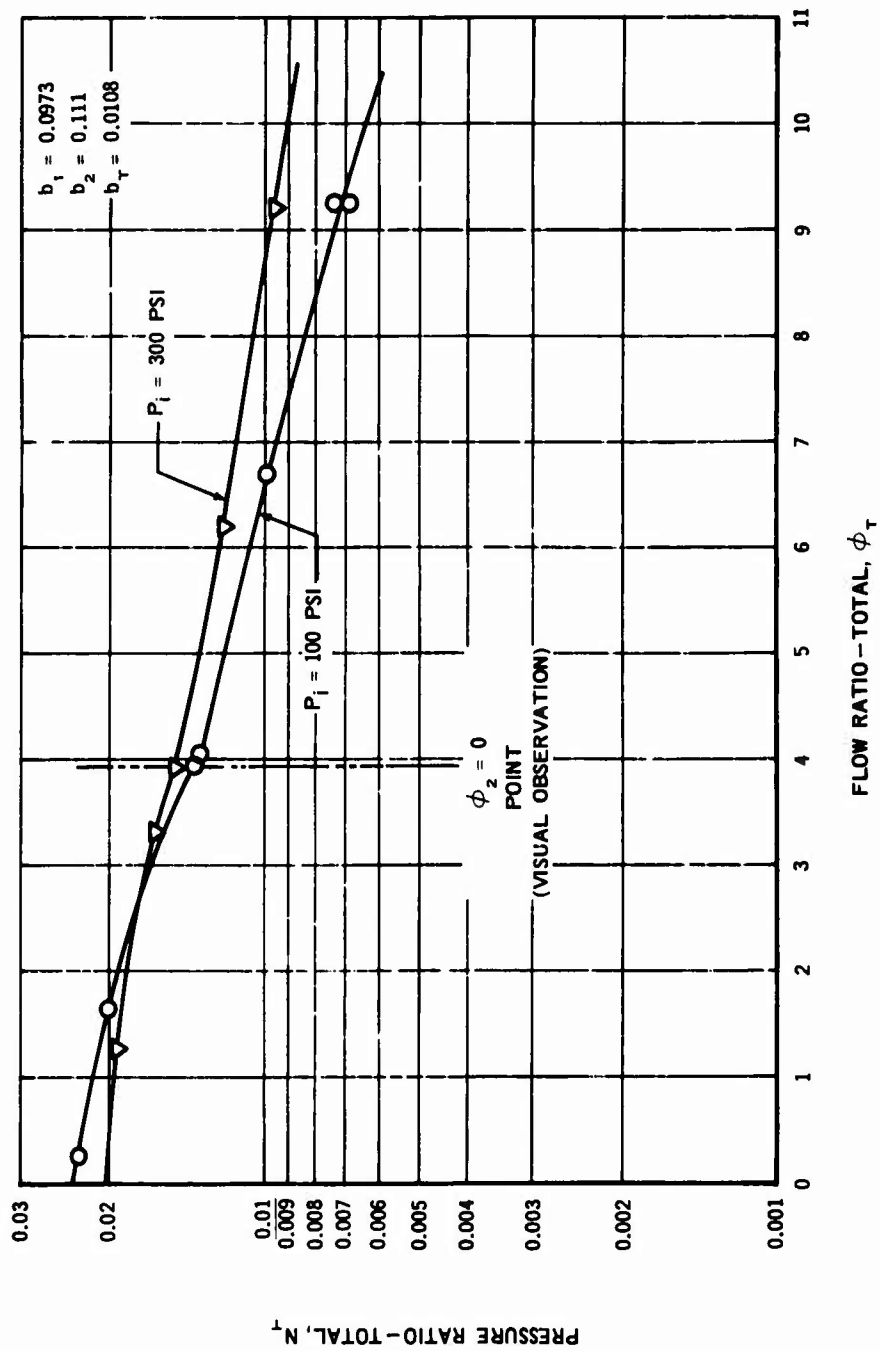


FIGURE 34. TEST CURVES FOR SERIES INDUCED PUMP

Since there is no induced flow at the second stage, the pressure drop from the second stage nozzle to the ejector discharge is, from equation (3);

$$(\bar{P}_i - \bar{P}_d)_2 = (\bar{P}_d - \bar{P}_o)_1 - (\bar{P}_d - \bar{P}_o)_1 = \frac{(\bar{P}_d - \bar{P}_o)_1}{(1 + K_1)_2} \left[1 + K_1 - 2b_2 + (1 + K_{34})_2 b_2^2 \right]$$

Since K_1 has been assumed to be 0.1 and $K_{34} = 0.25$

$$(\bar{P}_d - \bar{P}_o)_1 - (\bar{P}_d - \bar{P}_o)_2 = \frac{(\bar{P}_d - \bar{P}_o)_1}{1.1} [1.1 - 0.222 + 0.0154]$$

$$(\bar{P}_d - \bar{P}_o)_1 - (\bar{P}_d - \bar{P}_o)_2 = 0.81 (\bar{P}_d - \bar{P}_o)_1$$

$$(P_d - P_o)_2 = 0.19 (\bar{P}_d - \bar{P}_o)_1$$

For

$$(\bar{P}_d - \bar{P}_o)_1 \approx 21.4 \text{ psi}$$

$$(\bar{P}_d - \bar{P}_o)_2 = 4.06 \text{ psi}$$

For

$$(\bar{P}_d - \bar{P}_o)_1 \approx 6.5 \text{ psi}$$

$$(\bar{P}_d - \bar{P}_o)_2 = 1.23 \text{ psi}$$

From test data for these points $(\bar{P}_d - \bar{P}_o)_2 = 4.4 \text{ psi}$ and 1.34 psi for motive nozzle pressures of 300 and 100 psi respectively. Since the pressures calculated from the assumed K values are lower than test values it is assumed that the losses were actually less than those assumed.

Substituting test values for calculated values of pressure

$$(\bar{P}_d - \bar{P}_o)_{2(300)} = 4.4 = 21.4 (1 - K_e)$$

$$(\bar{P}_d - \bar{P}_o)_{2(100)} = 1.34 = 6.5 (1 - K_e)$$

$$1 - K_e \approx 0.206 \text{ for both cases.}$$

The second stage abrupt expansion loss is thus $K_e = 0.794$. A much used expression for abrupt expansion loss gives the total loss,

$$K_e \cong \left[1 - \frac{A_1}{A_2} \right]^2 = \left[1 - b \right]^2 \quad (18)$$

For

$$b = 0.111, K_e \cong \left[0.889 \right]^2 \cong 0.79$$

This expression simplifies analysis procedure by eliminating the need for laborious trial and error calculation using various assumed values of K_1 and K_{34} . It is only applicable at the ejector condition of $\phi = 0$, however, and only applicable for the nozzle to ejector discharge pressure drop.

From the results of these tests, it would appear that the first stage of the ejector sees the second stage as only an additional pressure drop in the feed system. The first stage will always operate at its maximum capacity commensurate with the pressure drop requirements dictated by second stage and feed line conditions. Since test data appear to confirm the constant value for K_e for equation (18), it is relatively easy to estimate the second stage loss and add it to the feed line loss when determining the first stage operating point. Before the second stage will begin to pump fluid, a discrete pressure drop across the stage must exist. The loss coefficient describing this pressure drop is a constant for any given value of area ratio, b .

Another configuration tested had a first stage area ratio $b_1 = 0.052$. The second stage area ratio was the same as the configuration shown in Figure 32, $b_2 = 0.111$. The points of operation at $\phi_2 = 0$ are as shown below.

$(\bar{P}_i - \bar{P}_o)_1$	ϕ_T	N_T
298 psi	2.64	0.0145
400 psi	2.42	0.0149
495 psi	2.53	0.0145

Since $N_2 \approx 0.260$ at $\phi_2 = 0$, the results shown are quite consistent with results obtained for the first configuration except that flow ratios are less. These flow ratios are quite realistic for the first stage area ratio used. Referring to Figure 7 for a $b = 0.05$ configuration and an $N_1 \approx 0.076$, the flow ratio is approximately $\phi_1 = 2.5$.

The series induced flow ejector configuration was considered under this contract because it appeared to offer a method of overcoming cavitation. The overall performance of this configuration does not appear to be an improvement over an equivalent simple ejector. Instead, a penalty is paid for the additional entrainment and mixing process required by staging.

From Cunningham's equation (Reference 1) for limiting flow ratio due to cavitation (equation (8)), values of limiting flow can be calculated for the first stage of the configuration shown in Figure 32. A comparison is shown below between these calculated values and the test values obtained for $\phi_2 = 0$. Y , in equation (8) is assumed to be $0.7P_{01}$.

Motive Nozzle Pressure:

$(\bar{P}_1 - \bar{P}_o)_1$	b_1	ϕ_{1L} calculated	ϕ_1 test
100	0.0973	3.20	3.94
300	0.0973	1.85	3.92

It is apparent that the first stage operation points exceeded those anticipated, considering the effects of cavitation for both nozzle pressure. From Figure 32 note that the nozzle plume diameter matches the mixing tube diameter at the throat entry, thus indicating an optimum S spacing. In addition, the flared tube throat entry is close to an optimum radiused configuration, and is short. The ratio of plenum diameter to throat diameter is

$$\frac{d_o}{d_m} = 8 ; \frac{A_o}{A_m} = 64$$

At the $\phi_1 = 3.92$ condition, using 300 psi nozzle pressure, the induced flow rate was 20,700 pounds per hour; $V_s \approx 1.29$ ft/sec;

$$\frac{V_s}{V_n} \approx \frac{1.29}{215} \approx 0.006$$

The limiting flow velocity ratio, from equation (9), modified for JP-5 air evolution is

$$\frac{V_s}{V_n} = \sqrt{\frac{0.7(1+K_1)P_o}{\bar{P}_i - \bar{P}_o}} \approx \sqrt{\frac{(0.7)(1.1)(14.7)}{300}} = 0.194$$

The ratio of these two values is

$$\frac{\lambda_{\text{Test}}}{\lambda_L} = \frac{0.006}{0.194} = 0.031$$

Thus it appears that a ratio of about 0.03 eliminates cavitation problems, at least up to flow ratios of 4.

It is of interest to note that the second stage mixing tube and diffuser was the same part used for the simple ejectors discussed in Section 4.2.5. From tests with the staged ejector, the loss coefficient K_{34} is less than 0.25, which further substantiates the assumption that the high K_{34} values obtained in the simple ejector tests are a function of induced flow aeration, or multiphase flow.

4.5.2 Series Staged Ejectors

A series staged ejector is one consisting of two or more simple ejectors arranged in series. Thus, the discharge pressure of one stage is the inlet pressure of the next stage downstream, or

$$P_{d1} = P_{o2}$$

The induced flow of the last stage is the sum of the induced flow of the first stage plus the motive flow of all stages. Thus for a two stage ejector configuration,

$$W_{s2} = W_{s1} + W_{n1}$$

$$W_{s2} = W_{n1}(\phi_1 + 1)$$

Reference 11 defines the total mass flow ratio of the system as the product of the mass flow ratios of the individual stages, where the mass flow ratio is defined as the total mass flow leaving the ejector or stage divided by the induced flow entering. Using this definition it can be shown that,

$$W_{n2} = \frac{\phi_1 + 1}{\phi_2} W_{n1}$$

Thus

$$\frac{W_{n1}}{W_{n2}} = \frac{\phi_2}{1 + \phi_1}$$

Reference 11 also defines that one of the design criteria be to have all stages operate at the same maximum available pressure. Thus $\bar{P}_{i_1} = \bar{P}_{i_2} = \bar{P}_i$. For a two stage ejector:

$$N_1 = \frac{\bar{P}_{d_1} - \bar{P}_o}{(\bar{P}_i - \bar{P}_o) - (\bar{P}_{d_1} - \bar{P}_o)} = \frac{\bar{P}_{d_1} - \bar{P}_o}{\bar{P}_i - \bar{P}_{d_1}}$$

$$N_2 = \frac{\bar{P}_{d_2} - \bar{P}_{d_1}}{\bar{P}_i - \bar{P}_{d_2}}$$

$$N_T = \frac{\bar{P}_{d_2} - \bar{P}_o}{\bar{P}_i - \bar{P}_{d_2}}$$

By mathematical manipulation

$$N_T = N_1 + N_2 (1 + N_1) \quad (18)$$

By definition

$$\phi_1 = \frac{W_s}{W_{n_1}} ; \quad \phi_2 = \frac{W_s + W_{n_1}}{W_{n_2}}$$

For a two stage ejector:

$$\phi_T = \frac{W_s}{W_{n_1} + W_{n_2}}$$

Thus it can be shown that

$$\phi_T = \frac{\phi_1 \phi_2}{1 + \phi_1 + \phi_2} \quad (19)$$

Substituting

$$\phi_2 = \frac{W_{n_1}}{W_{n_2}} (\phi_1 + 1)$$

for ϕ_2 in equation (19)

$$\phi_T = \frac{\phi_1 W_{n1}}{W_{n2} + W_{n1}}$$

To obtain highest total flow ration, W_{n2} must be zero and $\phi_T = \phi_1$. In other words, the optimum solution for maximum flow ratio reverts to the simple, single stage ejector. For $W_{n2} > 0$, ϕ_T will always be less than ϕ_1 .

For the two stage ejector configuration, it would appear that the first stage must be designed to give the best possible flow ratio. In the study of Reference 11 the discussion mainly concerned the pumping of gases. The conclusion drawn from this reference was that each stage should operate at or near its breakoff point, where the breakoff point was defined as that point at which the induced gas flow achieves sonic velocity in the throat of the ejector. The equivalent break point for the liquid pumping ejector is the cavitation limit. Thus, if it is assumed that cavitation is an incurable ailment of the ejector, the first stage must be designed to provide the required induced flow at the critical inlet or altitude condition within the flow ratio limit as determined by equation (8). Moreover, a minimum first stage discharge pressure can be prescribed by assessment of the vapor pressure of the liquid being pumped, so that liquid delivered to the second stage inlet is at a pressure equal to or higher than the vapor pressure.

For the staged ejector, it is best, at least at the critical design flow ratio, for each stage to operate at maximum efficiency: The maximum efficiency point or mep can be approximately determined from the simple equation defining the ejector mixing tube average Reynolds number, where, by continuity:

$$R_m = \sqrt{b \phi (1 + \phi) R_n}$$

where R_n = nozzle exit Reynolds number. At the condition for equality between mixing tube and jet momentum $R_m = R_n$. Thus the flow ratio at or near maximum efficiency is

$$\phi \cong \frac{1}{\sqrt{b}} - 1 \quad (20)$$

If ϕ of equation (20) is made to be ϕ_L for equation (8), then

$$\phi_{mep} \approx \phi_L = \frac{1-b}{b} \sqrt{\frac{(1+K_1) Y P_o}{P_i - P_o}} = \frac{1}{\sqrt{b}} - 1$$

Knowing the maximum available nozzle pressure, the desired flow ratio and the critical operating altitude, preliminary stage sizing can be defined by the above relationship.

4.5.3 Series - Parallel Staged Ejectors.

A Series - Parallel staged ejector operates in a similar manner to the series staged ejector except that some of the induced flow is allowed to flow to the intermediate and final stages of the ejector combination without benefit of initial pressure increase. Analysis of such an ejector becomes difficult because of the many variations of allowable intermediate stage induced flow that are possible. A two stage ejector, utilizing series and parallel flow, is shown in Figure 35. The first stage, a simple ejector, pumps fluid to the second stage. The second stage, in this case an annular nozzle, not only receives flow from the first stage but also from the inlet line directly.

This type of configuration has two advantages. For one thing, the total induced flow can be greater than for series staged configurations. This advantage, however, is secured at the expense of output pressure. The second advantage is that operation under throttled conditions can be accomplished without the accompanying high discharge pressure associated with series staged configurations. A series staged ejector will react to throttling by a corresponding decrease in first stage flow ratio.

The accompanying pressure rise is compounded by the second stage pressure rise. The discharge pressure will tend to rise sharply as the ejector is throttled. With an ejector combination permitting direct induced flow at the intermediate stages, throttling is accompanied by each stage, in succession starting with the last stage, following its own pump-down characteristic, until the directly induced flow of the stage is zero. As throttling is continued, the flow of the last stage will be increasingly recycled to the intermediate stages. The resultant pressure rise of the ejector at $\phi_1 = 0$ can be considerably less than the pressure rise of a series staged ejector depending on the amount of intermediate stage secondary flow inducement permitted i.e., the amount of stage recirculation permitted.

The performance of the series - parallel ejector of Figure 35 is shown in Figure 36. The lower curve is the performance of the second stage annular ejector operating without first stage boost. The upper curve shows the performance of the combined stages. In this case, stage motive nozzle pressures were not the same, as is indicated in Figure 36. Note that the curve slope changes at an induced flow of approximately 32 gpm. At lower induced flows, considerable recirculation between the two stages was noted. Better performance than that indicated is probable if the design of the stages is optimized. As was indicated in section 4.3 annular ejector design optimization requires further research. The flow characteristics can also be changed by either increasing or decreasing the second stage direct induced flow passage area. As was noted before, a multitude of variations are possible by this process.

4.5.4 Dual Operation Ejectors

Dual operation is possible for aircraft engine feed systems, where both non-afterburning and afterburning operating modes exist. This is made possible by the use of two engine driven pumps, one, the main engine pump for operation to military power, the other, the afterburner pump for operation up to full afterburner thrust.

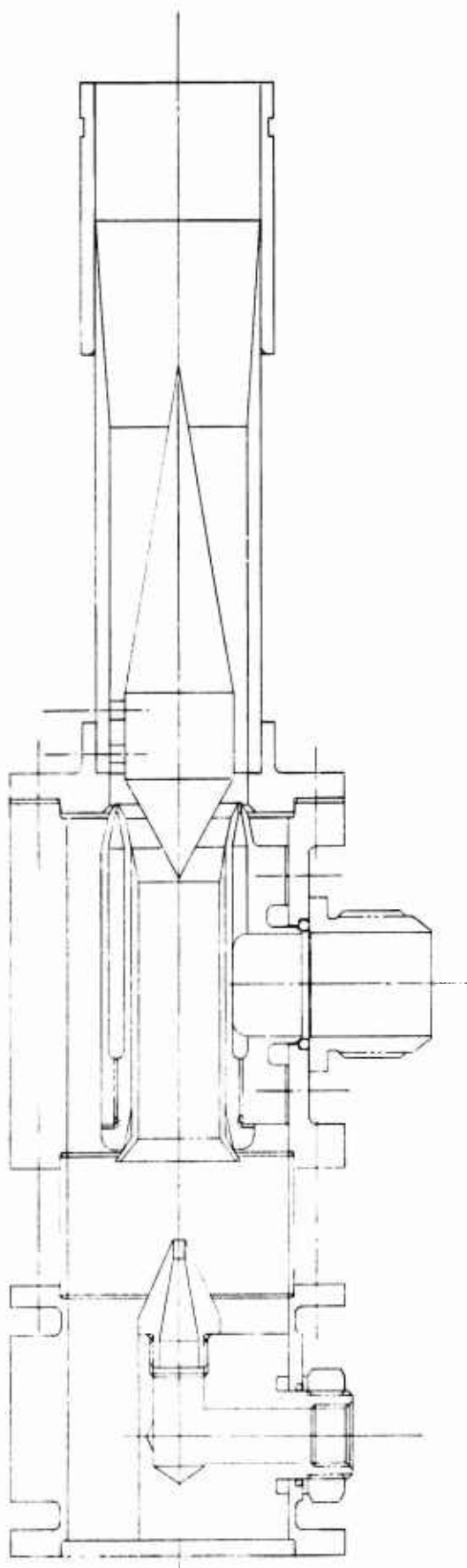


FIGURE 35. SERIES - PARALLEL STAGED EJECTOR

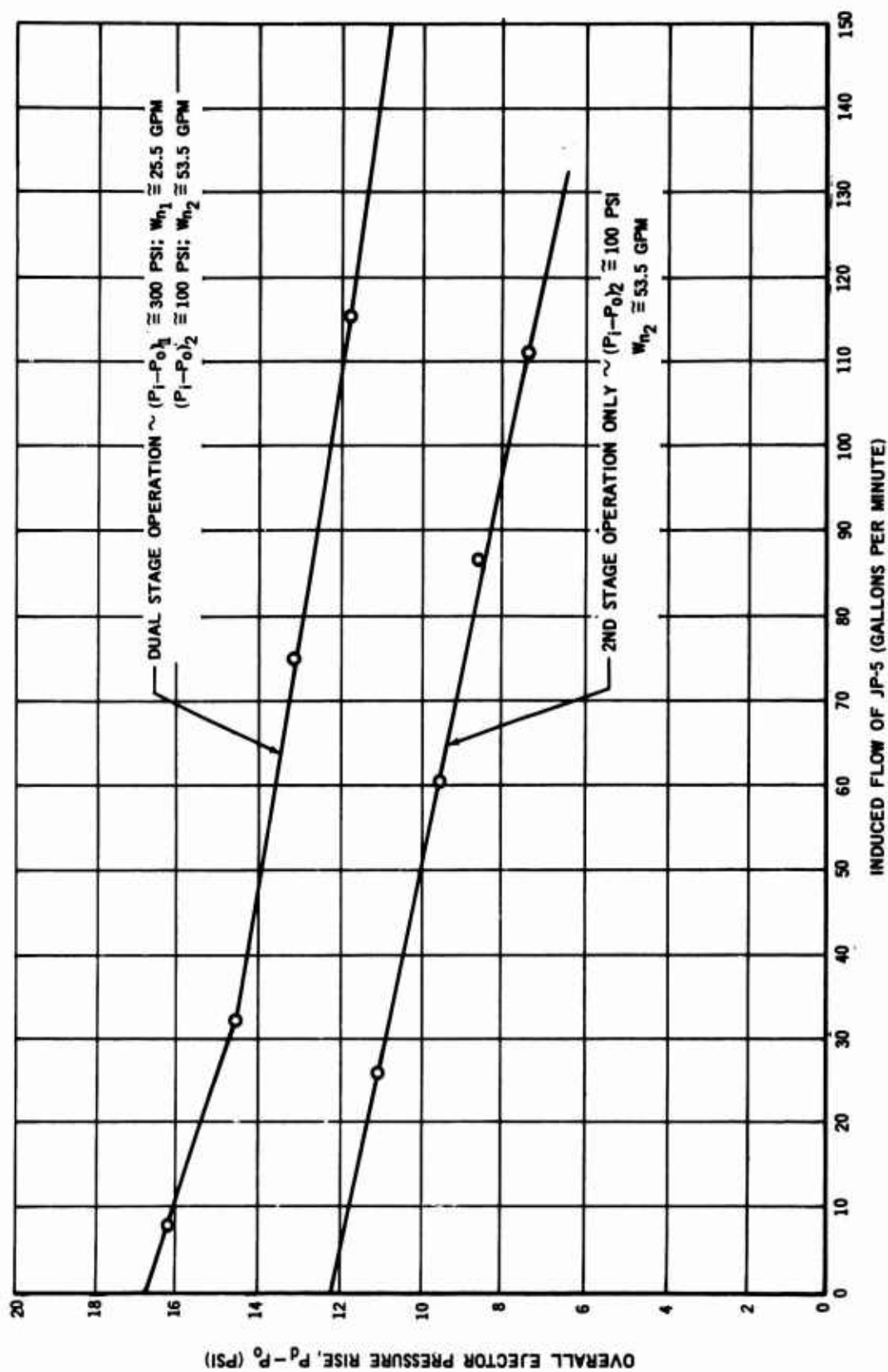


FIGURE 36. SERIES - PARALLEL EJECTOR PERFORMANCE SEA LEVEL OPERATION

The dual operation technique can be combined with the series staging, or series parallel staging configurations, or used with simple ejector configurations.

As applied to series, two stage ejectors the main engine pump could provide motive flow for the first stage of the ejector. This stage would be designed for high induced flow capacity such that at maximum afterburner thrust it could deliver the required induced flow, but at a low pressure. When throttled to military power flow this stage would deliver fuel at the desired output pressure. When in the afterburner mode, the second stage of the ejector, operated by fuel from the afterburner pump, would increase the ejector discharge pressure to the required level at the full afterburner flow demand. Applying dual operation to the series-parallel two stage ejector results in a different arrangement. To avoid interstage recirculation it is probably best to use the second stage to provide fuel to the engine up to full military power. The first stage could be used to augment pressure and flow for afterburner operation.

A dual operation simple ejector is shown in Figure 37. Dual operation is achieved by the use of two concentric motive nozzles. With this arrangement the flow to the smaller nozzle would be provided by the main engine pump and flow to the large nozzle provided by the afterburner pump.

Dual operation allows economies in motive fuel usage at lower engine power operating modes. Thus, for normal operation up to military power, less fuel is circulated than would be possible if single operation design were used.

4.5.5 Optimum Combinations

From the previous discussion, it appears that the series induced flow ejector configuration provides no advantages over the optimum simple ejector.

It has been shown that for maximum flow ratio, the series staged ejector reverts to a simple ejector configuration. If, however, high discharge pressure cannot be attained by simple ejector means, series staging may be a practical solution.

The series-parallel ejector combination may offer the advantage of higher induced flow capability and pressure boost. In this case, the second stage of the ejector combination must have high flow ratio capability. The first stage adds just sufficient high pressure flow so that the mixed flow pressure to the second stage inlet permits the attainment of the desired discharge pressure.

The series-parallel ejector combination shown in Figure 35 is unique in that the outer nozzle plume surface entrains fluid from an inlet pressure \bar{P}_0 while the inner plume surface entrains fluid from an inlet pressure \bar{P}_{d1} . It is considered that this combination may have advantages over series-parallel ejector combinations using simple ejector stages. More study of this configuration is needed to optimize design.

Of the combinations studied, the series-parallel ejector using an annular second stage, appears most promising. However, further development is required to achieve its potential.

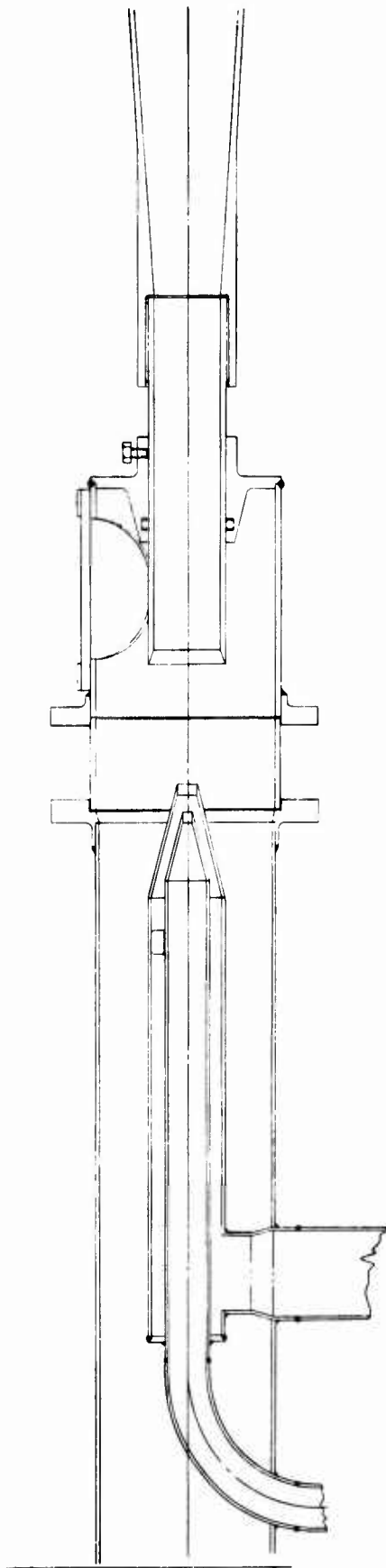


FIGURE 37. DUAL NOZZLE SIMPLE EJECTOR PUMP

A dual operation simple ejector was presented in Figure 37. Tests of this configuration with both nozzles supplied simultaneously show that the nozzle combination acts as a single nozzle. Thus, this configuration is a two-in-one-package ejector. For aircraft systems with both non-afterburning and afterburning modes of operation, this configuration is recommended.

4.6 LABORATORY TEST SETUP

The test setup for the ejector component development and climb tests is shown schematically in Figure 38. Figures 39 through 42 are photographs of the test setup. Figure 39 is an overall view showing the three insulated tanks, nozzle supply tank, sump tank, and receiver tank. Figure 40 shows the two J79 main engine pumps with the hydraulic pressure gages and pump fuel inlet, and discharge pressure gages. Figures 41 and 42 show the ejector pump.

4.7 SUMMARY

Over a hundred test runs, on sixteen different ejector configurations and ejector combinations were accomplished under this contract. The objectives of these test were:

- a. To determine the feasibility of using high motive nozzle pressure.
- b. To investigate low area ratio performance ($b = 0.1$ to 0.01).
- c. To confirm the accepted performance prediction analysis as established by Cunningham and others.
- d. To investigate the cavitation phenomenon, its predictability, and methods of eliminating it.
- e. To establish a uniform method for sizing and designing simple ejectors.
- f. To investigate unusual ejector designs (annular ejector).
- g. To investigate some of the less complicated ejector combinations.

Nozzle pressures up to 500 psig were used with considerable success. High nozzle pressure reduced the maximum attainable flow ratio. This reduction is due to cavitation and is predictable by use of Equation (8) with suitable values of Y and K_1 .

Area ratios from 0.0108 to 0.111 were tested. Test data showed that low area ratio ejectors have a higher flow capacity than higher area ratio ejectors. The use of Equations (1) through (4) will give good predictions of ejector performance, provided suitable values of K_1 , K_2 , and K_{34} are used. With regard to loss coefficients, motive nozzle loss can be satisfactorily represented by assuming $K_1 = 0.1$ for turbulent flow Reynolds numbers. $K_2 = 0$ will be a reasonable assumption especially if rounded entry configurations conforming to Figure 9 are used.

K_{34} can be predicted by use of Equations (6) and (7) and Figures 10 and 12, where all liquid flow can be assumed. For ejectors under cavitation conditions, the value as obtained for all liquid flow should be tripled to compensate for multiphase flow conditions.

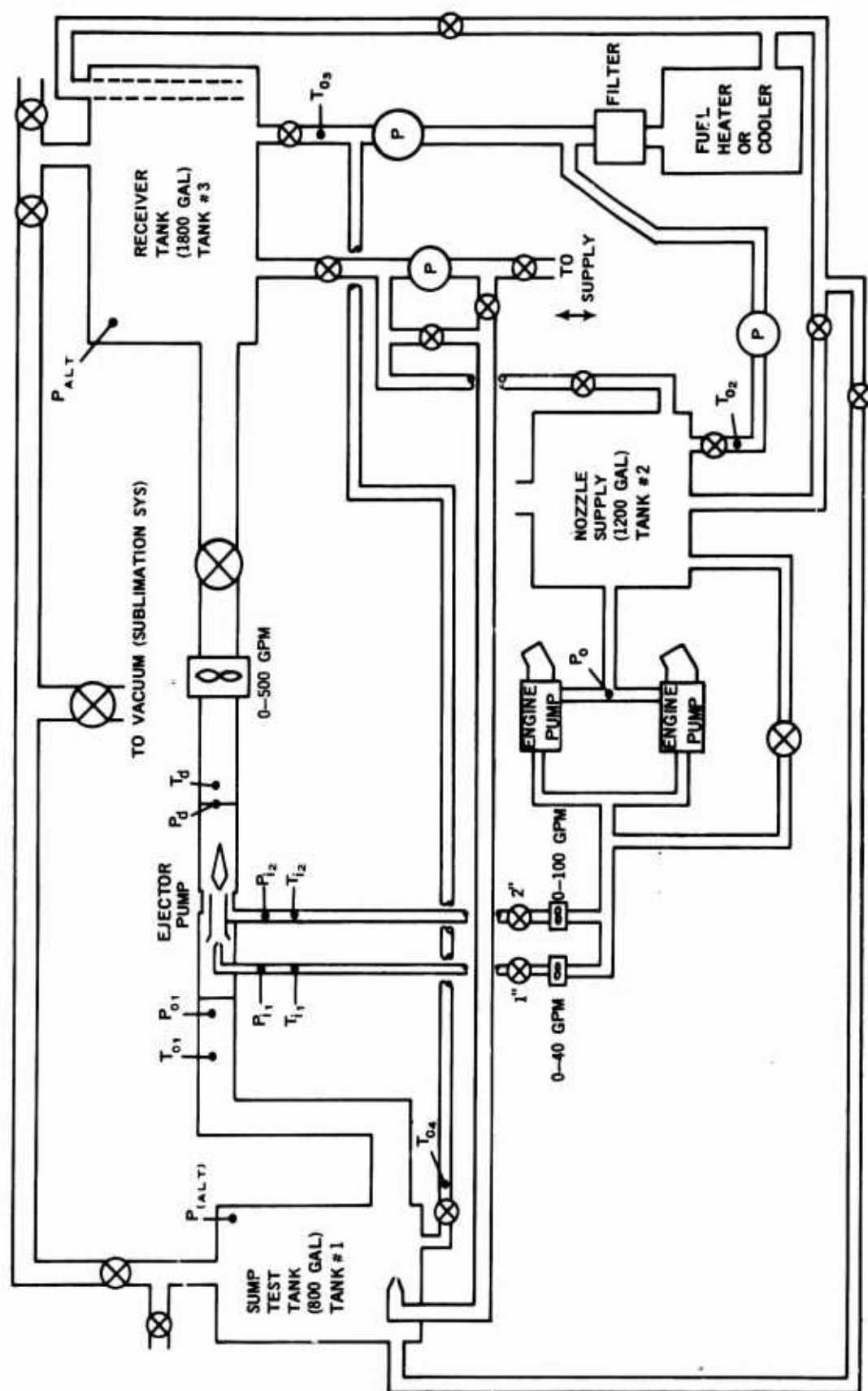


FIGURE 38. EJECTOR PUMP TEST SETUP

Altitude tests and high nozzle pressure tests provided many opportunities to study the cavitation phenomenon. Test results confirm the accuracy of Cunningham's cavitation equation (Equation (8)). For normal or cold temperature (-30 to 110°F) the value of $Y = 0.7\bar{P}_0$ should be used. For hot (135 - 200°F) fuel, either JP-4 or JP-5, $Y = 0.5\bar{P}_0$ provides a closer prediction of cavitation limiting flow ratio. The difference is due to the physical characteristics of the evolved gas in the cavitating pump. At low temperature, the gas



FIGURE 39. EJECTOR PUMP TEST FACILITY - GENERAL VIEW

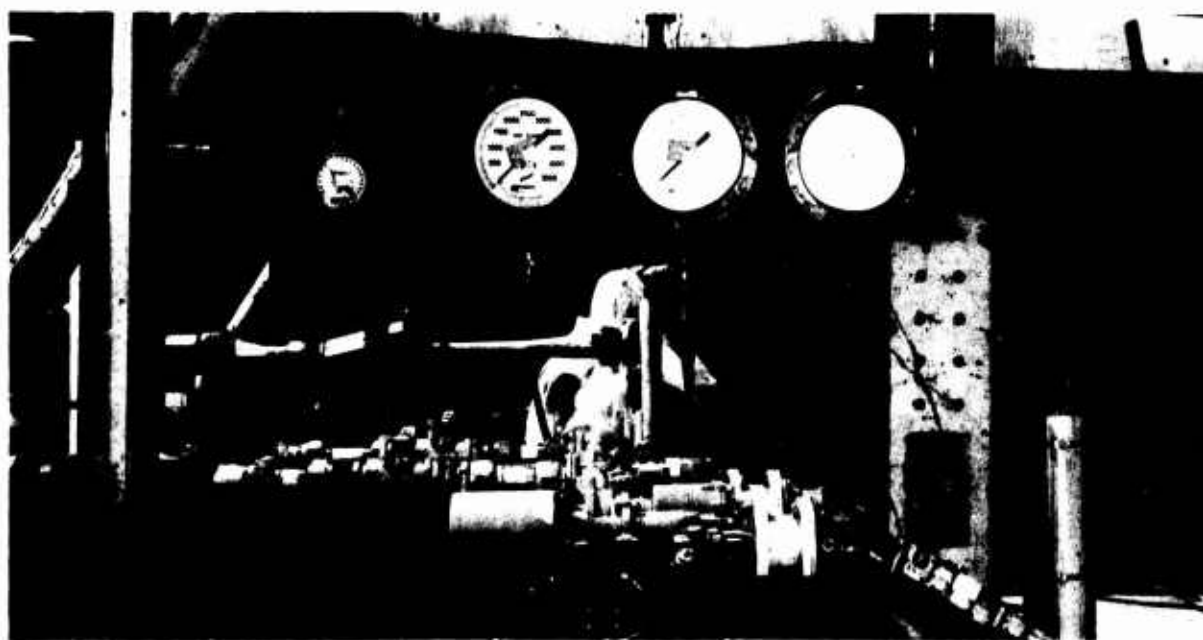


FIGURE 40. EJECTOR PUMP TEST FACILITY - MOTIVE NOZZLE SUPPLY PUMPS.

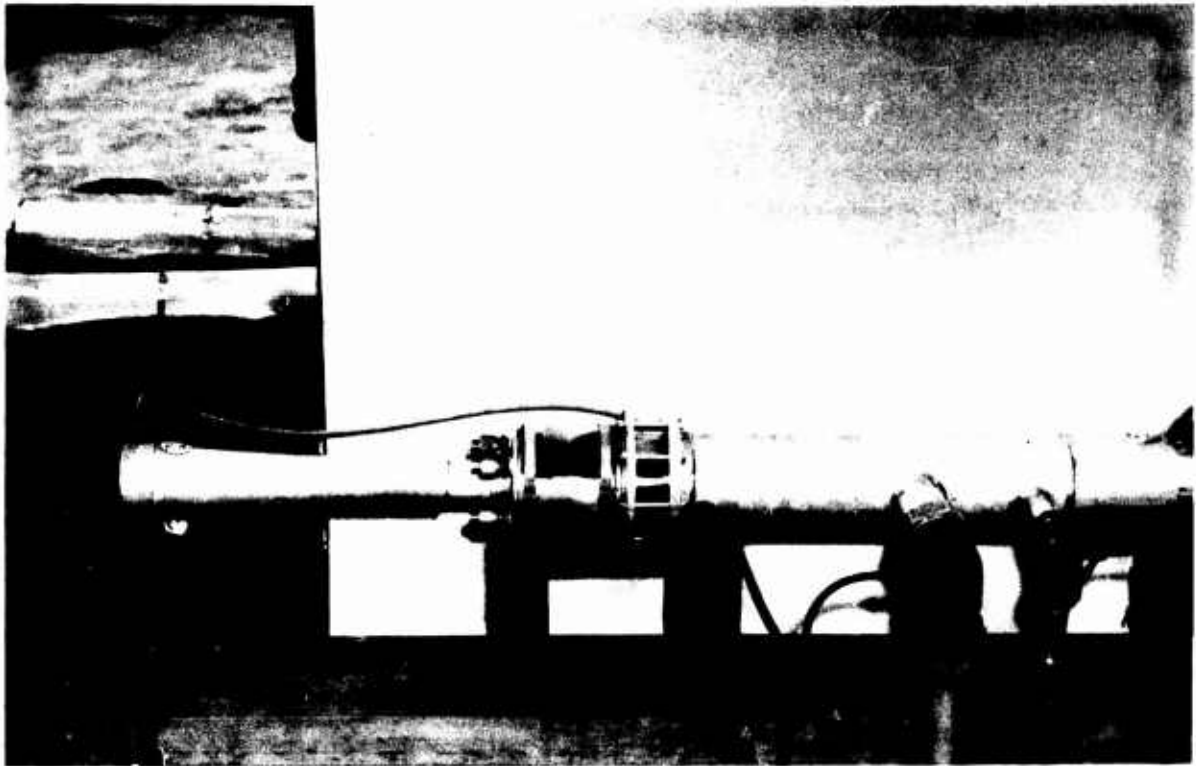


FIGURE 41. PUMP SECTION

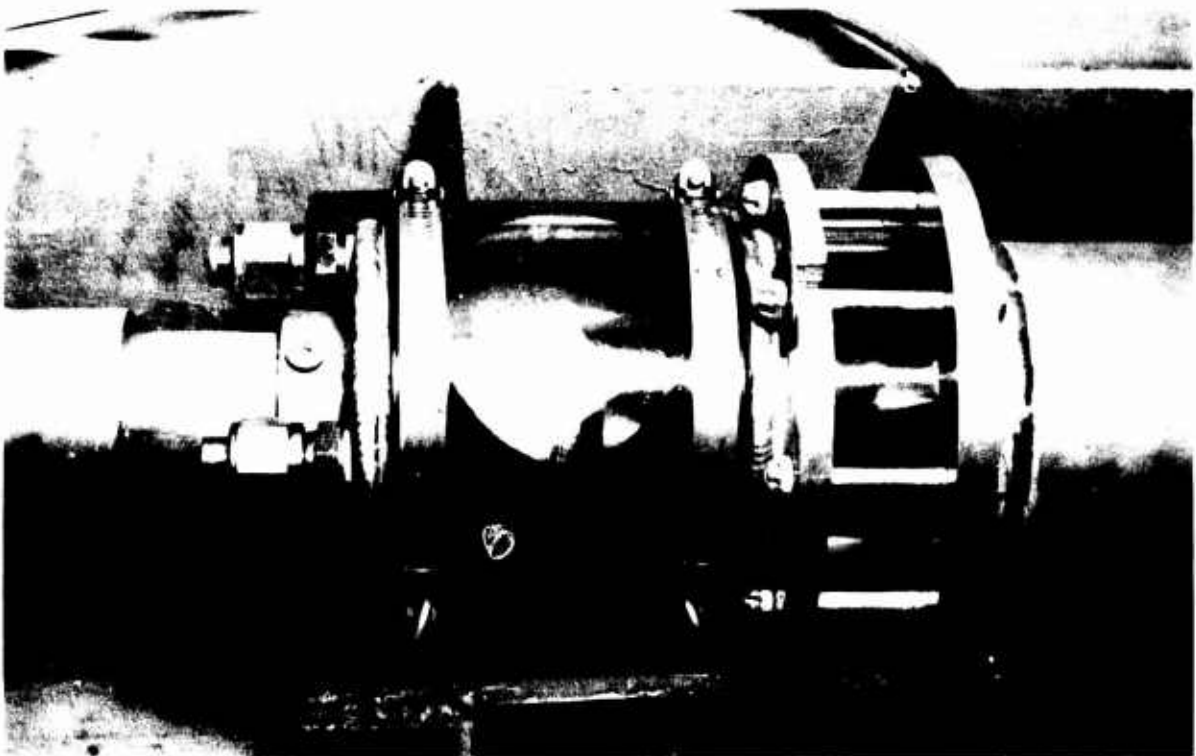


FIGURE 42. EJECTOR NOZZLE AND MIXING INLET AREA

is mostly air. At higher temperatures, the gas is predominantly vaporized fuel.

Elimination of the cavitation phenomenon in the ejector appears to depend upon the reduction of induced flow approach velocity. The prime requisite is that all desired induced flow entrainment must take place outside of the mixing tube. Nozzle to throat entry spacing S must be that distance at which the motive nozzle plume diameter is equal to the throat diameter. The mixing tube throat entry should be a rounded or radius type entry such that $K_2 = 0$ (See Figure 9).

The ejector plenum should be as large as possible to maintain V_s at as low a value as possible. Tests of a series induced flow ejector appear to substantiate the need for these design requirements and show that cavitation can be eliminated by use of careful design.

A theory has been presented whereby the ejector is designed around the motive nozzle plume model. Such a model was presented in Figure 14. The model for any motive nozzle size can be constructed by the use of simple trigonometric relationships. The basic equations are

$$S' = \frac{4.5d_n}{1 - (V_s/V_n)}$$

for sharp edged convergent nozzles, and the ratio $\frac{d_n}{d_{S'}} = 0.5143$. The model

has been developed by extensive investigations (Reference 6) of a round air jet at velocities characterized as turbulent and incompressible. Testing, accomplished under this contract, with fuel indicates that the same basic model is valid for liquid flow. It has been shown that the mixing tube should be terminated at the point where the plume 50% V_c cone impinges on the mixing tube wall. The 50% V_c cone can be determined by use of the relationship

$d_{S'50\%} = d_n$. The apex of the 50% V_c cone will be at the nozzle exit on the nozzle center line. The diffuser cone angle should be 6° preferably, for minimum losses. It is considered that a cone angle equal to the 50% V_c cone angle would not be detrimental. Testing accomplished under this contract appears to substantiate the motive nozzle plume model theory and ejector design approach.

Four annular ejector configurations were evaluated. The best configuration is shown in Figure 25, Configuration 4. The performance of the annular ejector is predictable with the same basic equations used for simple ejector performance evaluation. Further study is recommended to determine optimum design criteria.

Of the ejector combinations evaluated, the series-parallel combination with an annular ejector second stage shows promise. Additional development is required to optimize this configuration.

The simple ejector optimized in accordance with the motive nozzle plume model is considered the best approach for most engine feed system applications. For aircraft utilizing both afterburner and nonafterburner operating modes, the dual operation concentric motive nozzle configuration is recommended.

A dual operation ejector to satisfy the 70,000 lb per hour fuel flow, 200°F engine inlet temperature, JP-4 fuel supply, and system pressure loss as specified in the contract would require the following characteristics:

$$P_i = 500 \text{ psig}$$

$$b_1 = 0.016$$

$$b_2 = 0.04$$

$$d_{n1} = 0.218 \text{ inches}$$

$$d_{n2} = 0.344 \text{ inches}$$

$$d_n = 1.72 \text{ inches}$$

$$W_{n1} = 12,900 \text{ lb per hour}$$

$$W_{n2} = 31,200 \text{ lb per hour}$$

SECTION V
FUEL TANK SUMP

5.1 INTRODUCTION

The fuel in a main fuel tank of an aircraft normally is the last fuel used and the main tank is kept full by internal transfer from auxiliary tanks. The main tank usually has a sump area which is designed to capture fuel for consumption during negative gravity conditions. The fuel in the sump is then replenished when the aircraft is returned to normal gravity conditions.

In conditions of zero gravity, fluid orientation is essentially unpredictable and the fuel could be located randomly within the tank. As the fuel is removed from the sump for engine consumption, the fuel in the remainder of the main tank may not be able to flow into the sump to replenish the void area, thus air spaces may be created.

The ejector pump(s) used to supply fuel to the engine will work well when pumping either vapor or liquid. The fuel in the sump must be positioned to prevent large quantities of air from being pumped to the engine. This might be done by any of the following methods: (1) Provide an artificial gravity force, (2) provide a continually collapsing tank wall which follows the fuel and allows no vapor space, and (3) entrapping fuel by capillary action. Only the artificial gravity system was studied during this contract.

The artificial gravity is created by introducing a fluid jet into the sump area of the main tank. This jet contains sufficient energy to induce a fluid rotation (swirl) action in the sump with an angular velocity sufficient to produce a centrifugal force causing the fluid to always move toward the tank wall. The required jet velocity can be calculated based on the size of the sump and the selected centrifugal force. The jet source was not defined in the studies of this contract, however, possible sources include internal transfer from auxiliary tanks or from a fuel bleed from the engine. If fuel from the auxiliary tanks is used, the transfer pumps may become unported during zero gravity, thus cutting off the supply of the swirl jet. Under these conditions it may be necessary to use a small sustaining jet using fuel from the engine.

The fuel tank sump must contain a means of continuing the fuel pickup during the negative gravity conditions. This must be done by having a pickup at the top as well as at the bottom of the sump. To satisfy the desire for a minimum of movable parts, and considering that the ejector pump can not have two inlets (one of which might be unported), a flexible inlet tube was selected for this system. This will allow the fuel pickup to react to normal gravity environment in the same manner as the fuel itself does. That is, the pickup will rest on the tank bottom during normal gravity conditions in level flight and coordinated turns and by means of hose flexure will move to the top of the sump with a transition to negative gravity conditions. The inlet would be kept near the tank wall, to pick up the rotating fuel during the zero gravity condition.

The following symbols and definitions are used in this section of the report:

a	Ratio of cylinder height to radius ($\frac{h}{R}$)	--
a_n	Normal acceleration	feet/sec ²
b	Width of plate (perpendicular to flow)	feet
C_d	Drag coefficient	--
C_{dl}	Drag coefficient ($\pi a C_d$)	--
C_M	Moment coefficient	--
C_{Ml}	Moment coefficient ($\frac{C_M}{2}$)	--
C_T	Combined moment and drag coefficient ($C_{dl} + C_{Ml}$)	--
D	Drag-flat plate	pounds
D_T	Total drag of cylinder ($D + \frac{M}{R}$)	pounds
g	Acceleration of gravity	feet/sec ²
h	Cylinder height	feet
I	Moment of inertia	lb sec ² ft
m	Mass	pounds
\dot{m}	Mass flow	lb/sec
M	Moment	lb feet
M_A	Angular momentum	lb ft sec
P_S	Static pressure	inches of fluid
P_T	Total pressure	inches of fluid
R	Radius	feet
Re	Reynolds number	--
t	Time	seconds
v	Velocity	feet/sec
v_{jet}	Velocity of entering jet	feet/sec
v_{swirl}	Velocity of swirl at periphery	feet/sec
ν	Kinematic viscosity	ft ² /sec

ρ	Density	slugs/ft ³ or $\frac{\text{lb-sec}^2}{\text{ft}^4}$
ξ	Torque	lb feet
ω	Angular velocity	rad/sec
Ω	Precessional velocity	rad/sec
l	Length of plate (parallel to flow)	feet

5.2 DESIGN AND ANALYSIS

5.2.1 Swirl Analysis

The fuel to provide the swirling action is introduced along the circumference of the sump. A literature search did not reveal any existing methods of analysis for the swirl action. Therefore to provide a method of analysis, this fuel was assumed to act in a wheel type motion in a forced vortex. The flow regime was defined by Reynolds number as given in the following equation.

$$\text{Re} = \frac{\omega R^2}{\nu} \quad (\text{Ref 12, p. 547})$$

A normal acceleration at the tank wall equivalent to one g was selected. From Figure 43 the velocity to provide the required normal acceleration was chosen. ω can be obtained by $v = \omega R$. The swirling flow inside a cylindrical tank was assumed to be represented by the sum of the drags associated with a flat plate (side wall of the sump) and both sides of a rotating disc in an infinite fluid (top and bottom of sump).

5.2.1.1 Flat Plate Drag

The skin friction drag for a flat plate in parallel flow is given by

$$D = C_d \frac{\rho v^2}{2} b l \quad (\text{for one side only}) \quad (\text{Ref 13, p. 279-281})$$

Values of C_d are shown in Figure 44.

For a cylinder unrolled,

$$\begin{aligned} D &= C_d \frac{\rho v^2}{2} b l \\ &= C_d \frac{\rho v^2}{2} 2\pi R h \\ &= C_d \rho v^2 \pi R h \end{aligned}$$

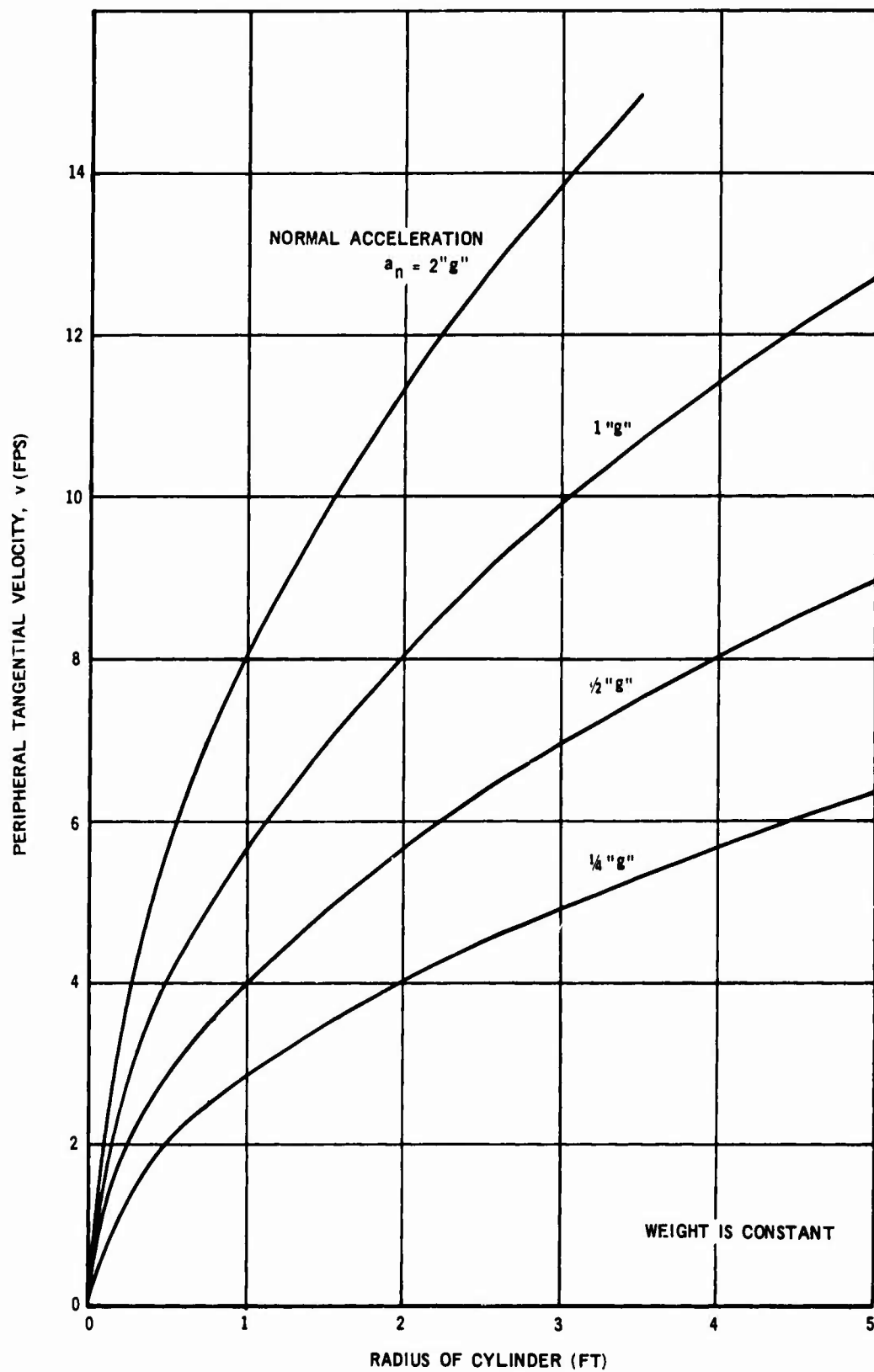


FIGURE 43. TANGENTIAL VELOCITY REQUIRED AT PERIPHERY TO DEVELOP VARIOUS LEVELS OF ACCELERATION

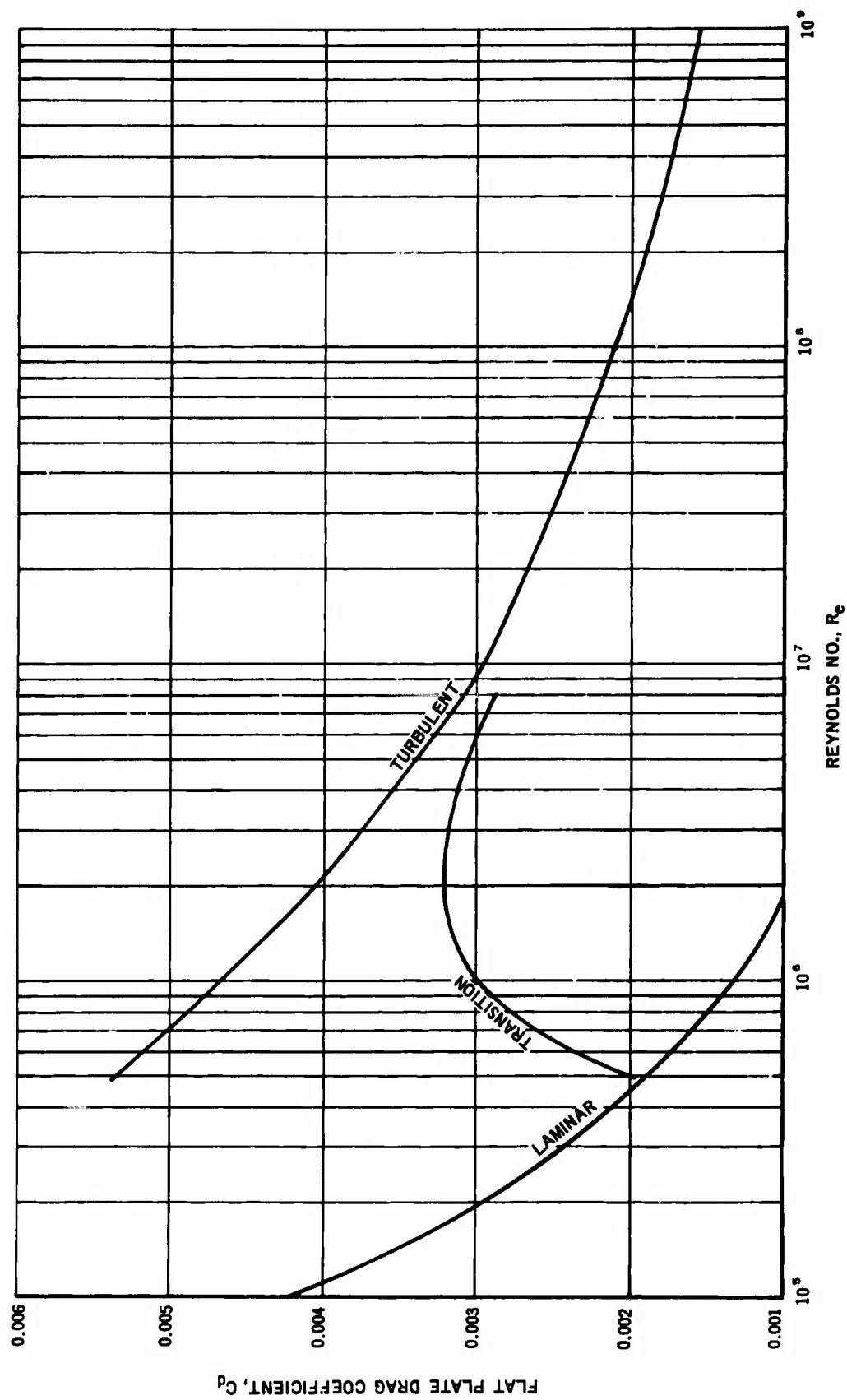


FIGURE 44. SKIN FRICTION DRAG COEFFICIENT FOR A SMOOTH FLAT PLATE PARALLEL TO FLOW

letting $\frac{h}{R} = \text{constant} = a$,

$$\begin{aligned} D &= \pi C_d \rho v^2 R a R \\ &= \pi a C_d \rho v^2 R^2 \end{aligned}$$

Letting $\pi a C_d = C_{d1}$

$$D = C_{d1} \rho v^2 R^2$$

5.2.1.2 Disc Drag

The torque required to rotate a disc in an infinite fluid is given as

$$M (\text{total}) = C_M \frac{\rho \omega^2}{2} R^5 \quad (\text{two sides of disc})$$

Where C_M for laminar flow ($Re > 3 \times 10^5$) is

$$C_M = \frac{3.87}{Re^{1/2}}$$

and for turbulent flow

$$C_M = \frac{0.146}{Re^{1/5}} \quad (\text{Ref 12, p. 547-548})$$

If the constant (1/2) in the total moment equation above is included,

$$\frac{C_M}{2} = C_{M1} = \frac{1.935}{Re^{1/2}} \text{ \& } C_{M1} = \frac{0.073}{Re^{1/5}}$$

The case of a disc rotating in a housing was also investigated, but it required less torque than for the infinite fluid case as shown in Figure 45. In order to be conservative, calculations were based on the disc rotating in an infinite fluid, thus providing a dimensionless coefficient, C_{M1} , to determine the force due to the moment on the disc. Substituting C_{M1} for $C_M/2$ and the linear velocity for the angular velocity ($v = \omega R$), the following equation for the force at the periphery resulting from the disc torque is obtained

$$\frac{M}{R} = C_{M1} \rho v^2 R^2$$

5.2.1.3 Total Drag

The total drag of the rotating fluid is expressed by the following:

$$D_T = D + \frac{M}{R} = (C_{D1} + C_{M1}) \rho v^2 R^2$$

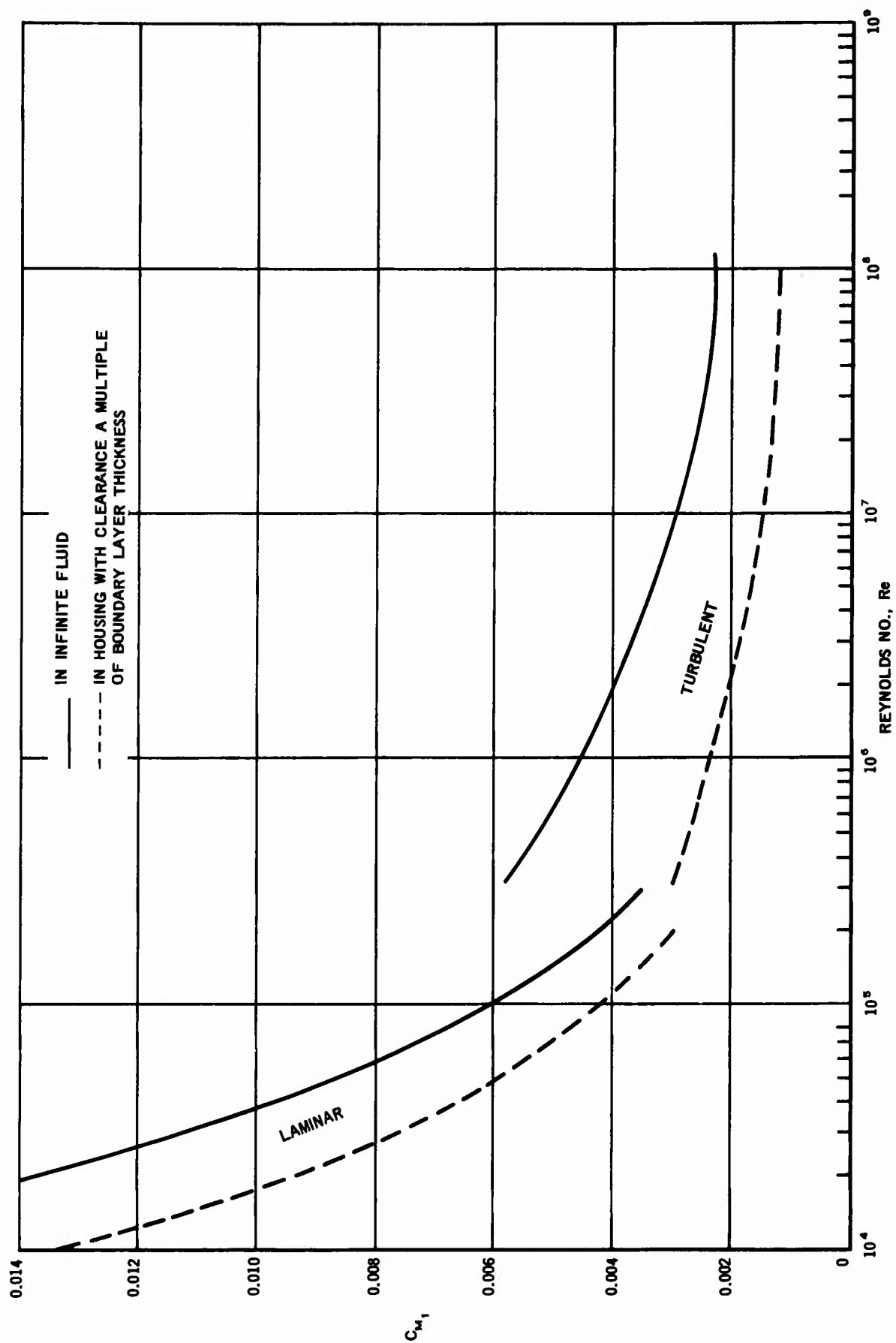


FIGURE 45. DIMENSIONLESS MOMENT COEFFICIENT FOR ROTATING DISK

Letting $(C_{dl} + C_{Ml}) = C_T$

$$D_T = C_T \rho v^2 R^2$$

C_T versus Reynolds number is graphed in Figure 46 for varying values of cylinder height to radius ratio (a).

The relation between torque and change in angular momentum is given by

$$\zeta dt = I d\omega \quad (\text{Ref 15, p. 177})$$

Assuming that the entering jet acts as a particle, its angular momentum may be defined as the product of its linear momentum and the perpendicular distance from the axis to its line of motion.

$$M_A = mvR \quad (\text{Ref 15, p. 175})$$

Assuming that the loss of momentum in the swirl will be made up by the jet nozzle to provide steady state, and inserting g to correct mass terms

$$\begin{aligned} \zeta dt &= \frac{m}{g} (v_{\text{jet}} - v_{\text{swirl}}) R \\ \text{but } \zeta &= D_T R \end{aligned}$$

Where D_T is the total drag referenced to the tank radius.

$$\begin{aligned} D_T R dt &= \frac{m}{g} (v_{\text{jet}} - v_{\text{swirl}}) R \\ D_T &= \frac{m}{g dt} (v_{\text{jet}} - v_{\text{swirl}}) = \frac{\dot{m}}{g} (v_{\text{jet}} - v_{\text{swirl}}) \end{aligned}$$

The two drag equations can be combined to determine the required nozzle momentum as follows:

$$\frac{\dot{m}}{g} (v_{\text{jet}} - v_{\text{swirl}}) = C_T \rho v_{\text{swirl}}^2 R^2$$

5.2.1.4 Aircraft Effects

Adverse effects on the airplane handling characteristics were checked by determining the gyroscopic moment of the fuel assuming solid body rotation during a snap roll. The precessional motion is governed by the following equation:

$$\zeta = I \omega \Omega \quad (\text{Ref 15, p. 182})$$

The polar moment of inertia is

$$I = \frac{mR^2}{2} = \pi R^4 \rho \frac{h}{2} \quad (\text{Ref 15, p. 174})$$

Giving

$$\zeta = \pi \omega \rho \frac{h}{2} R^4 \Omega$$

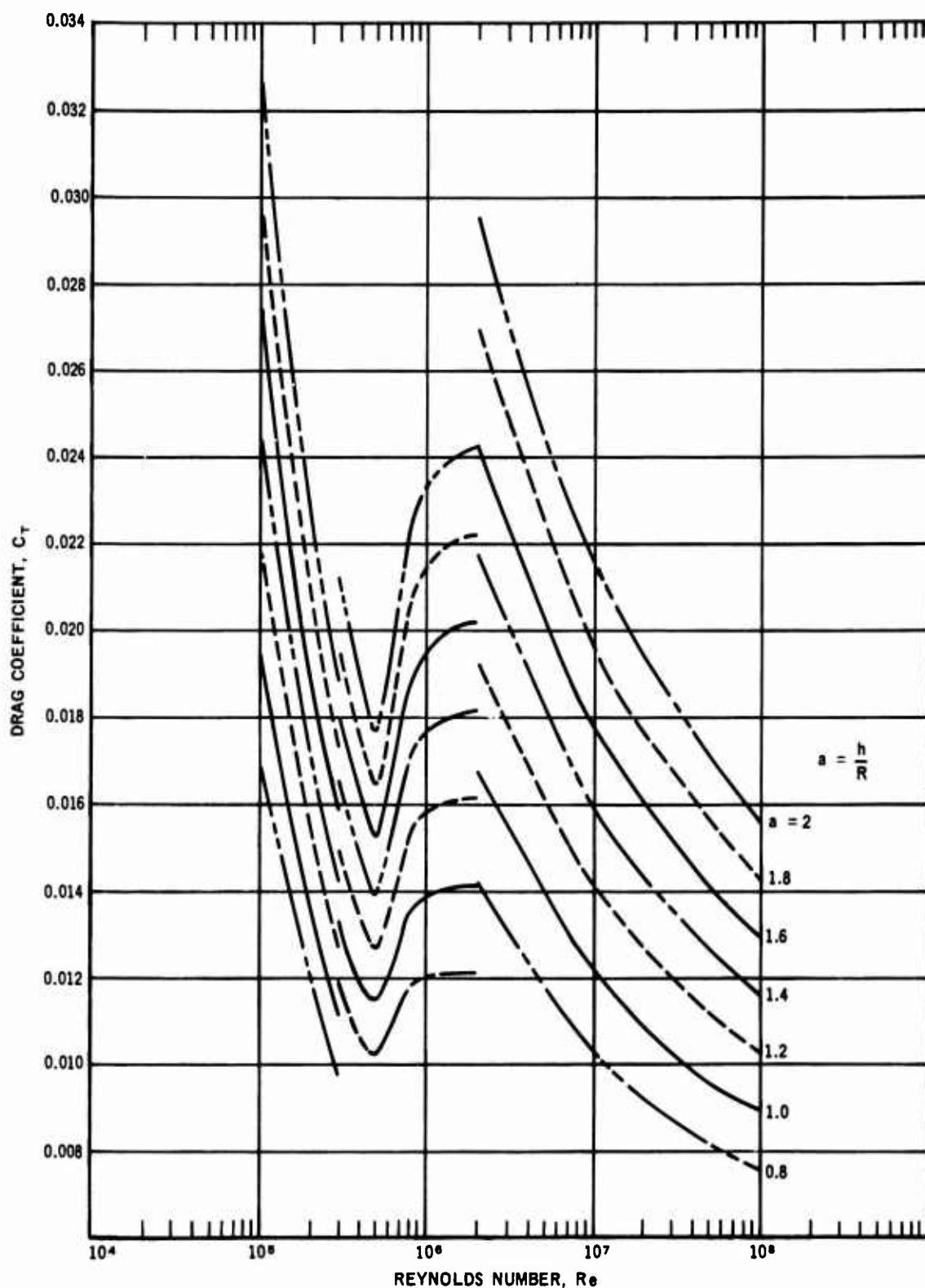


FIGURE 46. TOTAL DRAG COEFFICIENT FOR A CYLINDER

The required torque (or aircraft pitching moment) was calculated and found to be within the control capability of existing fighter or attack type aircraft, therefore no further study was done on aircraft effects.

5.2.2 Flexible Pickup

A flexible pickup was designed to be installed in the sump of the test tank. The pickup consisted of a three inch diameter flexible hose with a rigid metal pickup scoop mounted on the end of the hose as shown in Figure 47.

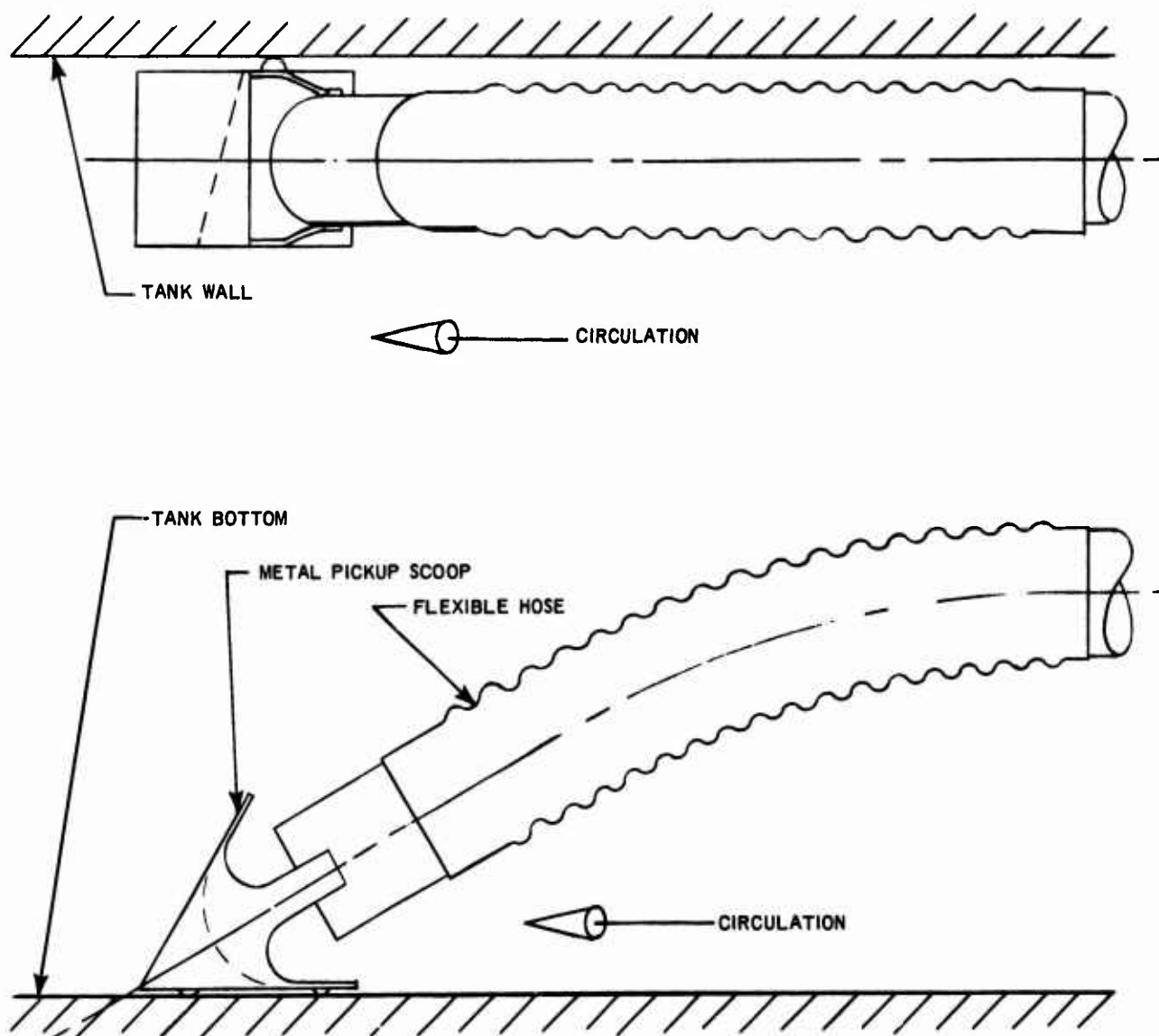


FIGURE 47. FLEXIBLE PICKUP

The hose is a convolute rubber hose reinforced with wire to reduce distortion during bending and to prevent collapse due to negative pressure caused by pump suction. The stiffness of the hose was designed for easy deflection so that the metal pickup would rest on the bottom of the tank under static conditions.

The metal pickup was designed with a scoop type entrance which would catch the fuel as it is rotating around the tank. The scoop is tilted at an angle of 15-20 degree so that the rotating fuel will produce a force tending to hold the pickup against the tank wall. The friction produced by this force was reduced by teflon buffers, which were attached to the scoop, to contact the wall. The size and shape of the pickup afterbody is a function of the angular deflection and depth of the sump. The weight of the pickup must be sufficient to allow the hose to flex from bottom to the top of the tank at a rate which would prevent air from entering the pump inlet.

5.3 FUEL TANK SUMP TESTS

The fuel tank sump and flexible inlet were set up as a system and tested to verify the analysis. The test was conducted in three phases; swirl test, tank sump test, and flight test.

5.3.1 Swirl Test

The swirl test was conducted to verify the results of the analytical model used to predict the behavior of the circulating fuel. A thirty six inch diameter cylindrical tank was used to approximate the aircraft tank. Closed vessel conditions of an aircraft tank sump located at the bottom of a tank were simulated by the installation of a transparent plastic baffle, at approximately half the height, which permitted visual examination of the swirling. A hole was cut in the center of the baffle to provide overflow for excess fuel. The test setup is shown in Figures 48 through 50.

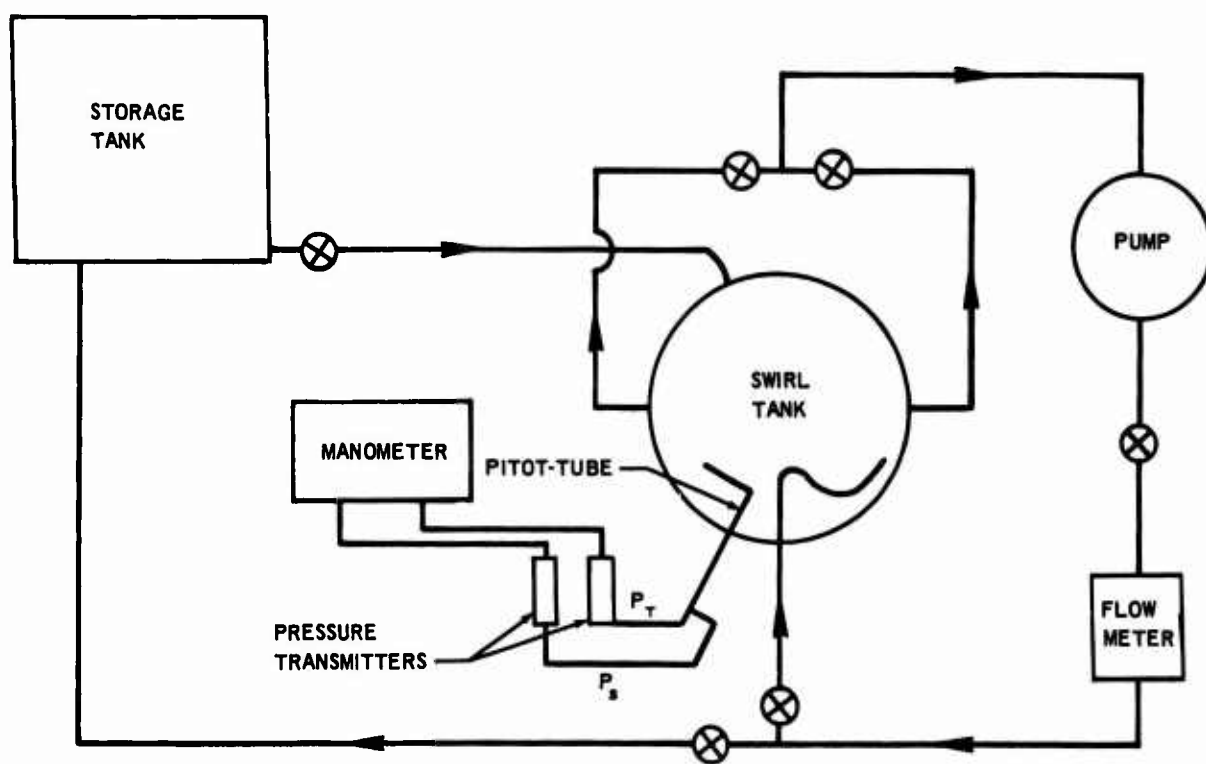


FIGURE 48. SWIRL TEST SYSTEM SCHEMATIC

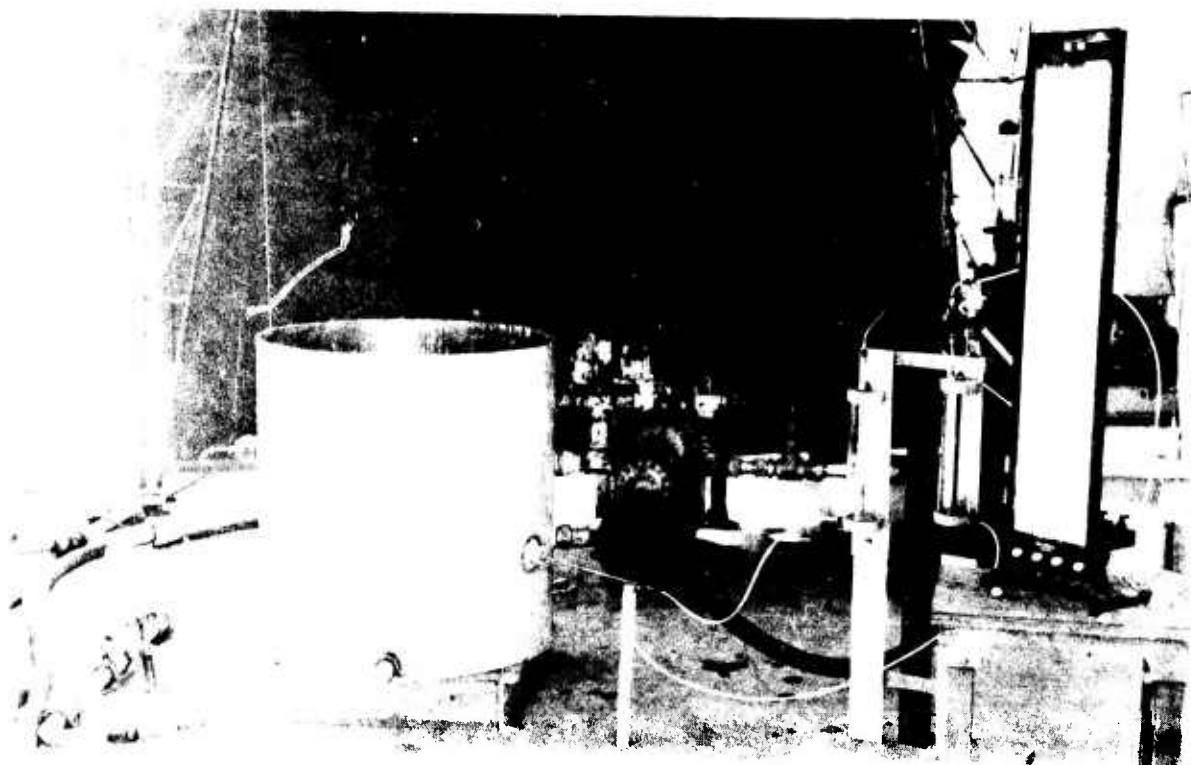


FIGURE 49. SWIRL TEST SETUP

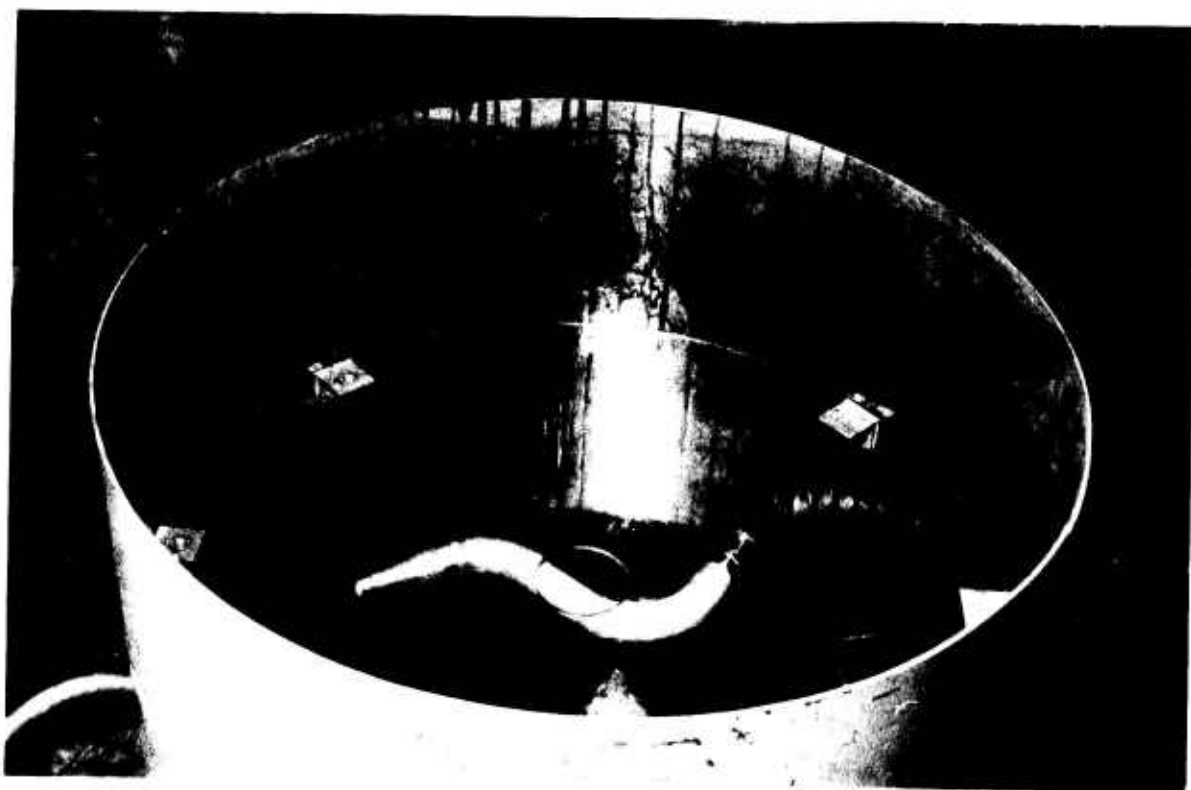


FIGURE 50. SWIRL TEST TANK

A Pitot tube was installed at midheight in the tank sump section such that the probe followed the streamlines as closely as possible. Air bottles were used as pressure transmitters to isolate the fuel from the manometers. Static and total heads were measured on a water manometer. The fuel was sucked from the swirl tank through two fittings located at the bottom and circulated as a closed system back through the nozzle which was located at midheight. Flow rates were monitored with a rotameter installed in the line. Tests were conducted to determine:

1. Tank velocity profile at steady state,
2. Variation of swirl velocity with time during, initiation and slowdown,
3. Effect of outlet location, and
4. Variation in Pitot velocity readings due to angular misalignment

The velocity profiles were determined by raking the Pitot tube in a radial direction.

Swirl tests in the cylindrical tank were conducted on several nozzle configurations. Different nozzle diameters were tested at varying flow rates to produce a large variation in the momentum of the swirl generating fluid, the largest velocity head being produced by the smallest nozzle operating at its maximum flow rate. The nozzles designed for low turning losses (smooth "S" bends with bend radius equal to two pipe diameters) produced good swirling action and behaved similarly. A bulkhead elbow was also installed as a nozzle to reduce obstruction in the swirl path, but it was discarded because it caused severe aeration in the fuel due to the sharp bend.

The Pitot tube was tested for accuracy with variation in angle of incidence of approaching fluid. Although the total and static readings varied, the velocity head was found to be insensitive to angular misalignments of plus or minus fifteen degrees. Figure 51 shows the variation in velocity head.

The velocity head profiles were plotted and the data formed in a consistent series of graphs. The swirl motion, however, did not conform to solid body rotation. Figure 52, plotted on logarithmic paper, reveals two regimes of straight lines with different slopes. On inner radii, up to approximately eleven or twelve inches, the slope was about six; indicating the velocity varied as the cube of the radius changed. From this break point out to the tank edge, the velocity head (slope of curve) appears to vary as the fourth power of the radius indicating that the velocity varies as the radius squared. The values were much smaller towards the center of the tank and consequently the relative reading error would be higher. Also the Pitot tube, being about eight inches long, was adversely affected as the radius decreased.

The drag force and momentum were calculated and compared to the theoretical values. Figure 53 shows that the predicted drag was substantially lower than the actual drag. Several factors contributed to this such as rough tank walls, piping, and turning losses. Figure 54 shows a correction factor plotted against Reynolds number which can be applied to the theoretical calculations.

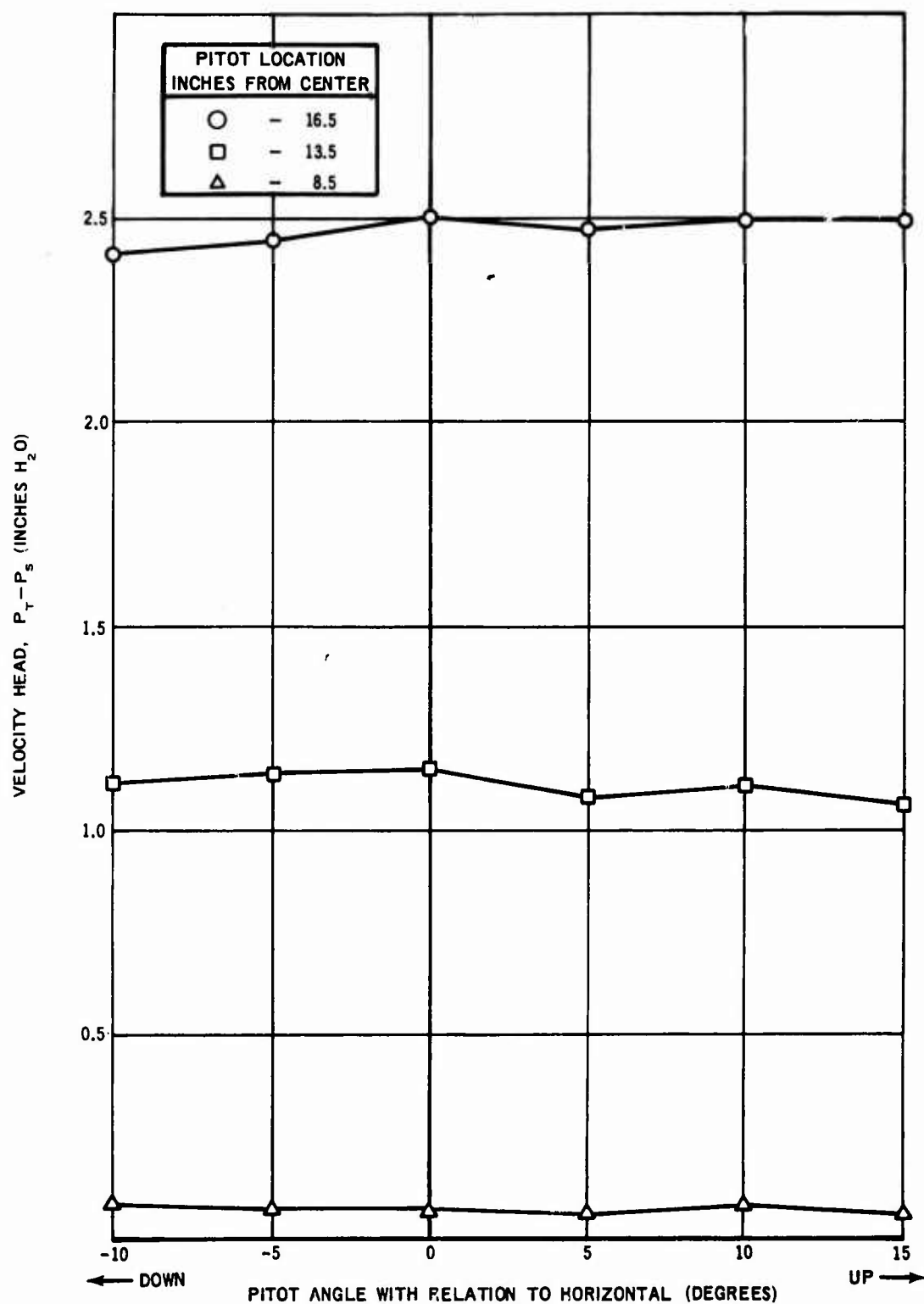


FIGURE 51. VARIATION IN PITOT READING WITH ANGLE OF INCIDENCE

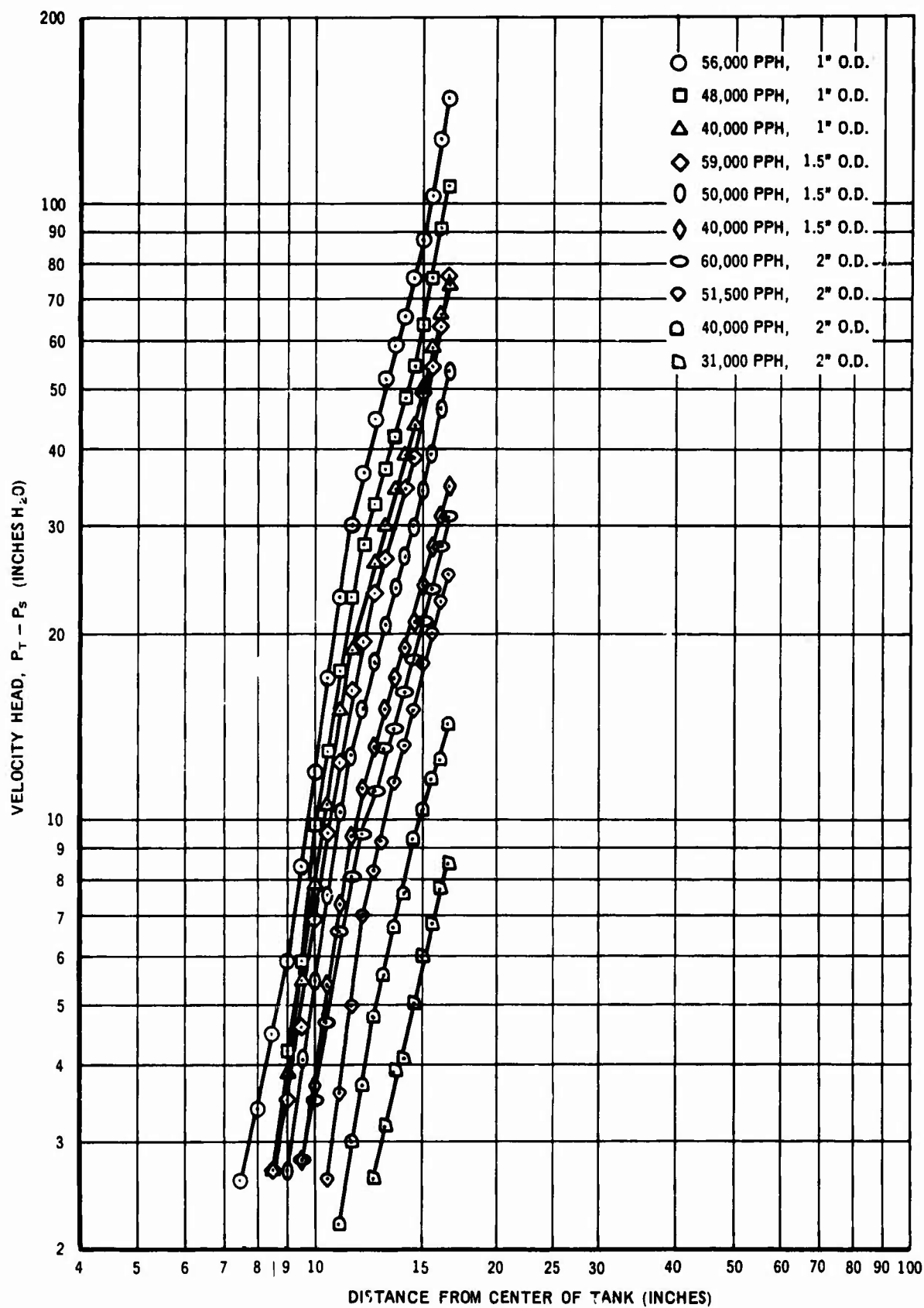


FIGURE 52. SWIRL VELOCITY VS DISTANCE FROM CENTER OF TANK

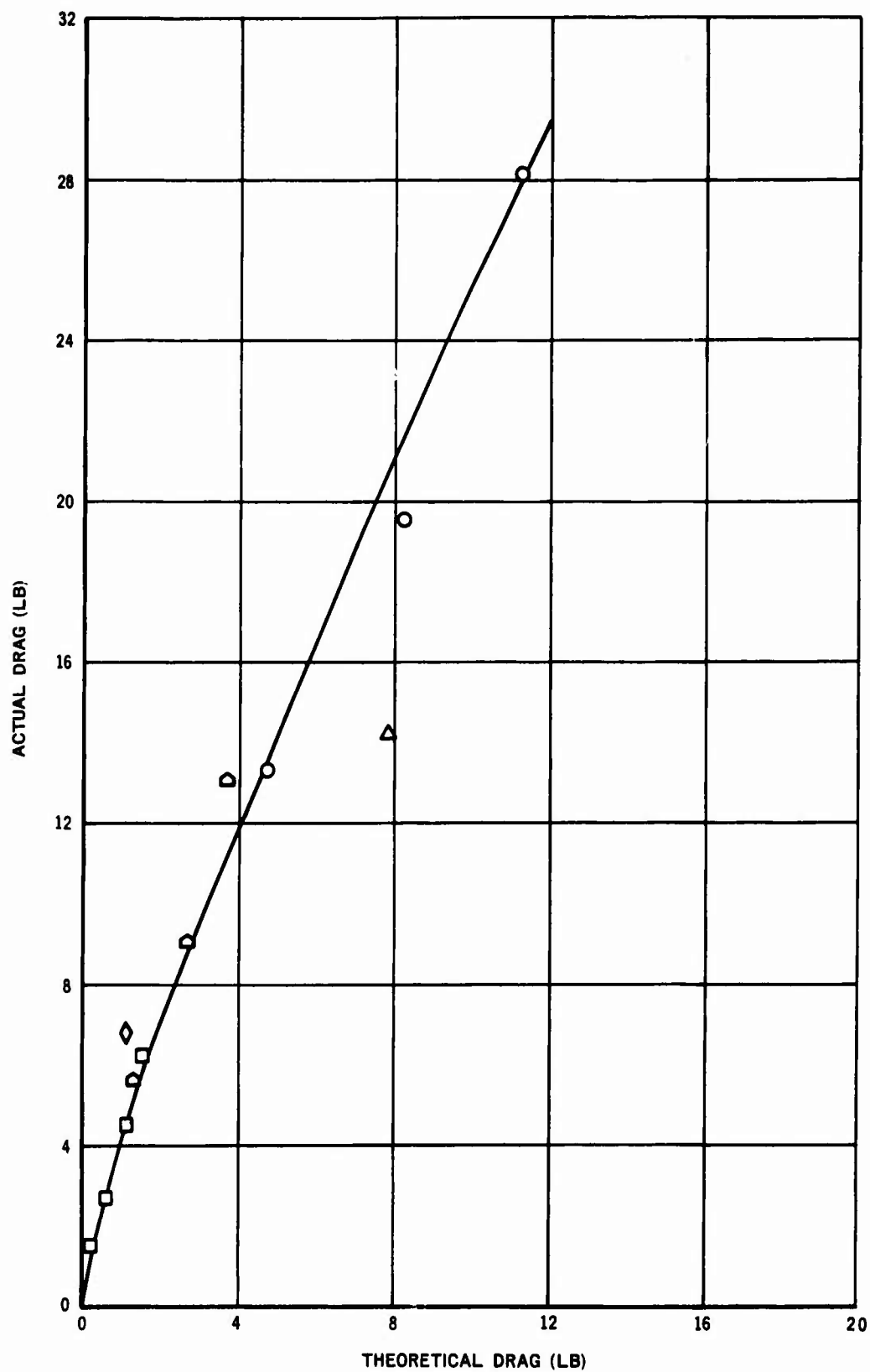


FIGURE 53. COMPARISON OF CALCULATED VERSUS OBSERVED DRAG

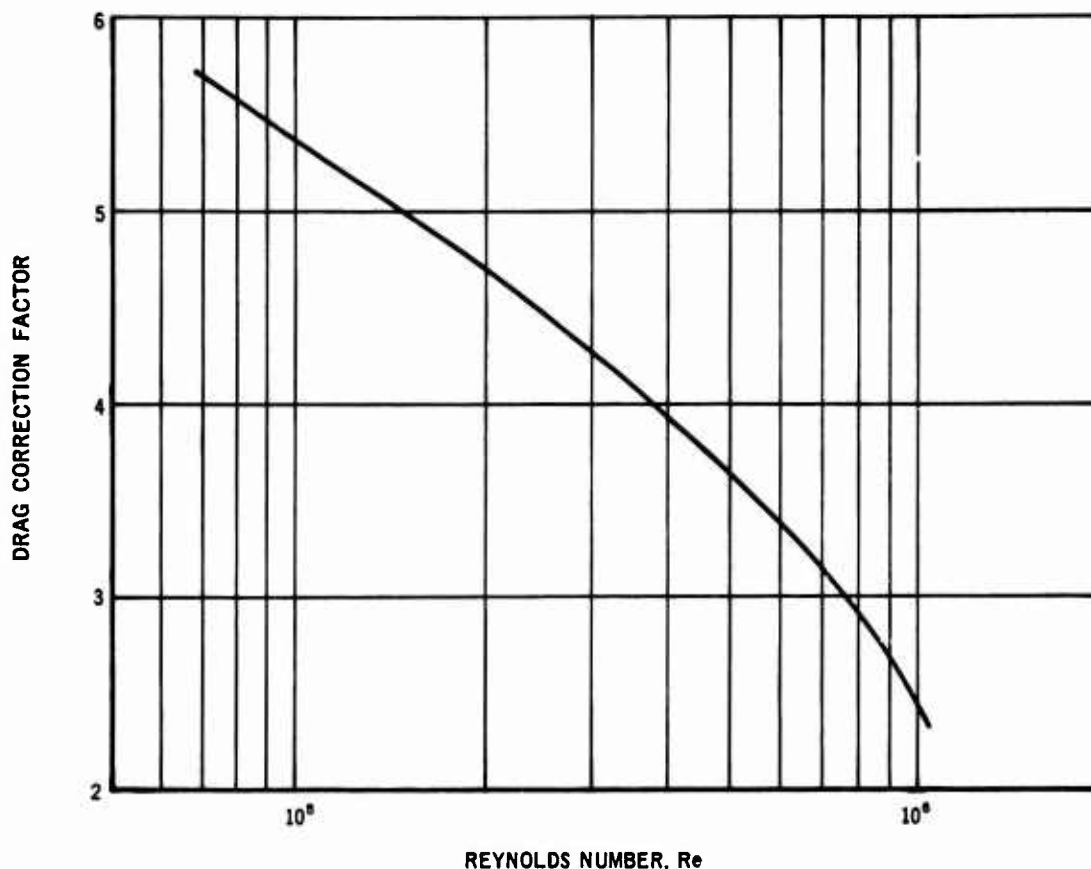


FIGURE 54. DRAG CORRECTION FACTOR

Variation in outlet location was checked but did not appear to have a significant influence (See Figure 55). Time traces of swirl initiation and decay are presented in Figures 56, 57, and 58. This indicates that swirl is essentially realized within thirty seconds after initiation for whatever the flow rate. Slowdown appears to be proportional to velocity head at cutoff and decreases exponentially with time. The following equation was derived from experimental data and may be used to predict the time decay.

$$P_T - P_S = 1.868 e^{-0.072 t}$$

Figure 59 presents estimated performance with a sustaining flow during slowdown.

5.3.2 Tank Sump Test

The purpose of this test was to obtain data on fuel rotation while varying flow rate with various geometrical configurations within the tank. A large rectangular tank was fabricated with a sump area sufficient for one minute of engine operation in afterburner. The sump was designed so that the corner radius could be varied between a full width circle and nearly square corners. This was done because the use of a cylindrical tank in an aircraft was not considered very practical. Thin metal baffles were installed to permit changes

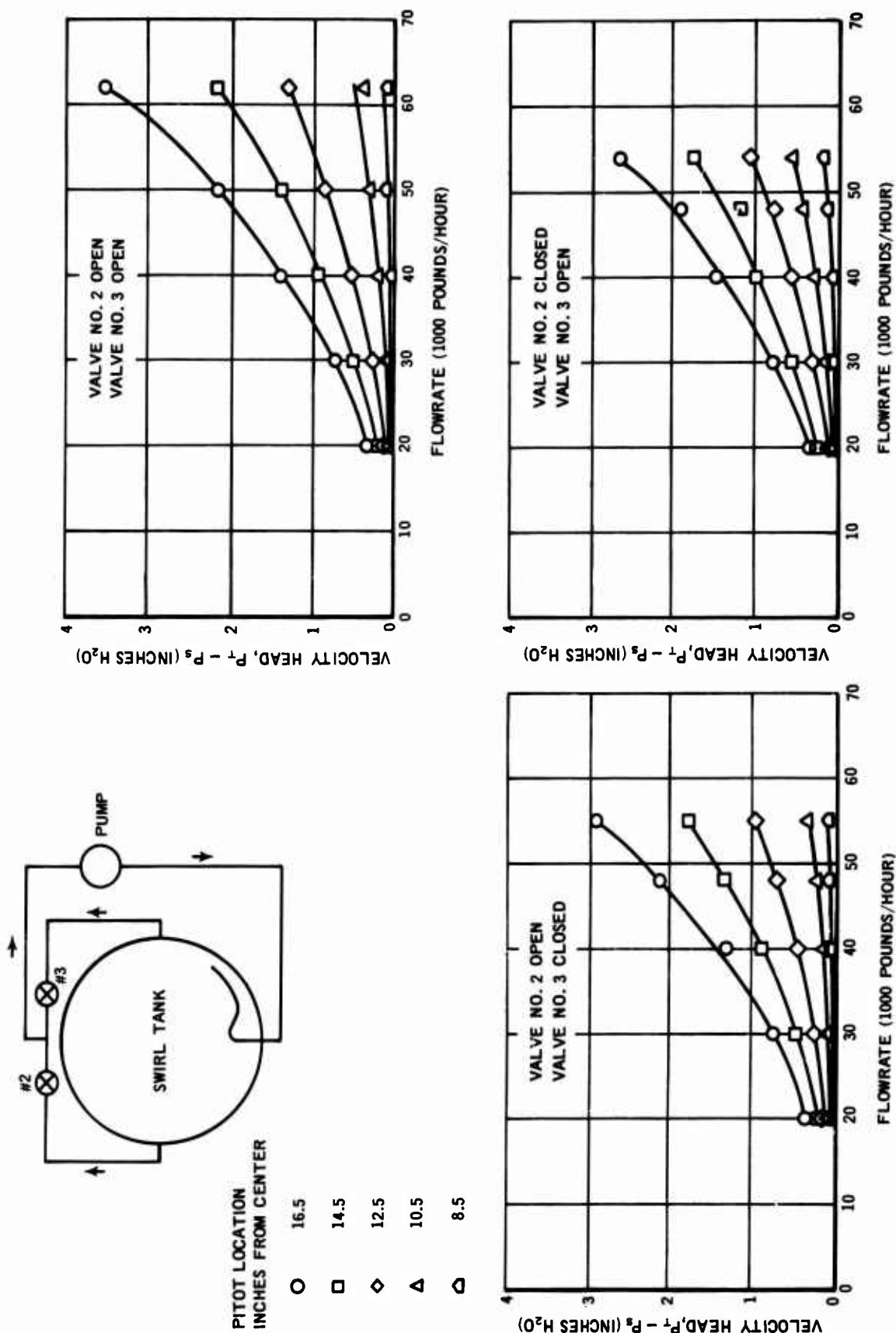


FIGURE 53. EFFECT OF OUTLET LOCATION ON VELOCITY HEAD

SYMBOL	NOZZLE FLOWRATE (POUNDS/HOUR)
○	20,000
□	30,000
◇	40,000
△	50,000
◻	60,000

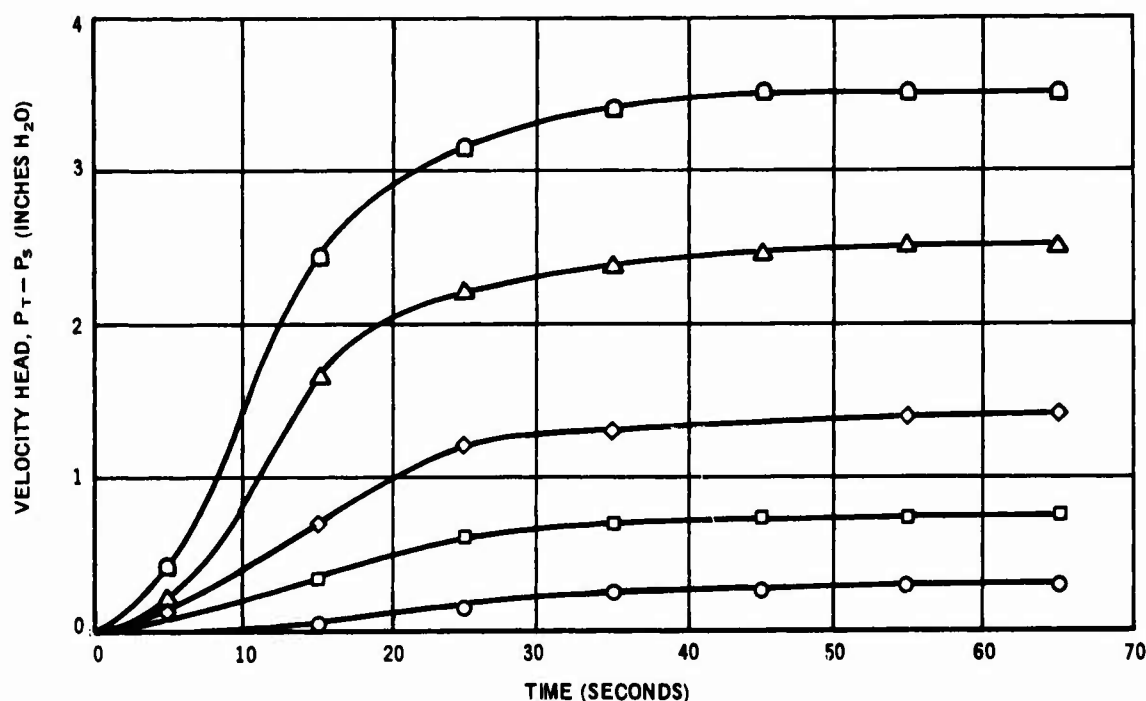


FIGURE 56. VELOCITY HEAD VS TIME FOR SWIRL INITIATION

in the corner radius by adjustment of the baffle attachments. Flexible fuel pickups were designed to simulate the aircraft installation. A closed vessel was formed by the installation of a transparent plastic baffle which permitted visual examination through plastic observation windows constructed in the tank. A hole was cut in the center of the plastic baffle to permit escape of entrained air and to provide an overflow passage for fuel. The test setup is shown schematically in Figure 60. The sump tank setup and tank are shown in Figures 61 and 62.

Three Pitot tubes were installed to determine the effect of Pitot location; at three-fourths sump height at the end of the straight section (Pitot No. 2) and at the beginning of the straight section (Pitot No. 1), and at one half sump height at the end of the straight section. These locations are shown on Figure 60. Static and total heads were measured with water manometers. The velocity profiles were determined by making a traverse with the Pitot tubes.

The fuel was pumped in a closed loop, sucking fuel from the tank using the fuel pickups and introducing it into the tank through the swirl generating nozzles. Flow rates were monitored with a rotameter installed in the line.

SYMBOL	NOZZLE FLOWRATE AT CUTOFF (POUNDS/HOUR)
○	20,000
□	30,000
◇	40,000
△	50,000
◻	60,000

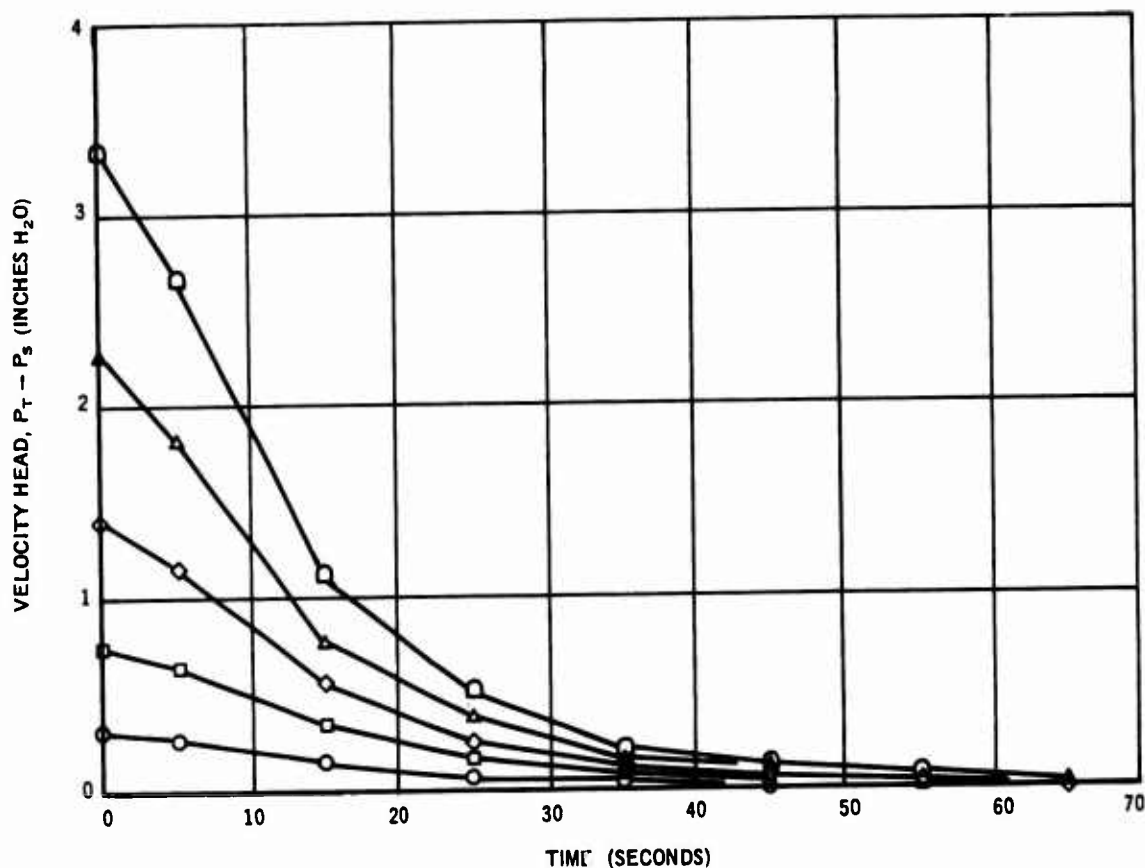


FIGURE 57. VELOCITY HEAD VS TIME FOR FRICTIONAL SLOWDOWN

Tests were conducted to determine swirling effectiveness with varying corner radius. An annular shape (made by inserting a center body) was also investigated to test the effect of a tank with a minimum low energy fuel in the center. During periods of zero gravity, when transfer fuel may not be available to maintain the swirl, the sump fluid will slow down considerably due to fluid friction and viscous losses and also because of removal of high energy fuel from the periphery of the sump. As high energy fuel is replaced by lower energy fluid from the sump interior, the swirl will slow down even more due to conservation of angular momentum. The centerbody was inserted to provide a case where the average swirl velocity would be higher. The centerbody provided an annular track eight inches wide and the full height of the sump.

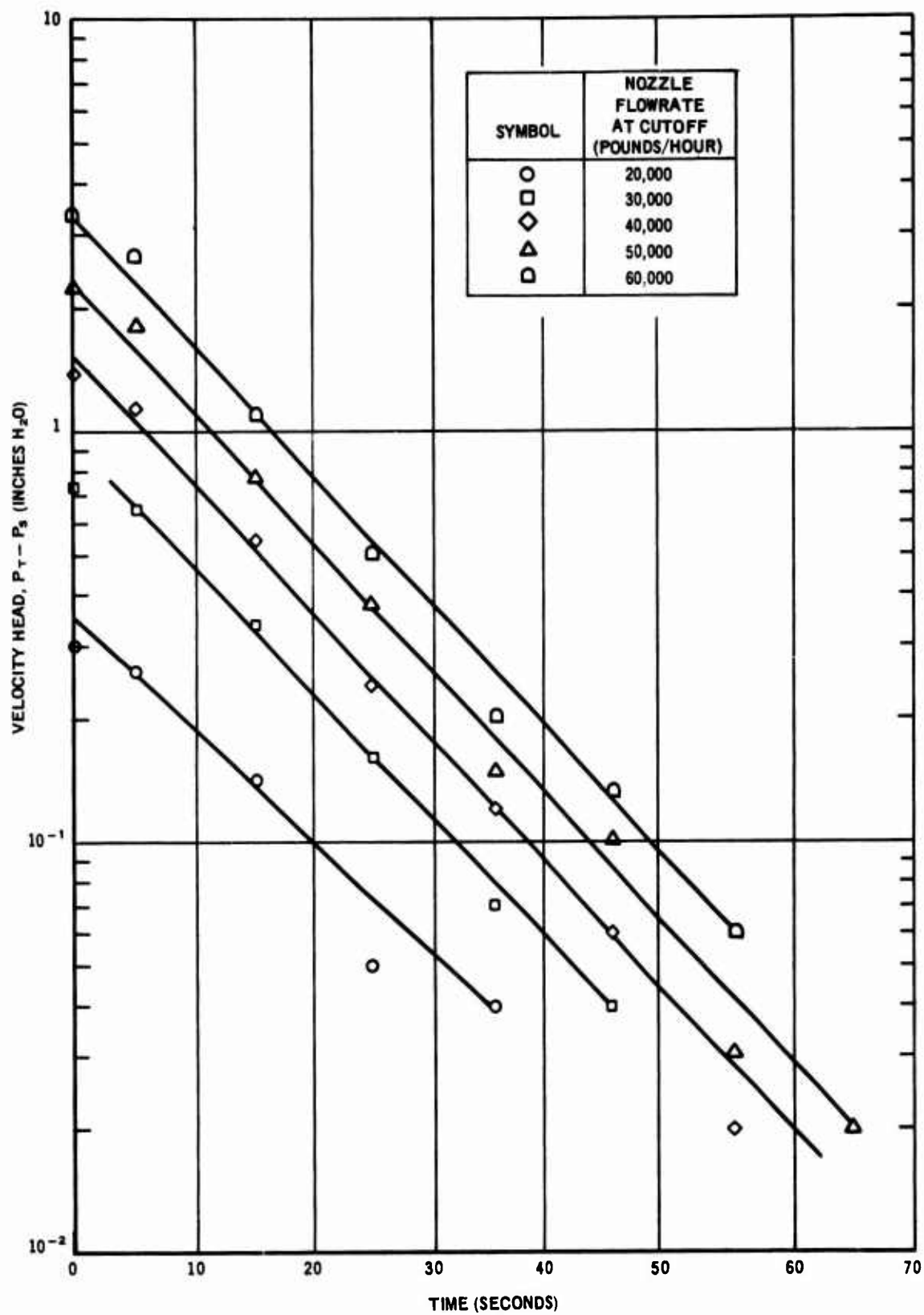


FIGURE 58. VELOCITY HEAD VS TIME FOR FRICTIONAL SLOWDOWN

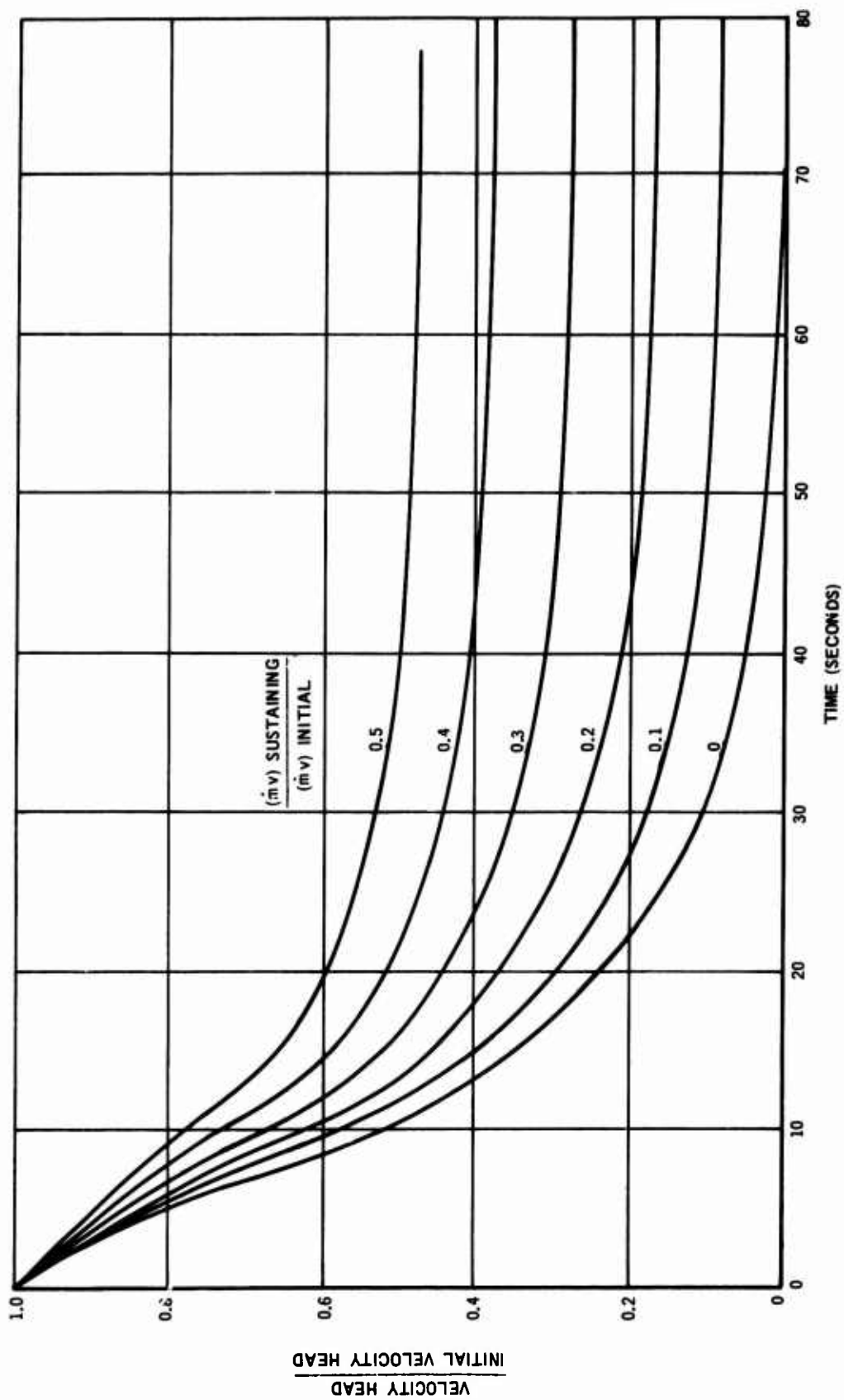


FIGURE 59. ESTIMATED PERFORMANCE WITH SUSTAINING FLOW DURING SLOWDOWN

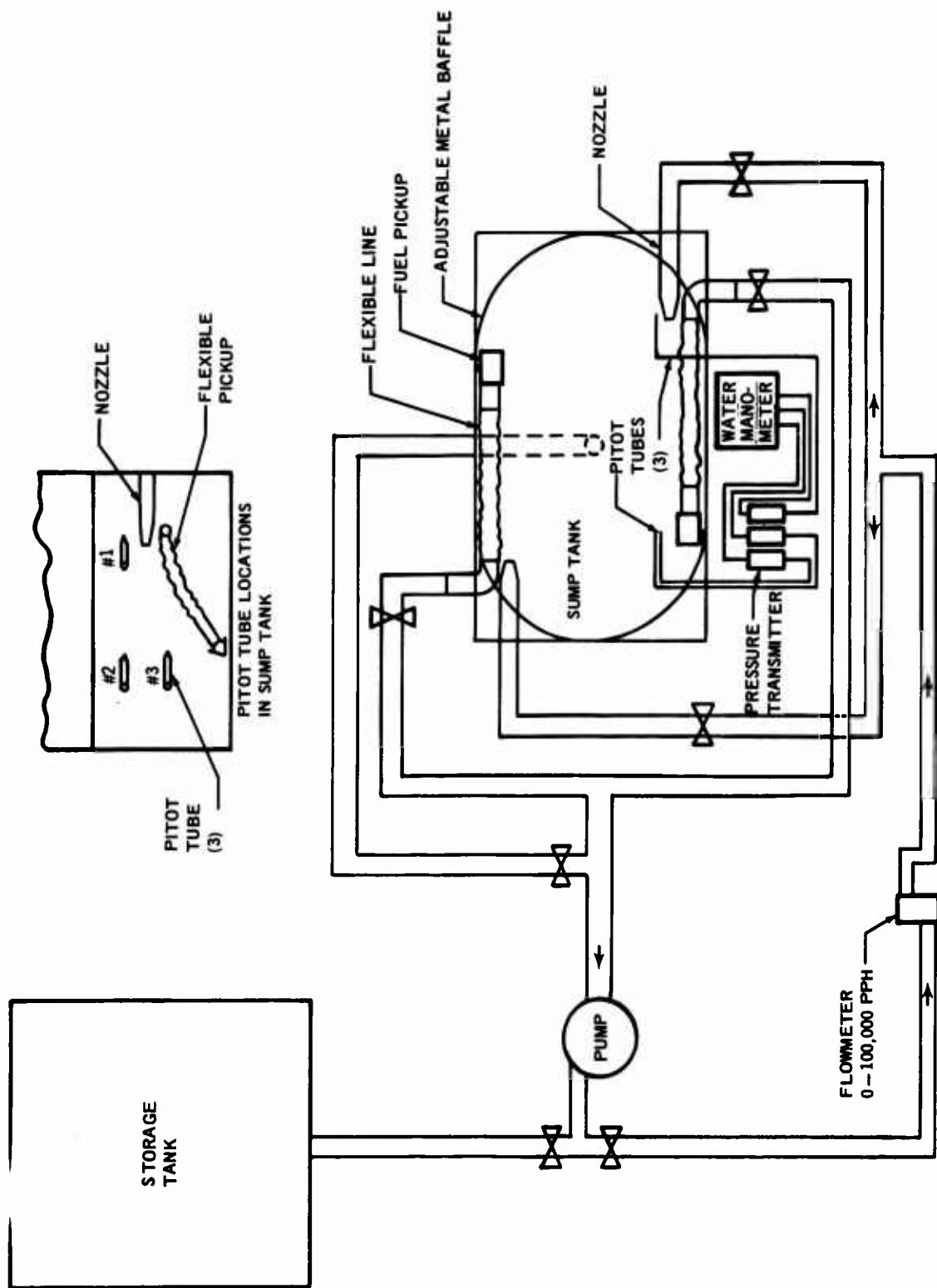


FIGURE 60. TANK SUMP SYSTEM SCHEMATIC

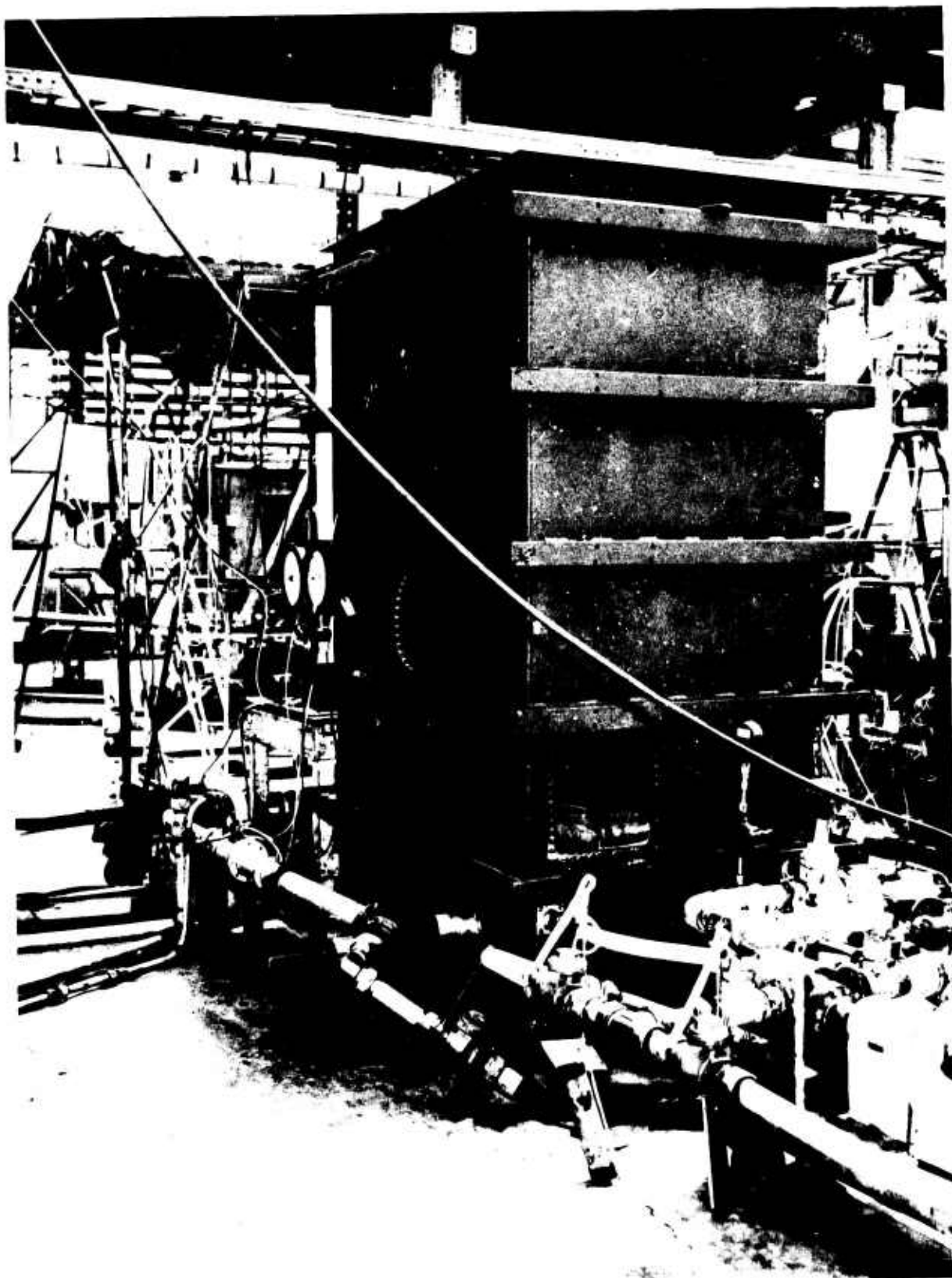


FIGURE 61. SUMP TANK SETUP

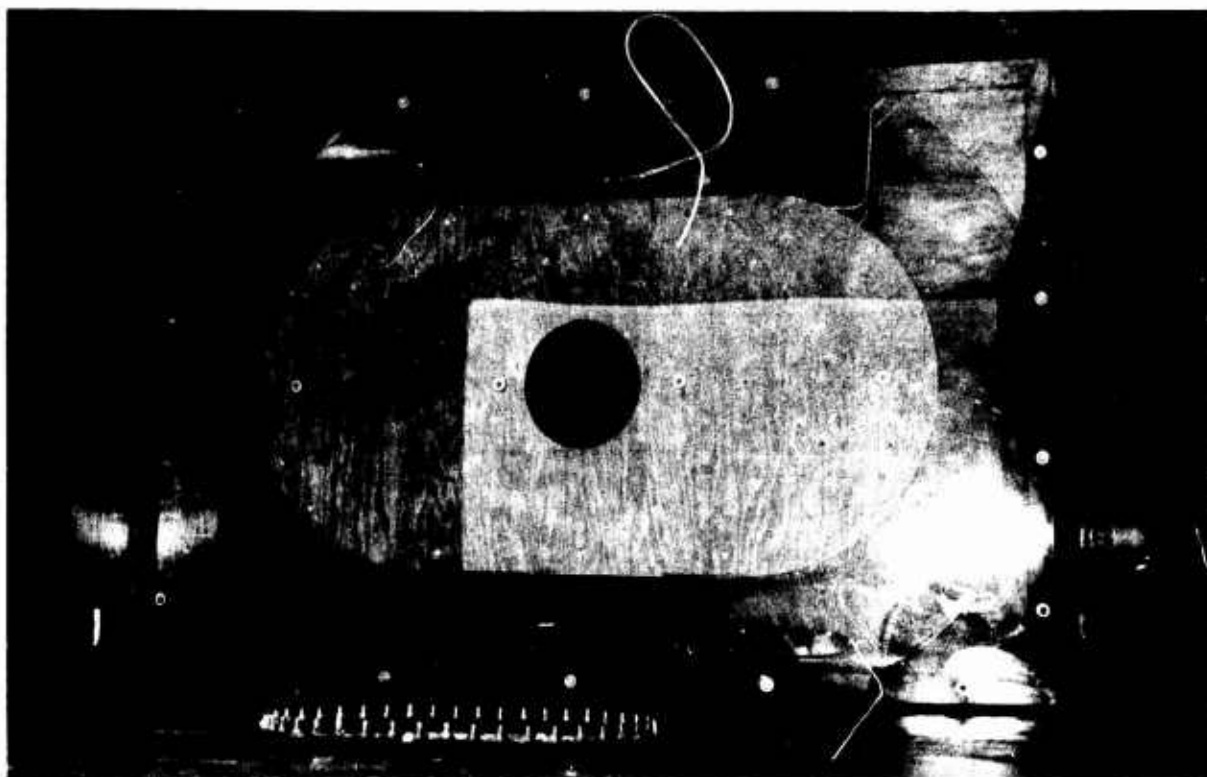


FIGURE 62. VIEW LOOKING DOWN INTO SUMP TANK SHOWING ADJUSTABLE BAFFLES AND CENTER BODY

The best shape for swirl generation appears to be that of a cylinder with a high volume to surface area ratio. This was corroborated by observation of the rectangular tank during slowdown which revealed eventual formation of circular flow before the motion ceased. That is, the fluid in the corners stagnated more rapidly than the fluid in the center resulting in a flow pattern which was very nearly round. Because this shape may not be practical for aircraft installations, varying sump configurations were tested. The corner radius was varied from three inches to twenty inches, which was the full radius of the minor dimension of the tank, using the adjustable baffles installed for that purpose.

The nozzles were originally located to exhaust at midheight into the sump on the center line of the minor dimension. The flexible pickup tube interfered with the swirl generation at this location and the nozzles were moved to three-fourths tank height directly over the inlet elbows for the pickup tube.

Pitot location was found to have a large influence on readings. The two Pitot tubes located at the end of the straight section appeared to be affected by the nozzle installation as they recorded consistently higher readings than the Pitot tube located at the beginning of the straight section. Figure 63 shows a typical plot of velocity head versus distance from the center of the sump. In many cases, negative readings were registered, probably due to eddies in the flow. It was felt that this would not affect the velocity head significantly since earlier experimentation showed the Pitots to be only slightly affected by angular misalignment. Pitot tube No. 1 was considered to provide the most consistent results for evaluations.

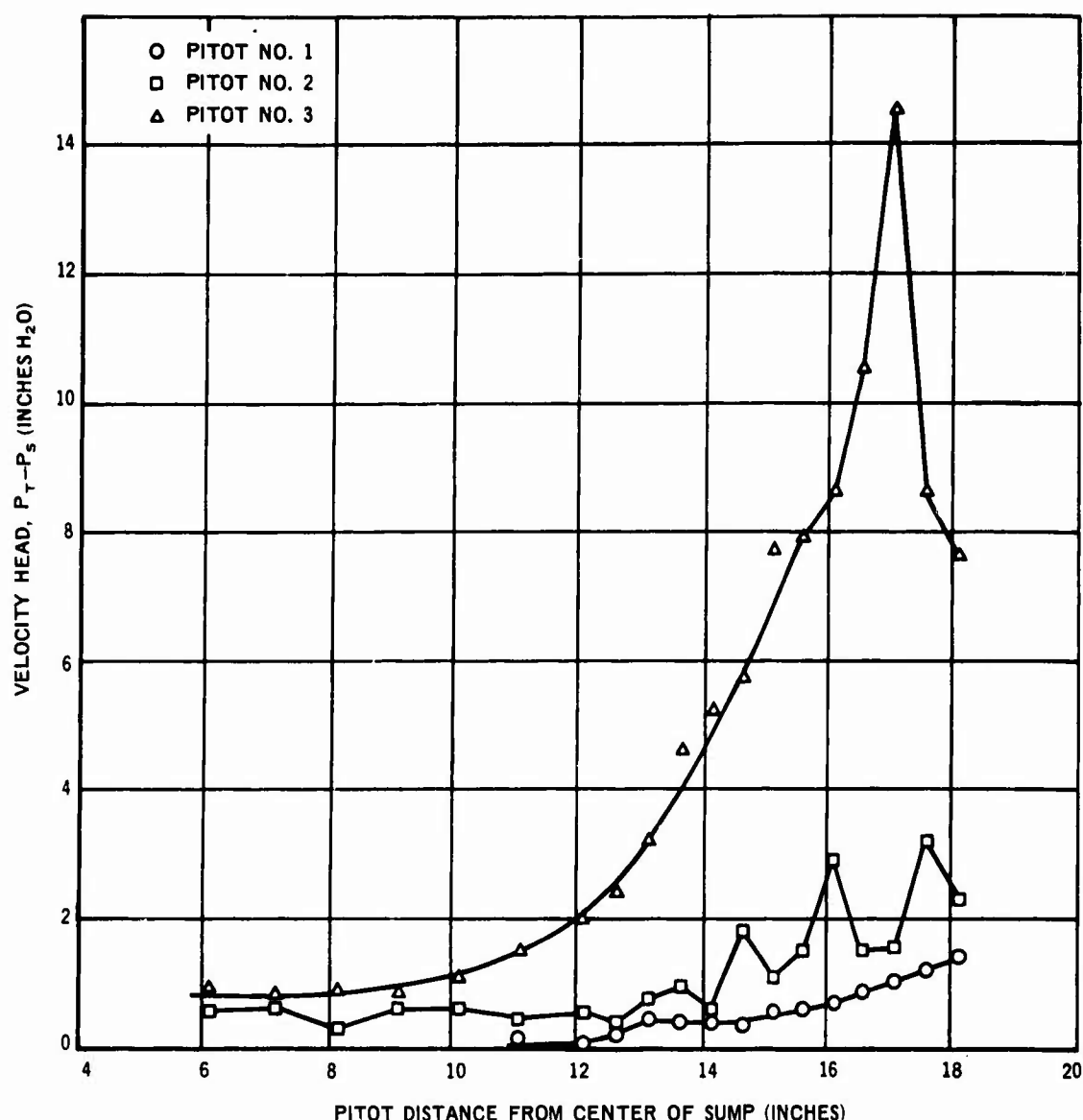


FIGURE 63. TYPICAL VELOCITY HEAD VS DISTANCE FROM CENTER

The corner radius was varied from three inches to twenty inches using the adjustable baffles installed for that purpose. The results indicate a substantial dropoff in fluid motion as the radius is decreased as shown in Figure 63. Change in radius reduced swirl more rapidly at large radii while relatively little difference was apparent in the range of three to six inches. A radius of twelve inches (radius ratio of 0.6) was considered to be the minimum corner radius for effective use of the swirl system.

The installation of the centerbody provided an increase in the average velocity in the annular track between the centerbody and the tank wall. The velocity near the tank wall (Pitot distance of 18 1/8 in.) was the same with or without the centerbody. The velocity near the centerbody (Pitot distance of 14 1/8 in.) was significantly improved with the twelve inch corner radius. The velocity plots can be seen in Figure 64.

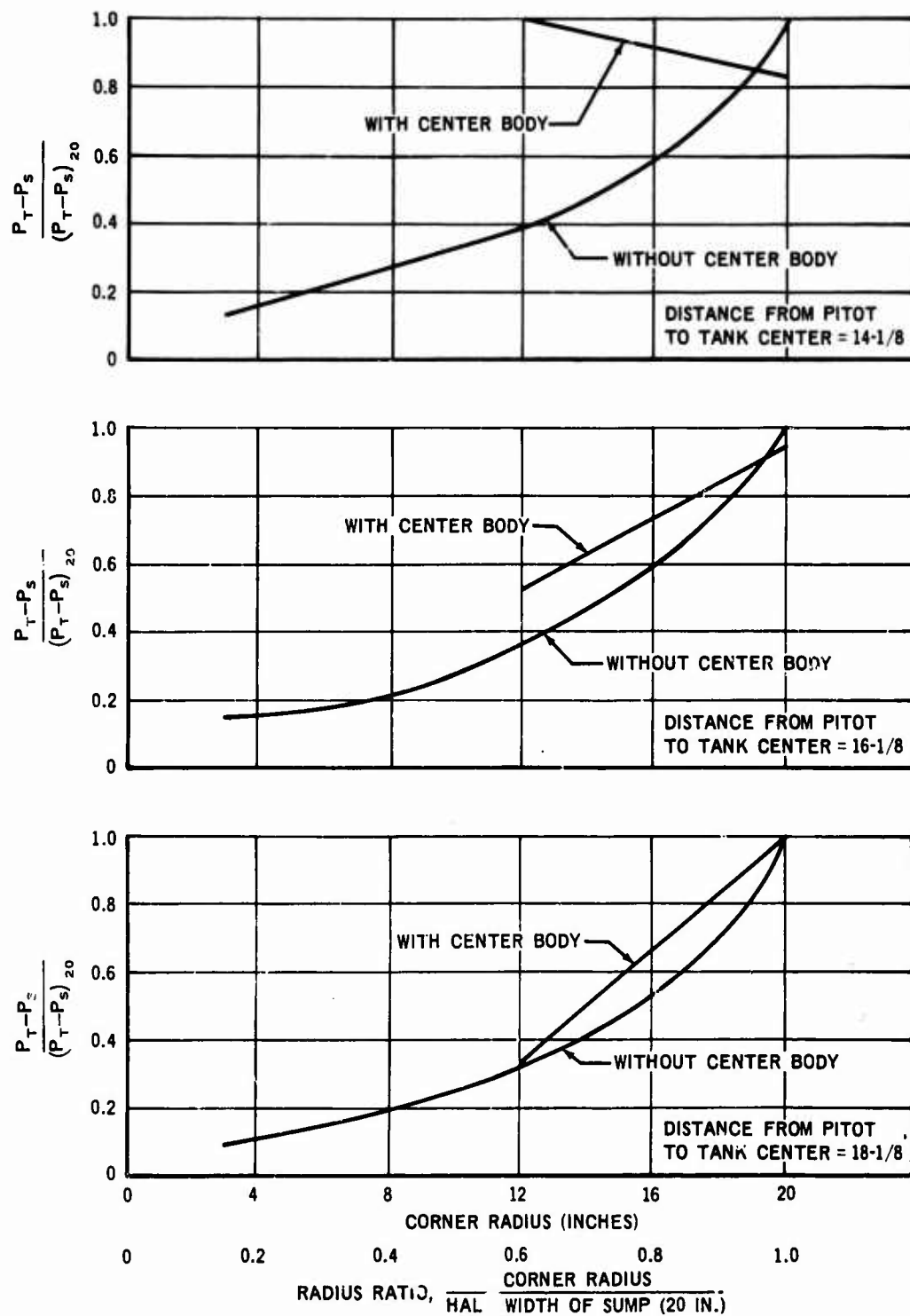


FIGURE 64. COMPARISON OF VELOCITY HEAD VS SUMP CORNER RADIUS

5.3.3 Flight Test

5.3.3.1 System Description

A flight test was conducted on a scale model of the sump and inlet configuration, mounted in the cabin of an Aero Commander, to verify the concept under flight conditions including zero and lateral gravity periods. The sump tank was simulated using a tank, of approximately one cubic foot volume, made out of transparent acrylic plastic. The vertical corners were rounded to a three inch radius (radius ratio of corner radius to the radius of an inscribed circle = 0.5) and fittings for fill, vent, swirl, and normal usage were attached in appropriate locations. The tank was mounted in a test box which was sized to fit in the passenger compartment of an Aero Commander test aircraft. Figures 65 through 70 show the system schematic and photographs of the installation. In addition to the sump tank, an auxiliary tank was installed in the baggage compartment to provide a reservoir for fill and drain of the sump tank. The auxiliary tank was mounted higher than the sump tank to provide gravity flow to fill the sump tank. Suitable valves and lines were installed to provide fill, drain, venting, and closed system circulation (swirl and fuel pickup). A movie camera was mounted to record events inside the tank. Instrumentation included a mechanical accelerometer, pump pressure gage, and sight glass - all mounted within the camera field of view. The tank and sight glass were backlighted through translucent panels while the accelerometer and pressure gage were frontlighted with a small flood light. All systems were designed for 28 vdc, to be compatible with the aircraft electrical system. The valves were mounted outside the flight box to permit manual operation. Instrumentation mounted above the aircraft instrument panel for the pilot included a gyro and a ping pong ball suspended on a thread.

The fluid was circulated by a positive displacement pump mounted inside the flight box. An air valve was installed upstream of the pump. This valve vented to ambient and was used to allow the pump to suck air into the line. This provided a visual indication, with bubble motion, of swirling in the tank. Two small polyurethane balls were placed in the tank as a further indication of motion. One of the balls was weighted with lead shot until it had the specific gravity of water, in order to show motion in lower parts of the tank.

The sight glass and pressure gage were used to provide an indication when the fuel pickup became uncovered and air was sucked into the system. This provided a means of assessing the effectiveness of the swirl in positioning the fluid in zero gravity conditions. Water was used instead of fuel as a safety precaution.

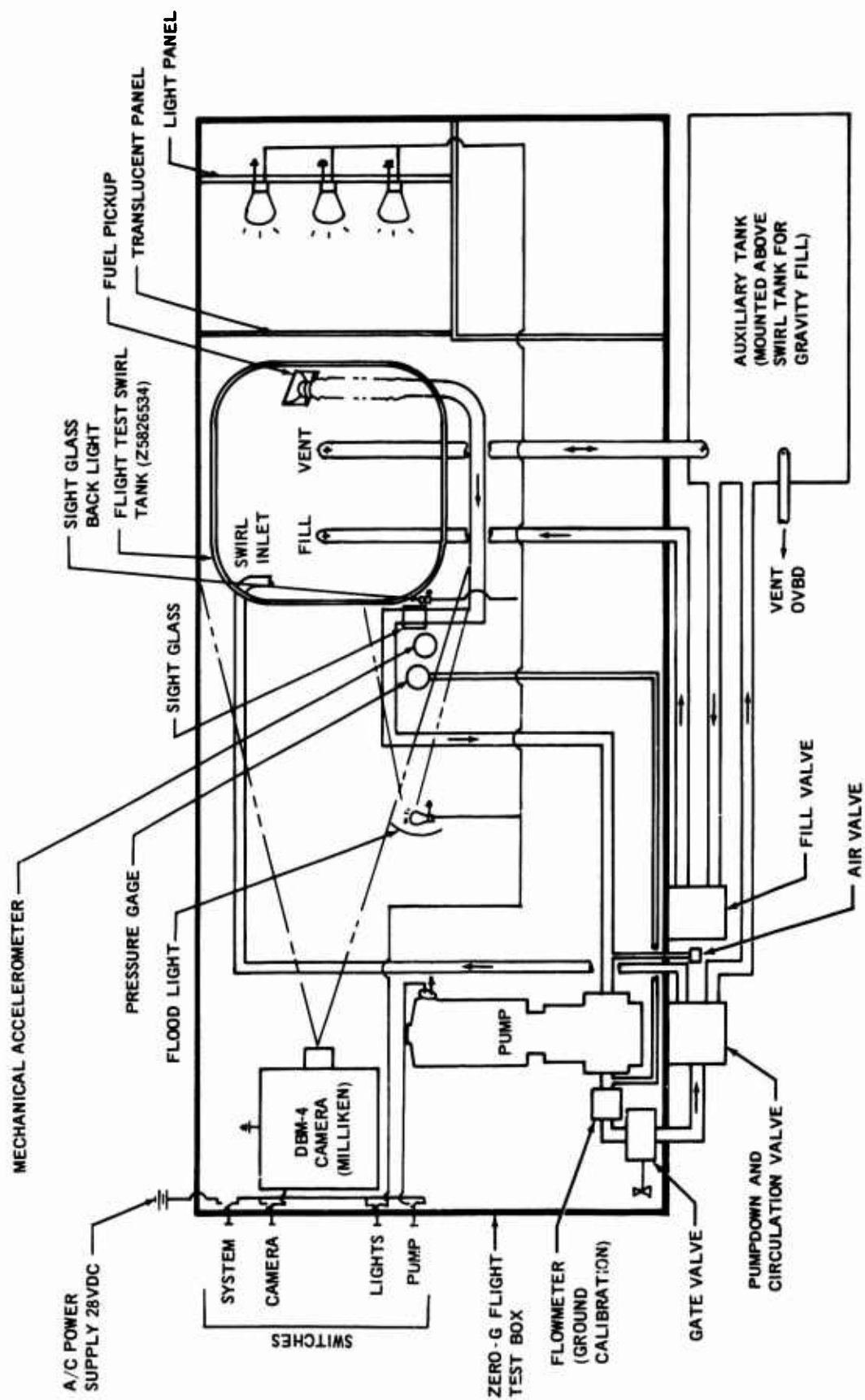


FIGURE 65. SCHEMATIC - ZERO-G FLIGHT TEST OF SWIRL TANK

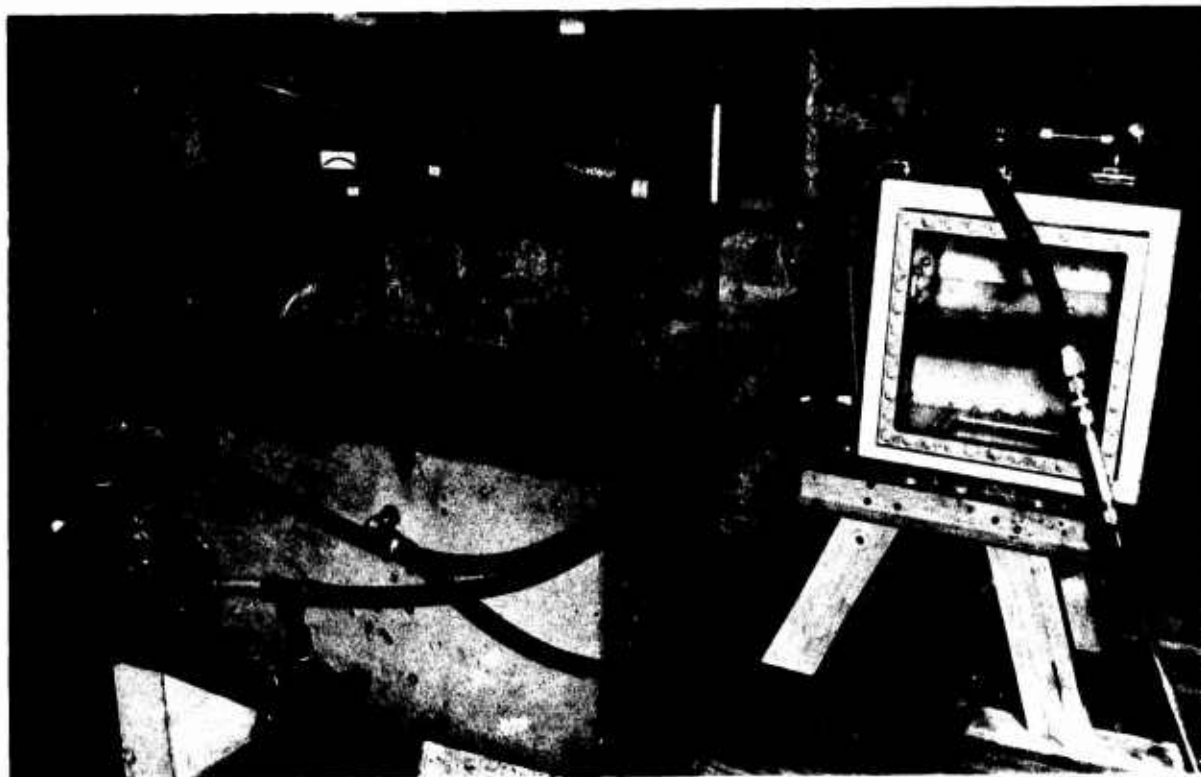


FIGURE 66. FLIGHT TEST SYSTEM - GROUND CHECKOUT

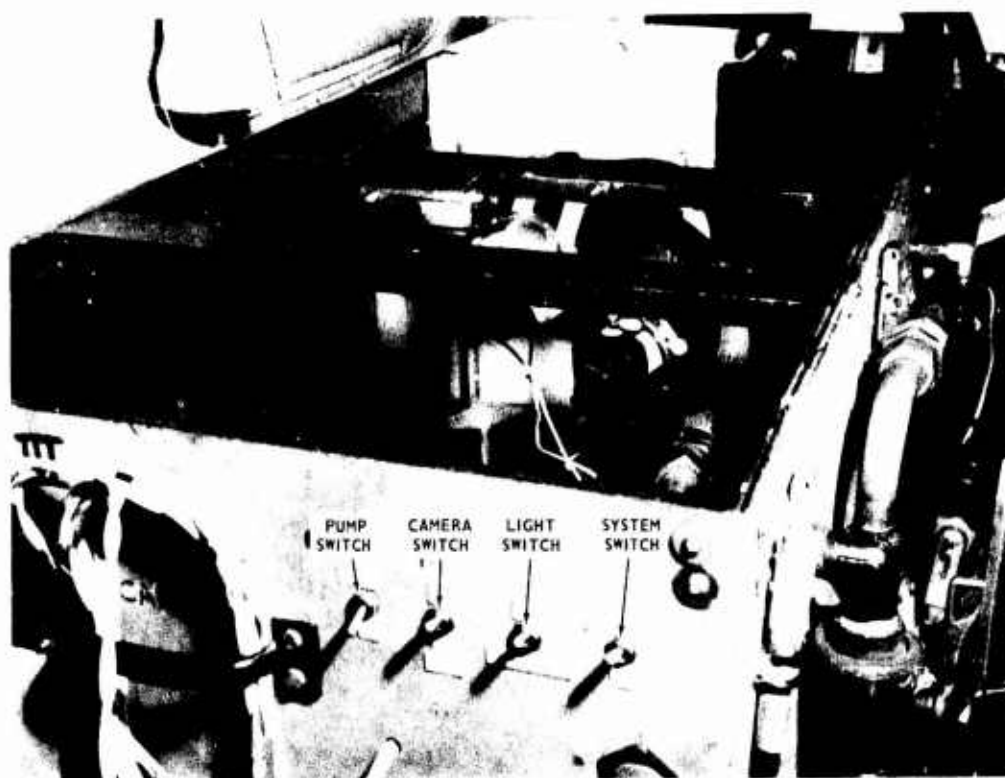


FIGURE 67. END OF TEST BOX WITH CONTROL SWITCHES

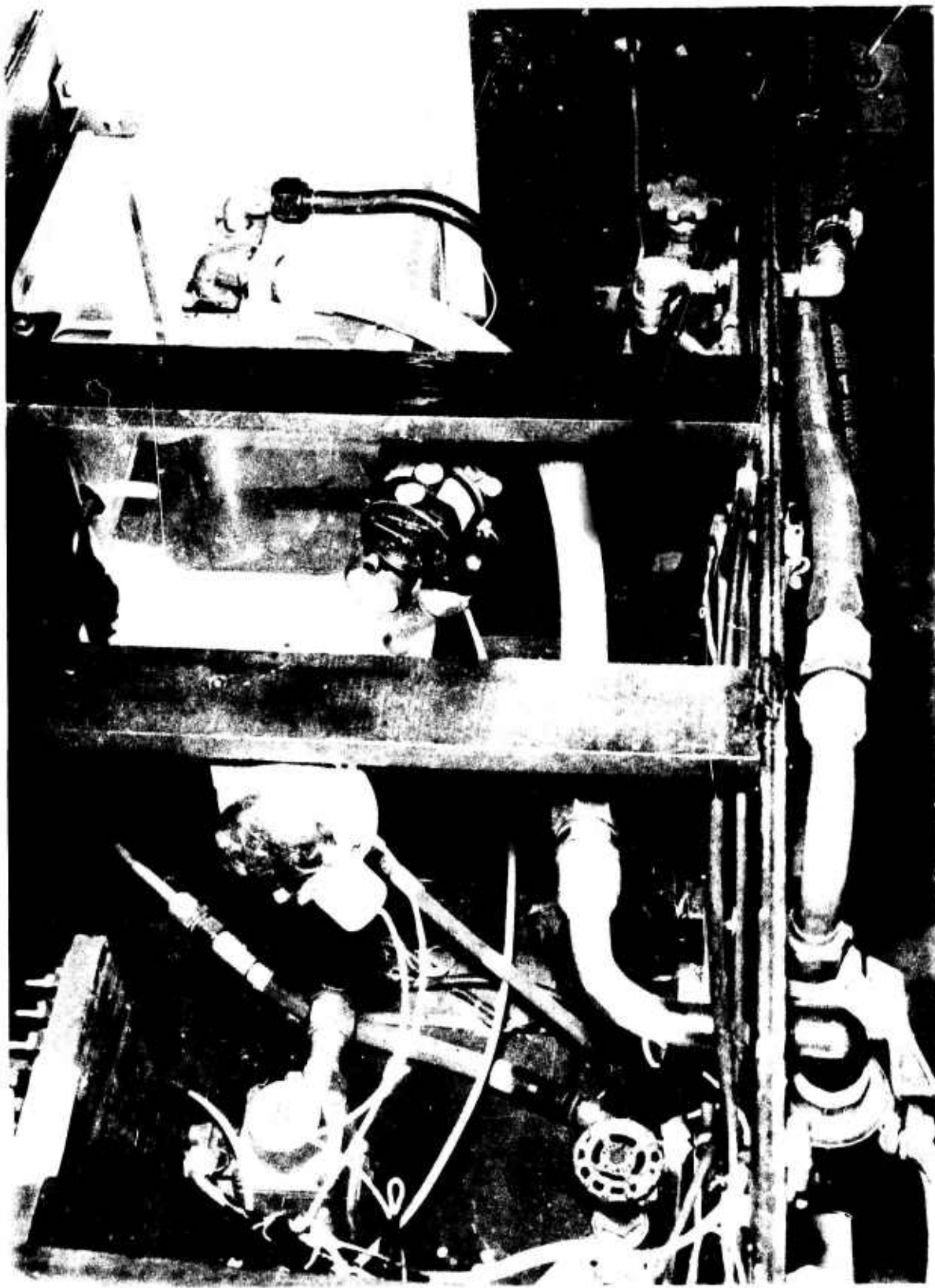


FIGURE 68. INSIDE VIEW OF TEST BOX

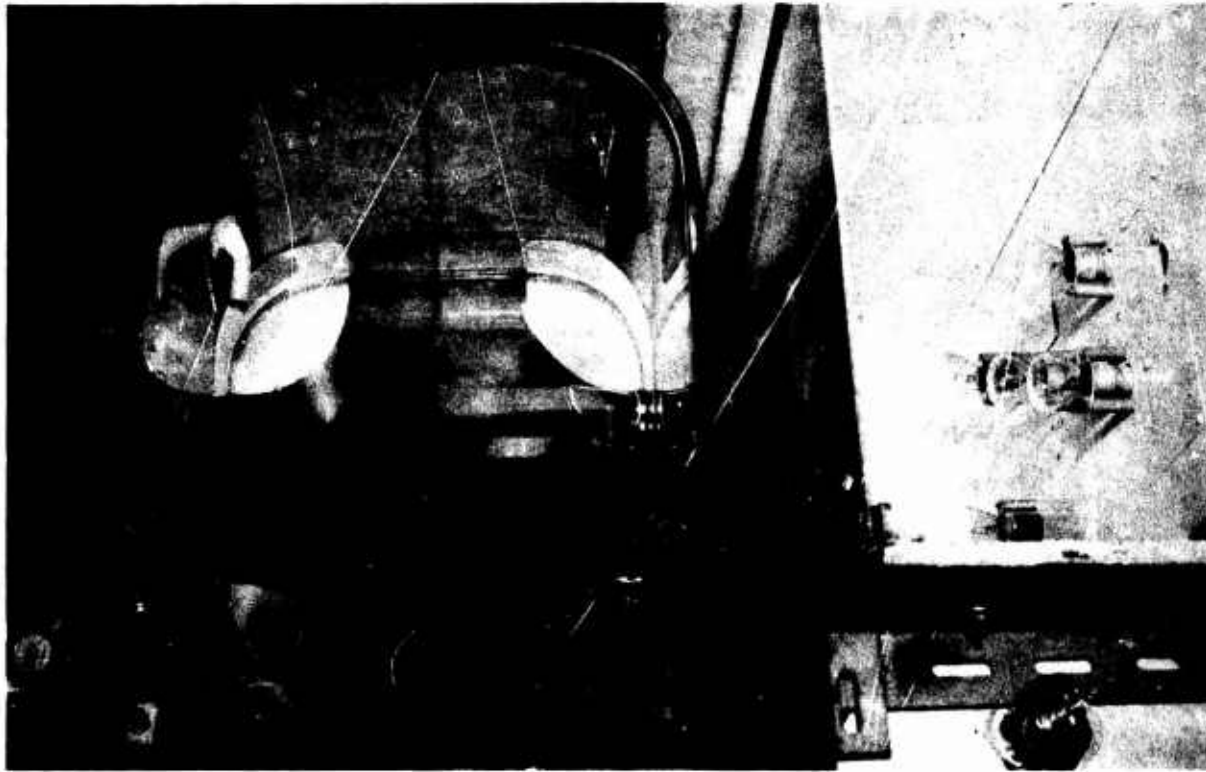


FIGURE 69. SWIRL TEST TANK MOUNTED IN TEST BOX

5.3.3.2 Flight Test Procedure

Tests were conducted to determine the feasibility of the swirl concept under zero gravity conditions. The Aero Commander provided periods ranging from six to nine seconds of near zero gravity. The aircraft is not designed for negative gravity, therefore that condition was not a part of the flight test program. The tests included:

1. Level flight with swirl – swirl nozzle off during pumpdown,
2. Zero gravity conditions
 - a. No swirl – base case of fluid in zero gravity
 - b. Swirl – swirl nozzle off during pumpdown
 - c. Swirl – swirl nozzle on during pumpdown (simulating a small jet of sustaining fluid during emptying of the tank), and
3. Dutch roll with swirl–swirl nozzle off during pumpdown (lateral gravity forces).

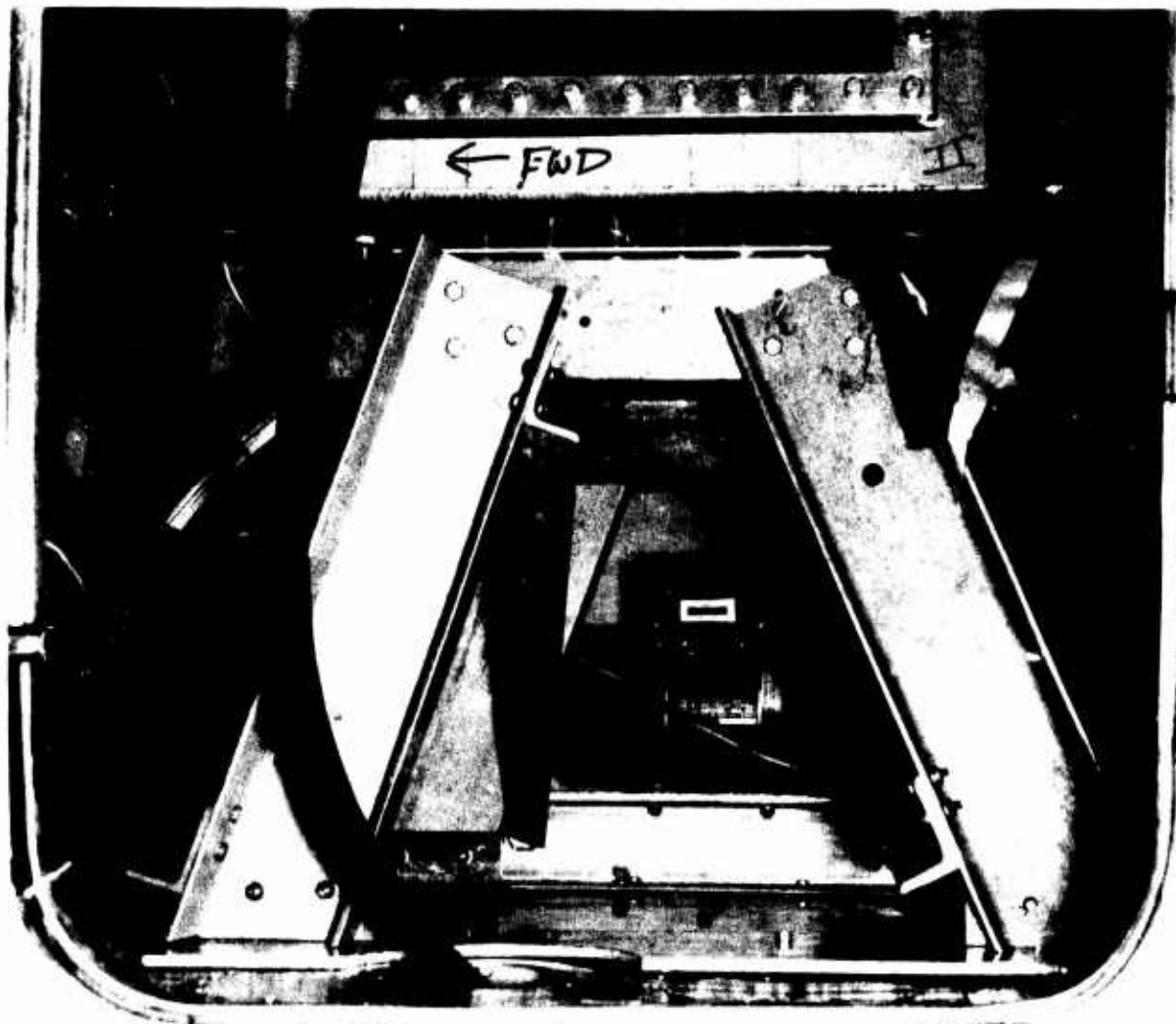


FIGURE 70. AUXILIARY TANK MOUNTED IN BAGGAGE COMPARTMENT

The flight test was conducted after several ground checkouts of the test rig. The sight glass proved to be a quick indication of loss of prime due to the pickup being uncovered. Pumpdown of the system (simulating loss of transfer fuel in the aircraft) eventually caused the pickup to unprime. The pressure gage did not react as quickly as the sight glass. The gage, however, served two purposes. It provided an indication of the exact time of start of pumpdown because the pressure drop of the two lines was different. That is, when the flow was diverted from swirl generation to pumpdown of the system the change was registered on the pressure gage as a decreased pressure. The gage also provided a measure of cavitation since the pressure output of the pump is a function of the vapor/liquid ratio entering the pump.

5.3.3.3 Flight Test Results

The flight test results were recorded on movie film. The photographs in Figures 71 through 91 are enlargements of single frames selected from the flight test film.

5.3.3.3.1 Level Flight. - Figures 71 through 74 illustrate a pumpdown of the tank during level flight to provide a base case under normal operating conditions of one g. Note that the accelerometer situated in the upper right hand corner reads one g. Figure 71 shows the balls circulating in a full tank. The plume out of the swirl generating nozzle is due to aeration of water when the air valve was opened to allow the pump to suck a mixture of air and water. The pressure gage, located at right center, reads about 12 psi indicating full flow through the nozzle. Figure 72 shows the tank approximately half full. The pressure gage reads about 8 psi indicating the fluid is being pumped to the reservoir tank in the baggage compartment. The fluid motion has slowed down. In Figure 73, the fuel pickup has started to suck a mixture of air and water. Note the mottled texture due to the bubbles in the sight glass at lower right. In Figure 74, the pickup is sucking a large portion of air and the pump output has dropped to approximately 3 psi.

5.3.3.3.2 Zero Gravity With No Swirl. - Figures 75 through 80 were taken from a sequence of tank pumpdown, without swirl, during zero gravity as a base case for weightlessness. In Figure 75, the aircraft is pulling out of a dive prior to entering zero gravity (the accelerometer reads approximately 1.5 g). In Figure 76, the system is experiencing zero gravity and the fluid has started to migrate. This motion continues (Figures 77 and 78) until in Figure 79, the pickup has unported; the pressure gage reads zero. In Figure 80, the pressure gage indicates about 9 psi, probably due to surge, but the sight gage is mottled indicating air in the line.

5.3.3.3.3 Zero Gravity With Swirl Prior to Pumpdown. - Figures 81 through 85 illustrate operation in zero gravity with initial swirl. Note the fuel pickup is positioned nearly horizontal (Figure 81) due to impingement of the swirling fluid. In Figures 82 and 83, air is being introduced into the swirl nozzle to help identify the fluid swirl motion. In Figure 84, pumpdown has started (note the pressure gage reading of approximately 8 psi). In Figure 85, the fluid has become randomly oriented, and the pump pressure has dropped to zero, a bubble has formed against the wall starting at the nozzle and continuing around the tank.

5.3.3.3.4 Zero Gravity With Sustaining Swirl. - Figures 86 through 89 illustrate the effect of a sustaining swirl during pumpdown of the tank in zero gravity. The aircraft is pulling out of a dive in Figure 86 (accelerometer reads 1.7 g). In Figure 87, the bubble has started to form at the top of the tank; the pickup has risen to a nearly horizontal position. In Figure 88, the bubble has started migrating down the center of the tank. The bubble has moved to a vertical position in the tank in Figure 89, however, it still maintains a coherent shape indicating the sustaining swirl has been effective in positioning the fluid.

5.3.3.3.5 Dutch Roll. - Figures 90 and 91 depict operation in dutch roll (simulating lateral gravity forces).

5.3.3.4 Flight Test Conclusions

The flight test indicated that the use of a small jet of circulation sustaining flow will be required to maintain effective fluid rotation. The rotation of the fluid in the tank provided a means of energizing the fluid near the walls and formed a pressure gradient which caused the less dense bubble to migrate

FLIGHT TEST
LEVEL FLIGHT WITH SWIRL
SWIRL NOZZLE OFF DURING PUMP DOWN

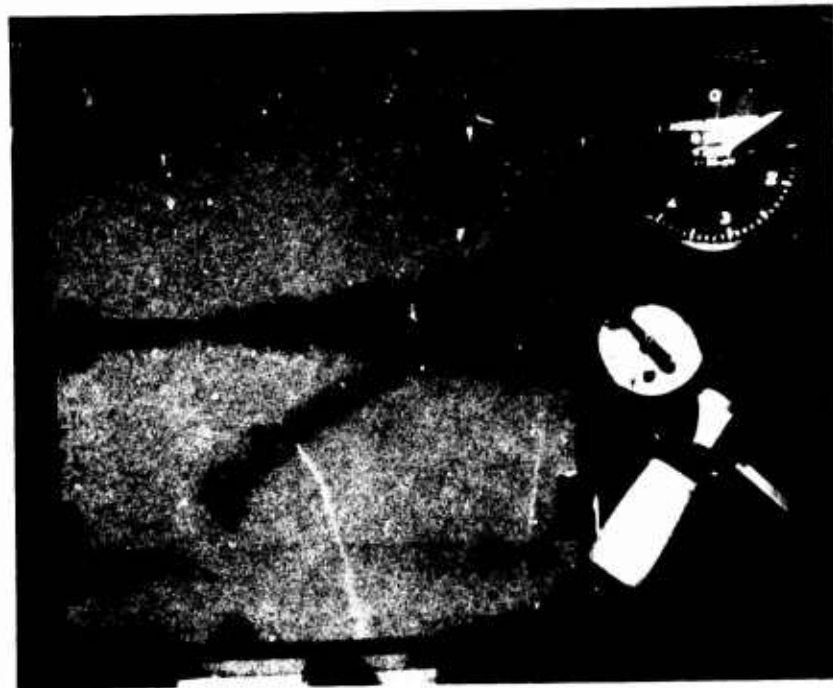


FIGURE 71. SWIRL JET "ON"



FIGURE 72. TANK PUMP DOWN

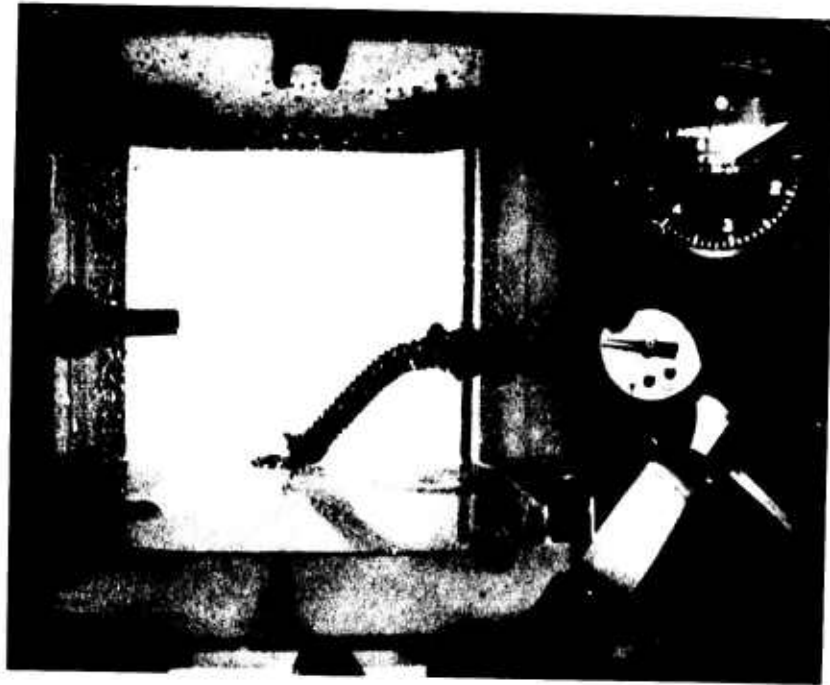


FIGURE 73. SIGHT GLASS CAVITATION

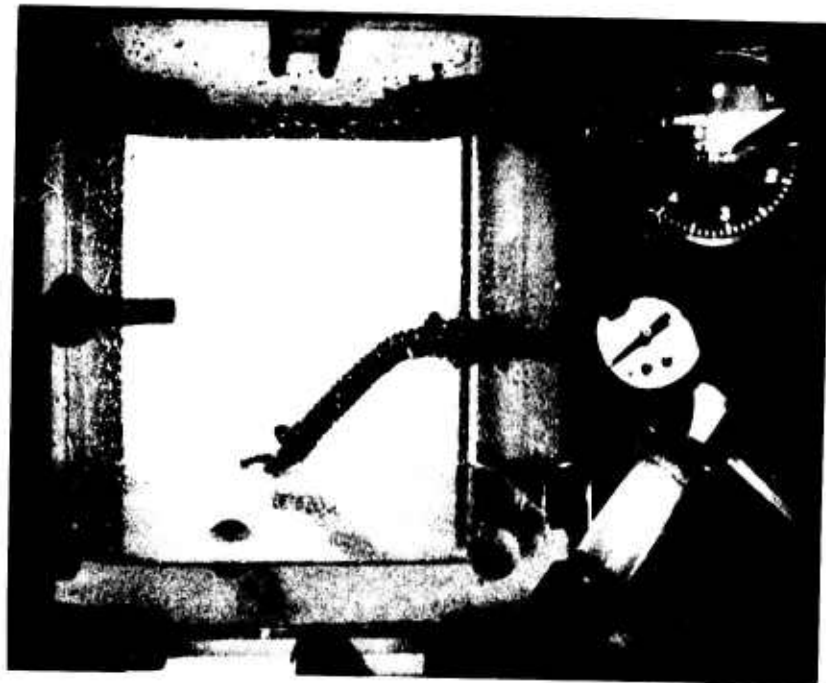


FIGURE 74. PUMP PRESSURE DECAY

FLIGHT TEST
ZERO GRAVITY WITH NO SWIRL

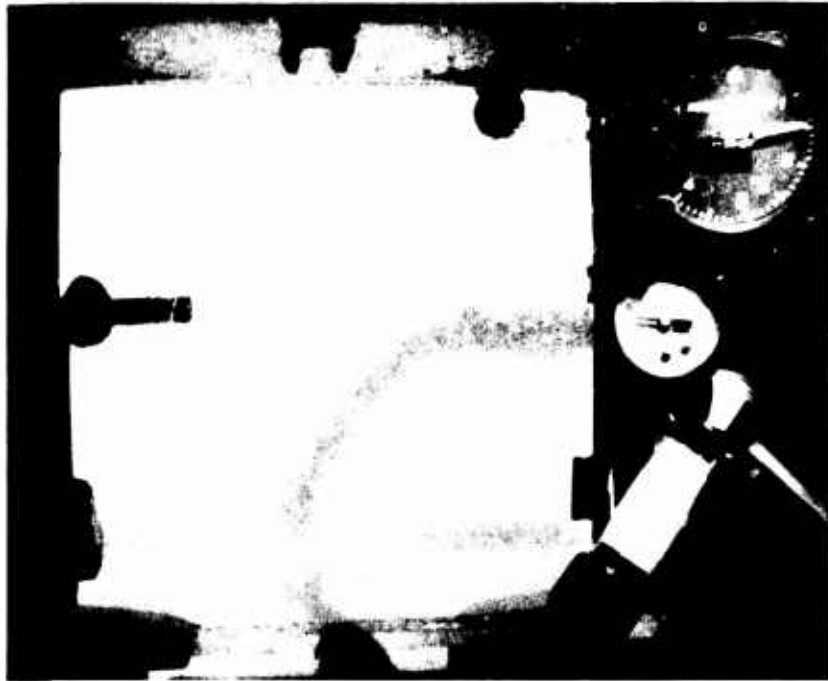


FIGURE 75. PULLOUT PRIOR TO WEIGHTLESSNESS

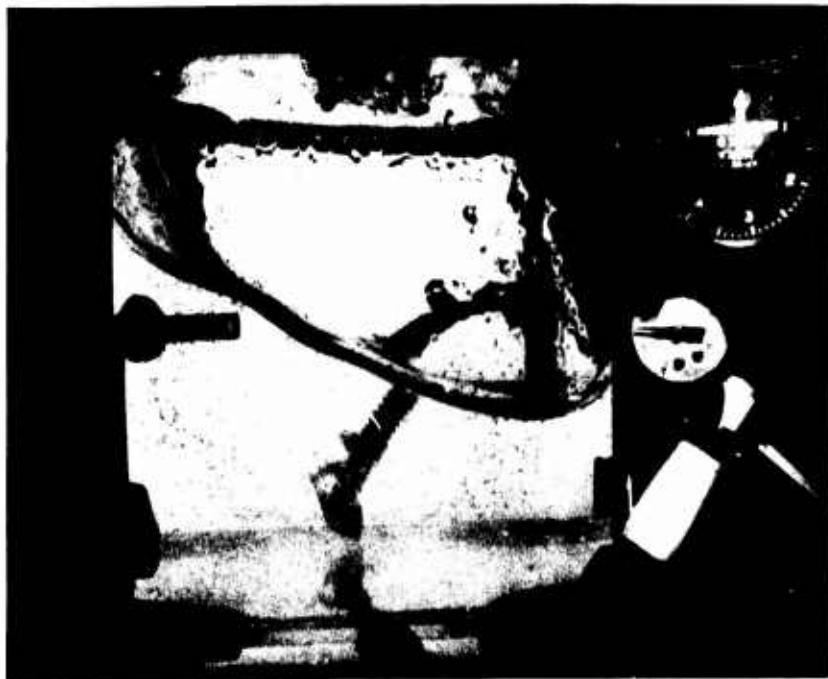


FIGURE 76. INITIAL MIGRATION OF FLUID

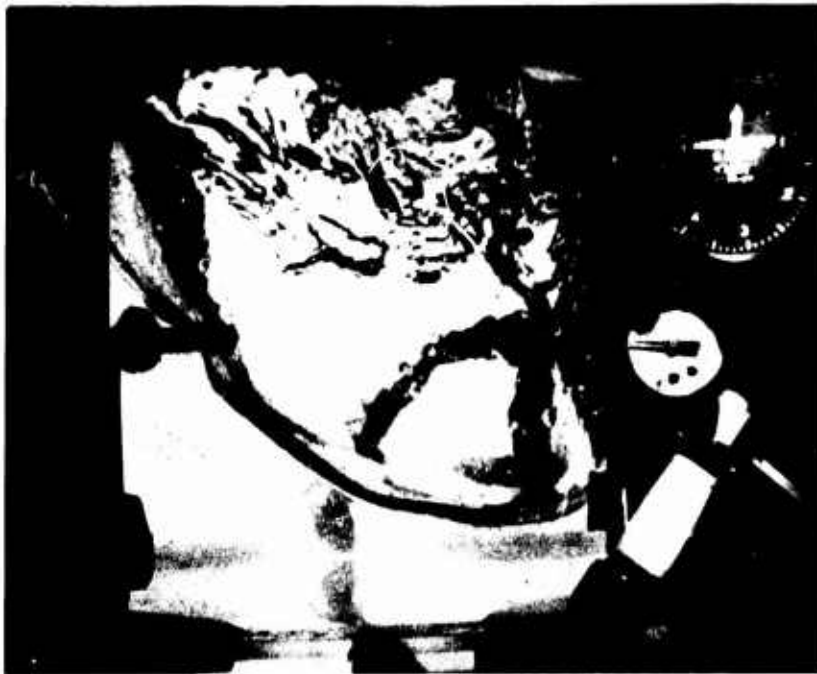


FIGURE 77. CONTINUED MIGRATION OF FLUID



FIGURE 78. CONTINUED MIGRATION OF FLUID



FIGURE 79. FUEL PICKUP UNPORTED

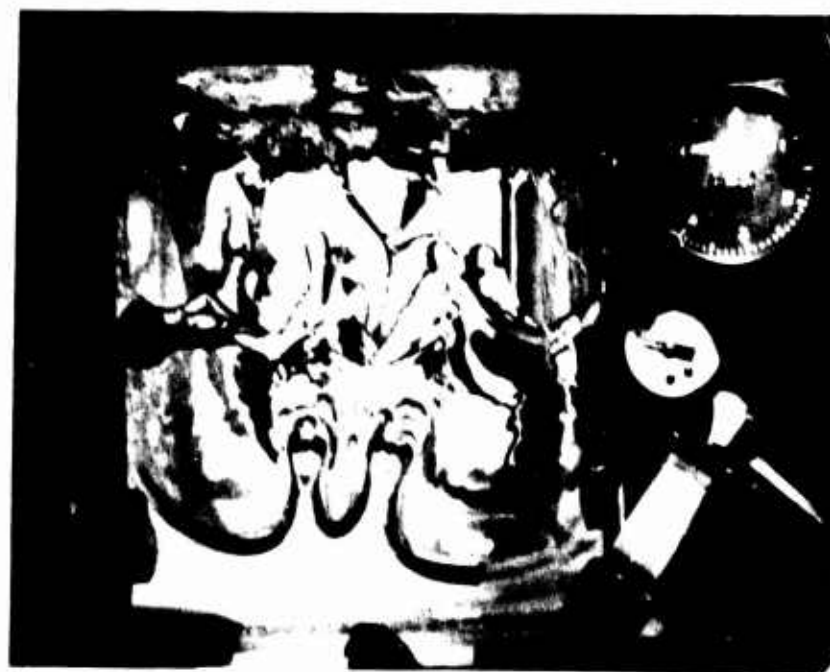


FIGURE 80. AIR IN SIGHT GLASS

FLIGHT TEST
ZERO GRAVITY WITH SWIRL
SWIRL NOZZLE OFF DURING PUMP DOWN



FIGURE 81. INITIAL ZERO GRAVITY



FIGURE 82. SWIRL JET ON



FIGURE 83. SWIRL JET ON



FIGURE 84. SIGHT GLASS INDICATES AIR

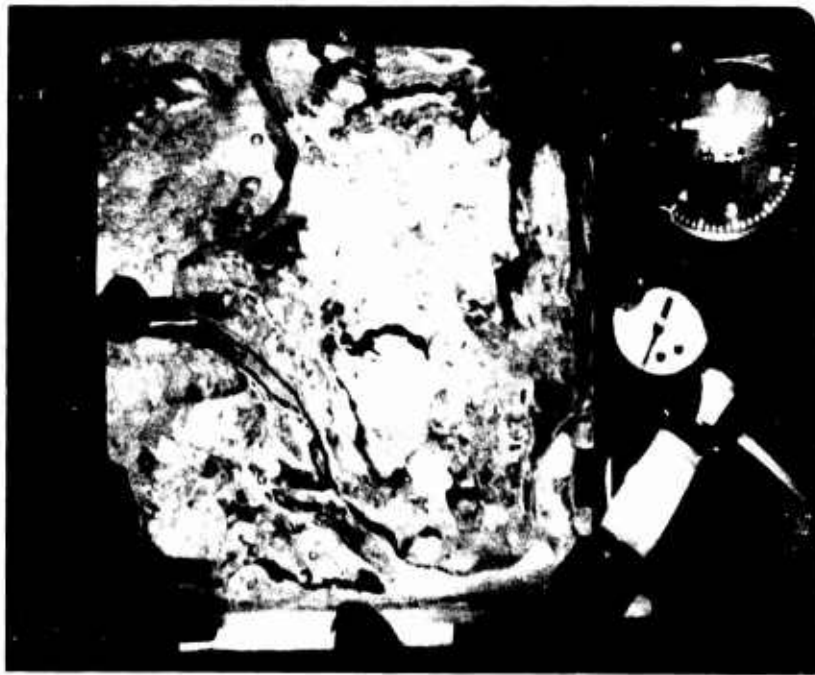


FIGURE 85. CAVITATION OF PUMP

toward the center. The bubble formed initially as a depression in the fluid toward the top of the tank and gradually filled the center as the tank was pumped down with sustaining flow. The air bubble prefers to be bound to the wall of the tank rather than free floating in the liquid, because the wall-bound state has a lower potential energy and is therefore the more stable state. (Ref 16, p. 397). The swirl appears to be more effective when the tank is full before entering zero gravity as it would be in actual flight. The pickup followed the fluid and positioned itself approximately midtank during zero gravity. (The swirl impingement was not strong enough to move the pickup under normal gravity conditions.)

FLIGHT TEST
ZERO GRAVITY WITH SWIRL
SWIRL NOZZLE ON DURING PUMP DOWN

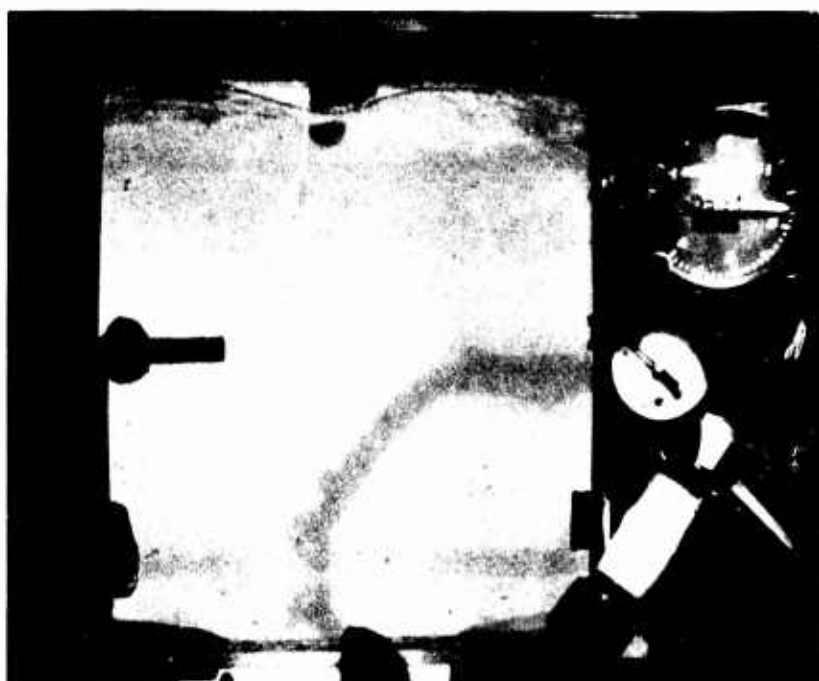


FIGURE 86. PULLOUT OF DIVE



FIGURE 87. BUBBLE FORMING AT TOP OF TANK



FIGURE 88. BUBBLE MIGRATES DOWN



FIGURE 89. COHERENT VERTICAL BUBBLE

5.3.3.3.5 Dutch Roll

Figures 90 and 91 depict operation in dutch roll (simulating lateral g forces).

FLIGHT TEST
DUTCH ROLL WITH SWIRL

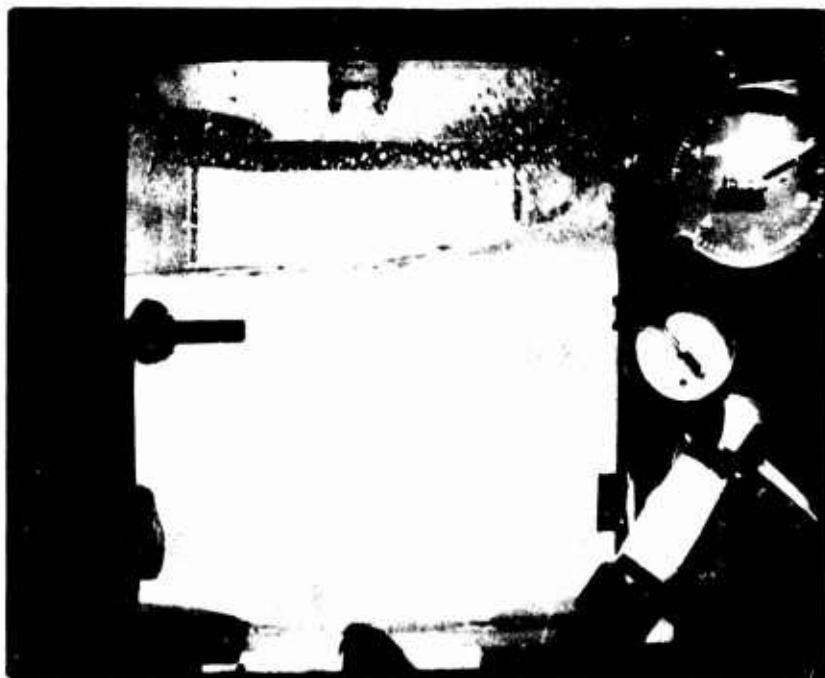


FIGURE 90. FLUID ACCELERATION TO RIGHT

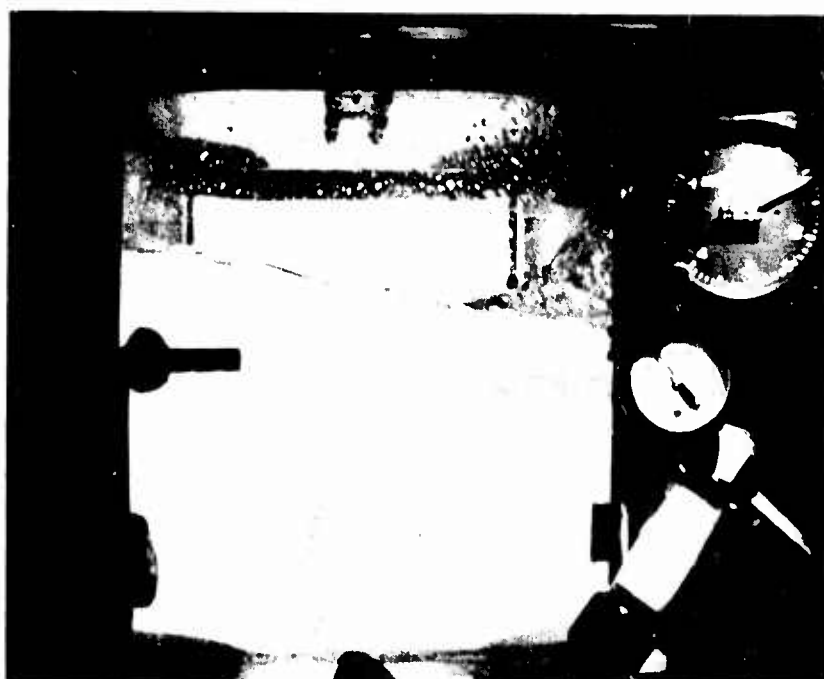


FIGURE 91. FLUID ACCELERATION TO LEFT

5.4 SUMMARY

The fuel tank sump, consisting of fuel circulation system and a flexible hose type fuel pump inlet line, has undergone a series of development tests in order to verify analysis and demonstrate the system capabilities.

The swirl testing showed that the theoretical drag must be increased by a correction factor in order to be compensated for losses estimated to be friction and turning losses not accounted for by the general equations. The correction factor, as a function of the Reynolds number of the rotating fuel, is presented in Figure 54.

Tests were conducted with a centerbody which formed an annular track in which the fuel could circulate. This eliminated the slow moving center fuel which only tended to dissipate the energy of the circulating fuel. The peripheral velocity at the outside wall did not change, however, the velocity at the inner wall increased substantially.

The corner radius of the tank has a strong influence on the resulting velocity. The best configuration was a full radius. As the corner radius was decreased, the velocity fell off rapidly. It was considered that at a radius equal to one quarter of the tank width, the velocity had decayed to the minimum acceptable level.

Flight test was conducted on a scale model of the sump system and flown in an Aero Commander to demonstrate the zero gravity conditions in the tank with and without the swirl jet operating. The flight test demonstrated that it is necessary to maintain the swirl action during the period of zero gravity. The flight test also showed that the flexible inlet tube will react as predicted to follow the gravity force, thus in negative gravity the pickup will move to the top of the sump as does the fuel and continue to supply fuel to the ejector pump.

SECTION VI

FLUIDIC AMPLIFIER

6.1 INTRODUCTION

A fluidic amplifier was studied as a possible control device for the ejector pump fuel feed system. This device would make use of fluid pressure(s) to regulate the flow and/or pressure output of the jet pump. The control flow would be bled from the ejector pump discharge such that as the discharge pressure increased the control flow would increase and divert a portion of the ejector nozzle flow. This loss in nozzle flow would in turn cut back the pump discharge pressure. The resulting action would maintain an ejector pump discharge pressure which would not exceed a desired maximum. This device would have high reliability in consonance with the design philosophy of no moving parts.

6.2 DESIGN

The fluidic amplifier shown in Figure 92 was designed as a proportional flow divider device. The power supply flow was introduced through a nozzle into

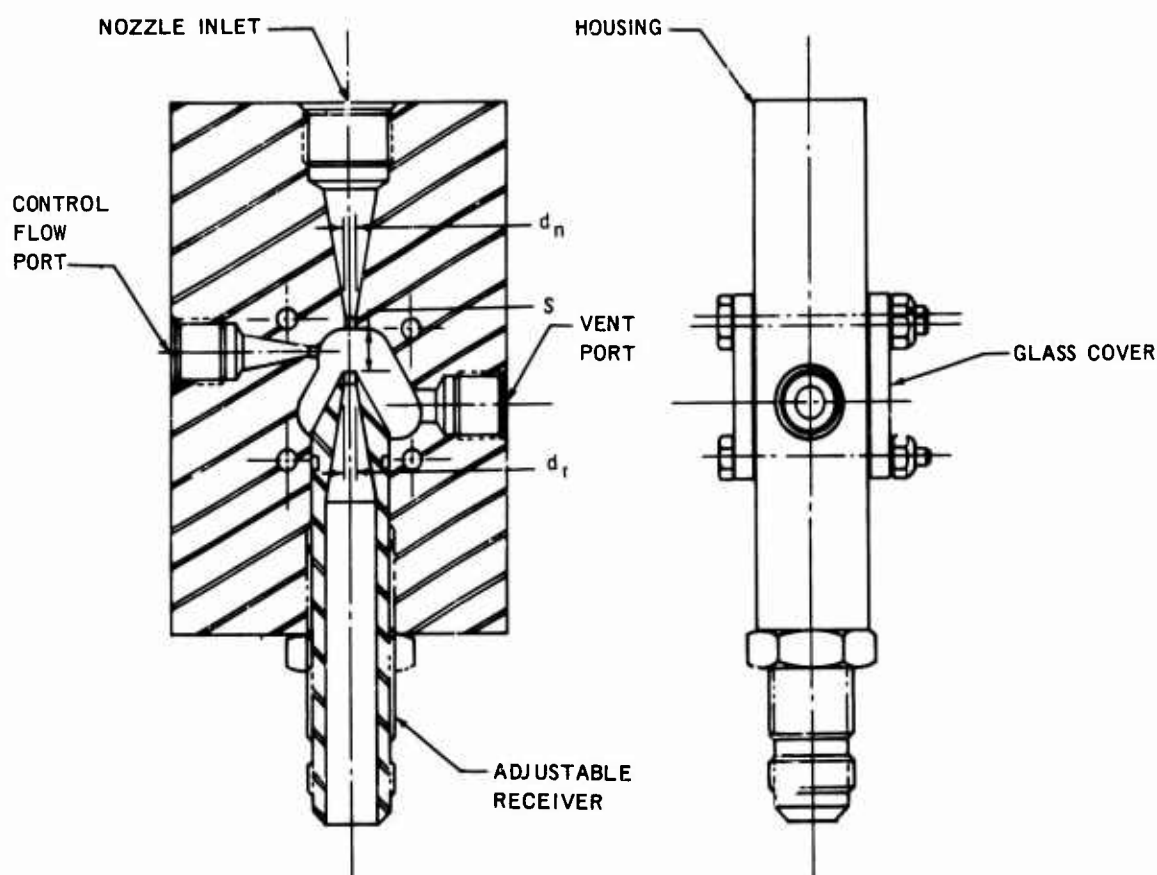


FIGURE 92. FLUIDIC AMPLIFIER

the amplifier such that it would pass through a cavity. A receiver opening with a downstream diffuser was located in the cavity downstream of the nozzle and collinear with it. Control flow was introduced into the same cavity at a 90° angle to the power supply flow. The momentum of the control flow was used to deflect the power supply flow as it passed from the nozzle exit to the receiver. This deflection resulted in both pressure and flow losses; the diverted flow was vented from the cavity into a catch tank. The larger the control flow the more the deflection of the main power flow.

To facilitate parametric studies, the amplifier was designed with a movable receiver to vary the power nozzle to receiver spacing. A series of runs were made with different nozzle spacing and varying receiver diameters. The power supply was set at a given pressure and control flow varied. Amplifier output flow and pressure were recorded with varying control flow. The test setup shown schematically in Figure 93.

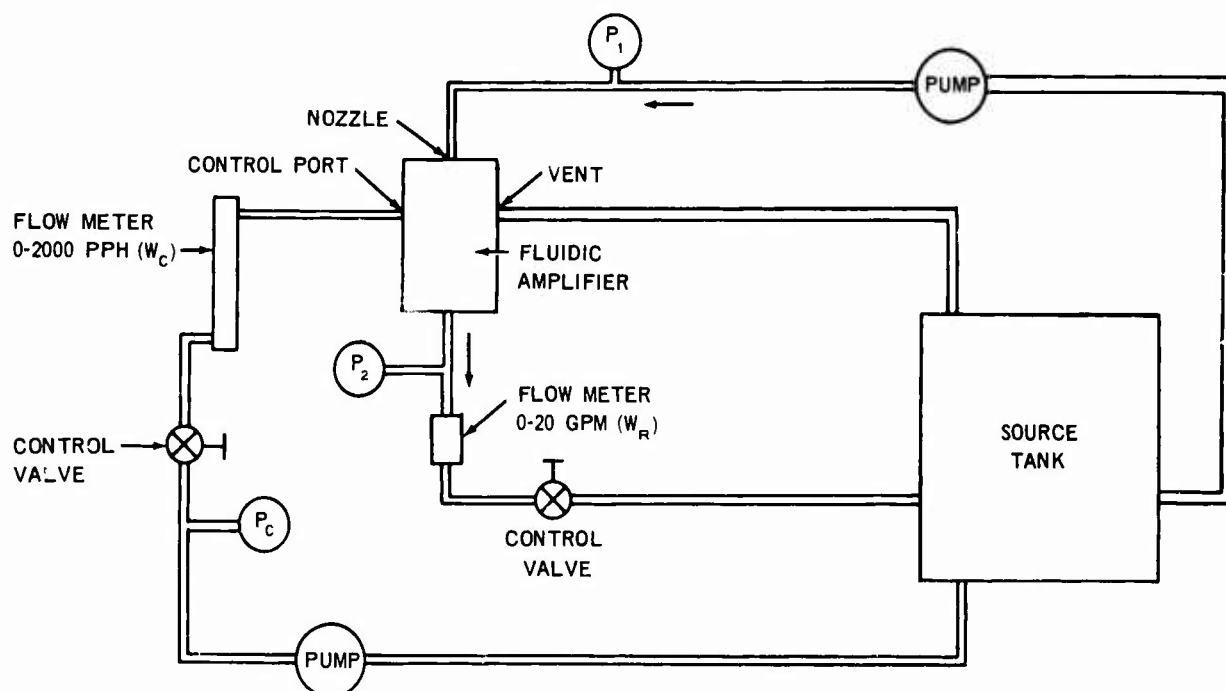


FIGURE 93. SCHEMATIC OF TEST SETUP FOR FLUIDIC AMPLIFIER

6.3 TEST RESULTS

Figures 94 and 95 present amplifier efficiency as a function of power loss versus pressure recovery across the amplifier with no control applied. The lower nozzle spacing ($s = 0.25$) resulted in significantly higher efficiencies as did increasing power supply pressure. The peak efficiency tended to occur at higher pressure ratios as spacing was decreased and supply pressure was increased. Increasing the receiver diameter resulted in lower peak efficiencies at lower pressure recovery ratios.

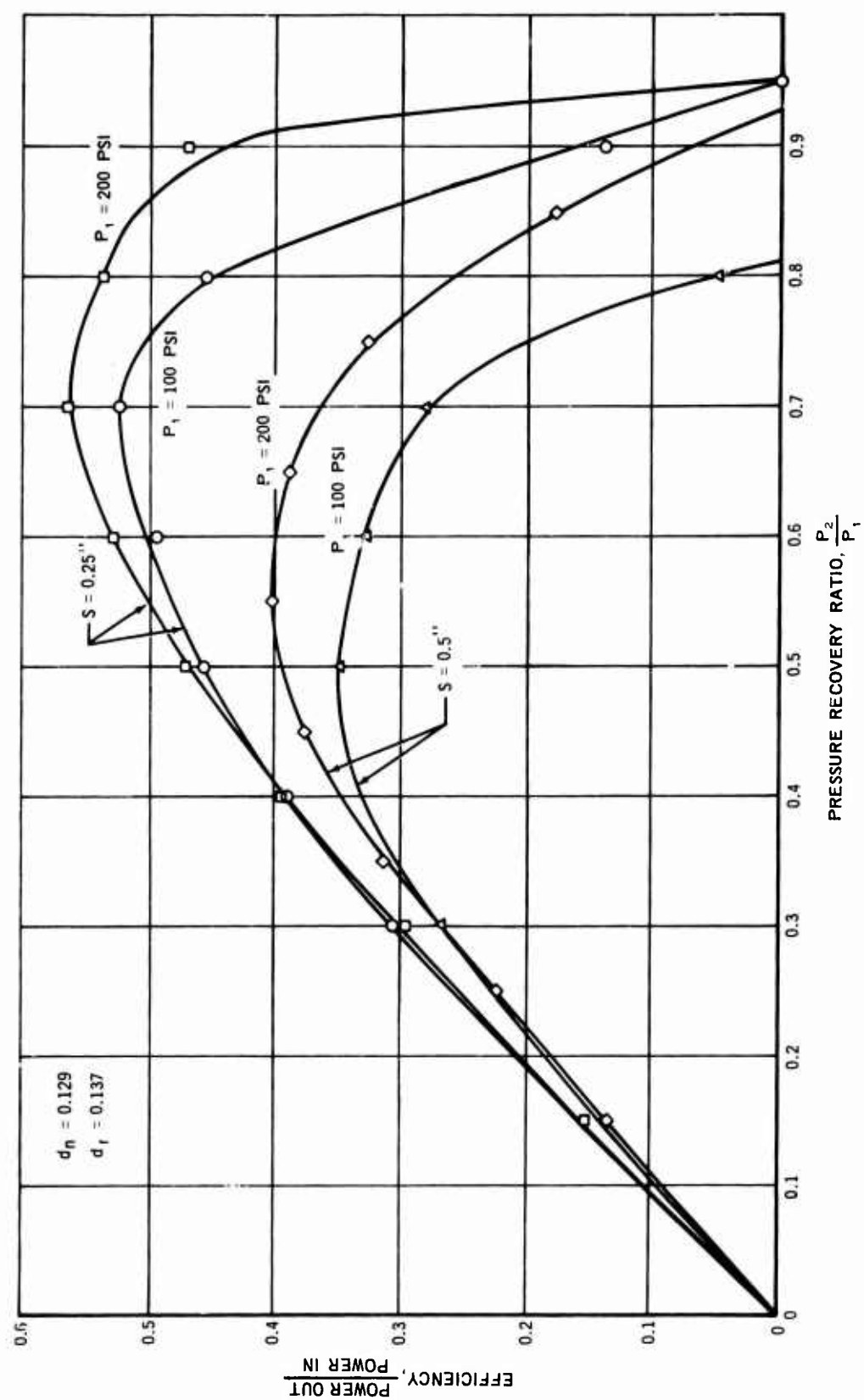


FIGURE 94. FLUIDIC AMPLIFIER PERFORMANCE

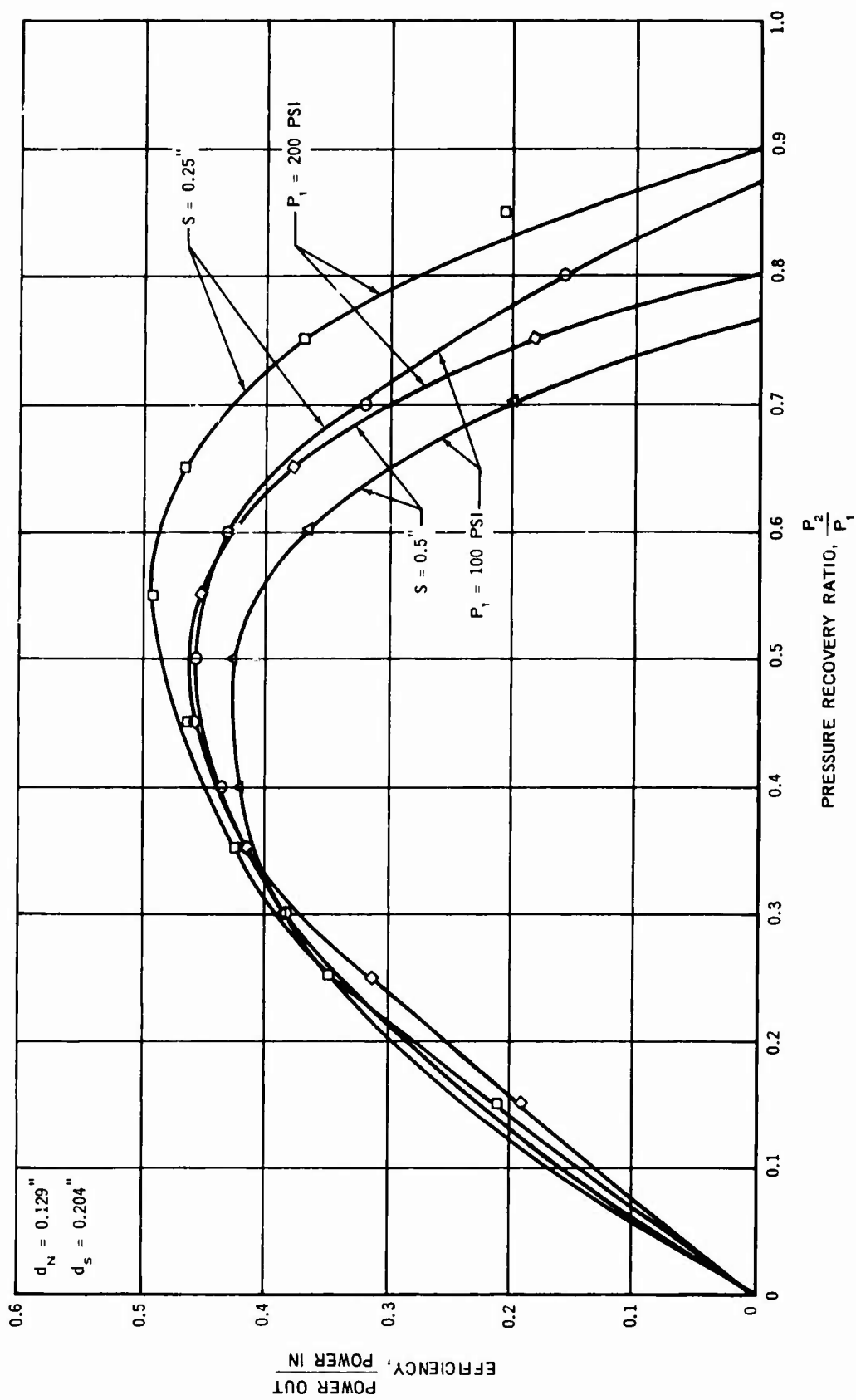


FIGURE 95. FLUIDIC AMPLIFIER PERFORMANCE

Figures 96 through 99 illustrate the effect of control flow on amplifier performance. The control flow is not effective at low pressure recovery ratios, the best results occurring with high control flow, low receiver diameter and large spacing. The parametric pressure recovery ratio is not graphed beyond the approximate peak efficiency point.

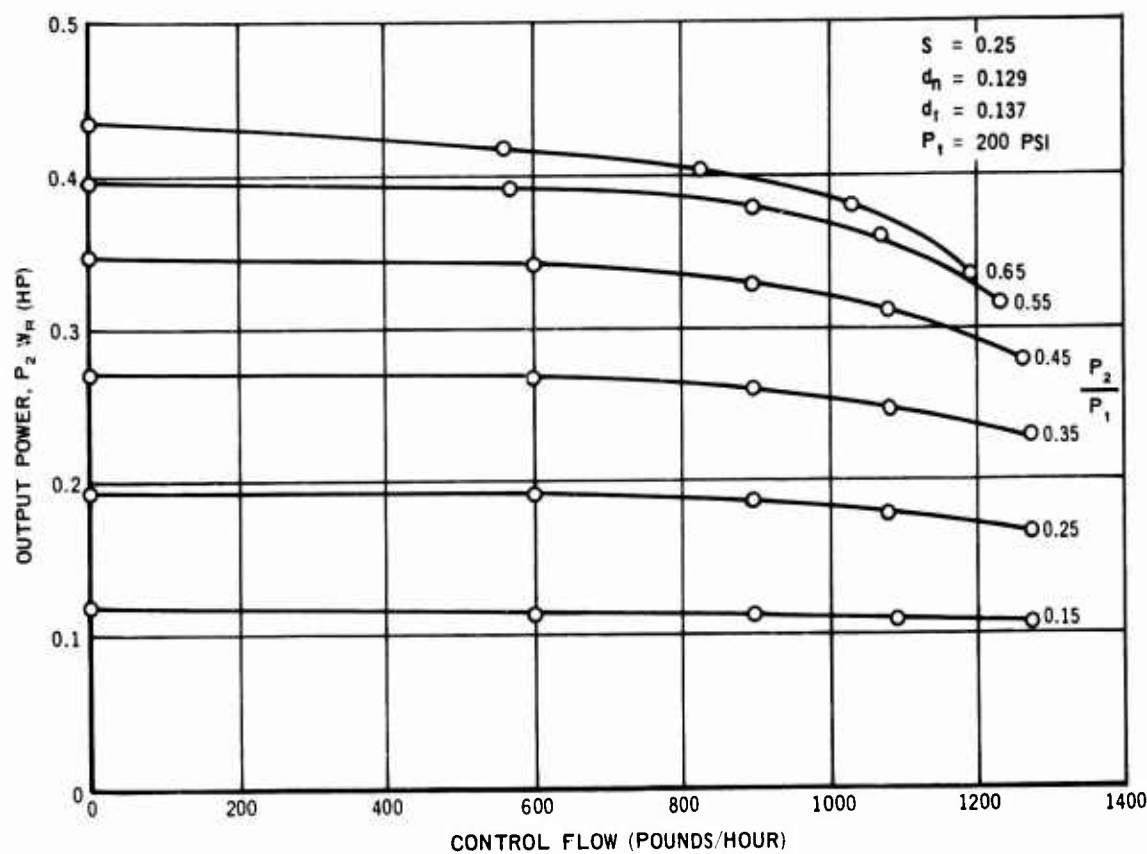


FIGURE 96. FLUIDIC AMPLIFIER PERFORMANCE

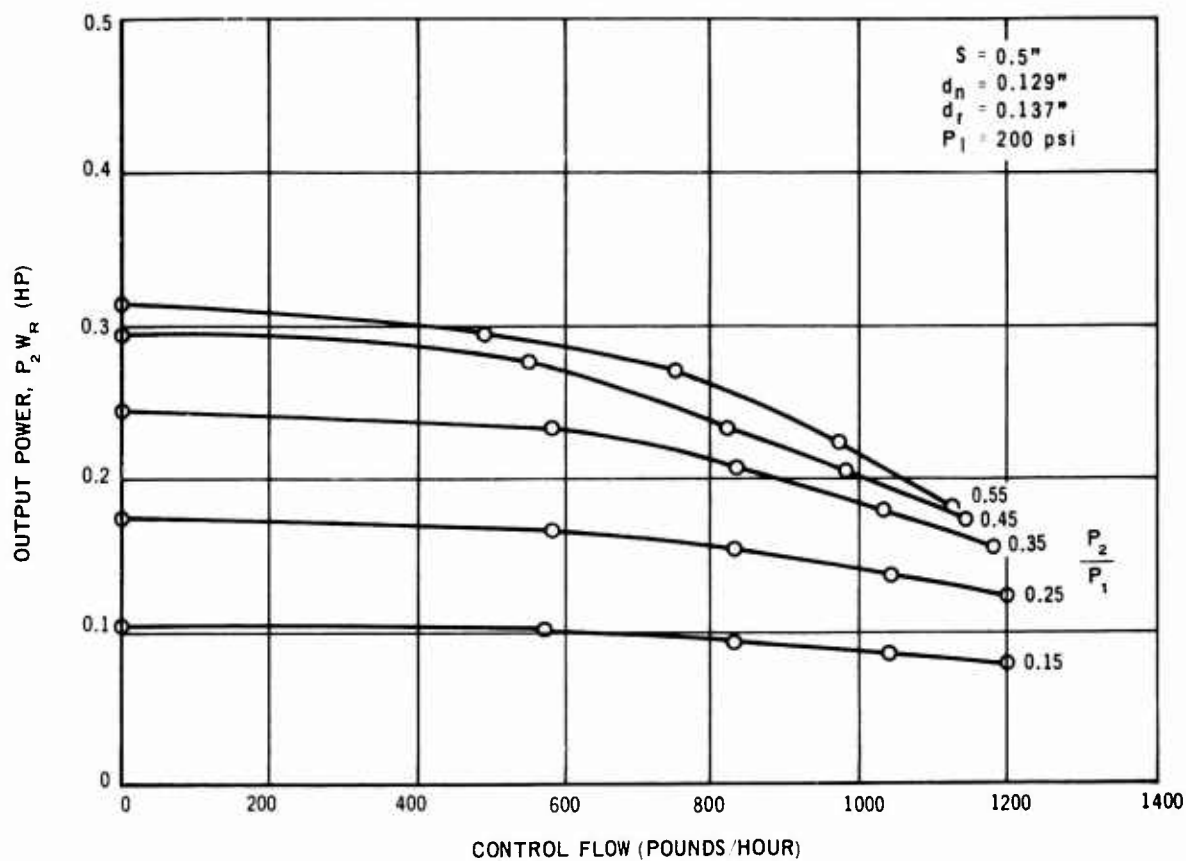


FIGURE 97. FLUIDIC AMPLIFIER PERFORMANCE

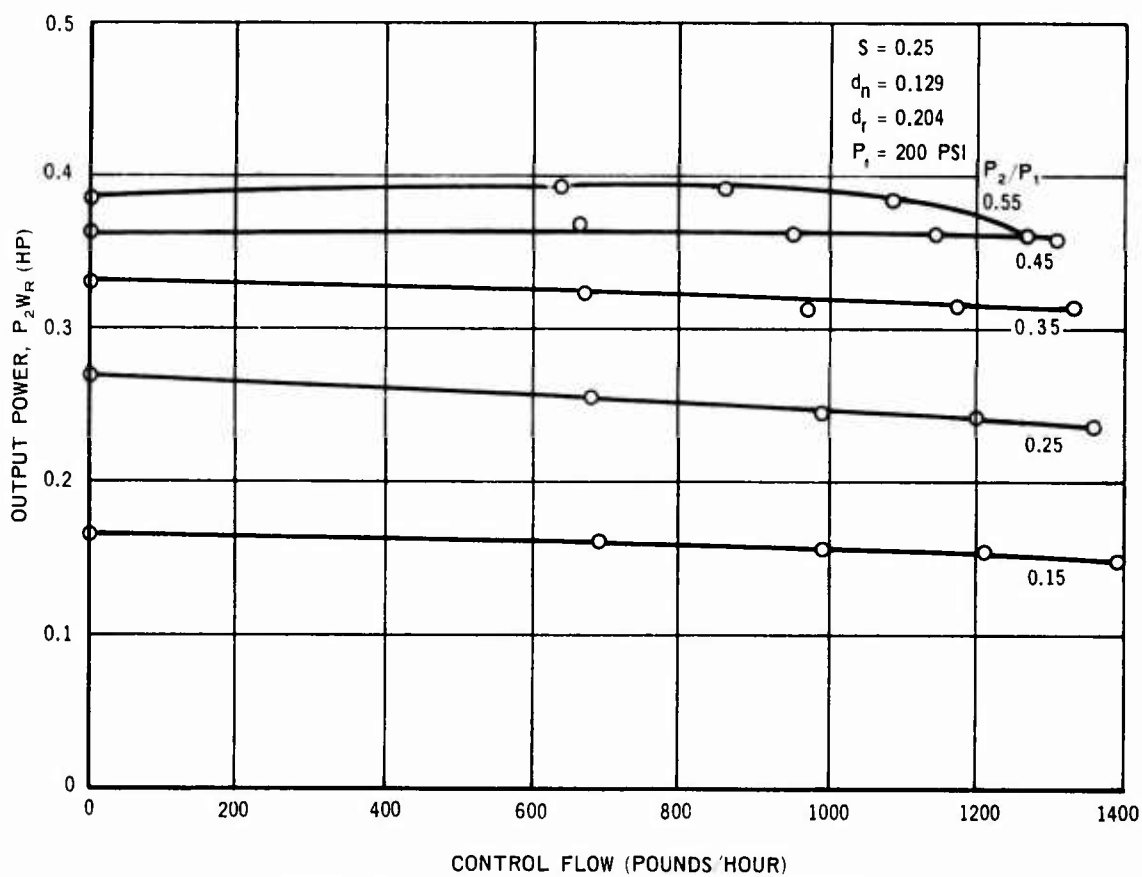


FIGURE 98. FLUIDIC AMPLIFIER PERFORMANCE

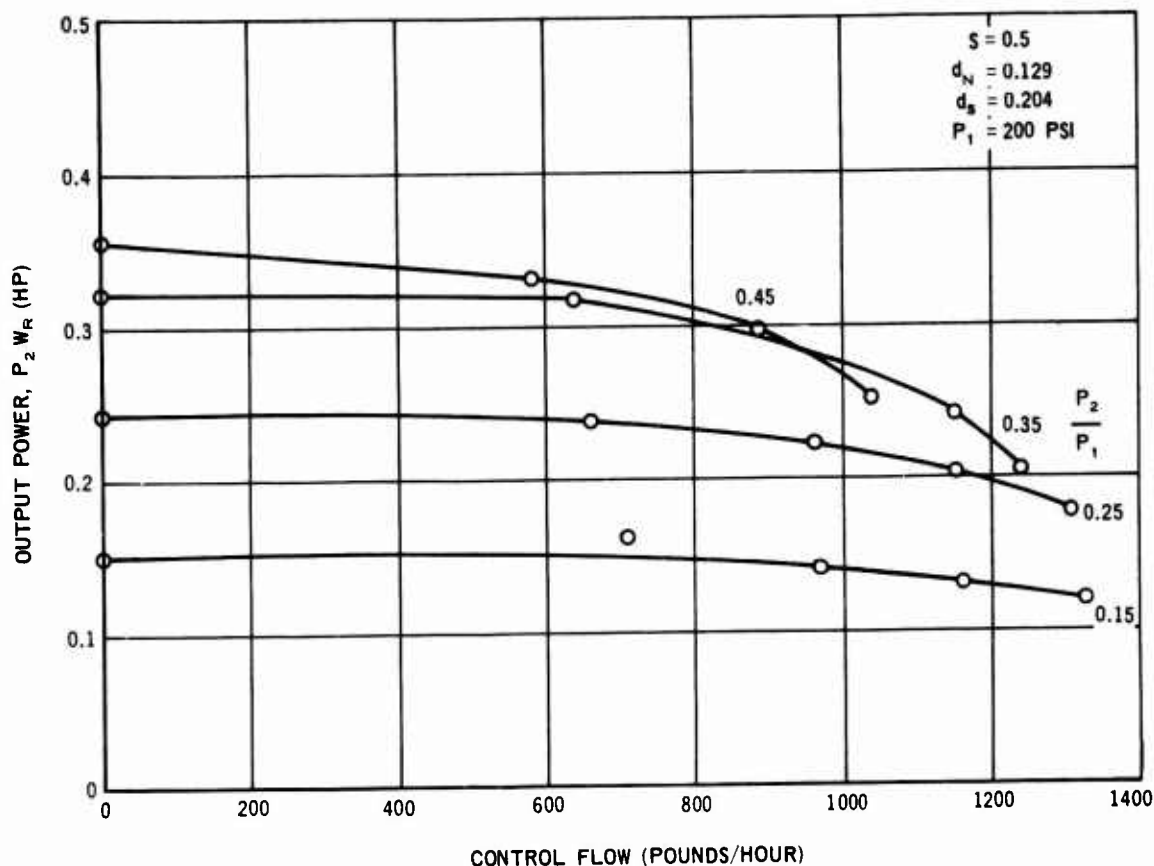


FIGURE 99. FLUIDIC AMPLIFIER PERFORMANCE

6.4 SUMMARY

The fluidic amplifier will require additional development. The model which was tested did not prove satisfactory as a power reducer for nozzle flow, as a function of control pressure.

The amplifier exhibited a characteristic high flow loss at all times as shown by its maximum efficiency of 57 percent. It was found that the fluidic amplifier was not required for the ejector pump and therefore additional testing and development was discontinued.

SECTION VII

EVALUATION OF EXISTING ENGINE FUEL PUMPS

7.1 INTRODUCTION

The ejector pump engine fuel feed system is being developed for possible use in connection with the F-4, A-5, or F-111 aircraft. The F-4 and A-5 both use the J79 engine and the F-111 uses the TF30 engine. To evaluate the use of an ejector system in these aircraft it must be determined if the fuel pumps, on either engine, have enough excess fuel to allow for bleedoff to operate the ejector pump.

7.2 J79 ENGINE

The J79 engine fuel system is so arranged that the fuel from the aircraft enters on a single line, divides and flows to the inlet of the main engine pump and the afterburner fuel pump. The main engine pump has two stages, a centrifugal boost stage and a high pressure gear stage. The afterburner pump is a high speed centrifugal pump. The system as developed for this contract would take fuel from the high pressure stage of the main pump for the primary stage of the ejector and would take fuel from the afterburner pump for the secondary stage.

7.2.1 Primary Stage

Based on the performance of the final ejector pumps tested for this contract, a pump can be scaled down to match the temperature and flow requirements in accordance with MIL-F-17874 for the F-4 aircraft using J79-GE-10 engine. It is estimated that the motive flow required for the primary stage of the ejector pump would be approximately 8,200 pounds per hour at a pressure of 500 psi. Figure 100 shows the fuel requirement for the engine and also the estimated main engine pump output for a worn pump, as obtained from the test data of reference 17. The difference between the two curves is the fuel available for bleed to use as motive fuel. The curve shows 11,400 pounds per hour available at military power. This number must be reduced by the amount of fuel consumed during transient conditions such as adjustment of the inlet guide vanes or afterburner signal which total 6,400 pounds per hour. This means that there is sufficient fuel for operating of the ejector pump during normal conditions but not enough during the transient conditions. To fully satisfy the ejector and engine, the engine pump output would have to be increased by approximately 3200 lb per hour or 12.5 percent.

7.2.2 Secondary Stage

The estimated flow required for the secondary stage would be a total of 16,000 pounds per hour at a pressure of 150-200 psi. Thus the required bleed from the afterburner pump would amount to approximately 8,000 pounds per hour. The afterburner pump normally does not have excess fuel available.

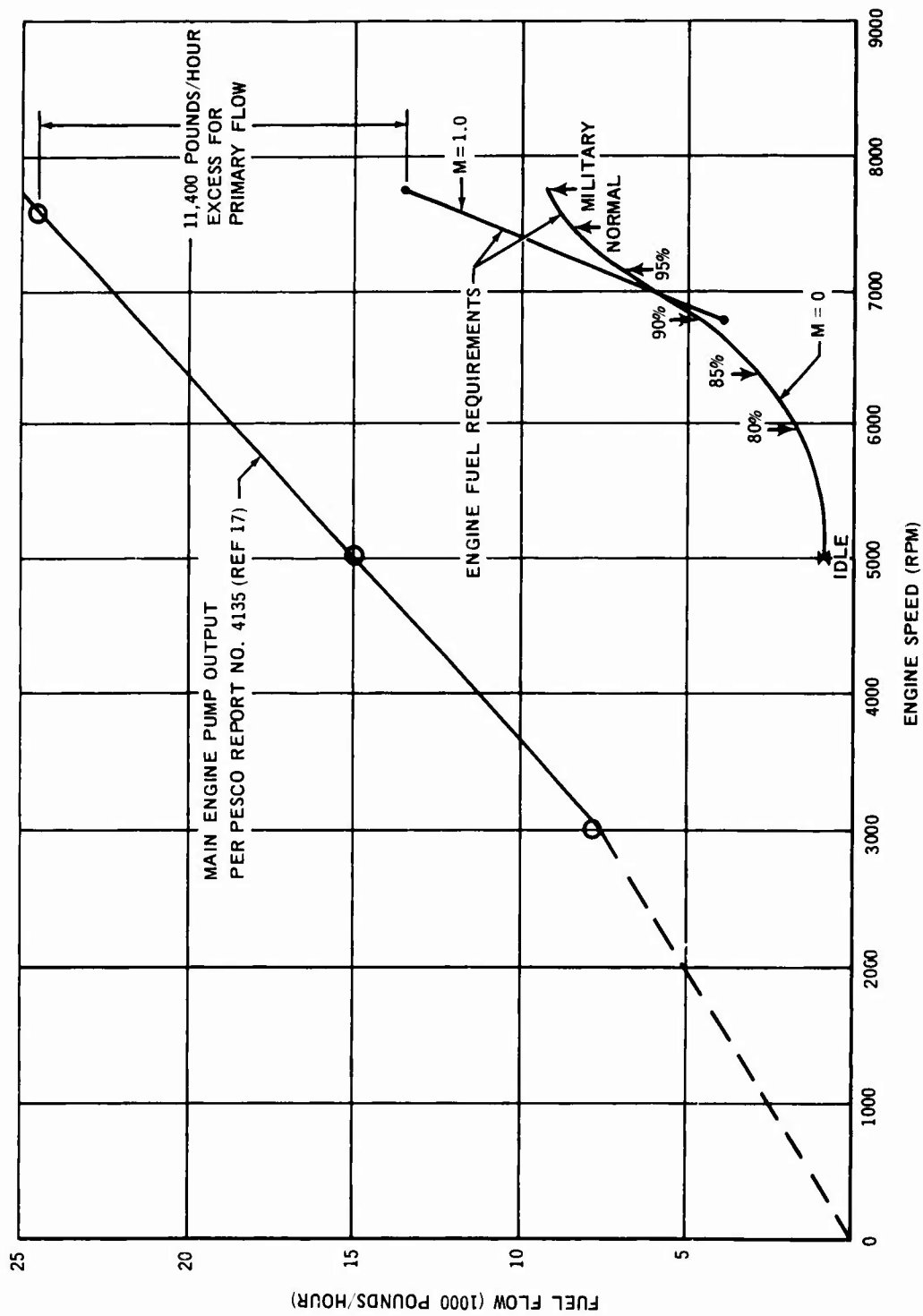


FIGURE 100. J79 MAIN ENGINE FUEL PUMP FLOW AT SEA LEVEL

Figure 101 shows the pump output performance curve which is extrapolated beyond the point which has been previously tested and reported in Reference 18 for a used pump. The extrapolation was done at a constant horsepower available at the inlet to the pump, which should be conservative. The flow is marginal and as a result the maximum afterburner performance may not be obtainable when using an existing afterburner fuel pump currently used on the J79 engine. To fully satisfy fuel flow requirements, the capacity of the pump needs to be increased by 8,000 pounds per hour or 12 percent.

7.3 TF 30 ENGINE

The main engine pump consists of a positive displacement gear stage with a boost impeller stage. The afterburner pump is a high speed centrifugal pump with an integral turbine driven inducer. The ejector motive fuel would be taken from the high pressure discharge from each of these pumps.

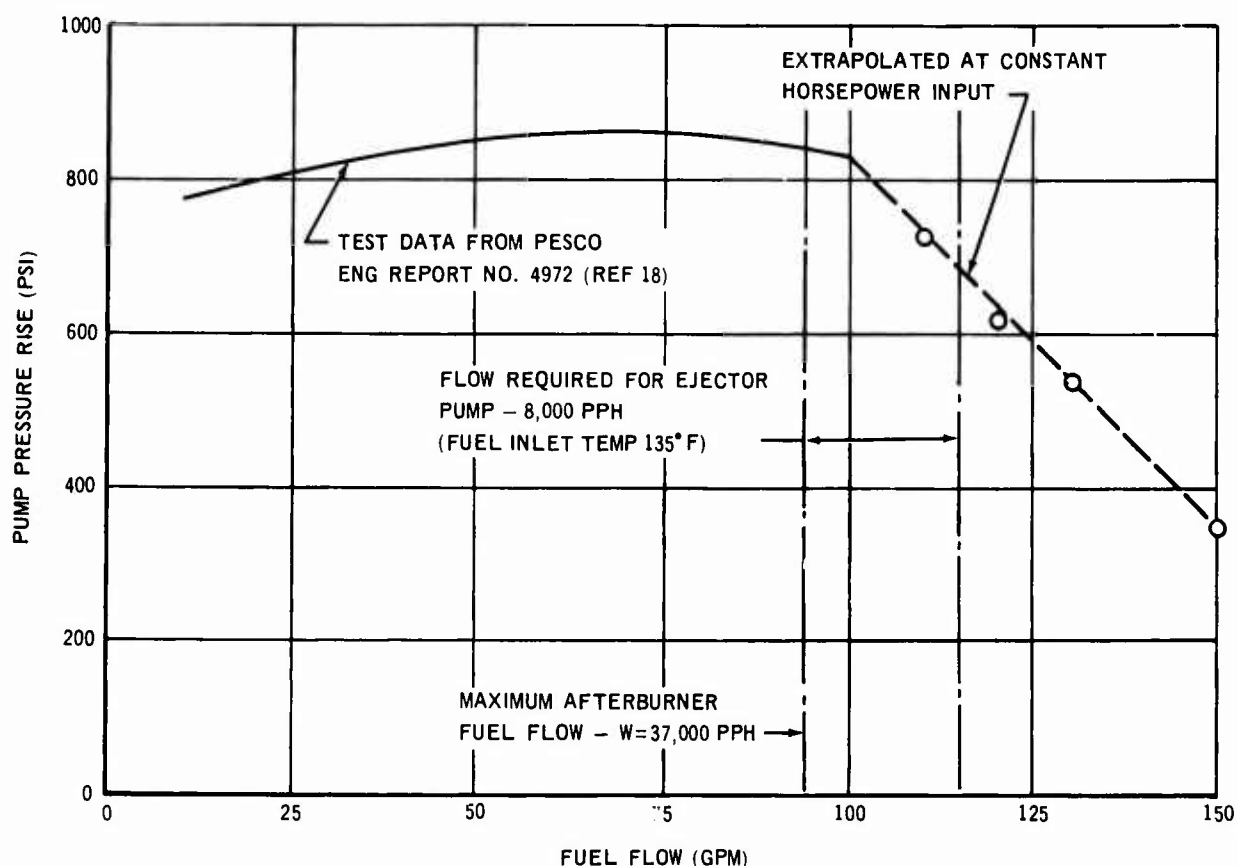


FIGURE 101. J79 AFTERBURNER FUEL PUMP PERFORMANCE

7.3.1 Primary Stage

It has been assumed that the flow requirements as specified in this contract are intended for use with the F-111. Based on the test work done, the motive flow requirements for the two engine military power conditions is equal to 12,900 pounds per hour. Figure 102 shows the main engine pump output as recorded in Reference 19 and shows the excess fuel at sea level military power at $M = 1.0$ to be 7,600 pounds per hour. This is not enough to satisfy the ejector pump requirements plus any transient fuel flows which the engine may require. These transients are unknown at this time, due to the confidential status of the engine. The pump capacity must be increased by at least 6,000 pounds per hour or 34 percent.

7.3.2 Secondary Stage

The secondary stage motive flow requirements on the ejector which was tested is approximately 31,200 pounds per hour. Figure 103 is plotted from data listed in Reference 20 and then extrapolated out. At the point where the flow curve crosses the minimum pressure curve, there is only a flow of approximately 13,600 pounds per hour which could be made available for ejector use. This means that an additional 17,600 pounds per hour of fuel must be made available for ejector operation. This is an increase of approximately 27 percent.

7.4 SUMMARY

The main engine fuel pump, on most engines, has a capacity beyond the engine requirements. This is not a specific amount and varies from one engine to the next. In order to bleedoff fuel for ejector fuel booster pump use, the size of the pumps needs to be increased. In the case of the J79 engine, the increase 12.5 percent whereas the TF-30 engine requires a 34 percent increase. This difference is attributed to the fuel temperature assigned to the requirements. For the F-4 (J79) case the temperature was assigned to be $+135^{\circ}\text{F}$ at the engine inlet whereas for the F-111 (TF30) the temperature of $+200^{\circ}\text{F}$, as specified in this contract, was used. On the TF30, if the temperature were reduced to $+135^{\circ}\text{F}$, the required increase would be reduced to approximately 10 percent.

The afterburner pumps are used up to their peak output and have very little excess, thus any bleed fuel taken must result in an increase in pump size. The temperature is the same as listed for the main engine fuel pump. The increase for the TF30 engine could be cut to approximately a 10 to 12 percent increase.

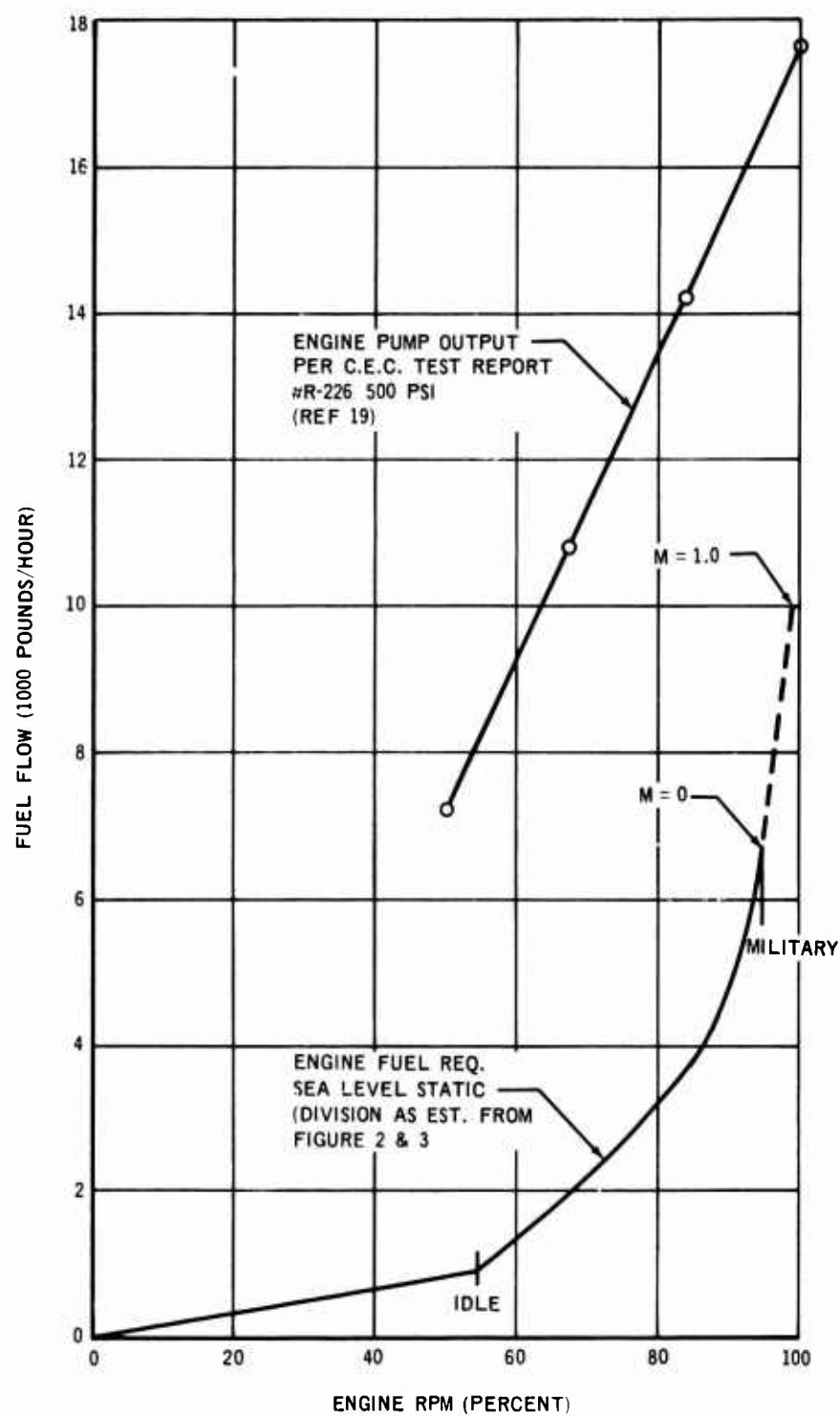


FIGURE 102. TF30 MAIN ENGINE PUMP PERFORMANCE - SEA LEVEL

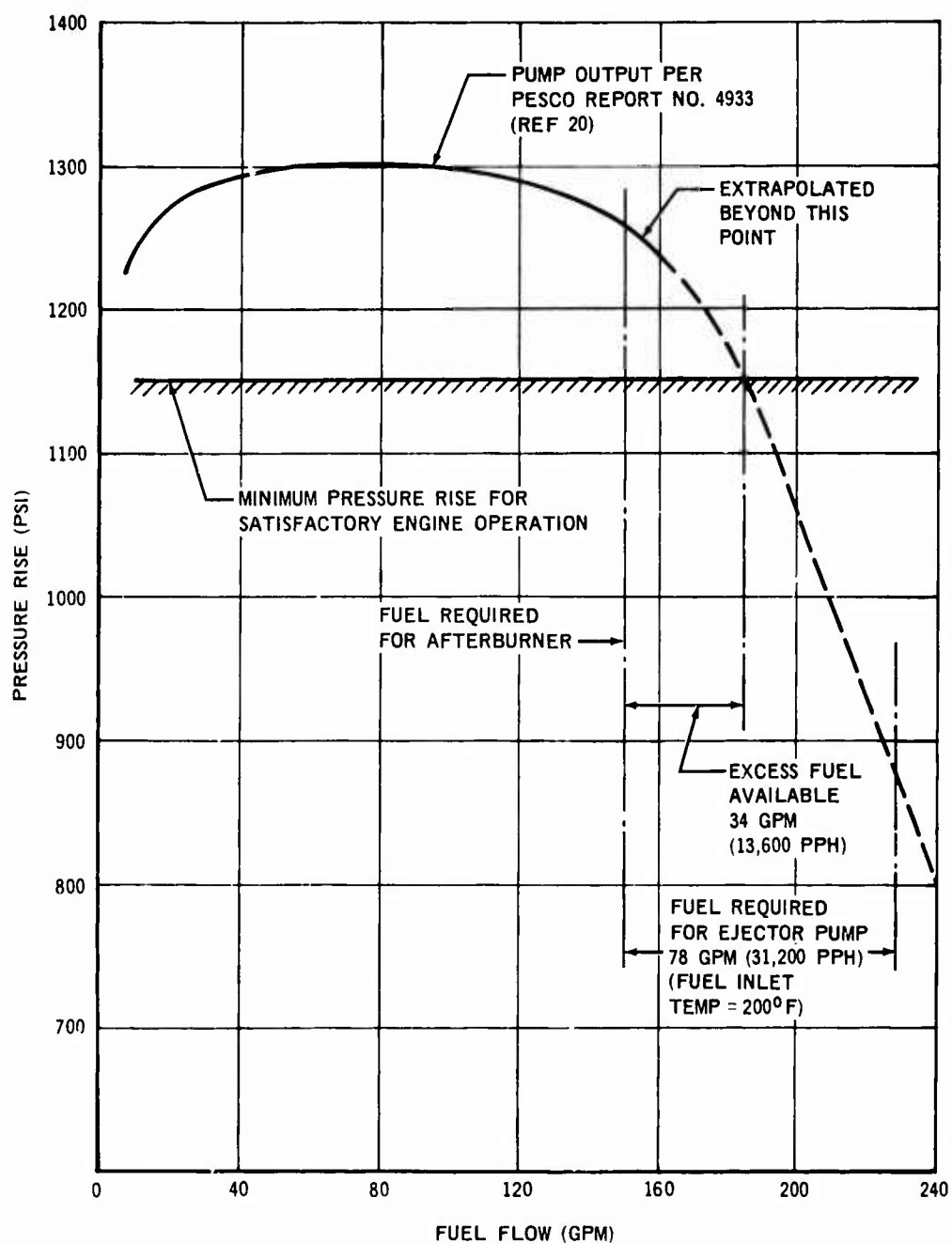


FIGURE 103. TF-30 AFTERBURNER PUMP PERFORMANCE

SECTION VIII

QUANTITATIVE TRADEOFF ANALYSIS

This section presents a tradeoff analysis method which could be used in determining the penalty differential associated with an ejector pump fuel feed system when compared with a conventional fuel feed system. Such a tradeoff analysis would provide a quantitative basis for selection of a system, and would be, preferably, expressed as a total system cost differential as discussed below.

The ejector pump fuel subsystem is below the third functional level (DOD Directive 3200.9); hence interdependence between this subsystem and another is either nonexistent or of little impact. Another characteristic is that the tradeoffs, or selection of an ejector pump system over a mechanically driven pump system, have virtually no influence on aircraft productivity during an emergency deployment. Therefore, the basis for evaluating trades can be either the total cost differential as determined by examining the expected total peacetime costs, or a user's cost, for a ten-year period of aircraft operation. The total cost method is preferable to the user cost method as the latter does not consider cost differentials in design, development, or production.

The first step in analyzing an alternative is to select a base case and then determine the deviation (ΔW) caused in the cost weight (where cost weight is the manufacturer's weight empty less weight of engine and rolling assembly). The weight differential may be positive, negative, or zero. If the deviation is not zero there will be an associated change in the baseline payload range.

Utilizing the concept of a fixed payload range for an aircraft in its design stage, the aircraft is restored to its baseline payload range through an incremental change in wing area (ΔS_W). Now the change in wing area will itself cause a change in cost weight. Therefore the change ΔS_W is made sufficiently large to account for both the incremental wing weight and the incremental weight associated with the trade element itself. The net change in cost weight represents a change in manufacturer's weight empty and is designated ΔMWE . Parenthetically, a ratio of 1.625 pounds of ΔMWE to 1 pound of subsystem weight was the ratio used by Douglas in the C-5A design effort.

The wing area differential (ΔS_W) causes a change in the fuel burn rate. The magnitude of this change is calculated as the difference between the fuel burn rates associated with the baseline configuration and the trade modified configuration. An additional increment for the fuel burn rate is necessitated, of course, by the specific requirements of the ejector pump fuel system under consideration. The resultant change in fuel burned rate generates a Δ change in the baseline total system cost, which represents the cost differential due to the fuel burn rate.

For the difference in Design, Development, Test and Evaluation effort required there are Δ costs.

Similarly, Δ costs are associated with Δ changes in reliability which in turn affect maintenance manhours per flight hour and spares provisioning and usage requirements. The cost differential associated with maintenance manhours is related to the total flying hours during a ten-year period based on a fleet of aircraft, flying a programmed number of flying hours per aircraft per day.

The individual Δ costs (which may be positive or negative) are then summed to give the total cost differential for the trade alternative and provides a quantitative basis for comparing alternatives. The cost difference computation is then the sum of

- Δ DDT&E cost
- Δ Production cost (total fleet)
- Δ Weight cost (including fuel differential)
- Δ MMH/FH cost
- Δ Spare parts cost

The preceding cost elements must consider a full operating cycle (generally ten years) for a full fleet of aircraft, flying at a specified number of hours per aircraft per year for each year of the life cycle.

In instances where existing aircraft are to be modified, there is the necessity to determine the change in the payload range curve and the difference in mission effectiveness. With procurement quantities already fixed, it appears unlikely that significant impact will result in mission effectiveness (other than maintenance costs which are treated separately).

The user cost method comprises only the differentials in operating cost, plus a specified cost for aircraft downtime due to unscheduled maintenance. First, a cost per occurrence is determined for each unscheduled maintenance action. A lambda value (reciprocal of mean time between unscheduled removal MTBUR) is multiplied by the sum of the aircraft down time cost plus the labor cost and then multiplied by the number of flying hours per aircraft in a ten-year period. To this is added the costs of scheduled maintenance, deferred maintenance, and spares. Additionally, the cost of incremental fuel consumption is also included. Comparisons are then made of the total user's costs.

SECTION IX

CONCLUSIONS AND RECOMMENDATIONS

9.1 CONCLUSIONS

The overall objective of this program has been to develop an ejector pump engine fuel feed system for aircraft with an afterburning mode of operation, such as the F-4, A-5, or the F-111. It is concluded that such an ejector pump engine fuel feed system for supplying both main engine and afterburner fuel quantities is feasible. The system that has been developed in this program complies with all contractual requirements.

9.1.1 Ejector Pumps

The ejector pump is a dual operation pump with two concentric nozzles. For main engine operation, the small nozzle is used with an area ratio of 0.016. For afterburner flow rates, the second nozzle is used with an area ratio of 0.04. The area ratio of an ejector pump is the means of expressing the performance characteristic of the given pump.

Sufficient development testing has been conducted to determine that the ejector pump can be sized by using established performance equations from reference 1 except that throat and diffuser loss coefficient K_{34} of approximately 0.6 must be used. $K_1 = 0.1$ and $K_2 = 0$ may be used. These equations are noted in Section 4.2.1 as equations (1), (2), (3), and (4) and also equation (8) as shown in section 4.2.3.3. In equation (8) $Y = 0.7P_o$ may be used for all conditions except for hot fuel above $+135^\circ\text{F}$ in which case $Y = 0.5P_o$ should be used.

It was found that ejector pump nozzle pressures up to 500 psi were acceptable. The high pressure is required to provide a relatively high ejector pump discharge pressure, however a low area ratio must be used to reduce the onset of flow limitation (cavitation). Nozzle pressures above 500 psi were not tested as it appeared that the engine fuel system of existing engines normally operates with 500 psi pump discharge pressure. There appeared, from testing, to be no reason to believe that higher pressures would cause any problems. From the testing done, there did not appear to be any limit to the total amount of fuel being pumped as long as there was sufficient motive fuel available. The analytical equations appear to work for any flow range.

9.1.2 Fuel Tank Sump

Located in the sump area of the main tank is a flexible hose fuel pickup which will pick up fuel from the bottom of the sump during normal flight conditions. Under negative gravity conditions, the end of the pickup will move up to the top of the sump and thus follow the fuel. The fuel in the sump will be circulated by means of a swirl jet of fuel introduced parallel to the tank wall. This swirl jet will provide fluid angular rotation sufficient to cause a normal force to keep the fuel at the tank wall during conditions of zero vertical gravity condition.

A normal force of 1 g appeared to be a good value as it required only 30 seconds to acquire the required speed.

A flight test was conducted of the sump system including the swirl jet and the flexible pickup. The test tank was scaled down to fit the cabin of an Aero Commander. In-flight motion pictures were taken during normal flight and zero gravity flight condition. The flight test showed that fuel is completely disoriented during zero gravity conditions. The swirl system does maintain the fuel orientation such as to keep the fuel at the tank wall. The flight tests showed a need for sustaining the swirl during the zero gravity condition to prevent the rapid decay of the centrifugal force. The tank sump should have corner baffles to aid in the reduction of fluid drag. This radius should be at least equal to one fourth of the tank width.

9.1.3 Fluidic Amplifier

The ejector pump system, as developed, does not require the fluidic amplifier to limit the maximum pressure at the engine to 30 psi.

The fluidic amplifier, as studied, did not produce satisfactory results, however the trend indicated that a fluidic device of this type could be developed to produce satisfactory reduction in pressure, if needed.

9.1.4 Engine Fuel Pumps

Fuel pumps of the J79 and the TF30 engine were studied for available fuel for ejector operation. The main engine pumps do have some excess fuel, however the amount appears to be marginal, when considering transient operations. The afterburner pumps do not have excess fuel and therefore would require an increase in size.

9.2 RECOMMENDATIONS

The ejector pump engine fuel feed system has progressed to a state of development such that the next phase should be a full scale flight test.

The flight test should be conducted in an aircraft capable of high altitude and high speed, and one that utilizes an afterburning engine. A suggested aircraft for the program would be an F-4B.

The system which would be flight tested would consist of a concentric nozzle dual operation ejector, a swirl system in the main fuel tank, and a flexible fuel pickup within the main fuel tank.

It is recommended that existing engine pumps be used in the flight testing even though maximum aircraft performance might be limited. It is also recommended that a trade study be conducted to determine the differential between an ejector pump engine fuel feed system and a conventional fuel feed system on the basis of total system cost.

SECTION X

REFERENCES

1. Cunningham, R.G., "The Jet Pump as a Lubrication Oil Scavenge Pump for Aircraft Engines," Wright Air Development Center Technical Report No. WADC-TR-33-143, July 1954.
2. Hansen, A.G. and Kinnavy, R., "The Design of Water-Jet Pumps," American Society of Mechanical Engineers Paper 65-WA/FE-31 presented in Chicago, Ill. Nov 1965.
3. Flugel, Gustav, "The Design of Jet Pumps" NACA Technical Memorandum No. 982, 1939.
4. Keenan, J.H. - Neumann, E.P. - and Lustewerk, F., "An Investigation of Ejector Design by Analysis and Experiment" ASME paper published in "Journal of Applied Mechanics," September 1950.
5. Stepanoff, A.J. Centrifugal and Axial Flow Pumps, 2nd Edition, John Wiley and Sons Inc, New York, 1957.
6. Küchemann, D. and Weber J., Aero Dynamics of Propulsion First Edition, McGraw-Hill Book Company Inc., New York, 1953.
7. Pekich, H.R., "Performance testing of Lear Jet Ejector Pump Assembly No. 2326023-1" Lear Siegler Inc. Test Report No. TR-1398, May 11, 1966.
8. Albertson, Maurice L.; Barton, James R. and Simons, Daryl B., Fluid Mechanics for Engineers, Prentice-Hall Inc., Englewood Cliffs, New Jersey, 1960, Chapter 6 Pages 239-245.
9. Weinstein, Alvin S., "Diffusion of Momentum from Free and Confined Slot Jets into moving secondary Streams," Air Force Cambridge Research Center Report No. AFCRC-TN-55-476 dated 4 May 1955 prepared at Carnegie Institute of Technology, Pittsburgh, Pennsylvania.
10. Hansen, A.G. and Sidhom, M., "A study of the Performance of Staged - Jet Pumps," American Society of Mechanical Engineers Paper 66-WA/FE-37 presented in New York, New York, November 1966.
11. Loth, J.L., "Theoretical Optimization of Staged Ejector Systems, Part I," Rocket Test Facility, Arnold Engineering Development Center, Air Force Systems Command, Arnold Air Force Station, Tennessee, Report No. AEDC-TR-66-2 dated March 1966.
12. Schlichting, H., Boundary Layer Theory, translated by Kestin, 4th edition, McGraw-Hill Book Co., New York, 1960.
13. Kaufmann, W., Fluid Mechanics, translated by Chilton, 2nd edition, McGraw-Hill Book Co., New York, 1963.

14. Dodge, R.A. and M.J. Thompson, Fluid Mechanics, McGraw Hill Book Co., New York, 1937.
15. Sears, F.W., and M.W. Zemansky, University Physics, Addison-Wesley Publishing Co., 1949.
16. Reynolds, W.C. and H.M. Satterlee, "Liquid Propellant Behavior at Low and Zero G, "Published in "The Dynamic Behavior of Liquids in Moving Containers," edited by H.N. Abramson, NASA SP-106, 1966, Ch. 11.
17. "Qualification Test of PESCO Model 024090-D14 main engine fuel gear pump for the General Electric J79 Series Jet Engines," PESCO Products Division, Borg-Warner Corporation Engineering Report No. 4135 dated May 18, 1960.
18. "Qualification Testing of PESCO Model 023521-022-01 High Speed Centrifugal Afterburner Fuel Pump," PESCO Products Division, Borg-Warner Corporation Engineering Report No. 4972, dated September 3, 1965.
19. "Qualification Test Report for Chandler Evans MFP-90 Model Fuel Pump," Chandler Evans Inc. Engineering Report No. R-226 dated January 28, 1965.
20. "Qualification Testing of PESCO Part No. 024536-202, High Speed Centrifugal Afterburner Fuel Pump for the Pratt and Whitney TF30 Aircraft Engine," PESCO Products Division, Borg-Wagner Corporation Engineering Report No. 4933, dated June 1965.

UNCLASSIFIED

Security Classification

DOCUMENT CONTROL DATA - R&D		
(Security classification of title, body of abstract and indexing annotation must be entered when the overall report is classified)		
1. ORIGINATING ACTIVITY (Corporate author) Douglas Aircraft Company, Aircraft Division 3855 Lakewood Boulevard Long Beach, California		2a. REPORT SECURITY CLASSIFICATION Unclassified
		2b. GROUP -
3. REPORT TITLE DEVELOPMENT OF AN EJECTOR PUMP ENGINE FUEL FEED SYSTEM		
4. DESCRIPTIVE NOTES (Type of report and inclusive dates) Final Report (June 1966 through July 1967)		
5. AUTHOR(S) (Last name, first name, initial) H. F. Winchester R. H. Van Dyne C. J. Moinat		
6. REPORT DATE July 1967	7a. TOTAL NO. OF PAGES 148	7b. NO. OF REFS 20
8a. CONTRACT OR GRANT NO. NOW66-0602-c	9a. ORIGINATOR'S REPORT NUMBER(S) DAC 61531	
b. PROJECT NO.		
c.	9b. OTHER REPORT NO(S) (Any other numbers that may be assigned this report)	
d.		
10. AVAILABILITY/LIMITATION NOTICES Qualified requesters may obtain copies of this report direct from DDG. THIS DOCUMENT IS SUBJECT TO SPECIAL EXPORT CONTROLS AND EACH		
11. SUPPLEMENTARY NOTES FOREIGN GOVERNMENTS OR FOREIGN NATIONALS MAY BE MADE ONLY WITH THE PRIOR APPROVAL OF COMMANDER, NAVAL AIR SYSTEMS COMMAND		12. SPONSORING MILITARY ACTIVITY Naval Air Systems Command Department of the Navy Washington, D. C. 20360
13. ABSTRACT An ejector pump engine fuel feed system was designed and developed. The system consists of an ejector fuel pump and a fuel tank sump with a swirl jet and a flexible fuel pickup tube. Several types of ejector pumps were tested which included the simple ejector, a dual series induced flow ejector, a parallel induced flow ejector and a dual operation ejector with two concentric nozzles. An annular ring-type nozzle was tested in addition to the normal central nozzle. The system as developed will pump JP-4 or JP-5 fuel at temperatures up to +200°F to an engine at a flow rate of 70,000 pounds per hour with a pump discharge pressure of 34 psia. The swirl jet in the sump tank provides fluid rotation and a resulting radial force to position the fuel at the wall of the sump tank at all times. This insures that fuel will be at a known location during periods of zero gravity. The fuel is then delivered to the ejector pump through a flexible hose-type fuel pickup tube. The end of the pickup is normally on the bottom at the tank wall. During periods of negative gravity, the pickup will bend upward to draw fuel from the top of the sump area. Flight tests were conducted on a scale model of the sump swirl system to demonstrate the zero gravity provisions.		

DD FORM 1473

1 JAN 64

0101-807-6800

UNCLASSIFIED

Security Classification

14. KEY WORDS	LINK A		LINK B		LINK C	
	ROLE	WT	ROLE	WT	ROLE	WT
Ejector pump Swirl jet Engine fuel feed system Flexible fuel pickup Simple ejector Dual ejector Concentric nozzles Annular nozzle Zero gravity Negative gravity Fuel tank						

INSTRUCTIONS

1. **ORIGINATING ACTIVITY:** Enter the name and address of the contractor, subcontractor, grantee, Department of Defense activity or other organization (*corporate author*) issuing the report.

2a. **REPORT SECURITY CLASSIFICATION:** Enter the overall security classification of the report. Indicate whether "Restricted Data" is included. Marking is to be in accordance with appropriate security regulations.

2b. **GROUP:** Automatic downgrading is specified in DoD Directive 5200.10 and Armed Forces Industrial Manual. Enter the group number. Also, when applicable, show that optional markings have been used for Group 3 and Group 4 as authorized.

3. **REPORT TITLE:** Enter the complete report title in all capital letters. Titles in all cases should be unclassified. If a meaningful title cannot be selected without classification, show title classification in all capitals in parenthesis immediately following the title.

4. **DESCRIPTIVE NOTES:** If appropriate, enter the type of report, e.g., interim, progress, summary, annual, or final. Give the inclusive dates when a specific reporting period is covered.

5. **AUTHOR(S):** Enter the name(s) of author(s) as shown on or in the report. Enter last name, first name, middle initial. If military, show rank and branch of service. The name of the principal author is an absolute minimum requirement.

6. **REPORT DATE:** Enter the date of the report as day, month, year; or month, year. If more than one date appears on the report, use date of publication.

7a. **TOTAL NUMBER OF PAGES:** The total page count should follow normal pagination procedures, i.e., enter the number of pages containing information.

7b. **NUMBER OF REFERENCES:** Enter the total number of references cited in the report.

8a. **CONTRACT OR GRANT NUMBER:** If appropriate, enter the applicable number of the contract or grant under which the report was written.

8b, 8c, & 8d. **PROJECT NUMBER:** Enter the appropriate military department identification, such as project number, subproject number, system numbers, task number, etc.

9a. **ORIGINATOR'S REPORT NUMBER(S):** Enter the official report number by which the document will be identified and controlled by the originating activity. This number must be unique to this report.

9b. **OTHER REPORT NUMBER(S):** If the report has been assigned any other report numbers (*either by the originator or by the sponsor*), also enter this number(s).

10. **AVAILABILITY/LIMITATION NOTICES:** Enter any limitations on further dissemination of the report, other than those

imposed by security classification, using standard statements such as:

- (1) "Qualified requesters may obtain copies of this report from DDC."
- (2) "Foreign announcement and dissemination of this report by DDC is not authorized."
- (3) "U. S. Government agencies may obtain copies of this report directly from DDC. Other qualified DDC users shall request through _____."
- (4) "U. S. military agencies may obtain copies of this report directly from DDC. Other qualified users shall request through _____."
- (5) "All distribution of this report is controlled. Qualified DDC users shall request through _____."

If the report has been furnished to the Office of Technical Services, Department of Commerce, for sale to the public, indicate this fact and enter the price, if known.

11. **SUPPLEMENTARY NOTES:** Use for additional explanatory notes.

12. **SPONSORING MILITARY ACTIVITY:** Enter the name of the departmental project office or laboratory sponsoring (*paying for*) the research and development. Include address.

13. **ABSTRACT:** Enter an abstract giving a brief and factual summary of the document indicative of the report, even though it may also appear elsewhere in the body of the technical report. If additional space is required, a continuation sheet shall be attached.

It is highly desirable that the abstract of classified reports be unclassified. Each paragraph of the abstract shall end with an indication of the military security classification of the information in the paragraph, represented as (TS), (S), (C), or (U).

There is no limitation on the length of the abstract. However, the suggested length is from 150 to 225 words.

14. **KEY WORDS:** Key words are technically meaningful terms or short phrases that characterize a report and may be used as index entries for cataloging the report. Key words must be selected so that no security classification is required. Identifiers, such as equipment model designation, trade name, military project code name, geographic location, may be used as key words but will be followed by an indication of technical context. The assignment of links, roles, and weights is optional.

UNCLASSIFIED

Security Classification